AIR FORCE INSTITUTE OF TECHNOLOGY

AIR UNIVERSITY
UNITED STATES AIR FORCE

AN ANALYTICAL AND EXPERIMENTAL STUDY OF AIRCRAFT HYDRAULIC LINES INCLUDING THE EFFECT OF MEAN FLOW

DISSERTATION

AFIT/DS/AA/79S-1

John H. Pletcher, Major

SCHOOL OF ENGINEERING

WRIGHT-PATTERSON AIR FORCE BASE, OHIO

AFIT/DS/AA/79S-1

(9) Doctoral Thesis,

(6)

AN ANALYTICAL AND EXPERIMENTAL STUDY OF AIRCRAFT HYDRAULIC LINES INCLUDING THE EFFECT OF MEAN FLOW

DISSERTATION

(14) AFIT/DS/AA/79S-1 (10) John H. Pletcher, Jr
Major USAF

(11) May 79

(12) 236

Approved for public release; distribution unlimited.

(16) 3145

(17) 30

ϕ12 225

YB

AN ANALYTICAL AND EXPERIMENTAL STUDY OF AIRCRAFT HYDRAULIC LINES INCLUDING THE EFFECT OF MEAN FLOW

DISSERTATION

Presented to the Faculty of the School of Engineering

of the Air Force Institute of Technology

Air University

in Partial Fulfillment of the

Requirements for the Degree of

Doctor of Philosophy

by

John H. Pletcher, Jr., M.S.
Major USAF

May 1979

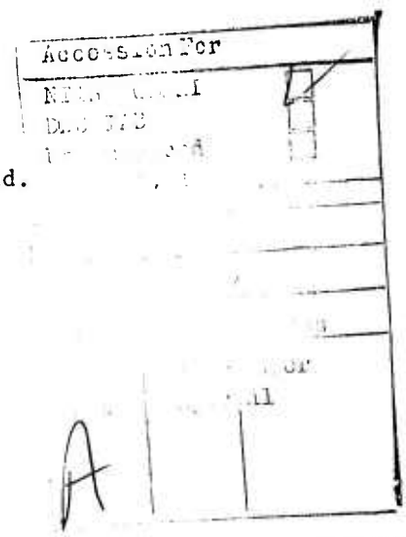

Preface

This dissertation is part of a continuing series of studies conducted at the Air Force Institute of Technology concerning fluid transmission line technology, with emphasis on aircraft hydraulic systems. The aim of the dissertation was twofold. First an analysis was developed which included the effect of mean flow coupled with oscillatory fl. via the convective term in the axial momentum equation. The second aim was an experimental study of a hydraulic system to determine how the frequency response is affected by the mean flow, bends, line geometry, temperature, and fluid properties.

This combined analytical and experimental effort resulted in a large amount of computer results as well as a large quantity of experimental data. The computer programs and the experimental data are available at the Air Force Institute of Technology to any student continuing research in this area.

I have many people to thank. Major John A. Wright and Major Shraga Katz provided much experimental data on the use of the clampon transducer. Mrs. Mollie Bustard, the librarian, and her husband, Mr. William Bustard, who was in charge of computer facilities, saved me countless hours by obtaining needed reference materials and solving difficult computer problems. Mr. Ed Binns, Mr. Paul Lindquist, and Mr. Harold Lee deserve special thanks for their help in designing the experimental setup, including the instrumentation, and in obtaining meaningful data. They also provided valuable engineering insight when problems arose. I also wish to thank my Advisory Committee, Dr.

Milton E. Franke, Dr. David A. Lee, Major James T. Karam, Jr., and Captain Richard Merz, for their guidance. Dr. Franke deserves special thanks for the sound technical advice and constant encouragement he provided throughout this effort. Likewise, Dr. Lee, who spent many hours working with me on mathematical developments and numerical evaluation techniques, deserves special thanks. Most importantly, I wish to thank my wife [redacted] for her constant support and understanding and for keeping our family together and happy for so long.

John H. Pletcher, Jr.

Contents

Contents (cont'd)

Contents (cont'd)

List of Figures

List of Tables

List of Symbols

Symbol	Description	Units
A	$2\overline{u_o}R^2/(\gamma L)$	dimensionless
a	$1/2 - B/(8D_2)$	dimensionless
$\hat{a}$	argument of the confluent hypergeometric function, $M(\hat{a},b,-\hat{z}/\hat{a})$	dimensionless
$(a)_K$	$a(a+1)(a+2)(a+3)\ldots(a+K-1)$, $(a)_0 = 1$	dimensionless
B	$-A - j\omega R^2/\nu$	dimensionless
B_m	fluid bulk modulus	psi
b	argument of the gamma function $\Gamma(b)$, and the confluent hypergeometric function, $M(\hat{a},b,-\hat{z}/\hat{a})$	dimensionless
c	speed of propagation	in/sec
c_f	calibration factor	$psi/volts_{rms}$
c_K	coefficient of z^K in infinite series for W(z)	dimensionless
c_m	coefficient of z^m in infinite series for W(z)	dimensionless
c_p/c_v	ratio of specific heats	dimensionless
c_o	corrected adiabatic speed of sound	in/sec
c_{of}	speed of propagation for zero mean flow	in/sec
c_2	$\overline{u_o\Omega}/c_o$	dimensionless
c_3	$j\omega L\overline{\Omega}/c_o$	dimensionless
c_4	coefficient defined by Eq (106)	dimensionless
D	positive real number	dimensionless
D_2	$j\sqrt{A}/2$	dimensionless
E	modulus of elasticity	psi
$E(\epsilon)$	function used to separate variables (see Eq (40))	dimensionless

Symbol	Description	Units
e	2.71828...	dimensionless
$F(\gamma)$	function defined by Eq (89)	dimensionless
F_w	$(8\omega/\omega_\nu)^{1/2}$	dimensionless
F_x	axial force per unit volume	lbf/in^3
$G(\gamma)$	function defined by Eq (96)	dimensionless
J	summation index	dimensionless
J_o	Bessel function of the first kind, order zero	dimensionless
J_1	Bessel function of the first kind, order one	dimensionless
j	$\sqrt{-1}$	dimensionless
K	summation index	dimensionless
K_m	line mounting factor	dimensionless
K_1	arbitrary constant	dimensionless
K_2	$K_1/(8D_2)$	dimensionless
k	c_p/c_v for an ideal gas and B_m/P_o for a liquid	dimensionless
L	transmission line length	in
M	Mach number	dimensionless
M(-,-,-)	confluent hypergeometric function	dimensionless
m	summation index	dimensionless
n	summation index	dimensionless
P_{max}	maximum amplitude of the standing pressure wave	psi
Pr	Prandtl number	dimensionless
P_o	average or steady-state pressure	psi
P_1	peak pressure 7.19 in. from the pump (Ch. VII) forward wave pressure	psi dimensionless

Symbol	Description	Units
P_2	peak pressure 96.25 in. from the pump (Ch. VII) reflected wave pressure	psi dimensionless
P_3	peak pressure 197.25 in. from the pump	psi
p	pressure	psi through Eq (33) dimensionless after Eq (33)
R	transmission line radius	in
r	radial coordinate	in
T	temperature	^oF
t	time	sec
u	axial velocity	in/sec through Eq (33) dimensionless after Eq (33)
u_r	radial velocity	in/sec
u_θ	velocity in the circumferential velocity	in/sec
u_o	through-flow velocity, $u_o(\varepsilon)$	in/sec
$\overline{u}_{C/L}$	maximum centerline velocity	in/sec
V_1	voltage reading before data run	$volts_{rms}$
V_2	voltage reading after data run	$volts_{rms}$
W	wall thickness	in
W(z)	function used to transform variables (see Eq (49))	dimensionless
x	axial coordinate	in
Y_m	Young's modulus	psi
Y'_o	normalizing constant, $1/(c_o\rho_o)$	$in^3/(lbf\text{-}sec)$
Y_{11}	forward driving point admittance	$in^3/(lbf\text{-}sec)$
Y_{12}, Y_{22}	admittance parameters	$in^3/(lbf\text{-}sec)$
Y_{21}	forward transfer admittance	$in^3/(lbf\text{-}sec)$

Symbol	Description	Units
Z_c	characteristic impedance	psi/cis
Z_{ca}	adiabatic characteristic impedance	psi/cis
z	$2D_2\varepsilon^2$	dimensionless
$\hat{z}$	argument of the confluent hypergeometric function, $M(\hat{a},b,-\hat{z}/\hat{a})$	dimensionless
α	attenuation	dimensionless
β	phase constant	dimensionless
Γ	propagation factor	in^{-1}
$\Gamma(b)$	Gamma function	dimensionless
γ	separation constant and propagation constant	dimensionless
ε	r/R	dimensionless
η	x/L	dimensionless
η_o	reference point for pressure boundary condition	dimensionless
θ	circumferential coordinate	radians
μ	absolute viscosity	$lbf\text{-}sec/in^2$
ν	kinematic viscosity	in^2/sec
π	3.14159...	dimensionless
ρ	density	$lbf\text{-}sec^2/in^4$ through Eq (33) dimensionless after Eq (33)
ρ_o	average or steady-state density	$lbf\text{-}sec^2/in^4$
ϕ	phase angle	radians
Ω	weighting function	dimensionless
ω	frequency	rad/sec in equations, Hz on figures
ω_ν	viscous characteristic frequency, $8\nu/R^2$	rad/sec

Symbol	Description	Units
Subscripts		
o	zero mean flow	
1	forward wave	
2	reflected or backward wave	
Superscripts		
'	derivative with respect to z	
-	average value of a function across the line cross-section	
~	mean quantity	
_	(underscore) small perturbation about a mean quantity	

Abstract

A mathematical model of a fluid transmission line was developed which includes the effect of laminar mean flow coupling with oscillatory flow. The equations of motion and a frequency dependent pressure-density relation are solved for the attenuation and phase constant of a pressure wave traveling either with or against the mean flow. Using these, the pressure and velocity are calculated using an appropriate line model. The analysis centered on solving the nonhomogeneous confluent hypergeometric equation with complex parameters using an infinite series and evaluating the solution using Ward's method.

Experiments were run using an aircraft hydraulic system. The frequency response, vibration displacement, and the standing pressure half wave were measured in a straight line and a line with bends for flow rates up to 9.5 gpm. The bends had very little effect on the pressure measurements; however, the vibration displacement was greater near the bends than in a straight line section. The mean flow had no significant effect on the frequency response or the standing pressure half wave. A clampon transducer, which did not disturb the flow and could be easily moved, was used for the pressure measurements. Vibration displacements in excess of 0.001 in. peak-to-peak caused significant measurement errors. However, in the absence of vibration, the clampon transducer pressure measurements were within 5% of readings taken with a conventional Statham in-line transducer. The clampon transducer should be a valuable tool for the hydraulic engineer.

A sensitivity analysis showed the effect of small changes in geometry, temperature, steady-state pressure, fluid properties, entrained air content, and element volume. The resonant frequency was lowered moderately by a small increase in line length, temperature, or entrained air content. Peak pressure was lowered significantly by a small increase in entrained air content or element volume. Also the attenuation was lowered significantly by a small decrease in line radius or temperature, and increased significantly by a small increase in kinematic viscosity.

Using the analysis, the attenuation and phase constant were calculated for hydraulic and air lines. Results were compared with experiments and the published work of Nichols, Brown, Orner and Cooley and that of Katz, Hausner and Eisenberg. The agreement was good. For typical hydraulic line flow rates, results showed no significant difference from the no-flow results. Velocity profile data were also obtained which compared favorably with the results of Richardson and Uchida. The air line results show that the attenuation and phase constant increase with frequency. The reflected or backward wave attenuation and phase constant increase with flow, while the forward wave attenuation and phase constant decrease with flow and by a smaller amount than the increase for the reflected wave for a given increase in flow. Results are presented in terms of the deviation from the no-flow values and as a ratio with the no-flow values. The difference between flow and no-flow values is significant in this case, especially for frequencies near and below the viscous characteristic frequency. For air with a mean flow Mach number of 0.1, the forward wave attenuation decreased to 34% of the no-flow value and the

forward wave phase constant decreased to 83% of the no-flow value. This effect was greater at higher mean flow Mach numbers, but smaller at higher frequencies. The data were reasonably linear for high frequencies but nonlinear for frequencies near and below the viscous characteristic frequency. The new analysis and line model provide a means for the fluid systems designer to accurately account for mean flow effects.

AN ANALYTICAL AND EXPERIMENTAL STUDY OF AIRCRAFT HYDRAULIC LINES INCLUDING THE EFFECT OF MEAN FLOW

I. Introduction

Background

Hydraulic lines and fluid transmission lines in general have been studied for many years due to their application to aircraft systems, gas and oil transmission, fluidics, and acoustics. Studies included some early work on the effects of waterhammer by Joukowsky (40) in 1898 and Allievi (36) in 1903. In the same time period Heaviside (37) developed his operator theory to solve electrical transmission line problems. His work provided the analytical tools needed to solve fluid transmission line problems. In 1929 Richardson and Tyler (27) experimentally studied the velocity profile of air oscillating in a pipe and later in 1956 Uchida (32) studied the same phenomena with the oscillating flow superimposed on a laminar mean flow.

Viscous dissipation was included in fluid transient analyses by Wood (43) in 1937 and Rich (41) in 1945 via a loss term proportional to the velocity transients, effectively a linear friction term. In 1950 Iberall (39) developed a solution for the viscous attenuation in lines using frequency dependent dissipation. Rohmann and Grogan (42) in 1957 solved Iberall's problem in terms of electrical transmission line analogies. In 1962 Brown (7) and Nichols (22) published their work on pneumatic transmission lines with Brown covering the transient response and Nichols the frequency response.

A continuing research effort in fluid transmission line technology is being conducted at the Air Force Institute of Technology. In 1970 Franke, Karam and Lymburner (38) experimentally determined the frequency response and effect of flow for fluidic transmission lines. Later Moore (20) studied the effects of turbulence and noncircular cross-sections for pneumatic lines. In 1977 Wright (35) performed an experimental study of the frequency response of hydraulic systems. Two more experimental efforts with hydraulic systems took place in 1978. Katz (16) studied measuring techniques for oscillatory and transient pressures while Zur (44) studied the transient response and the effect of bends. In all this research, mean flow effects have been ignored or approximated based on limited experimental data.

Problem

The primary intent of this research was to develop an analytical model of a hydraulic line which included mean flow effects. The main stumbling block that caused prior researchers to employ approximations or ignore the effect of mean flow altogether was the nonlinear convective term in the axial momentum equation, udu/dx. Orner (24) linearized this equation but could not solve the resulting relations. These equations are solved by the author, providing for the first time an accurate analytical method to access the effect of laminar mean flow in a fluid transmission line (either liquid or gaseous). Results are compared with experimental data and the results of other researchers to verify the validity of the method.

Several analytical and experimental studies of hydraulic lines were conducted. The analytical studies used the new analytical method to show the effect of flow and other parameters of interest.

Also the results of an effort (3) by the McDonnell Aircraft Company under contract with the Air Force Aero Propulsion Laboratory were used, especially the hydraulic system frequency response computer program (HSFR) which calculated the dynamic pressure and velocity at any point in an aircraft hydraulic system. Resonant frequencies and pressure standing wave amplitude and positi re also calculated by the program. Using these two analytic ols, a sensitivity analysis was accomplished to determine the t of small changes in line geometry and fluid properties.

Experimental studies were undertaken to provide data to verify the analytical results and to study the effect of bends in a hydraulic line. Also a new pressure measuring instrument, the clampon transducer, was studied to determine if its unique qualities would make it a valuable tool for the aeronautical engineer. Tests were designed to ensure that significant vibration was present, as aircraft hydraulic systems are typically subject to vibration. The effect of this vibration on the clampon transducer was then studied.

Overview and Summary of the Problem

In the theory section, the solution to the problem of the fluid transmission line with mean flow is obtained. All assumptions and mathematical techniques are given. Several lengthy mathematical demonstrations have been relegated to the appendices. A mathematical model of a hydraulic line using the analytical solution is also given. Chapter III describes the experimental equipment used and the tests that were run. In Chapter IV the use of the clampon transducer is discussed, as well as the results of several tests involving the clampon transducer. The effect of vibration on the clampon transducer

is covered in Chapter V. The results of experiments run to determine the effect of bends on the frequency response of a hydraulic system are given in Chapter VI. Chapter VII contains the sensitivity analysis for a hydraulic line showing the effect of changes in line geometry and fluid properties. Analytical results for the attenuation, phase constant and velocity profile in a hydraulic line with laminar mean flow are given in Chapter VIII. In Chapter IX analytical results for the frequency response and standing pressure half wave in a hydraulic line with mean flow are compared with experimental data. The effect of flow on the attenuation, phase constant and velocity of propagation for large mean flow velocities in air lines is given in Chapter X. Analytical results for air lines are compared with the published results of other researchers in Chapter XI. A summary with recommendations for future research follows in Chapter XII and the appendices with the mathematical demonstrations conclude the dissertation.

As many diverse topics are discussed herein, the reader may wish to review only topics of particular interest. For the reader interested in the analysis of a fluid transmission line and the mathematical details of the solution, Chapters II, VIII, XI and the Appendices are recommended. The reader interested in the experimental study of hydraulic systems is referred to Chapters III, IV and V. For one interested in the effect of mean flow, Chapters VIII, IX and X should be reviewed. The reader interested in the clampon transducer, and the effect vibration has on it, should read Chapters IV and V. Those interested in the effect of bends should go to Chapter VI, and those interested in the effect of changes in line geometry and fluid properties should review Chapter VII.

II. Theory

Problem Definition

The basic problem is to determine the dynamic response of a fluid transmission line (Fig. 1) with through-flow to perturbations to the average velocity, $\bar{u}_o$, and/or pressure, p_o. The solution then must relate the velocity, which is averaged over the cross-section, to the pressure at any point in the line. The fluid transmission line is a rigid, circular tube of length L, inside radius R, and wall thickness W. The fluid is compressible and Newtonian with kinematic viscosity ν, density ρ, and bulk modulus B_m. This is the problem addressed by Orner (24).

Assumptions

1. The fluid is continuous, Newtonian and barotropic, meaning that the fluid density depends only on the pressure.

2. All fluid properties, namely the adiabatic speed of sound, the ratio of specific heats, c_p/c_v, Prandtl number, Pr, kinematic viscosity and bulk modulus, are assumed constant. This implies small temperature variations and isothermal tube walls.

3. The flow, both steady and unsteady, is assumed to be laminar. This implies that the Reynolds number based on tube diameter is 2000 or less.

4. $R \ll L$ and $\omega R/c_o \ll 1$. The wavelengths and the line length must be large compared to the line radius to insure that end effects and transverse wave propagation are negligible. For MIL-H-5606B

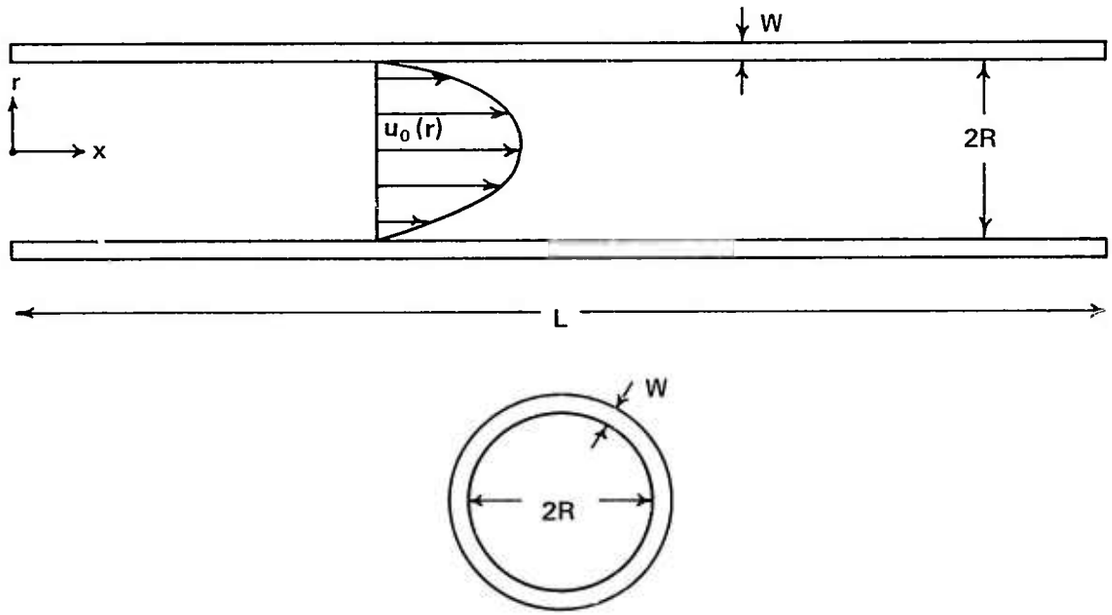

Figure 1. Fluid Transmission Line

hydraulic fluid at 70^{o}F in a standard 5/8 in. OD line, this requires $L \gg 0.25$ in. and $\omega \ll 2.2 \times 10^{5}$ rad/sec.

5. The velocity and the change of all dependent variables in the circumferential direction are negligible due to rotational symmetry.

6. The tube walls are rigid. This means that the elasticity of the pipe walls may be neglected when compared with the compressibility of the fluid. An analysis showing the validity of this assumption can be found in D'Souza and Oldenburger (10). The speed of sound in a liquid is corrected to account for the elasticity of the walls

$$c_o = \sqrt{\frac{B_m}{\rho_o \left(1 + \frac{K_m R B_m}{EW}\right)}} \qquad (1)$$

c_o is the corrected adiabatic speed of sound in the fluid, E is the modulus of elasticity of the line material and K_m is the line mounting factor. An appropriate value for K_m is given in Reference 2 (K_m = 1.8).

7. The bulk viscosity is assumed to be zero. A group of studies (28) on the second coefficient of viscosity found that very high frequencies (10^{12} Hz and higher) were required before the second coefficient of viscosity could be measured in liquids. However, at these high frequencies the second coefficient was large, up to 200 times larger than the first coefficient of viscosity, and positive, not negative as the Stokes hypothesis requires. Strictly speaking, Stokes hypothesis is good only for low density monatomic gases. However, as long as the frequency is well below the relaxation frequency (21,24), i.e.,

$$\omega << c_o^2/\nu \tag{2}$$

the effect of the bulk viscosity is negligible. For MIL-H-5606B hydraulic fluid at 70^oF, this requires

$$\omega << 6.4 \times 10^{10} \text{ rad/sec} \tag{3}$$

and for air at standard temperature and pressure

$$\omega << 8 \times 10^9 \text{ rad/sec} \tag{4}$$

8. Second and higher harmonics of pressure, velocity and density may be neglected. This is analogous to assuming small amplitude perturbations in an analysis using time-averaged mean flow quantities and perturbations thereof. The assumption is needed in the analysis of the nonlinear convective acceleration term of the axial momentum equation. D'Souza and Oldenburger (10) show that to justify the omission of the nonlinear convective term, $u\partial u/\partial x$, in the momentum equation, the Mach number, M, must be small, i.e., $M = \frac{\overline{u}_o}{c_o} << 1$. Also, in experiments using air, Kantola (14) found a noticeable deviation from small amplitude theory at M = 0.05. This indicates the nonlinear convective term must be considered for even relatively small Mach numbers to account for the coupling of the mean flow with the velocity perturbations.

9. There are no significant body forces acting on the fluid transmission line.

10. The quasi-steady through-flow is incompressible, established, and unaffected by the oscillatory flow. For this laminar analysis, a Hagen-Poiseuille velocity profile is assumed; i.e.,

$$u_o(\varepsilon) = 2\overline{u}_o \ (1-\varepsilon^2) \tag{5}$$

$$\varepsilon \equiv r/R \tag{6}$$

where $\overline{(\cdot)}$ denotes the average value of the function across the line cross-section; i.e.,

$$\overline{(\cdot)} \equiv 2\int_0^1 \varepsilon(\cdot)d\varepsilon \tag{7}$$

11. The pressure is constant across the cross-section of the tube; i.e.,

$$p = p(\eta,t) \tag{8}$$

$$\eta = x/L \tag{9}$$

This follows from the further assumption that the radial velocity is negligible compared to the axial velocity. As shown by Brown (7), the assumption is valid as long as

$$\frac{\nu}{Rc_o} << 1 \tag{10}$$

For MIL-H-5606B hydraulic fluid at 70^{o}F, this requires

$$R >> 8.6 \times 10^{-7} \text{ in.} \tag{11}$$

As given by Brown (7), this and most of the other restrictive inequalities are derived by representing p and u as sine waves traveling at the speed of sound and using these in the momentum and continuity equations as well as the equation of state.

12. The second derivative of the axial velocity is small compared to the radial derivatives.

$$\frac{\partial^2 u}{\partial x^2} << \frac{1}{r}\frac{\partial}{\partial r}\left(r\frac{\partial u}{\partial r}\right) \tag{12}$$

This is valid whenever

$$\frac{\nu\omega}{c_o^2} << 1 \tag{13}$$

which is the same restriction noted earlier when the frequency was required to be well below the relaxation frequency of the fluid.

Differential Equations

The mass conservation and axial momentum equations written in cylindrical coordinates are

Continuity:

$$\frac{\partial \rho}{\partial t} + \frac{1}{r}\frac{\partial}{\partial r}(r\rho u_r) + \frac{1}{r}\frac{\partial}{\partial \theta}(\rho u_\theta) + \frac{\partial}{\partial x}(\rho u) = 0 \tag{14}$$

Axial Momentum:

$$\rho\left(\frac{\partial u}{\partial t} + u_r\frac{\partial u}{\partial r} + \frac{u_\theta}{r}\frac{\partial u}{\partial \theta} + u\frac{\partial u}{\partial x}\right) = -\frac{\partial p}{\partial x} + F_x + \mu\left(\frac{\partial^2 u}{\partial r^2} + \frac{1}{r}\frac{\partial u}{\partial r} + \frac{1}{r^2}\frac{\partial^2 u}{\partial \theta^2} + \frac{\partial^2 u}{\partial x^2}\right) + \frac{\mu}{3}\frac{\partial}{\partial x}\left[\frac{1}{r}\frac{\partial}{\partial r}(ru_r) + \frac{1}{r}\frac{\partial u_\theta}{\partial \theta} + \frac{\partial u}{\partial x}\right] \tag{15}$$

where u_r is the velocity in the radial direction, u_θ is the velocity in the circumferential direction, and F_x is the axial body force term.

After applying the above assumptions, the basic differential equations are:

Continuity:

$$\frac{\partial \rho}{\partial t} + \rho\frac{\partial u}{\partial x} + u\frac{\partial \rho}{\partial x} + \rho\frac{\partial u_r}{\partial r} + \rho\frac{u_r}{r} + u_r\frac{\partial \rho}{\partial r} = 0 \tag{16}$$

Equation of Motion: axial direction

$$\rho\left(\frac{\partial u}{\partial t} + u\frac{\partial u}{\partial x}\right) = -\frac{\partial p}{\partial x} + \mu\left[\frac{\partial^2 u}{\partial r^2} + \frac{1}{r}\frac{\partial u}{\partial r} + \frac{1}{3}\frac{\partial}{\partial x}\left(\frac{\partial u_r}{\partial r} + \frac{u_r}{r}\right)\right] \tag{17}$$

Process Relation

Orner (24) gives a process relation

$$\frac{\rho_1}{\rho_o}(r,x,\omega) = \Omega(r,\omega)\frac{p_1}{p_o}(r,x,\omega) \tag{18}$$

where ρ_1 and p_1 are perturbations of density and pressure respectively about the mean quantities ρ_o and p_o, ω is the radian frequency, and $\Omega(r,\omega)$ is a weighting function. For liquids, Ω is a constant,

$$\Omega = p_o/B_m \tag{19}$$

However, for gases, the energy equation must be used to develop an expression for $\Omega(r,\omega)$. This was done by Orner (24) with the following result:

$$\Omega(r,\omega) = 1 + \frac{\left(\frac{c_p}{c_v} - 1\right)}{c_p/c_v}\left[\frac{J_o\left(\frac{r}{R}\sqrt{-jPr\omega/\omega_\nu}\right)}{J_o\left(\sqrt{-jPr\omega/\omega_\nu}\right)} - 1\right] \tag{20}$$

$$\omega_\nu \equiv 8\nu/R^2 \tag{21}$$

where J_o is the Bessel function of order zero. In addition to the assumptions given here, Orner also assumed in his development of Eq (20) an ideal gas, no heat generation due to external sources and that the axial convective heat transfer and viscous dissipation in the energy equation are negligible for the through-flows considered; i.e., Mach numbers 0.3 and less.

Eq (20) is a frequency-dependent process relation. An alternative relation, not frequency-dependent, could be used also. The simplest is the isentropic perfect gas law. Since this is perhaps an oversimplification, both Eq (20) and the isentropic perfect gas law

$$\frac{(\rho)^{c_p/c_v}}{p} = \text{CONSTANT} \tag{22}$$

will be used and results compared.

Reduction to Simplified Forms

Two methods are typically used to reduce Eqs (16), (17) and (18) to forms that can be solved analytically. The first method is the attack taken by Orner (24) where one lets

$$u(r,x,t) = \sum_{n=0}^{\infty} u_n (r,x) \exp (jn\omega t) \tag{23}$$

$$u_r(r,x,t) = \sum_{n=0}^{\infty} u_{r_n}(r,x) \exp (jn\omega t) \tag{24}$$

$$p(r,x,t) = \sum_{n=0}^{\infty} p_n (r,x) \exp (jn\omega t) \tag{25}$$

$$\rho(r,x,t) = \sum_{n=0}^{\infty} \rho_n (r,x) \exp (jn\omega t) \tag{26}$$

Substituting into Eqs (16), (17) and (18), subtracting out the steady state equations (n=0), the first order equations (n=1) are:

$$j\omega\rho_1 + \rho_o \left[\frac{\partial u_{r_1}}{\partial r} + \frac{u_{r_1}}{r}\right] + \rho_o \frac{\partial u_{r_1}}{\partial x} + u_o \frac{\partial \rho_1}{\partial x} = 0 \tag{27}$$

$$j\omega u_1 + u_o \frac{\partial u_1}{\partial x} + u_{r_1} \frac{\partial u_o}{\partial r} + \frac{1}{\rho_o} \frac{\partial p_1}{\partial x} = \nu \left[\frac{\partial^2 u_1}{\partial r^2} + \frac{1}{r} \frac{\partial u_1}{\partial r} + \frac{1}{3} \frac{\partial^2 u_{r_1}}{\partial x \partial r} + \frac{1}{3r} \frac{\partial u_{r_1}}{\partial x}\right] \tag{28}$$

In these equations second and higher harmonics have been neglected, and also

$$u_r = \frac{\partial u_o}{\partial x} = \frac{\partial \rho_o}{\partial x} = \frac{\partial \rho_o}{\partial r} = 0 \tag{29}$$

by assumptions 10 and 11. If one assumes the axial gradient of u_{r_1} is of the order $\frac{\omega L u_{r_1}}{c_o}$, the last two terms in Eq (28) can be ignored.

Note that they vanish when integrated across the cross-section with respect to r from r=0 to r=R; i.e.,

$$\frac{1}{3}\frac{\partial}{\partial x}\int_o^R 2\pi r\left(\frac{\partial u_r}{\partial r}+\frac{u_r}{r}\right)dr = 0 \tag{30}$$

where

$$u_r(o,x) = u_r(R,x) = 0 \tag{31}$$

For the same reason the terms $\frac{\partial u_r}{\partial r}+\frac{u_r}{r}$ in the continuity equation can be neglected also. Assumptions 3, 4 and 11 (negligible radial flow, R<<L and laminar through-flow) allow the term $u_{r_1}\frac{\partial u_o}{\partial r}$ to be neglected also. The resulting equations are

$$j\omega\rho_1 + \rho_o\frac{\partial u_1}{\partial x} + u_o\frac{\partial \rho_1}{\partial x} = 0 \tag{32}$$

$$j\omega u_1 + u_o\frac{\partial u_1}{\partial x} + \frac{1}{\rho_o}\frac{\partial p_1}{\partial x} = \nu\left(\frac{\partial^2 u_1}{\partial r^2}+\frac{1}{r}\frac{\partial u_1}{\partial r}\right) \tag{33}$$

These equations less the through-flow term, $u_o\frac{\partial u_1}{\partial x}$, have been studied by many researchers (7, 22, 23) and are the basis of most fluid transmission line work, including the frequency and transient response of lines. However, the effect of the omitted term, which represents the coupling of the laminar mean flow to the oscillatory flow, has not been adequately studied before. The solution of Eq (32) with the through-flow term included has not been done before and is the end result of this analysis.

At this point it is convenient to nondimensionalize the equations. Let

$$u \equiv \frac{u_1}{c_o} \qquad \rho \equiv \frac{\rho_1}{\rho_o} \qquad p \equiv \frac{p_1}{p_o}$$

$$\eta \equiv \frac{x}{L} \qquad \varepsilon \equiv \frac{r}{R} \tag{34}$$

Then Eqs (32), (33), and (18) become

$$\frac{j\omega u L}{c_o} + \frac{u_o}{c_o}\frac{\partial u}{\partial \eta} = \frac{L\nu}{R^2 c_o}\left[\frac{\partial^2 u}{\partial \varepsilon^2} + \frac{1}{\varepsilon}\frac{\partial u}{\partial \varepsilon}\right] - \frac{1}{k}\frac{dp}{d\eta} \tag{35}$$

$$\frac{j\omega L \rho}{c_o} + \frac{\partial u}{\partial \eta} + \frac{u_o}{c_o}\frac{\partial \rho}{\partial \eta} = 0 \tag{36}$$

$$\rho = \Omega p \tag{37}$$

where $k = c_p/c_v$ for an ideal gas and B_m/p_o for a liquid. Also assumption 11, which states that the pressure is constant across the cross-section, has been invoked and thus the last term in Eq (35) is written appropriately as p is now a function of η only.

The method of perturbations is the second method that can be used to reduce Eqs (16) and (17) to the final forms (35) and (36). In this method one writes

$$\begin{aligned} \rho &= \tilde{\rho} + \underline{\rho} & u &= \tilde{u} + \underline{u} \\ p &= \tilde{p} + \underline{p} & v &= \tilde{v} + \underline{v} \end{aligned} \tag{38}$$

where the underscored variables represent small perturbations about the mean quantity, (~). These can be substituted into Eqs (16) and (17), mean quantities subtracted out, and products of perturbation quantities neglected as they are small. When the same assumptions as applied in the first method are used, the Laplace transform taken, and the continuity equation integrated across the cross-section; the

result is the same as Eqs (35) and (36). Moore (20) developed similar equations in this manner.

Solution

The intent of the analysis is to obtain a relationship between the average velocity and the pressure valid at any point in the line. Eq (35) will be solved subject to the radial boundary conditions

$$u(1,\eta) = \frac{\partial u}{\partial \varepsilon}(o,\eta) = 0 \tag{39}$$

After substituting Eq (37) into Eq (36) to eliminate ρ, the results will be integrated across the tube cross-section to yield a third condition that must be satisfied. First separate variables by letting

$$u(\varepsilon,\eta) \equiv \exp(\gamma\eta)E(\varepsilon) \tag{40}$$

The exp $(\gamma\eta)$ term in Eq (40) is used as one expects to find a solution in terms of the dimensionless propagation constant, γ, whose real part is the attenuation, α, and whose imaginary part is the phase constant, β. Thus, the solution should yield some of the allowable modes of longitudinal wave propagation. The result is

$$\frac{d^2E}{d\varepsilon^2} + \frac{1}{\varepsilon}\frac{dE}{d\varepsilon} + (A\varepsilon^2 + B)E = K_1 \tag{41}$$

$$E(1) = 0$$

$$E'(0) = 0$$

$$K_1 \exp(\gamma\eta) = \frac{c_o}{kL\nu}\frac{dp}{d\eta} \tag{42}$$

where the Hagen-Poiseuille velocity profile has been substituted in for $u_o(\varepsilon)$, i.e.,

$$u_o(\varepsilon) = 2\frac{\bar{u}_o}{c_o}(1-\varepsilon^2) \tag{43}$$

Also

$$A \equiv \frac{2\bar{u}_o R^2}{\nu L} \tag{44}$$

$$B \equiv -A - j\frac{\omega R^2}{\nu} \tag{45}$$

$$\gamma \equiv \text{separation (propagation) constant} \tag{46}$$

$$K_1 = \text{arbitrary constant} \tag{47}$$

The development to this point is the same as Orner's (24). Orner proceeded to solve Eq (41) and gave his result as

$$u(\varepsilon,\eta) = \frac{R^2 c_o}{kL\nu}\frac{dp}{d\eta}\frac{\exp\left[j\frac{\varepsilon^2\sqrt{A}}{2}\right]}{(B+2j\sqrt{A})}\left[1-\frac{M\left(\frac{1}{2}-\frac{B}{4j\sqrt{A}};\ 1;\ j\varepsilon^2\sqrt{A}\right)}{M\left(\frac{1}{2}-\frac{B}{4j\sqrt{A}};\ 1;\ j\sqrt{A}\right)}\right] \tag{48}$$

where M is the confluent hypergeometric function.

He then used Eq (48) and continuity, Eq (36), to attempt to solve numerically for the separation constant, γ. This he was unable to do. The approach seemed sound, however, and the fact that the confluent hypergeometric function appeared lent credence to a solution of this form as the same function has appeared in studies by Womersley (34) on pulsatile blood flow and by Brown, Margolis and Shaw (8) on turbulent flow in fluid transmission lines.

The details of the solution leading to Eq (48) were not given by Orner (24) and substitution of his solution back into the original differential equation does not yield an identity, but rather a contradiction. See Appendix A for the details. It is interesting to note, however, that Orner's solution does meet the boundary conditions and

in the limiting case of zero through-flow does reduce to the well-known Bessel function velocity profile, the result given by Brown (7), Nichols (22), and Oldenburger (23). The facts that there are no published tabulations of the confluent hypergeometric function, that numerical methods of evaluating γ from Eqs (36), (41) and (42) are involved, and of course that Orner's solution is incorrect all contributed to his inability to complete the solution for the problem.

To find a correct solution to Eq (41) it is convenient to transform variables. Let

$$E(\varepsilon) \equiv e^{-D_2\varepsilon^2} W(\varepsilon) \tag{49}$$

$$z = 2D_2\varepsilon^2 \tag{50}$$

$$D_2 = \frac{j\sqrt{A}}{2} \tag{51}$$

Eq (41) then becomes

$$zW''(z) + (1-z)W'(z) - \left(\frac{1}{2} - \frac{B}{8D_2}\right)W(z) = \left(\frac{K_1}{8D_2}\right)e^{z/2} \tag{52}$$

$$W(2D_2) = 0$$

$$W'(0) = 0$$

Also define

$$a \equiv \frac{1}{2} - \frac{B}{8D_2} \tag{53}$$

$$K_2 = \frac{K_1}{8D_2} \tag{54}$$

The final form of the equation to be solved is then

$$zW''(z) + (1-z)W'(z) - aW(z) = K_2 e^{z/2} \tag{55}$$

Assume an infinite series solution of the form

$$W(z) = \sum_{m=0}^{\infty} c_m z^m \tag{56}$$

If a recursion relation for the coefficients, c_m, can be found and if the series converges uniformly, then numerical methods can be used to evaluate the series.

The existence of a convergent series as a solution for a linear second order differential equation with a singular point at the origin is proved by Kaplan (15) for the homogeneous case. For the nonhomogeneous equation, Kaplan states that his results can be extended to cover this special case and gives a reference, Picard (26). As will be shown later, for the particular differential equation in question, a uniformly convergent infinite series can be found as would be expected in the light of Kaplan's remarks.

By substituting this infinite series, Eq (56), in the differential equation and equating coefficients of like powers of z, a recursion relation results. For

$$W(z) = \sum_{m=0}^{\infty} c_m z^m \tag{57}$$

$$W'(z) = \sum_{m=0}^{\infty} m c_m z^{m-1} \tag{58}$$

$$W''(z) = \sum_{m=2}^{\infty} c_m m(m-1) z^{m-2} \tag{59}$$

Substitution yields:

$$z\sum_{m=2}^{\infty} m(m-1)c_m z^{m-2} + (1-z)\sum_{m=1}^{\infty} mc_m z^{m-1} - a\sum_{m=0}^{\infty} c_m z^m = K_2 \sum_{m=0}^{\infty} \frac{z^m}{2^m m!} \quad (60)$$

noting that

$$e^{z/2} = \sum_{m=0}^{\infty} \frac{z^m}{2^m m!} \quad (61)$$

Let $m-1 = K$ so that $m = K+1$ (62)

$$\sum_{1}^{\infty} K(K+1)c_{K-1} z^K + \sum_{0}^{\infty} (K+1)c_{K+1} z^K - \sum_{1}^{\infty} Kc_K z^K - a\sum_{0}^{\infty} c_K z^K - K_2 \sum_{0}^{\infty} \frac{z^K}{2^K K!} = 0 \quad (63)$$

Coefficient of z^K:

$$K(K+1)c_{K+1} + (K+1)c_{K+1} - Kc_K - ac_K - \frac{K_2}{2^K K!} = 0 \quad (64)$$

$$[K(K+1)+K+1]c_{K+1} - (K+a)c_K - \frac{K_2}{2^K K!} = 0 \quad (65)$$

$$(K+1)^2 c_{K+1} = (K+a)c_K + \frac{K_2}{2^K K!} \quad (66)$$

$$c_{K+1} = \frac{K+a}{(K+1)^2} c_K + \frac{K_2}{2^K K!(K+1)^2} \quad (67)$$

This is the desired two-term recursion formula. Note that for $K=0$,

$$c_1 = ac_o + K_2 \quad (68)$$

c_o is arbitrary and will be determined from the boundary condition $E(1)=0$ which transforms to $W(2D_2)=0$.

In order to find a general term, start with the recursion relation which is good for all K.

$$c_{K+1} = c_K \left[\frac{K+a}{(K+1)^2}\right] + \frac{K_2}{2^K K!(K+1)^2} \tag{69}$$

$$c_K = c_{K-1} \left[\frac{K-1+a}{K^2}\right] + \frac{K^2}{2^{K-1}(K-1)!K^2} \tag{70}$$

$$c_{K-1} = c_{K-2} \left[\frac{K-2+a}{(K-1)^2}\right] + \frac{K^2}{2^{K-2}(K-2)!(K-1)^2} \tag{71}$$

$$c_2 = c_1 \left(\frac{a+1}{4}\right) + \frac{K_2}{8} \tag{73}$$

$$c_1 = c_o a + K_2$$

Putting this all together yields,

$$c_{K+1} = \frac{K_2}{2^K K!(K+1)^2} + \left[\frac{K+a}{(K+1)^2}\right]\left[\frac{K_2}{2^{K-1}(K-1)!K^2} + \left(\frac{K-1+a}{K^2}\right)\left[\frac{K_2}{2^{K-2}(K-2)!(K-1)^2}\right.\right.$$

$$\left.\left. + \left[\frac{K-2+a}{(K-1)^2}\right]\left[\cdots\left[\frac{K_2}{8} + \left[\frac{a+1}{4}\right]\left[K_2 + ac_o\right]\right]\cdots\right]\right]\right] \tag{74}$$

This can be written as:

$$c_{K+1} = \sum_{J=1}^{K+1} \frac{K_2 (a+J)_{K+1-J}}{(J)^2_{K+1-(J-1)} (J-1)! 2^{J-1}} \frac{c_o (a)_{K+1}}{[(K+1)!]^2}, \quad K = 1,2,3,\ldots \tag{75}$$

where

$$(a)_K \equiv a(a+1)(a+2)\ldots(a+K-1), \quad (a)_o \equiv 1 \tag{76}$$

The evaluation of c_o follows directly from the boundary condition,

$$W(2D_2) = 0 \tag{77}$$

and noting that

$$M(a,1,z) = \sum_{K=0}^{\infty} \frac{(a)_K z^K}{(K!)^2} \tag{78}$$

The result is:

$$c_o = \frac{-1}{M(a,1,2D_2)} \sum_{K=1}^{\infty} \left\{ \sum_{J=1}^{K} K_2 \left[\frac{(a+J)_{K-J}}{(J)^2_{K+1-J}(J-1)!2^{J-1}} \right] (2D_2)^K \right\} \tag{79}$$

Thus

$$W(z) = K_2 \sum_{K=1}^{\infty} \left\{ \sum_{J=1}^{K} \left[\frac{(a+J)_{K-J}}{(J)^2_{K+1-J}(J-1)!2^{J-1}} \right] \left[z^K - (2D_2)^K \left(\frac{M(a,1,z)}{M(a,1,2D_2)} \right) \right] \right\} \tag{80}$$

Reversing the transforms and incorporating the other half of the separated equation, the final result is:

$$u(\varepsilon,\eta) = \frac{R^2 c_o}{kL\nu} \frac{dp}{d\eta} \frac{1}{8D_2} e^{-D_2\varepsilon^2} \sum_{K=1}^{\infty} \left\{ \sum_{J=1}^{K} \left[\frac{(a+J)_{K-J}}{(J)^2_{K+1-J}(J-1)!2^{J-1}} \right] \left[(2D_2)^K \left(\varepsilon^{2K} - \frac{M(a,1,2D_2\varepsilon^2)}{M(a,1,2D_2)} \right) \right] \right\} \tag{81}$$

One may ask if this solution meets the second boundary condition; namely,

$$\frac{\partial u(o,\eta)}{\partial \varepsilon} = 0$$

$$\frac{\partial u}{\partial \varepsilon} = \frac{R^2 c_o}{k L \nu} \frac{dp}{d\eta} \frac{1}{8D_2} \left(-2D_2 \varepsilon e^{-D_2 \varepsilon^2}\right) \sum_{K=1}^{\infty} \left\{ \sum_{J=1}^{K} \left[\frac{(a+J)_{K-J}}{(J)^2_{K+1-J} (J-1)! 2^{J-1}} \right] \right.$$

$$\left. \otimes \left[(2D_2)^K \left(\varepsilon^{2K} - \frac{M(a,1,2D_2\varepsilon^2)}{M(a,1,2D_2)} \right) \right] \right\} + \frac{R^2 c_o}{KL\nu} \frac{dp}{d\eta} \frac{1}{8D_2} e^{-D_2\varepsilon^2}$$

$$\otimes \sum_{K=1}^{\infty} \left\{ \sum_{J=1}^{K} \left[\frac{(a+J)_{K-J}}{(J)^2_{K+1-J} (J-1)! 2^{J-1}} \right] \right] \left[(2D_2)^K \left(2K\varepsilon^{2K-1} \right.\right.$$

$$\left.\left. - \frac{4D_2\varepsilon}{M(a,1,2D_2)} \frac{dM(a,1,2D_2\varepsilon^2)}{d(2D_2\varepsilon^2)} \right) \right] \right\} \tag{82}$$

From the Handbook of Mathematical Functions (13),

$$\frac{dM}{dz}(a,b,z) = \frac{a}{b} M(a+1,b+1,z) \tag{83}$$

Thus,

$$\frac{dM(a,1,2D_2\varepsilon^2)}{d(2D_2\varepsilon^2)} = aM(a+1,2,2D_2\varepsilon^2) \tag{84}$$

Now evaluating Eq (82) at ε=0, all terms drop out as they are multiplied by ε. Also, M(a+1, 2, 0) is finite; in fact,

$$M(a,1,0) = M(a+1,2,0) = 1 \tag{85}$$

as can be seen from the series representation

$$M(a,b,z) = \sum_{n=0}^{\infty} \frac{(a)_n z^n}{(b)_n n!}, \quad b \neq 0 \tag{86}$$

Thus the boundary condition $\frac{\partial u(o,\eta)}{\partial \epsilon} = 0$ is met.

The proof showing uniform convergence of the series given by Eq (56) is in Appendix B. Also a demonstration that the solution (81) is indeed a solution of the differential equation is given in Appendix C. Appendix D shows that the solution as given in Eq (81) does reduce to the well-known Bessel function velocity profile equation in the limiting case of zero through-flow.

Evaluation of the Separation Constant, Υ

Using Orner's approach to evaluate the separation constant, Υ, it is necessary to put the solution, Eq (81), and the continuity equation, Eq (36), into a form suitable for numerical methods. First the solution must be integrated across the tube cross-section which is easily done if the confluent hypergeometric function is written in its series representation. Due to its uniform convergence property, term-by-term integration is then possible. The result is

$$\bar{u}(\eta) = \frac{R^2 c_o}{kL\nu} \frac{dp}{d\eta} \frac{e^{-D_2}}{8D_2} \sum_{K=1}^{\infty} c_K \sum_{J=0}^{\infty} \frac{(D_2)^J}{(K+1)_{J+1}}$$

$$- \sum_{n=0}^{\infty} \frac{(a)_n (2D_2)^n}{(n!)^2 M(a,1,2D_2)} \sum_{J=0}^{\infty} \frac{(D_2)^J}{(n+1)_{J+1}} \qquad (87)$$

where

$$c_K \equiv (2D_2)^K \sum_{J=1}^{K} \frac{(a+J)_{K-J}}{(J)^2_{K+1-J} (J-1)! 2^{J-1}} \qquad (88)$$

Let

$$F(\gamma) \equiv \frac{R^2 c_o e^{-D_2}}{kL\nu\ 8D_2} \sum_{K=1}^{\infty} c_K \sum_{J=0}^{\infty} \frac{(D_2)^J}{(K+1)_{J+1}}$$

$$- \sum_{n=0}^{\infty} \frac{(a)_n (2D_2)^n}{(n!)^2 M(a,1,2D_2)} \sum_{J=0}^{\infty} \frac{(D_2)^J}{(n+1)_{J+1}} \qquad (89)$$

Thus

$$\bar{u}(\eta) = F(\gamma) \frac{dp}{d\eta} \qquad (90)$$

Using Eq (40),

$$\frac{d\bar{u}}{d\eta} = \gamma \bar{u} \qquad (91)$$

Substituting the process relation, Eq (37), into the continuity equation, Eq (36), and integrating across the tube cross-section yields

$$\frac{j\omega L \bar{\Omega} p}{c_o} + \frac{d}{d\eta}\left(\frac{\overline{u_o \Omega} p}{c_o}\right) = -\frac{d\bar{u}}{d\eta} \qquad (92)$$

where by assumption 11

$$p = \bar{p}(\eta) \qquad (93)$$

Substituting Eq (92) into Eq (91) gives

$$\frac{dp}{d\eta} = \frac{j\omega L \bar{\Omega} + \frac{d}{d\eta}\left(\frac{\overline{u_o \Omega}}{c_o}\right)}{\frac{\overline{u_o \Omega}}{c_o} + \gamma F(\gamma)} p \qquad (94)$$

The term

$$\frac{d}{d\eta}\left(\frac{\overline{u_o \Omega}}{c_o}\right)$$

can be neglected as u_o, Ω, and c_o are assumed not to be functions of η. This is a good assumption as long as the mean flow axial dissipation and convection is small compared to that in the radial direction. This is compatible with assumption 10 (incompressible mean flow) and assumption 12 (small axial dissipation). From Eq (42) it is seen that

$$\frac{dp}{d\eta} = \gamma p \tag{95}$$

Substituting Eq (95) into Eq (94) yields the final form of the continuity equation, the form suitable for numerical evaluation.

$$G(\gamma) = \gamma^2 F(\gamma) \pm c_2\gamma + c_3 = 0 \tag{96}$$

$$c_2 = \frac{\overline{u_o\Omega}}{c_o} \tag{97}$$

$$c_3 = \frac{j\omega L\overline{\Omega}}{c_o} \tag{98}$$

This equation must be solved for right traveling waves that move in the direction of the mean flow and for left traveling waves that move against the mean flow. Thus Eq (96) has a plus or minus sign in front of the $c_2\gamma$ term, corresponding to positive and negative values of the mean flow.

As Eq (96) is a nonlinear equation with complex-valued coefficients and functions, care had to be taken to find an appropriate numerical method. Several were attempted including Newton's method (9) and Muller's method with deflation (9). Muller's method was contained in the International Mathematical and Statistical Libraries

which were available for use on the Control Data Corporation (CDC) Cyber 74 computer that was used for the computing. Neither method gave satisfactory results and Ward's method (9) was tried next. This, programmed in double precision (29 significant digits), worked well. It does not employ derivatives but rather minimizes the sum of the absolute values of the real and imaginary parts of the function $G(\gamma)$. Starting with an initial guess for γ, $G(\gamma)$ is calculated and set as the reference value. Then, the routine iterates by stepping, both plus and minus, the real and imaginary parts of γ. At each step a new value of $G(\gamma)$ is calculated and compared with the reference value of $G(\gamma)$. If the sum of the absolute values of the real and imaginary parts of the new $G(\gamma)$ are smaller than that of the reference value, the reference value is replaced by the new $G(\gamma)$. The value of γ yielding this smaller value is then taken as the starting point for the next iteration. Should no point yield a decrease, the step size is then halved and the iteration continued. The iteration is terminated when either a criterion on the minimum step size is satisfied (typically 1×10^{-16} was used) or when the sum of the absolute values of the real and imaginary parts of $G(\gamma)$ reaches a suitably small number (typically 1×10^{-16} was used). Critical to this method is the initial guess as a bad guess will greatly increase the computer time required. A suitable initial guess is the value of the propagation constant calculated for zero through-flow which is derived from the Bessel function velocity solution and is given by Kirshner and Katz (18) as

$$\gamma = \frac{j\omega}{c_o} \left\{ \left[1 + \frac{2\left(\frac{c_p}{c_v} - 1\right) J_1\left(j^{3/2}\sqrt{Pr}\, F_w\right)}{j^{3/2}\sqrt{Pr}\, F_w J_o\left(j^{3/2}\sqrt{Pr}\, F_w\right)} \right] \Bigg/ \left[1 - \frac{2J_1\left(j^{3/2}F_w\right)}{j^{3/2}F_w J_o\left(j^{3/2}F_w\right)} \right] \right\}^{1/2} \tag{99}$$

where

$$F_w = \left(\frac{8\omega}{\omega_\nu}\right)^{1/2} \tag{100}$$

$$\omega_\nu = \frac{8\nu}{R^2} \quad \text{for circular lines} \tag{101}$$

This value of γ was then adjusted for the effect of through-flow by multiplying it by $\frac{c_o}{c_o+\bar{u}_o}$ for the right running wave and $\frac{c_o}{c_o-\bar{u}_o}$ for the left running wave.

To evaluate $G(\gamma)$, it was also necessary to evaluate the confluent hypergeometric function for complex parameters. This proved difficult because, though the series eventually converged in the regions of interest, a large amount of destructive cancellation occurred. Typically there were terms of the order 10^{19} and the resulting sum was order 10^{9}. For high frequency, low frequency, and large through-flow calculations, the destructive cancellation became much worse. These cases were not of interest though and in fact violated assumptions 3, 4 and 7 used in the analysis. Due to this destructive cancellation, double precision arithmetic had to be used on all calculations. Typically over 100 terms in the series had to be taken until the convergence criterion was met. The same problem occurred in the evaluation of the infinite series for $F(\gamma)$. As a result, considerable computer time was required to evaluate γ. Typically 400 seconds of execution time were required on the CDC Cyber 74 to calculate γ for the left and right running waves in hydraulic fluid and 250 seconds for air. The required computer time is increased when the frequency, radius or mean flow is increased and when the kinematic viscosity is decreased.

Line Model

Once numerical values for the propagation constant have been determined, it is necessary to develop a model of a transmission line that uses these calculated values to determine other results of interest such as pressure, velocity and characteristic impedance. The model consists of superposing the forward traveling wave and the reflected wave subject to two boundary conditions. The first boundary condition is the pressure at some point, η_o, in the line. The phase of the pressure at η_o is taken as zero and serves as a reference for all other phase angle calculations. This is convenient as the experimental data which is used for this boundary condition consists of pressure magnitude data only.

The second boundary condition is that the velocity at the end of the line is the through-flow velocity only, i.e., the perturbation velocity is zero. For zero mean flow, there is no flow whatsoever through the closed valve at the end of the line. For small through-flows, the perturbation velocity is still taken to be zero. This follows since, at the low flow rates (0 to 9.5 gpm) used in the experiments, the area ratio of the annular opening in the needle valve to the line cross-sectional area is much less than one. This causes the valve gain and the load impedance to be very large. For instance, at 2.5 gpm, the valve gain was 2360 psi/gpm.

Zero perturbation velocity does not imply a simple reflection of the pressure wave at the valve. This is due to differing pressure-velocity relationships for the forward and reflected waves. In particular, the phase difference between the velocity and pressure for

the forward wave is not the same as that for the reflected wave and this must be accounted for. This can be done by using Eqs (40), (90), (95) and (96). First one writes the pressure at the end of the line by superposing the two waves:

$$p(1) = P_1(1) + P_2(1) \tag{102}$$

where P_1 is the pressure due to the forward wave and P_2 is the pressure due to the reflected wave. Then note that

$$u(\eta) = \gamma F(\gamma) p(\eta) \tag{103}$$

in particular

$$u_2(1) = \gamma_2 F(\gamma_2) P_2(1) \tag{104}$$

Using this and applying Eqs (40) and (95), the result is

$$p(\eta) = C_4 e^{\gamma_1 \eta + (1-\eta)(\beta_1+\beta_2)j} + C_4 \left[\frac{\gamma_1 F(\gamma_1)}{\gamma_2 F(\gamma_2)}\right] e^{\gamma_1 + (1-\eta)(\alpha_2-\beta_2 j)} \tag{105}$$

where

$$C_4 = \frac{p(\eta_0)}{e^{\gamma_1 \eta_0 + (1-\eta_0)(\beta_1+\beta_2)j} + \left[\frac{\gamma_1 F(\gamma_1)}{\gamma_2 F(\gamma_2)}\right] e^{\gamma_1 + (1-\eta_0)(\alpha_2-\beta_2 j)}} \tag{106}$$

The term

$$\frac{\gamma_1 F(\gamma_1)}{\gamma_2 F(\gamma_2)}$$

accounts for the phase difference in pressure between the forward wave and the reflected wave at the end of the line. Also the term

$$e^{(1-\eta)(\beta_1+\beta_2)j}$$

accounts for the lag between the reflected wave and the forward wave, i.e., it is a measure of how far the reflected wave is ahead of the forward wave. Using Eq (105), the pressure gradient is found to be

$$\frac{dp}{d\eta} = C_4(\gamma_1-\beta_1 j-\beta_2 j)\ e^{\gamma_1\eta+(1-\eta)(\beta_1+\beta_2)j}$$

$$+ C_4(-\alpha_2+\beta_2 j)\left[\frac{\gamma_1 F(\gamma_1)}{\gamma_2 F(\gamma_2)}\right] e^{\gamma_1+(1-\eta)(\alpha_2-\beta_2 j)} \qquad (107)$$

This model superposes only two waves when there are actually an infinite number of waves passing a given point at a given time. This is due to the reflection of the left-running reflected wave from the pump. Until the wave is completely attenuated, it will continue reflecting up and down the line. Thus a limitation of this model is that there can be no significant reflection from the pump. This can happen two ways. First, the wave could attenuate to such a degree that by the time it reaches the pump, its amplitude would be negligible. The second way is that the wave does not reflect from the pump to any appreciable degree. The actual line length used in the experiments was not long enough for the wave to attenuate significantly; however, the reflection from the pump was negligible. This was verified experimentally using the testing procedure described in Chapter III.

Using this model and the calculated values of the propagation constant at a given frequency, the pressure standing wave, the average

velocity and velocity profile at any point in the line, and the characteristic impedance were calculated. These additional calculations took about 60 additional seconds of computer time with the velocity profile calculations accounting for most of the additional time.

When the transmission line is not terminated by a valve, but rather is open, a different model is required as the boundary condition at the end of the line is not that the perturbation velocity is zero, but that the perturbation pressure is zero, i.e.,

$$p(1) = P_1(1) + P_2(1) = 0 \tag{108}$$

The resulting pressure relations are the same as Eqs (105) and (106) with the exception that the term

$$\frac{\gamma_1 F(\gamma_1)}{\gamma_2 F(\gamma_2)}$$

is replaced by minus one.

For calculations of the characteristic impedance, a matched line must be used. This means that there is no reflection from the end of the line. In this case

$$\frac{\gamma_1 F(\gamma_1)}{\gamma_2 F(\gamma_2)}$$

is replaced by zero in Eqs (105) and (106).

The results calculated using this analysis and line model are only as good as the boundary condition, $p(\eta_o)$. This boundary condition must be accurate. If the point at which the boundary condition is taken is near a pressure node, great care must be exercised. Considering the small dynamic pressures near a pressure node, an error

of one or two psi may be equivalent to a large error percentage-wise and analytical results using this erroneous boundary condition will be unreliable at best. Data for the boundary condition ideally should come from a point near an antinode or a point where the dynamic pressure is known as accurately as possible.

Using the theory developed in this chapter, analytical results for hydraulic lines and air lines were calculated and these are given in Chapters VIII and X respectively.

III. Experimental Equipment

Test System

A schematic diagram of the hydraulic system designed for this study is shown in Fig. 2. A fifteen horsepower motor was used to drive an Abex nine cylinder piston hydraulic pump. Connected to this pump, through a pump manifold and bulkhead fitting, was a 0.625 in. OD stainless steel line. Several "T" fittings were installed in the line to allow mounting of resonators, filters, Statham transducers and a U-shaped section of tubing. Terminating the line was a pressure relief valve set for 3750 psig. Tests with flow were conducted by adding three inches of 0.625 in. OD stainless steel tubing which joined the pressure relief valve to a manually operated needle valve.

This needle valve was connected to 0.5 in. OD copper line leading to a 2.43 gal. reservoir. The outlet of the pressure relief valve was also connected to this copper line. Reservoir pressure was maintained at 20 psig via compressed nitrogen gas from a high pressure tank with a pressure regulator. A second line, the pump case drain, was also connected to the reservoir. At the inlet to the reservoir, two filters (one for the pump case drain line and one for the return line from the needle valve) were installed to remove any particles in the hydraulic fluid as well as to warn of pump deterioration. The hydraulic fluid on the return or suction side of system was routed through two heat exchangers where the oil was cooled by cold tap water.

To reduce system vibrations, the line was braced in seven locations. Five of the braces were constructed from 2 in. x 4 in. wood

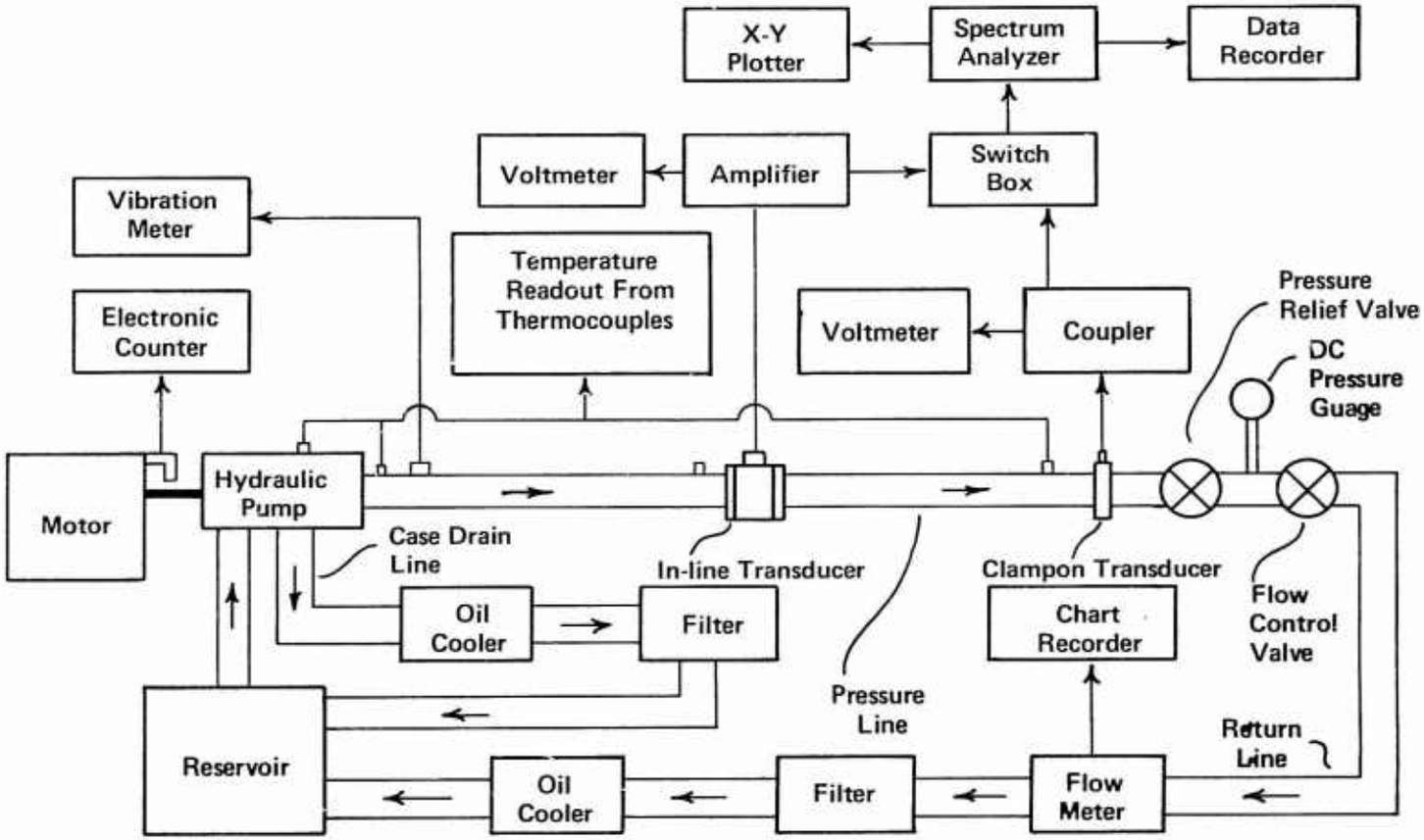

Figure 2. Schematic Diagram of Hydraulic System and Instrumentation

studs and the other two braces were made with steel frames. The wooden braces were placed under the line, the line taped to the brace and at least two shot bags placed over the line. The line was taped to the side of one steel frame and clamped via an adele clamp to the other steel frame. The hydraulic pump was rigidly attached to the motor which was bolted firmly to a large iron platform.

The fluid used in this study was MIL-H-5606B hydraulic fluid. This fluid was chosen as it is the hydraulic fluid used in most United States Air Force aircraft. The fluid properties of MIL-H-5606B are well-known and have been documented in the Society of Automotive Engineers Aerospace Information Report 1362 (30). The only disadvantage in using MIL-H-5606B was that this hydraulic fluid is slightly non-Newtonian.

System Setup

1. Configuration One had a resonator at the output port of the pump followed by a U-shaped section of line. The purpose of the bend was to simulate actual aircraft hydraulic system designs which require several bends in the line to route hydraulic fluid from the pump on the engine to a hydraulic actuator some distance away. The resonator was at the upstream end of the U-shaped bend and a "T" fitting was at the other end. These formed ninety degree bends while the other two bends, formed by physically bending the line, were 93.5 deg and 97.5 deg with radii of curvature of 2.75 in. and 4.94 in. respectively. The length of the U-shaped section was 39.5 in. and the total line length was 208.09 in. The resonator, with an internal volume of 19 $in.^3$, was used to reduce the amplitude of the pressure ripple.

2. Configuration Two was similar to Configuration One. Beyond the first 90 deg bend, the setup was the same as Configuration One. The resonator was replaced by a filter cavity with a volume of 15.9 $in.^3$ which is 17% less than the resonator volume. Thus the effect of a smaller volume, and the resulting larger pressure ripple, could be measured.

3. Configuration Three was again similar to Configuration One and indeed identical past the first 90 deg bend. In this configuration, there was no volume element. Data taken with the system in the first three configurations can be compared to determine the effect of a volume element on frequency response and reduction of pump ripple.

4. Configuration Three/Modification One was the line as described under Configuration Three with a manually-operated needle valve at the end of the line. This valve allowed metered flow in the line. Tests conducted in Configuration One, Two, and Three were all no-flow, blocked line experiments.

5. Configuration Four consisted of moving the U-shaped section of line from the output port of the pump to a point near the end of the line. With the bends far from the pump and the associated large mechanical vibrations generated by the pump and the motor, a better study of the effect of the bends could be conducted. The flow control valve was in this setup and tests were run with flow varying from 0 to 9.5 gpm. The total line length was 209.75 in.

6. Configuration Four/Modification One consisted of the addition of a brace under the bend of the U-shaped section. Otherwise, this configuration was the same as Configuration Four. This brace was needed to reduce vibrations in the U-shaped section.

7. Configuration Four/Modification Two was the same as Configuration Four/Modification One except that fittings for two Statham transducers had been put in the U-shaped section. These Statham transducers, which measure the pressure directly, were not affected by vibrations as were the clampon transducers. Thus accurate pressure measurements could be made in the region of the bends and the effect of the bends better studied.

8. Configuration Five consisted simply of a straight line from the pump to the flow control valve. Data taken in this configuration were used to compare with data from Configuration Four to determine how bends affect a system. Also these data were used to verify analytical results. The total line length, components (pump, valves, etc.) and the instrumentation were the same in each case. Figure 3 depicts all the configurations.

Component Description

A detailed model of each component in the pressure side of the system, i.e., from the hydraulic pump to the flow control valve, was essential if good system response prediction from the HSFR program was desired.

1. Hydraulic Pump. A nine cylinder, piston hydraulic pump (model AP10V-2) made by the Aerospace Division of the Abex Corporation was used. It was a constant pressure, variable displacement pump with a rated volumetric flow rate of 25 gpm and a rated steady state pressure of 3000 psig. Pressure was controlled by a pressure compensator which sensed the pressure at the output port of the pump and adjusted the swash plate angle as required to maintain 3000 $\pm$ 10 psig.

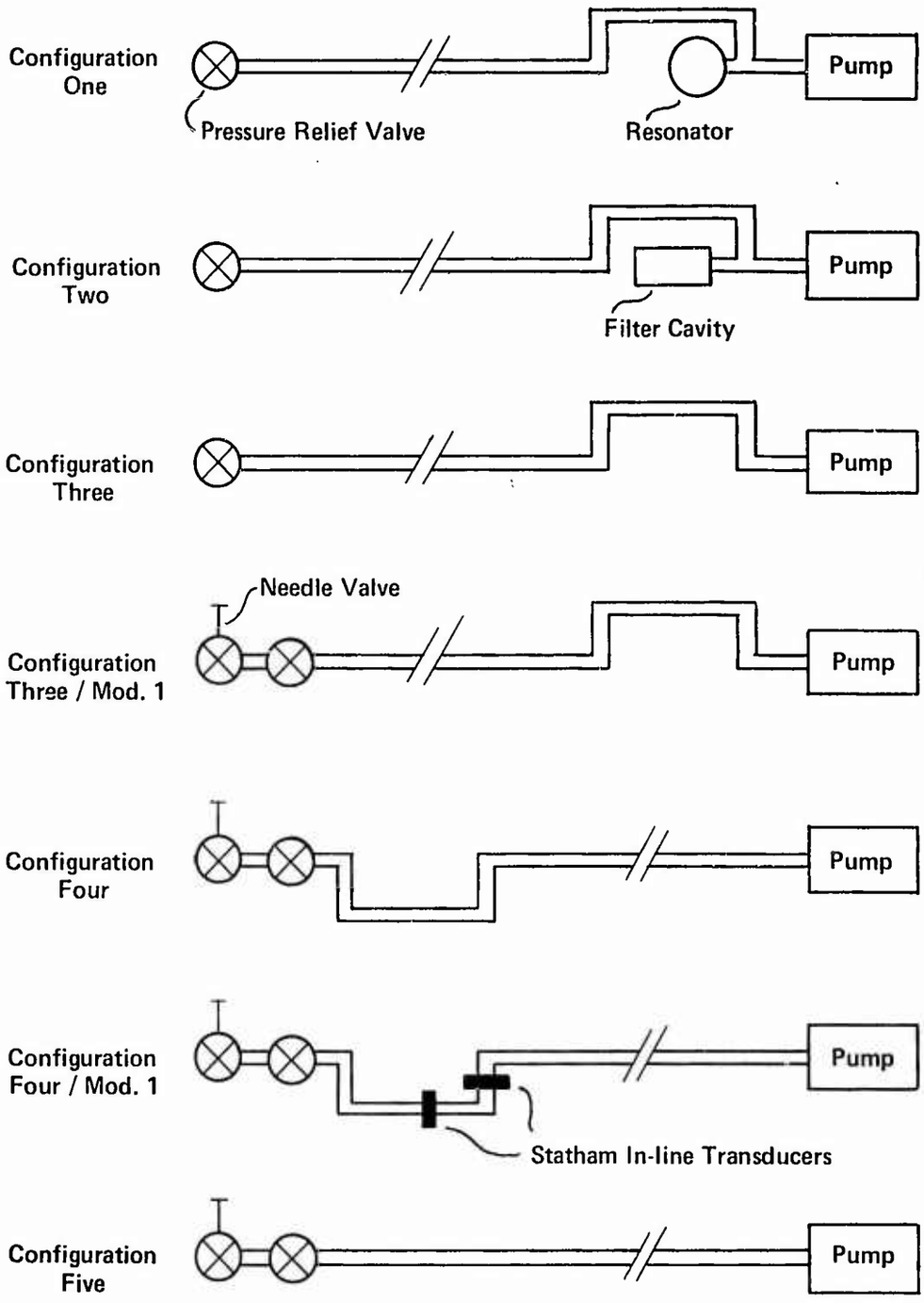

Figure 3. Line Configurations

This pump was chosen as it is in wide use on Air Force aircraft, such as the F-4, and because it was the pump used by McDonnell Douglas Corporation in their tests (3). Thus the results of this study can be compared with those of McDonnell Douglas. A detailed description of the pump components and the pump characteristics is given in (2).

2. Motor. The hydraulic pump was driven by a 15 HP, variable drive motor manufactured by US Motors. It had a speed range of 1100 to 5500 rpm. No tests were run above 4800 rpm as both the vibration level and the pump temperature became excessively high. Temperatures in excess of 225^{o}F result in the decomposition of the hydraulic fluid and thus no data were taken when the temperature exceeded 200^{o}F.

3. Hydraulic Line. The hydraulic line was standard MIL 5845304 seamless, stainless steel tubing with an outside diameter of 5/8 in. and a wall thickness of 0.065 in. This line was used on the pressure side of the system. On the suction or return side of the system, copper tubing was used. It had an outside diameter of 1/2 in. and a wall thickness of 0.030 in. The stainless steel line was the same as is used on United States Air Force aircraft and was the same as McDonnell Douglas used.

4. Oil Coolers. Two tube-type heat exchangers were used to cool the hydraulic fluid. Cold tap water served as the cooling fluid. The smaller heat exchanger was used to cool hydraulic fluid from the pump case drain and the larger heat exchanger was installed in the return line to cool the hydraulic fluid before it reached the reservoir. Preheating the system was expedited by leaving the cold tap water off until the system reached a desired operating temperature.

5. Filters. Two filters were installed to remove contamination from the hydraulic fluid and thus prevent pump deterioration and failure. One filter, a case drain filter made by the Bendix-Skinner Division of Bendix Aviation Corporation, was mounted between the heat exchanger and the reservoir. The second filter, a Pall non-bypass filter, was mounted in the return line just prior to the heat exchanger. This filter had a special pop-up button that, when exposed, indicated the filter was contaminated.

6. Reservoir. The reservoir used was designed and fabricated by technicians from the Air Force Aero Propulsion Laboratory. It was made of stainless steel and had a capacity of 2.43 gal. In normal operation, 2.75 gal. of hydraulic fluid were used to fill the lines and reservoir to normal operating level.

7. Nitrogen Bottle and Pressure Regulator. A 2100 psig nitrogen bottle with a pressure regulator made by Harris Colorific Company was used to maintain return system and reservoir pressure at 20 psig. The nitrogen was fed in at the top of the reservoir.

8. Resonator. An F-4 aircraft resonator was used to reduce pump ripple. The resonator, with a volume of 19 $in.^3$, was installed at the pump outlet and significantly decreased the amplitude of the pump ripple.

9. Valves. An 1/8 in. Walworth needle valve was used to supply hydraulic fluid under line pressure to a pressure gauge at the end of the line. During test runs, this valve was closed and only opened momentarily to check line pressure. A 1/2 in. Crane needle valve was used as the flow control valve. This valve was manually operated to obtain desired flow rates. To protect against large overpressures, a

Denison pressure relief valve was used at the end of the line. The cracking pressure was set at 3750 psig.

10. Bracing. Due to significant vibration generated by pump ripple and the motor, the system had to be braced. The intent was not to rigidly secure the line and thus eliminate all vibrations. This would be desirable from the standpoint of avoiding vibration errors in the clampon pressure transducer data and thus allow better comparison with analytical results. However, to better simulate actual aircraft hydraulic systems, the system was braced in seven places down the 209.75 in. line as well as at the beginning and end of the line. This setup also made possible the vibration tests that were run to determine the effect of pump and motor generated vibrations as well as vibrations generated by pump ripple. Five of the braces were made of wooden two-by-fours nailed together in the shape of a "T". The line was taped to the top board and shot bags placed over the line. The other two braces were made of steel. The line was taped to one brace and clamped via an adele clamp to the other.

Instrumentation

The primary intent of the experiments was to measure the amplitude of the pump ripple or AC line pressure as well as the amplitude of the vibration. Several tests were also run to determine parameters required for the analytical model of the system as well as to check out the primary instrumentation. The following instrumentation was used during the tests.

1. Pressure Transducers. Two Kistler piezoelectric clampon transducers and two Statham, strain gauge type, in-line transducers were used to measure AC pressure amplitude. The Kistler clampon

transducer was especially useful for the tests in that it could be moved easily and did not disturb the flow. The clampon transducer fitted into a specially made mount that was manufactured by AMSA Hydrodynamics. This mount was secured to the line and the transducer torqued down, all in accordance with manufacturer's installation procedures. The piezoelectric transducer then sensed the expansion and contraction of the tube wall caused by the AC pressure. Since the piezoelectric head touched the outside of the hydraulic line, no holes needed to be drilled in the line and no flow disturbance was generated. Unfortunately, the transducer sensed any movement of the tube wall relative to the transducer head, including vibration generated movement. Several tests were run to show the effect of vibration on the clampon transducer. Fortunately, the Statham in-line transducer was not sensitive to vibration. It was flush mounted on the inside of the hydraulic line. Thus the sensing head was in direct contact with the fluid and measured the AC pressure amplitude directly. Special "T" fittings were designed to hold the Statham transducers and allow them to be mounted anywhere a "T" fitting could go. There were only four places in the line a "T" fitting could go without cutting the line and adding even more disturbance to the flow. Each time the in-line transducer was moved, the system had to be depressurized and replumbed, a time-consuming and messy project due to the spillage of hydraulic fluid. This was why the majority of the tests used the clampon transducers, with the in-line transducer always at the same location. Tests were run in the absence of vibration which showed good agreement between the clampon and in-line transducers.

2. Coupler. The Kistler piezoelectric clampon transducer was connected to a Kistler 587D Piezotron Coupler which furnished current-limited DC power to the internal impedance converter in the clampon transducer.

3. Amplifier. A Bell and Howell Model 8-114 amplifier was used to amplify the output of the Statham in-line transducer.

4. Wave Analyzer. In the early tests a Hewlett Packard Model 302A wave analyzer was used to measure the amplitude of the signal from either of the pressure transducers at any desired frequency. The wave analyzer was basically a tunable voltmeter. It had a voltage accuracy of 5% of full scale and a frequency dial accuracy of $\pm$ (1% + 5 cps). When tuned to the pump speed, the wave analyzer gave the rms amplitude of the AC pressure signal at the frequency of the pump. Typically, the pressure signal oscillated slightly, especially near resonant speeds. This, combined with the error associated with the required manual tuning, resulted in unneeded error. To overcome this problem, a spectrum analyzer was used.

5. Spectrum Analyzer. To measure more accurately the pressure oscillation, a Nicolet Scientific Corporation 444A Mini-Ubiquitous FFT Computing Spectrum Analyzer was used. The advantage of this instrument was that it sampled the signal a preset number of times (16 samples were used for most tests), performed a fast Fourier transform, averaged the results and displayed them on a cathode ray tube display. The display plotted rms signal amplitude versus frequency. The frequency range displayed was set to include the pump speed and several harmonics thereof. The pressure amplitude at any frequency was obtained by running a cursor to the desired frequency. The rms

amplitude was displayed on the screen to three significant figures. The spectrum analyzer had a frequency accuracy of 0.01% of full scale and amplitude linearity of $\pm$ 0.05% of full scale. The spectrum analyzer also had a storage capability and dual display option which allowed a stored signal to be compared with the incoming signal. The excellent capabilities of this spectrum analyzer allowed immediate in depth analysis of the signal. For example, with a proper frequency scale selection, the fundamental resonance and higher harmonics can be seen and accurately measured. A further advantage of the spectrum analyzer was that it came with a data recorder.

6. Data Recorder. A Nicolet Scientific Corporation 144A data recorder with a 144A-1 data recorder cartridge was used to record any desired display on the spectrum analyzer. The advantage gained with this instrument was that data taken during a test could be recorded and then analyzed later at the convenience of the researcher. Also the recorded data could be displayed on the spectrum analyzer and then plotted on an X-Y plotter automatically.

7. X-Y Plotter. A Hewlett-Packard Model 7046A X-Y plotter was used to obtain hard copy plots of the displays from the spectrum analyzer that were recorded. Only the line depicting the frequency response and none of the annotaton or scale markings could be graphed automatically. Complete depictions of spectrum analyzer displays were possible using a Nicolet Scientific Corporation Model 131B X-Y plotter.

8. Voltmeters. A Cubic Corporation Model V-70 Digital Voltmeter was used to calibrate the clampon pressure transducer. The output of the clampon transducer was fed through the piezotron coupler into the voltmeter to determine the transducer output associated with

a known change in DC line pressure. Also a Weston Model 1294 DC digital readout voltmeter was used to measure the DC signal from the in-line transducer. This was used primarily to check the reservoir pressure before the pump was started and to check the DC line pressure during data runs.

9. Pressure Gauge. A second way of measuring the DC line pressure was with an Ashcroft pressure gauge which was installed at the end of the line. A needle valve was also installed so that the pressure gauge could be isolated from the hydraulic line when not in use.

10. Magnetic Pickup. An Electro 3010 magnetic pickup was mounted on the drive shaft of the motor opposite the gear teeth.

11. Counter. The output of the magnetic pickup was connected to a Hewlett-Packard Model 522B electronic counter. The counter displays rpm which had to be converted to cycles per second taking into account that the hydraulic pump was a nine cylinder pump. This meant that for every revolution of the drive shaft, nine compression cycles were generated.

12. Flowmeter. A Potter Model 1/2"-1 flowmeter was installed in the return line to measure the flow rate. Flow rates up to 10 gpm could be measured to within 0.1 gpm. The output of the flowmeter was connected to a chart recorder.

13. Chart Recorder. A Minneapolis Honeywell/Brown Electronix Division chart recorder Model SY153X was used to record the output of the flowmeter. For each pressure reading taken, the chart was annotated with the pump speed.

14. Thermocouples, Switchbox and Readout. Five iron-constantine thermocouples were used to measure line temperature. One was mounted on the hydraulic pump, three spaced down the hydraulic line and the fifth was movable and also used to measure room temperature. All thermocouples were connected to a 24-position switch box which provided selective readout on a drum-type temperature readout instrument.

15. Strobatac. A General Radio Company Type 1531-A Strobatac was used to determine the approximate line vibration frequency and to determine at what points along the line vibration was most severe. The strobatac was used to determine the frequency of the vibration and an approximate value for the amplitude of the vibration. More exact measurements of the vibration amplitude were required however.

16. Vibration Pickup. For more exact vibration measurements, a Bell and Howell Model 09394 Transducer-Vibration-Velocity Pickup was employed. The pickup was rigidly secured to an aluminum mount which could be bolted onto the hydraulic line at any desired location and orientation. This allowed vibration measurements at every point where clampon transducer data were taken with the sensitive axis of the vibration pickup in two orientations, vertical and horizontal.

17. Vibration Meter. The output of the vibration pickup was connected to a Dubrow Development Company Model 381 Vibration Meter. This meter had three high-pass filters: 30, 70 and 110 Hz. The use of one of these allowed low frequency mechanical vibration to be filtered out of the signal, leaving the high frequency vibration of interest. Of course, the signal could be left unfiltered, allowing measurement of the low frequency vibration also. The electronics by

which the vibration meter provided a signal to an external jack distorted the amplitude of the signal. This prevented measurements of the vibration amplitude on the spectrum analyzer; however, frequency measurements were accurate. Vibration amplitude had to be manually read on the face of the vibration meter.

18. Camera. A Tektronix C-11 Oscilloscope Camera, which used a Polaroid camera, was used to photograph displays on the scope of the spectrum analyzer. To obtain good pictures, the camera mount had to be physically held next to the scope with drapes placed around the lens to prevent stray light from entering.

Instrument Calibration

All instruments except the Kistler clampon transducer were calibrated by technicians from the Instrument Shop of the Air Force Aero Propulsion Laboratory. The Kistler clampon transducer had to be calibrated prior to each data run. After the transducer was secured to the line at the desired location with the bolts torqued to 2-4 ft-lbf, the sensing element of the transducer was slowly torqued to 2-4 ft-lbf. While this was being accomplished, the output of the transducer was monitored on a DC digital voltmeter. Tightening of the sensing element was stopped when the output reached 2 volts. In the event that 2 volts could not be obtained within the torque range of 2-4 ft-lbf, shims of varying thickness were added or removed as required and the procedure repeated until a satisfactory reading was achieved. With the transducer thus installed, readings on the DC digital voltmeter were taken with and without system pressure (2970 psi) in the line, before and after each data run. These readings provided a calibration factor,

$$C_f = \frac{(2970 \text{ psig} - 20 \text{ psig})\sqrt{2}}{V_1(2970) - V_1(20 \text{ psig}) + V_2(2970 \text{ psig}) - V_2(20 \text{ psig})} \frac{\text{psi}}{V_{rms}} \qquad (109)$$

where V_1 is the voltage reading before the run and V_2 is the voltage reading after the run. Thus P_{peak} (psi) = C_f . V_{rms} (volts rms). According to the manufacturer's data (5), this procedure will result in a linearity of typically better than $\pm$ 1%, with a maximum of $\pm$ 2%. The Statham in-line transducer which was calibrated in the Instrumentation Shop using dead weights had a linear response of 400 psi per volt from zero to 4000 psi.

Frequency Response and Vibration Tests

Prior to any test, all instrumentation was warmed up for at least thirty minutes. The nitrogen supplying pressure to the reservoir was turned on as well as the tap water going to the oil coolers. The clampon transducers were then mounted loosely to the hydraulic line. Then the motor was started and the system allowed to warm up to an average steady-state operating temperature for the flow rate being run (115^{o}F for 2.5 gpm, 140^{o}F for 5.0 gpm and 155^{o}F for 7.5 gpm). Sometimes this process was expedited by leaving the water going to the oil coolers turned off, and running the motor at a high rpm. Once the average steady-state temperature was attained, the motor was turned off and the clampon transducers torqued down as described in the previous section. Often it was necessary to hammer a shim down to a very thin thickness to obtain a good calibration. With the transducers mounted, the motor was turned on and off three times to seat the clampon transducers. This was necessary to assure accurate calibration readings as typically the readings taken on the initial motor start up varied by up to 30% from readings taken after

the motor had been turned on and off three times. With the coupler set in the DC mode, readings from the clampon transducers with only 20 psig pressure in the line were taken. The motor was turned on and another reading quickly taken with the line pressurized to 2970 psig. This was done quickly so as to avoid any error due to the DC output voltage from the coupler decaying. The voltage decayed with a typical time constant of 1500 seconds which means that readings taken over a 15 second period would cause a decay error of 1%. With the transducer calibration now complete, the motor rpm was set to the highest rpm desired. It was necessary to start at the highest rpm and work down as the pump would stall at low rpm's and high flow rates. Also the line temperature varied less as it took a considerably longer time for the line to cool from the steady-state temperature at high rpm's than it took to heat up from the lower steady-state temperatures at low rpm's.

Once the rpm had been set to either 4500 rpm (675 Hz) or 4800 rpm (720 Hz) depending on the test being run, pressure and/or vibration readings were taken. The coupler was set to the AC mode and the spectrum analyzer was set in the "SUM" mode with 16 averages. Tests were run in the "PEAK" mode with 32 averages. Many readings were identical and all readings were within 0.5% of each other. Once an average had been taken, the cursor on the spectrum analyzer was moved to the pressure spike at the pump frequency or any desired frequency, such as a higher harmonic, and a reading taken. The reading was the rms amplitude in millivolts of the pressure at the frequency displayed on the spectrum analyzer. If the data displayed were particularly noteworthy, they were recorded on the data recorder

for future reference. All recordings were uniquely identified and noted in a log book for easy reference later.

For vibration readings, the vibration meter was set to measure displacement with an appropriate filter setting selected. Since most of the low frequency vibration occurred at 20 Hz and below, it made little difference which setting, i.e., 30, 70 or 110 Hz, was selected. The vibration pickup was torqued down after the line was preheated, just as the clampon pressure transducers. Once the motor rpm was set, a reading was taken. Without any filter, the needle on the vibration meter oscillated considerably and an average had to be taken. However, with the high-pass filters, the needle settled down and readings were easily taken.

At the beginning of each scan, after the motor rpm was set, temperature readings were taken at four points down the line as well as a reading of room temperature. At the end of the test run these temperature readings were repeated. For tests with flow, the rpm was set close to the desired value and then the flow control valve at the end of the line was manually adjusted to obtain the desired flow rate. Since a change in the valve opening changed the load on the motor, and thus the rpm, the rpm had to be readjusted to the desired value. Then the flow would be adjusted if required, and the rpm rechecked. Typically, the second flow adjustment and the third rpm adjustment were not required. The rpm was noted on the chart recorder that recorded the flow rate.

Pressure and/or vibration readings were taken every 100 rpm (15 Hz) from 4800 rpm (720 Hz) down to 1200 rpm (180 Hz) for flow rates of 5.0 gpm and less. Readings for flow rates of 7.5 gpm and

9.5 gpm could only be obtained down to 1700 rpm (255 Hz) and 2000 rpm (300 Hz) respectively as the motor would stall. When a pressure or vibration peak was encountered, readings were taken every 50 rpm in the vicinity of the peak to more accurately define the peak. At the end of the run, in addition to temperature readings, a second set of clampon pressure transducer calibration readings were taken in the same manner as at the beginning of the run. These two calibration readings were typically very close and were averaged for data reduction purposes. If the line temperature at the time of the second calibration reading varied by more than 20°F from the temperature at the time of the first, then the calibration reading would vary somewhat. This is one reason why the line was preheated prior to the first calibration. The second reason was that comparisons with analytical data were better if the line could be maintained at a reasonably constant temperature.

Wave Reflection Tests

A series of tests were run to determine what percentage of a left-running reflected wave was reflected from the pump. Configuration Five, the straight line, was used for tests with slight modifications. For these tests measuring the reflection from the pump, the pressure relief valve was removed from the line as the valve volume diffused the pressure wave and resulting measurements were not truly indicative of the wave reflection. The instrumentation was identical to that used in the frequency response tests. The spectrum analyzer was used in the real time mode which gave a display similar to a standard oscilloscope. The trigger level was set and the wave automatically captured. The trigger point is displayed as well as 128

memory samples prior to the trigger and 895 after the trigger. The time scale had to set so as to allow appropriate delay time for the wave to travel from one transducer to the pump and back while still appearing on the display. The Statham in-line transducer was used for the tests to eliminate any error due to vibrations. Time domain displays could not be recorded on the data recorder so Polaroid pictures were taken of the displays to allow data reduction at a later time.

The test procedures started in the same manner as the frequency response tests. Instruments were allowed to warm up 30 minutes, the reservoir was pressurized, the water to the oil coolers was turned on, and the pump was started. The pump rpm was set at a low rpm with a low AC pressure amplitude. With the valve fully closed, the valve handle at the end of the line was struck sharply with a mallet. The expansion wave traveled upstream past the transducer, triggering the spectrum analyzer, continued to the pump and reflected back to the transducer. The amplitude of the wave before and after the reflection was recorded.

Sudden valve closing was also attempted. The results were not good, however, as the valve would not close suddenly. The initial movement, which was rapid, was not enough to close the valve and generate a transient of reasonable amplitude for measurements. The sudden valve opening, however, was rapid enough to generate a transient of reasonable amplitude. Also, the results were repeatable.

IV. Use of the Clampon Transducer

Introduction

As mentioned in the previous chapter, the clampon transducer was used extensively for dynamic pressure measurements. This instrument is relatively new and had only been used by its designer, Mr. Gerald Amies, who is affiliated with the McDonnell Aircraft Company. Mr. Amies used this clampon transducer for tests in support of a contract with the Air Force concerning aircraft hydraulic systems analysis. The sponsoring Air Force agency, the Aero-Propulsion Laboratory, bought several of these transducers and was interested in learning under what conditions they could be used and likewise under what conditions they would give unreliable measurements.

Advantages of the Clampon Transducer

The clampon transducer is preferred over other pressure measuring devices for two reasons. First, the clampon transducer is a roving transducer, flush mounted to the outside of the hydraulic line at any point along the line. Secondly, it does not disturb the flow and thus alter the dynamic pressure. On the other hand, an in-line transducer requires a "T" fitting in the line for mounting and becomes a permanent part of the hydraulic system. Even with the best of machining, the flow will probably be disturbed at the head of an in-line transducer.

Comparison with the In-line Transducer

The first concern was whether or not the clampon transducer measured dynamic pressure accurately. This, of course, was purported by the manufacturer who had performed tests to verify this. However, since the clampon transducer was new and to the author's knowledge had not been independently tested, tests were run. Several tests were completed by Wright (35) and Katz (16) who worked with the author on the same equipment as described in Chapter III. In Wright's tests, a clampon transducer and an in-line transducer were mounted as close as possible to each other. Pressure data were taken and corrected for the separation between the transducers assuming a sinusoidal standing wave. He reported good agreement between the two transducers. Later tests by Katz showed that the clampon transducer was adversely affected by mechanical vibrations. However, when the mechanical vibration was small, the pressure data from the clampon and in-line transducers agreed well.

Encouraged by these results, the author performed only one more test, a test without any vibration present. To do this, the line could not be driven by a pump and motor which produce large vibrations. Instead, two clampon transducers were mounted on a short line connected to a hand pump. The line was terminated by a manual valve which was used to deplete the pressure. A DC pressure gauge was also installed in the line. The transducers were calibrated according to the manufacturer's instructions. Starting with the line pressurized to the normal operating pressure of 3000 psi, the pressure was then raised and lowered with pressure measurements taken at each new

pressure. The results demonstrated that the line had to be pressurized and depressurized at least twice before a stable, repeatable calibration could be obtained. It appeared that the transducer had to seat itself. Pressure data from both clampon transducers, using a calibration factor thus obtained, showed excellent agreement with the DC pressure gauge which had a resolution of 25 psi. The data were within 5% of the data taken with the DC pressure gauge 90% of the time.

Effect of Temperature

Experiments conducted later showed another effect, that of temperature. A calibration factor determined at an initial temperature would be smaller than one determined later at a higher temperature. For a significant change in calibration factor, a temperature change of approximately 20^{o}F was required. This necessitated preheating the line to an average steady-state temperature as described earlier under test procedures. To further reduce the effect of temperature, a calibration factor was determined at the beginning of each test and another at the end. These were then averaged and the averaged calibration factor used for data reduction. If the calibration factor at the beginning of the run differed significantly from the one at the end of the run, the data were considered unreliable and the test was run again. This was not required, however, as long as the line was properly preheated.

Effect of Clamp Torque and Preload Voltage

There were two required tolerances that had to be met during the installation and calibration of the clampon transducer. The first was that when the mounting clamp was installed on the line, both screws

had to be torqued to 2-4 ft-lbf. This was to hold the mounting clamp securely to the line. For the hydraulic lines and mounting clamps used in this research effort, 2 ft-lbf did not securely hold the mounting clamp to the line, but 4 ft-lbf did and this was the torque setting used for all installations for pressure data runs. However, tests were run with torque settings above and below 4 ft-lbf to determine how sensitive the transducer output was to the mount torque setting. Data were taken using torque settings of 3, 4 and 5 ft-lbf with all other variables held constant. Considering all the variables, in particular dynamic pressure, temperature and vibration, the best method of holding these constant was to run with the line blocked immediately downstream of the pump. The two clampon transducers were mounted 12.5 in. and 14.5 in. from the pump which was far enough that the line temperature remained constant. Due to the blockage, there was no dynamic pressure. Also, with effectively no load on the pump, the vibration did not change significantly when the pump frequency was changed. The clampon transducers were effectively measuring the displacement due to vibration which was large due to the proximity of the pump. The results for the transducer 14.5 in. from the pump are shown in Figure 4. The recommended mount torque setting gave the best sensitivity, i.e., the largest reading for a given displacement. The results for the transducer 12.5 in. from the pump were similar. Thus the effect of overtorquing or undertorquing the mount bolts was a decreased sensitivity of the transducer. Regardless of the torque setting, the data should be reasonably accurate as the calibration factor adjusted for the decreasing voltage output per unit displacement.

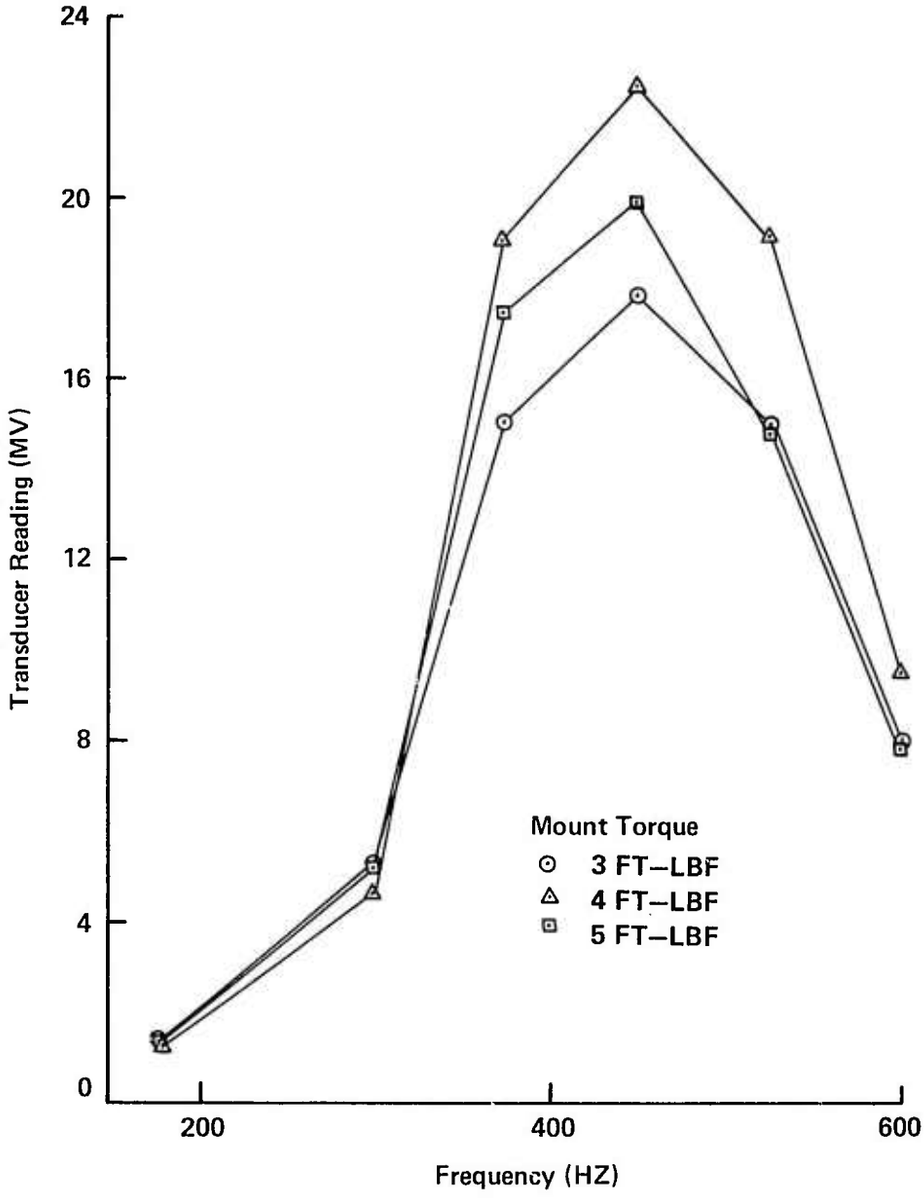

Figure 4. Effect Of Mount Torque On A Clampon Transducer (Voltage Preload 2.0 Volts)

The second required tolerance was the voltage preload on the transducer itself. The manufacturer's instruction manual called for 1-2 volts. To test the sensitivity of the transducer to the voltage preload, the same test procedure was followed as in the sensitivity test for the mount torque. The only difference was that the mount torque setting was held at a constant 4 ft-lbf, and the voltage preload allowed to vary from 1 to 2.5 volts. Preloads above 2.5 volts were not attempted for fear of possible permanent damage to the transducer. The results for the transducer 14.5 in. from the pump are shown in Figure 5. In this case the 2.0 volt preload gave the highest sensitivity and the 2.5 volt preload caused a large decrease in sensitivity. Again the results for the transducer 12.5 in. from the pump showed the same trend. Thus for best results, the transducer should be torqued down to a 2.0 volt preload setting, but no more. This was done for all data runs. The transducers were set as close to 2.0 volts as possible during calibration.

Repeatability

To best demonstrate repeatability of data, tests had to be run where the dynamic pressure was large, the vibration reasonably small, and the temperature nearly constant. These factors all pointed to a test with a limited frequency range at high rpm, at a point well downstream of the pump. At high rpm's, the vibration had the lowest amplitude but yet the dynamic pressure was high. The limited frequency range prevented the temperature from varying significantly. The results for both the clampon transducer and the in-line transducer are shown in Figure 6. Since the transducers were located 37 in.

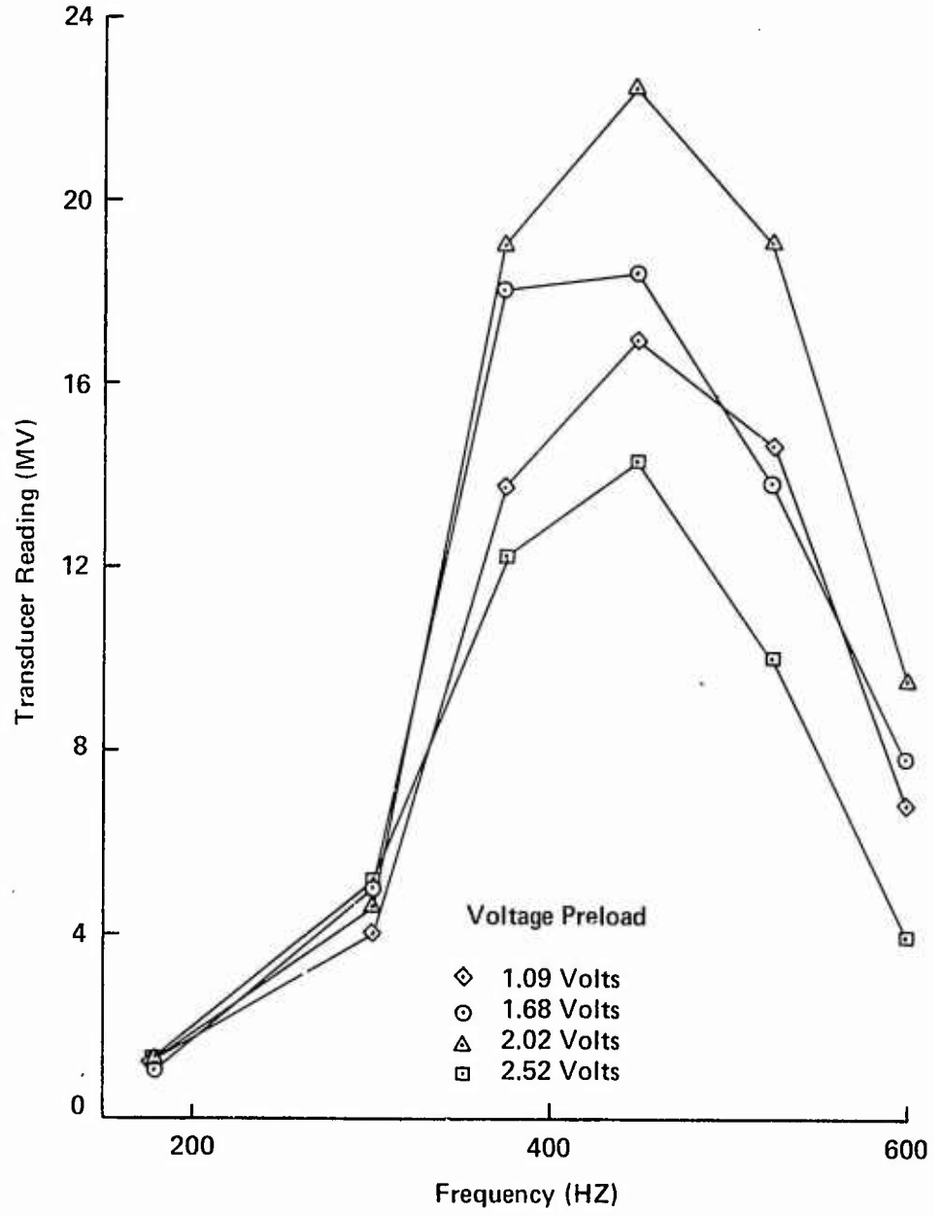

Figure 5. Effect Of Voltage Preload On A Clampon Transducer (Mount Torque 4 FT–LBF)

apart, one would not expect to see identical curves, but rather identical trends. The test was started, after the line had been preheated, at 4650 rpm (697.5 Hz). Measurements were taken every 50 rpm (7.5 Hz) down to 4400 rpm (660 Hz) and back up to 4650 rpm (697.5 Hz). Then several random readings were taken. The repeatability was excellent. The largest difference, which was an 8.7% change, occurred between the readings at the beginning and the end of the test and was probably the result of a slight increase in temperature and a small change in the vibration level.

Summary

The clampon transducer, properly installed and calibrated, is an excellent instrument for measuring dynamic pressure in hydraulic systems where vibration is not significant. However, the effect of vibration on the clampon transducer needs to be determined. The only study in this area is that of Katz (16) and more work is required if the data produced using the clampon transducer are to be trusted.

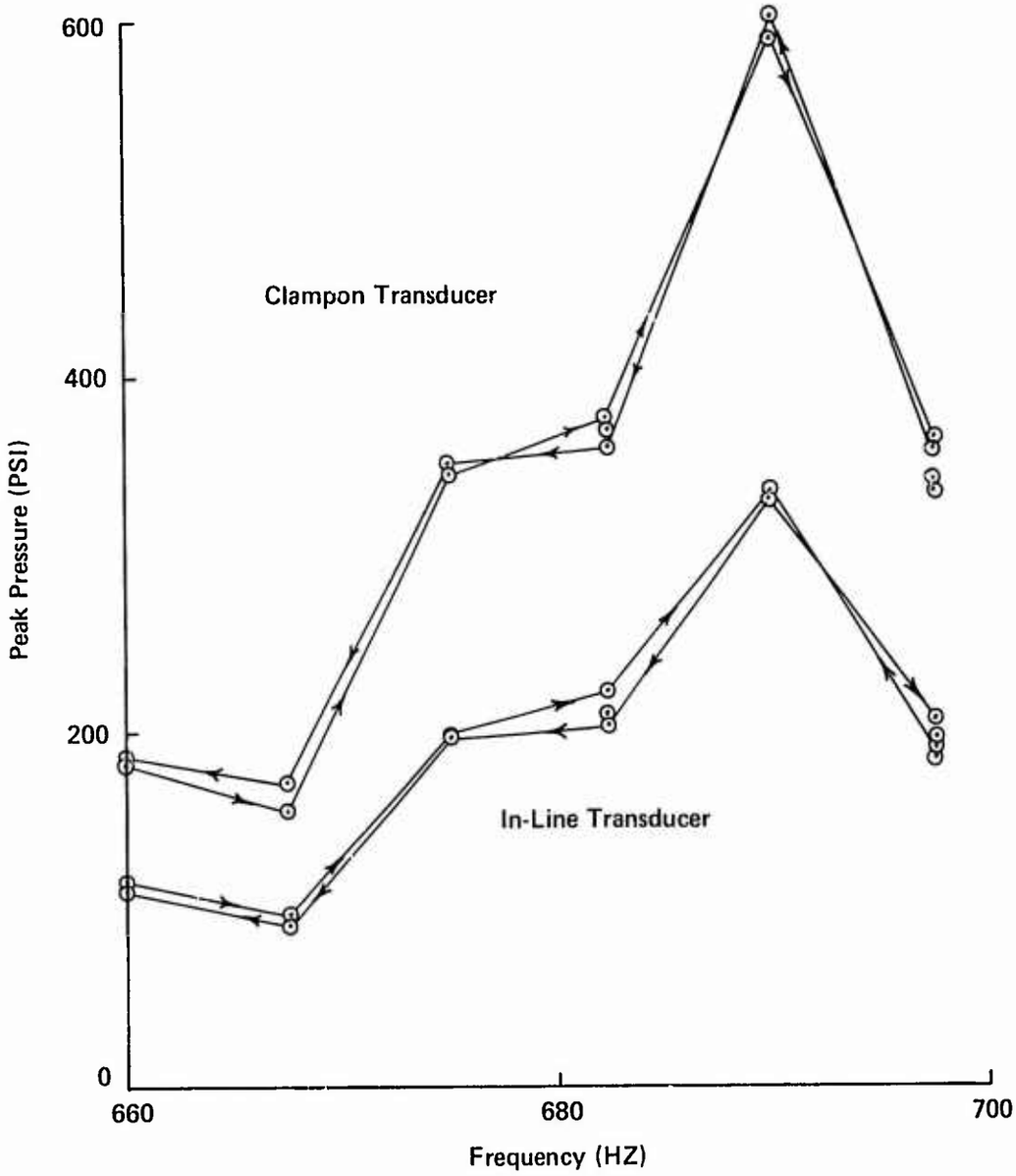

Figure 6. Repeatability Of Data
Clampon Transducer 64.5 In. From Pump
In-Line Transducer 101.5 In. From Pump

V. Effect of Vibration on the Clampon Transducer

Introduction

Despite the fact that the intent of the experimental research was to study the fluid mechanics associated with hydraulic systems, it was also necessary to consider vibration of the experimental system. This was due to the fact that the effect of vibration on the clampon transducers was unknown. Several experiments were conducted to quantify vibrational effects. The intent was to justify using the clampon transducer for pressure measurements by showing when the output of the transducer was not significantly affected by vibrations.

Based on the work of Amies (4), it was anticipated that there would not be any significant vibrational effect. He reported no problems due to vibration under the conditions of his tests. When the physical system was looked at, however, it was easy to postulate significant vibrational effects. Considering that the clampon transducer measured the displacement of the outer tube wall as it expanded and contracted due to the oscillatory pressure on the inside of the tube, it seemed conceivable that the displacement of the outer tube wall due to vibrational bending modes would also be measured. Also the frequency of the oscillation was the same in both cases as the primary energy source for both the vibration and the dynamic pressure was the hydraulic pump. Of course, higher harmonics were present as well as low frequency structural vibrations.

Vibrational Harmonics

The vibrational harmonics were measured to ascertain their relative magnitude in comparison with the fundamental. The first harmonic of vibrational displacement was the only one of significant amplitude and a plot of the ratio of the amplitude of the first harmonic to the amplitude of the fundamental is given in Figure 7. Note that the ratio is one-third or less.

Low Frequency Vibration

The low frequency structural vibrations were not a major concern since, due to their long wavelengths compared to the wavelengths at the pump operating frequencies of interest, the change in displacement was very slow compared to the change in displacement at the higher frequencies. This was true as long as the frequencies were at least an order of magnitude apart. This was the case in the experiments as the low frequency vibrations occurred at 0-20 Hz, while the pump frequencies were 180-720 Hz. Furthermore, the 110 Hz filter on the vibration meter was used to filter out all low frequency signals when vibration measurements were taken. Also, when pressure measurements were taken using the spectrum analyzer, only the displacement of the tube wall at the frequency of interest was recorded.

The low frequency vibrational displacement did have significant amplitude compared to the high frequency displacement. Figure 8 compares data taken with the 110 Hz high-pass filter, which eliminated the low frequency vibration, to data taken without the filter. The relative amplitude of the low frequency vibration can thus be seen At 2000 rpm (300 Hz) the low frequency vibration, which was superposed onto the vibration at the pump frequency, is small. The vibration at

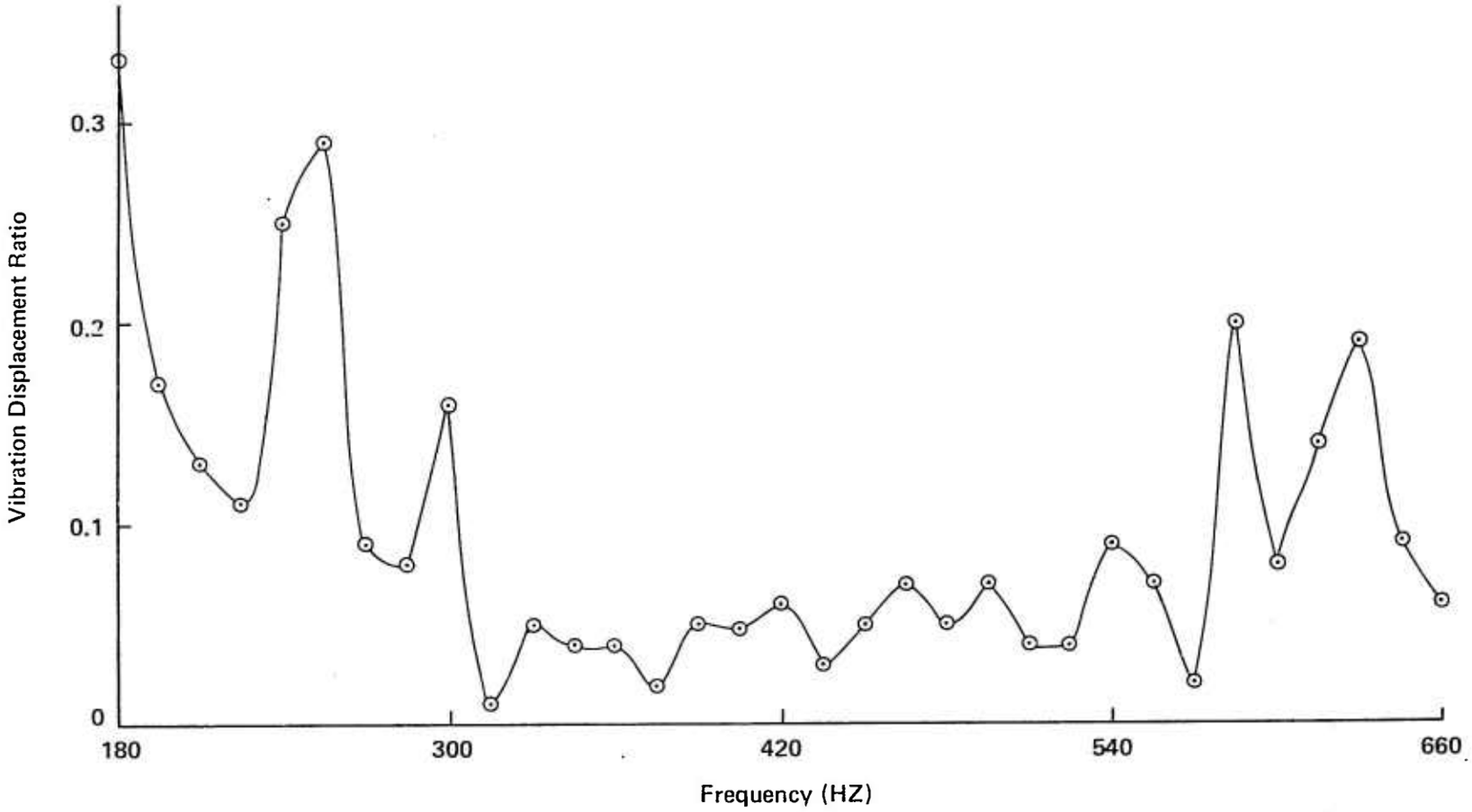

Figure 7. Ratio Of The Amplitude Of The First Harmonic Of Vibration Displacement To The Fundamental

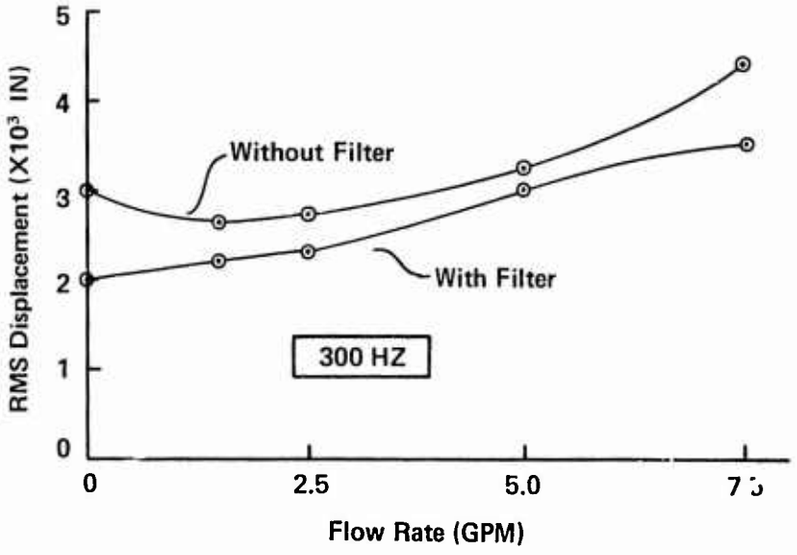

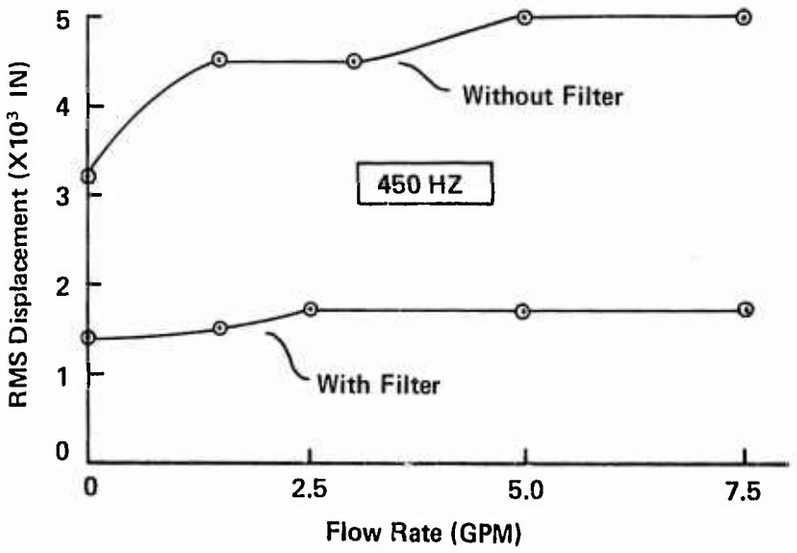

Figure 8. Vibration Displacement Measurements At
300 and 450 Hz With and Without an 110 Hz High-Pass Filter

the pump frequency was relatively large in this case. The situation at 3000 rpm (450 Hz) was considerably different. The low frequency vibrational displacement increased and the displacement at the pump frequency decreased. Figure 9 shows the displacement at resonant rpm's. These resonant rpm's were frequencies where dynamic pressure spikes occurred. Under these conditions the low frequency displacement was very large while the high frequency vibration was small. Here a second source of energy for the vibration is present, namely the large dynamic pressure oscillations. Pressure readings were often more than 700 psi peak-to-peak. This caused a tremendous increase in the noise level and necessitated the wear of ear protectors by all personnel in the laboratory. It was interesting to note that even with the addition of the large dynamic pressure, the vibration at the pump frequency actually decreased slightly while the low frequency displacement and the noise level increased greatly. This smaller vibration at the higher pump frequencies was expected since the attenuation of the vibration becomes much greater at high frequencies. Figure 9 also shows data for a pump frequency of 4000 rpm (600 Hz) which was just slightly higher than the resonant frequencies. The dynamic pressure was still significant at this frequency but much smaller than at the resonant frequency. The vibration at the pump frequency was still small due to the large attenuation at this high frequency, but the low frequency vibration changed, increasing at 1.5 and 2.5 gpm and decreasing at the other flow rates. At 4000 rpm (600 Hz) and all high frequencies, the motor driving the hydraulic pump generated significant noise and vibration, while at the lower frequencies, 3000 rpm (450 Hz) and below, the motor ran relatively quietly.

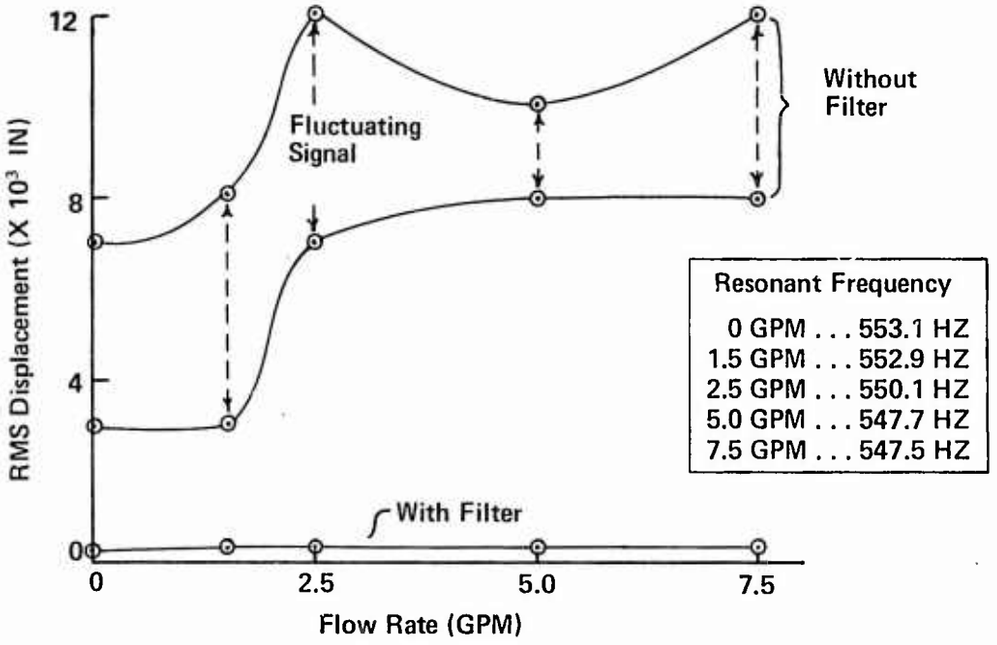

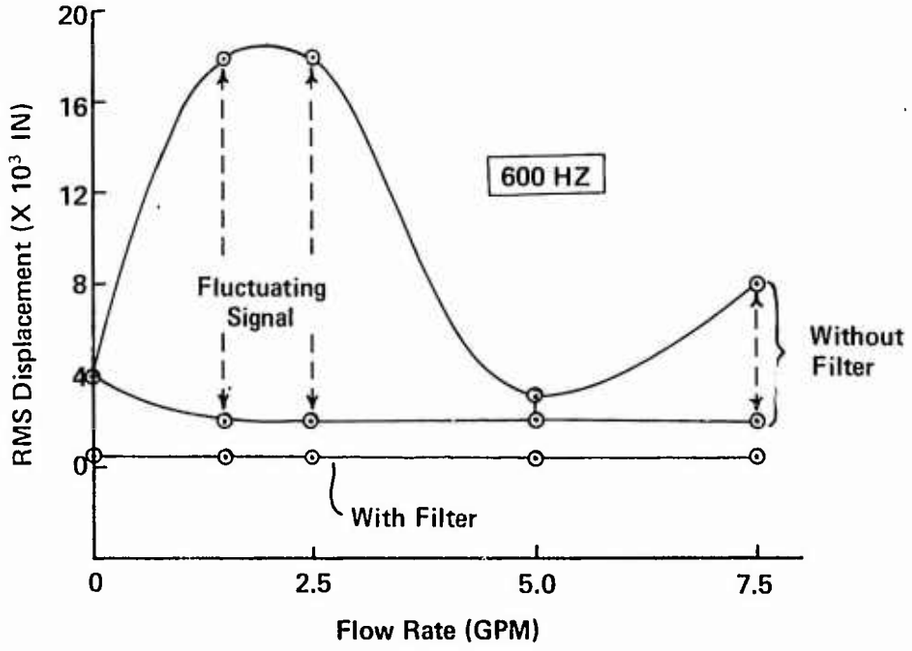

Figure 9. Vibration Displacement Measurements At Resonant Frequencies and 600 Hz With and Without an 110 Hz High-Pass Filter

Energy Sources for Vibration

As noted above, there were several significant energy sources for the vibration. The first source was the hydraulic pump which was a source for vibrations at the same frequency as the dynamic pressure and thus was a problem for clampon transducers. A second source was the motor driving the pump. With all of its belts and pulleys, vibrations at many frequencies, especially low frequencies, were generated. A third source was the dynamic pressure in the line. This again was a problem for the clampon transducer. A fourth source came from the experimental setup itself. There were sharp bends and tees in the lines that caused the flow to turn abruptly. Since part of the energy source here was the steady-state through-flow, the vibration generated was probably at the natural frequency of the system, approximately 20 Hz, which was much lower than the lowest pump frequency of interest, 180 Hz. The other portion of the energy source was the oscillatory flow. Since the flow was oscillating at the pump frequency, vibrations at this frequency were likely to be produced when the flow was abruptly turned. This was observed experimentally. Vibration both at 20 Hz and below and at the pump frequency was significantly higher near bends than in straight line sections.

Blocked Line Experiments

Since there were three primary sources for vibration at the pump frequency, it was desirable to isolate one, the vibration caused by the hydraulic pump and motor. To do this, the hydraulic line was blocked 3.625 in. downstream of the pump. The line was filled with hydraulic fluid, but there was no flow. The vibration generated by the pump could still travel down the tube walls, but there was no

dynamic pressure in the line and thus no vibration due to it. Likewise, there was no vibration due to abrupt turning of the flow since there was no flow, oscillatory or steady-state. Data were taken at four points down the line and compared with data taken with the line unblocked but with no flow. All data were taken with a clampon transducer. The results are shown in Figures 10-13. Figure 10 shows results at a short distance downstream of the blockage. The curve for the unblocked line shows the superposition of the dynamic pressure and the vibration, while the curve for the blocked line is due to vibration only. The blocked line "pressure" reading induced by the vibration is a significant fraction of the overall "pressure" reading as depicted by the curve for the unblocked line. If the vibration and the dynamic pressure were in phase, the difference between the curves would be representative of the true dynamic pressure, barring nonlinearities. However, the two signals are not in phase or else negative dynamic pressure, an impossibility, would be present in the line from 1800 to 2100 rpm (270 to 315 Hz). One reason why the vibration and the dynamic pressure are out of phase is that the vibration travels along the tube walls at approximately four times the velocity that pressure waves travel in the hydraulic fluid.

Figure 11 shows data for blocked and unblocked lines about 8 in. downstream of the point where data were taken for the previous graph, Figure 10. The "pressure" reading induced by the vibration in the blocked line is still large and the data for the unblocked line are changed somewhat, primarily due to the fact that the data are from a different point on the standing pressure wave in the line. The first significant decrease in the "pressure" reading induced by the

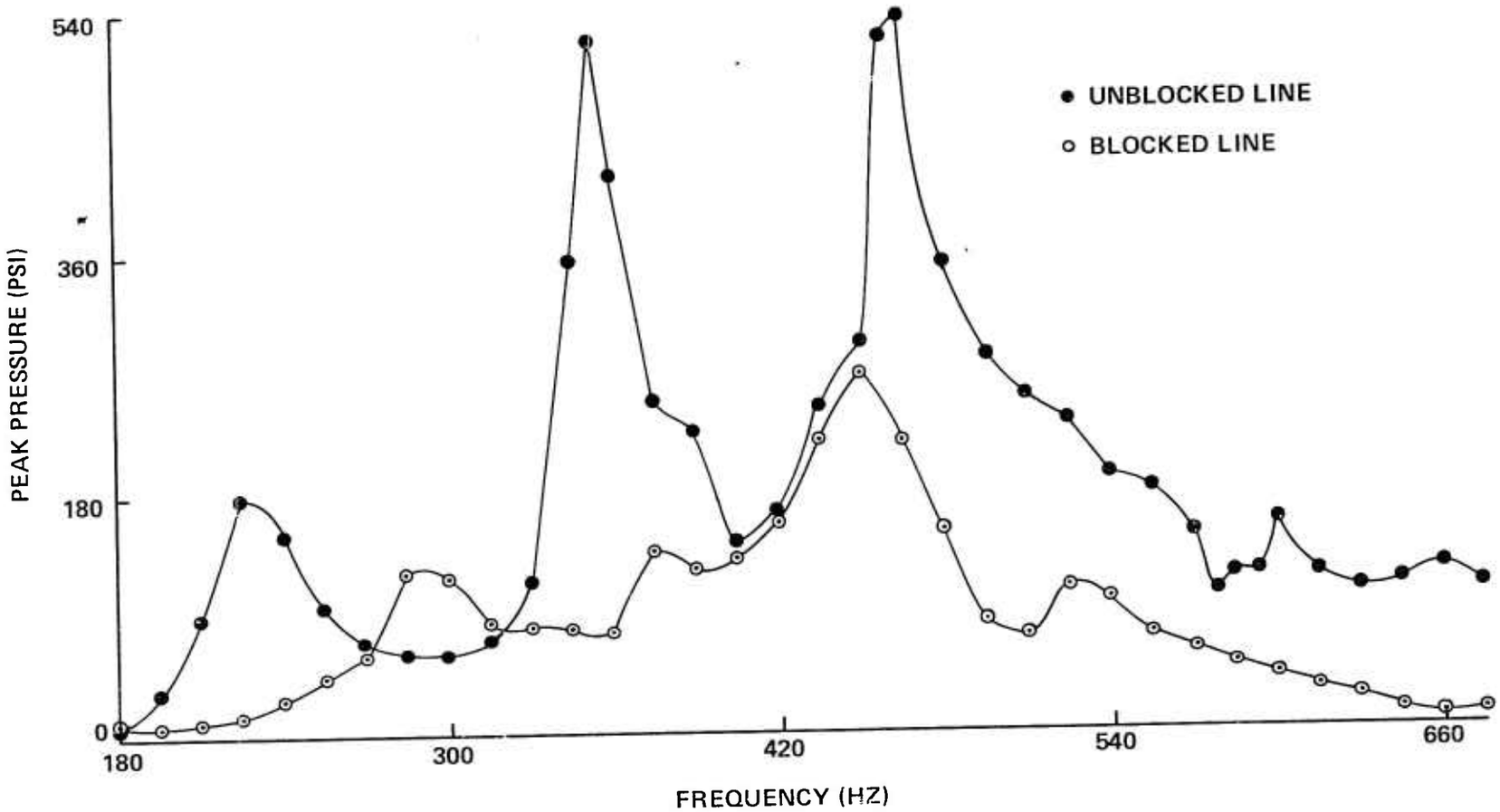

Figure 10. Clampon Transducer Pressure Measurements 7.1875 In. from Pump

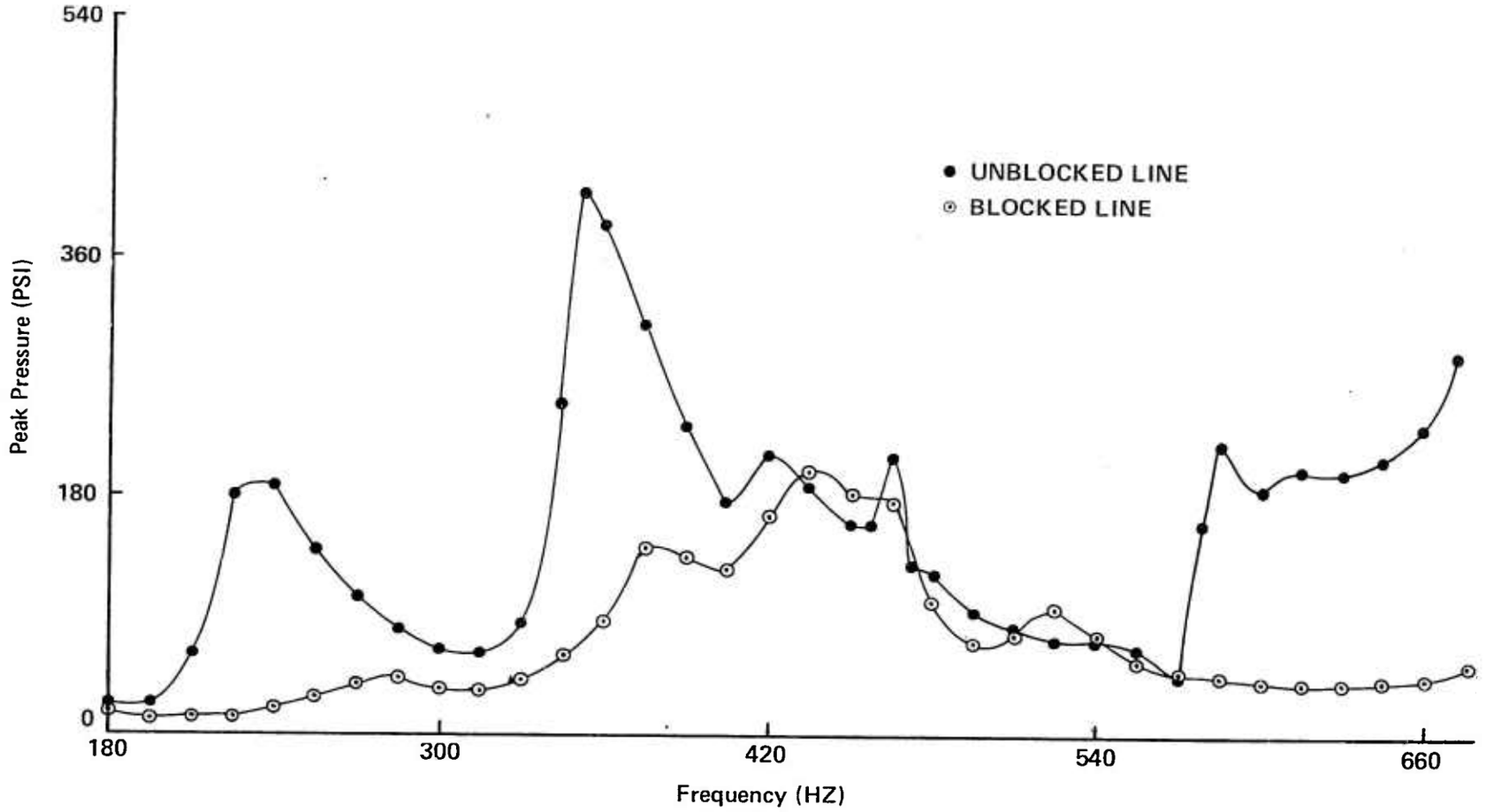

Figure 11. Clampon Transducer Pressure Measurements 13.5 In. From Pump

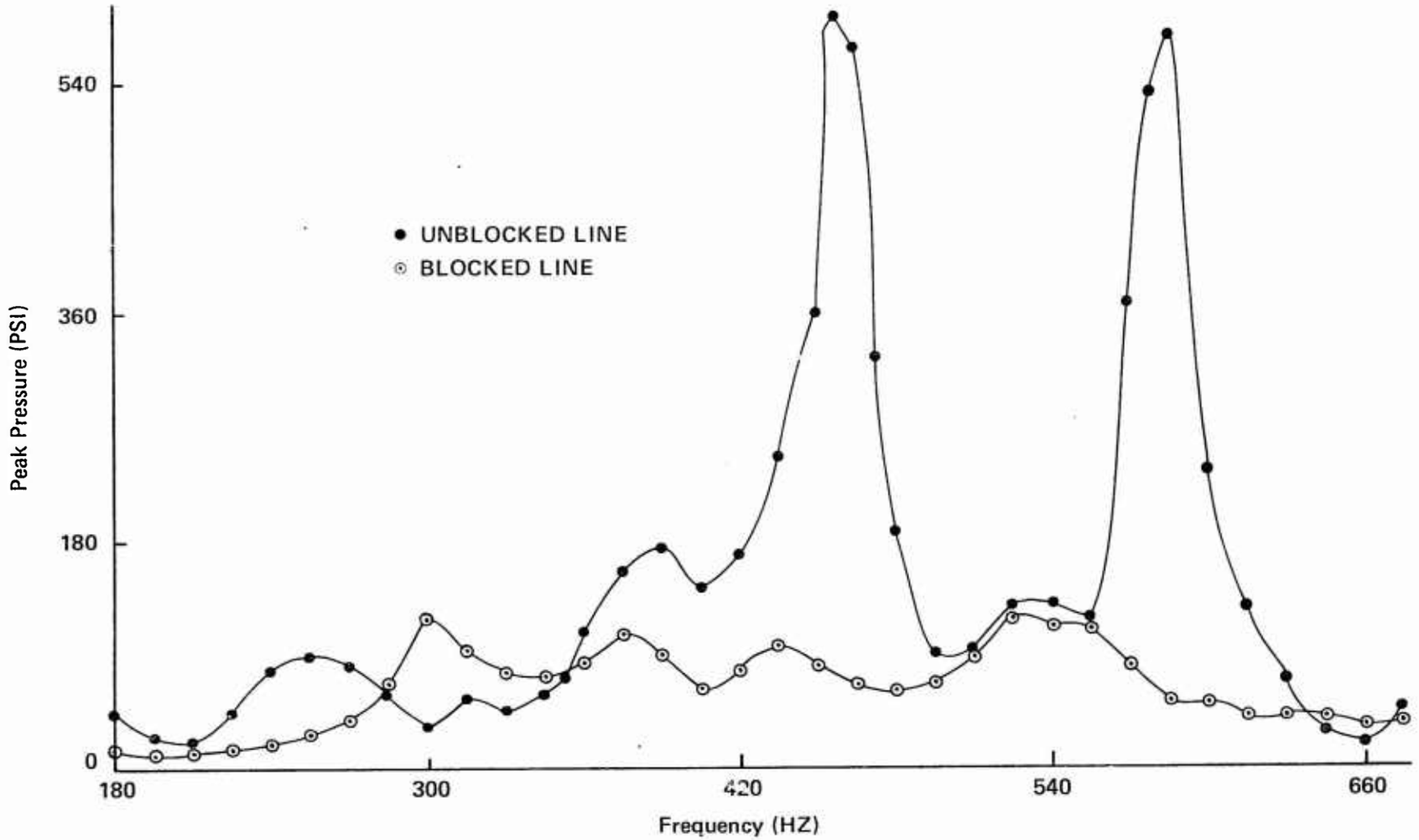

Figure 12. Clampon Transducer Pressure Measurements 32.5 In. From Pump

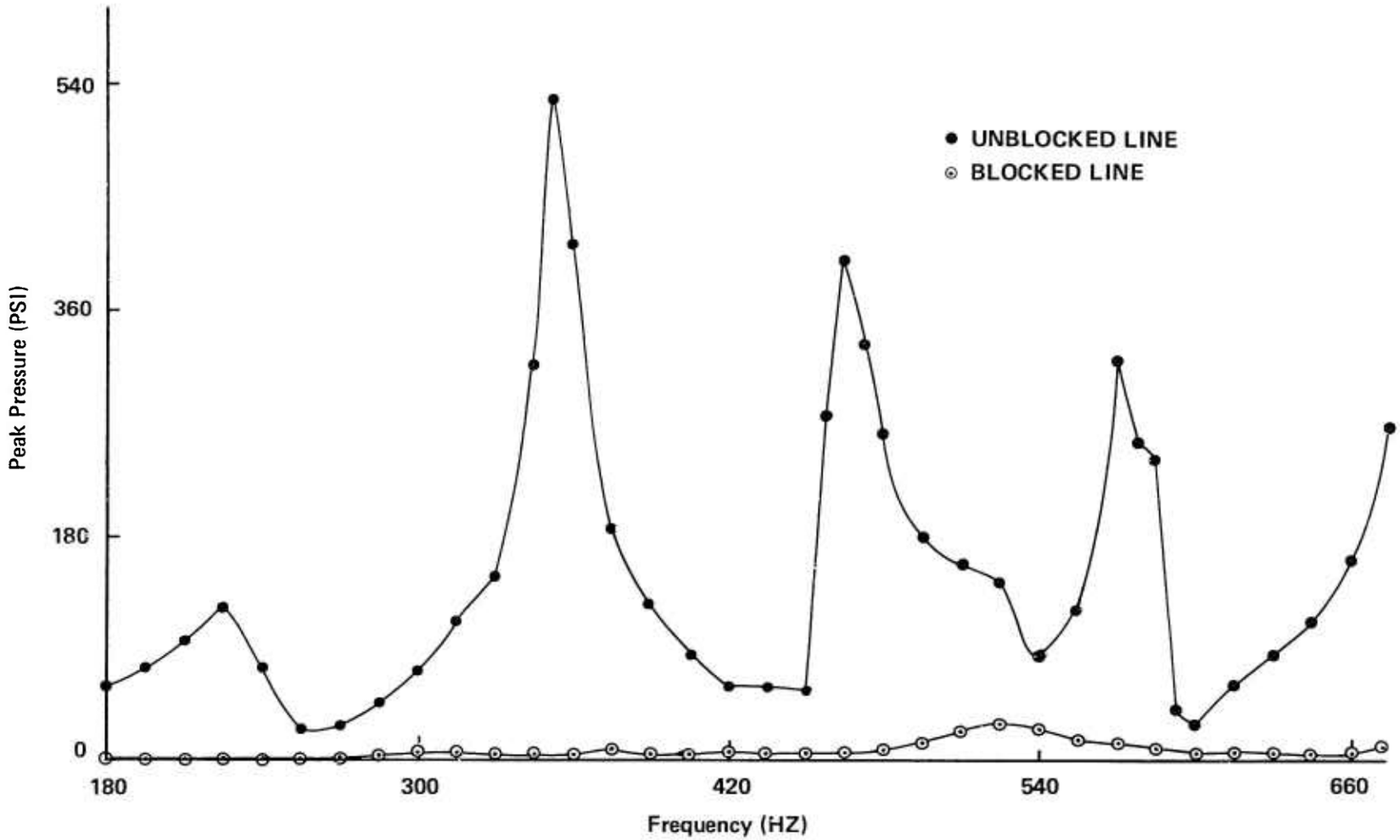

Figure 13. Clampon Transducer Pressure Measurements 64.5 In. From Pump

vibration shows up in Figure 12, where the largest pressure is 120 psi compared to 200 psi in the previous figure. The primary reason for this large decrease is that the data were taken 19 in. further downstream, which is 32.5 in. from the pump and just 2 in. upstream of the first brace. This brace reduced the amplitude of the displacement due to vibration but had no effect on the dynamic pressure. The damping brought about by the braces is shown in Figure 13. In this plot, the "pressure" readings induced by vibration have decreased to the point that they are no longer significant, while the dynamic pressure is still at normal levels. The reason for this large drop is that the data were taken 64.5 in. from the pump, downstream of the second brace which had three shot bags over it. The braces and the shot bags dampened the vibration from the pump and motor enough that it was no longer significant. Data taken from points further down the line, past more braces and shot bags, showed ever decreasing vibration levels.

The primary conclusion drawn from these experiments is that significantly high vibrational displacements caused by the hydraulic pump and motor can seriously affect the measurements taken with a clampon transducer. The peak displacements for the data runs near the pump, Figures 10 and 11, were 0.004 in. peak-to-peak; 0.0029 in. peak-to-peak at 32.5 in. from the pump (Figure 12); just 0.0011 in peak-to-peak 64.5 in. from the pump (Figure 13); and only 0.00045 in. peak-to-peak 156.75 in. downstream of the pump. A second conclusion is that braces, shot bags and other damping devices suitably placed can reduce the vibration generated by the hydraulic pump and motor to a level that does not affect the clampon transducer significantly.

One reason why Amies had no vibration problems in his experiments is that his lines were securely anchored and braced. The resulting vibrational displacements were probably very low. It appears that a good rule of thumb is to keep the vibrational displacements down to 0.001 in. peak-to-peak or less for normal hydraulic system applications of the clampon transducer.

Pressure-Induced Vibrations

At this point only part of the problem has been addressed. The remainder, the vibration induced by the dynamic pressure oscillations, is left. Since this vibration is generated anywhere when dynamic pressure is present, and hence where dynamic pressure measurements would be taken, a serious problem exists if the vibration is significant enough to affect the clampon transducers. Several experiments were run in which a clampon transducer was mounted upstream of the in-line transducer, as close as possible to it without touching. Vibration data were also taken. Then pressure data from the clampon transducer were compared with that from an in-line transducer. The in-line transducer, by virtue of the fact that it sensed the dynamic pressure directly by being flush-mounted in the line, was not affected by vibrations as were clampon transducers. The results of the experiments are shown in Figure 14. Assuming no vibrational effects, one would expect only small differences in pressure readings due to the transducers being mounted at slightly different locations along the line. However, at frequencies where the measured vibration was high, the clampon transducer read extremely high, nearly twice the reading given by the in-line transducer. When the vibration was low, agreement was much better. Only where the vibrational displacement was

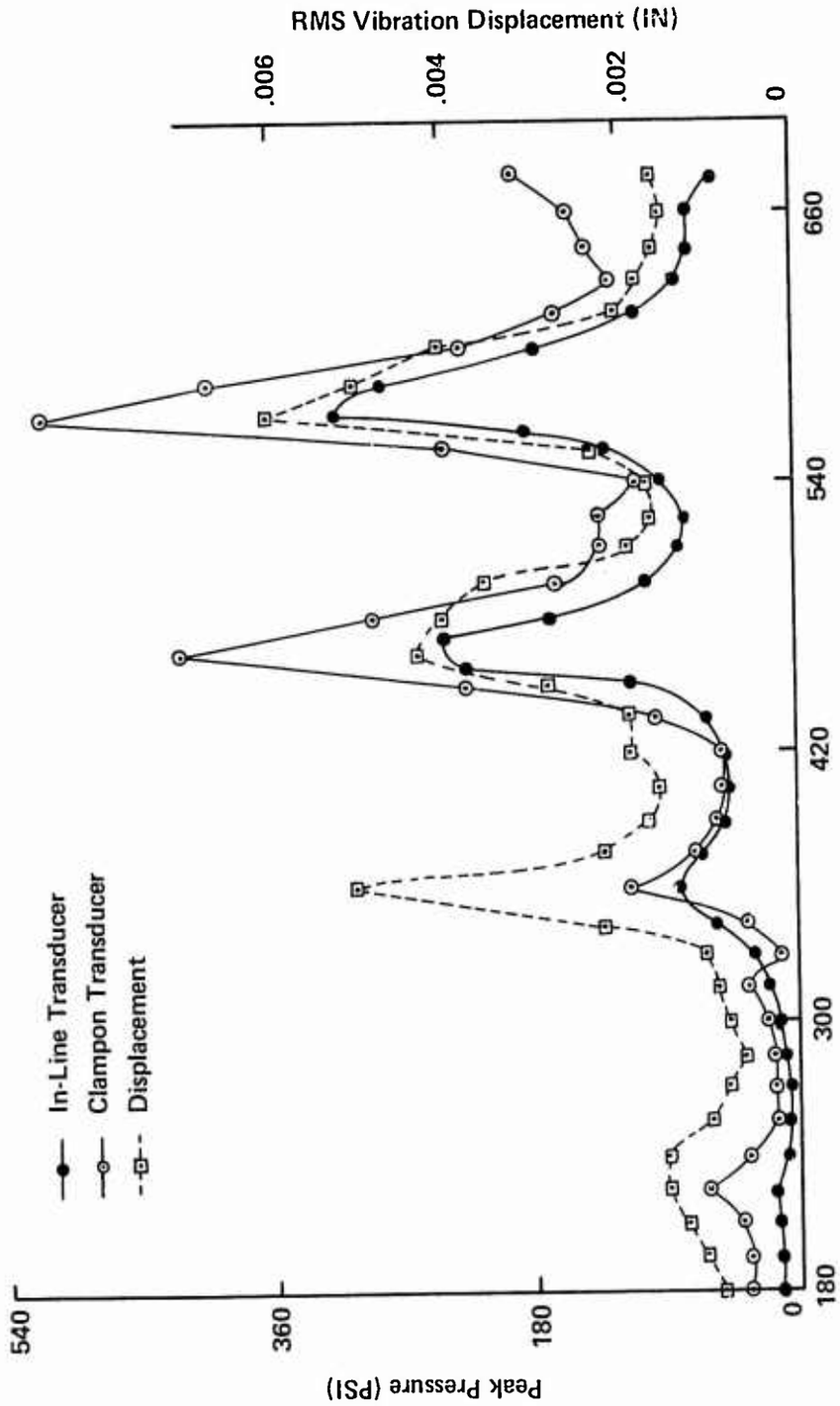

Figure 14. Comparison of Clampon and In-line Transducer Readings

low, near 0.001 in. peak-to-peak, did the clampon transducer agree well with the in-line transducer.

The results indicate that dynamic pressure itself does generate vibration at the same frequency as the pressure oscillation. When the pressure oscillations are large enough, the resulting vibration will affect a clampon transducer since it is measuring vibrational displacements as well as pressure-induced displacement. The resulting pressure readings are high, especially at frequencies where pressure peaks occur. The experiments were designed to allow large vibrational displacements. This was done by placing the transducers as far as possible from any brace or support that would dampen the vibration. With more bracing and thus lower displacement, the agreement would be better. The experimental setup of Amies (4) was better braced but still his data show the same trend, pressure readings taken with a clampon transducer that are consistently higher than predicted by theory.

Further tests were conducted by Katz (16) using the same instrumentation and equipment as used by the author. The difference was that his line was securely anchored with variable span between anchors. Katz compared clampon transducer data with in-line transducer data. The results are given in Table I. The span most closely approximating that used in the author's experiments is 30 in. The +25% correction for high frequencies and large dynamic pressures shows the same trend as the experimental data of the author; namely, pressures measured with the clampon transducer that were much higher than predicted. Even at the lower frequencies and pressures, the corrections are significant, indicating the effect of vibration cannot

Table I

Differences (Percents) Between In-Line
and Clamp-On Transducers
(Related to the In-Line Transducer)

Span	10 in.		30 in.	
(RPM)	1500-3300	3300-4500	1500-3300	3300-4500
Frequency (Hz)	225-500	500-675	225-500	500-675
Pressure > 100 PSI	± 10%	+ 20%	± 10%	+ 25%
Pressure < 100 PSI	± 10%	± 15%	± 15%	± 20%

Span	50 in.		70 in.	
(RPM)	1500-3300	3300-4500	1500-3300	3300-4500
Frequency (Hz)	225-500	500-675	225-500	500-675
Pressure > 100 PSI	± 10%	+ 25%	± 15%	+ 20%
Pressure < 100 PSI	± 20%	± 25%	± 15%	± 15%

Span	90 in.		110 in.	
(RPM)	1500-3300	3300-4500	1500-3300	3300-4500
Frequency (Hz)	225-500	500-675	225-500	500-675
Pressure > 100 PSI	+ 15%	+ 25%	+ 15%	+ 25%
Pressure < 100 PSI	± 15%	+ 20%	± 15%	+ 25%

be neglected. The data in Table I confirm that the better secured the line is, the smaller the effect of the vibration on the clampon transducer.

Summary

When vibration that produces significant displacements is present, pressure measurements using a clampon transducer will definitely be affected. In most cases the measured pressure will be significantly higher than the actual pressure. In the experiments run, the clampon transducers were not significantly affected by the vibration until the vibrational displacements became greater than 0.001 in. peak-to-peak. The vibrational displacements were typically large near the hydraulic pump, the motor, sharp bends and tees in the line. Mounting the clampon transducer as far as possible from these areas will help reduce vibration effects. Perhaps the best method of reducing vibrational displacements is by securely anchoring the line at as many points as possible, especially near points where a clampon transducer is to be mounted. Margolis and Brown (19) used this method to eliminate vibration when they buried their entire fluid line in 4 in. of concrete. When less effective damping methods are employed, vibrational displacement measurements must be taken to assure the damping is sufficient.

A third method of eliminating the effect of vibrations is to mount two clampon transducers directly opposite each other, i.e., 180 deg around the tube from the other. Both transducers would have to be calibrated separately. Then adjustments would have to be made so that both transducers had the same effective calibration factor. This could possibly be done by using an amplifier to raise the voltage of

the transducer with the lower calibration factor. Any error due to bending moments caused by vibration should be cancelled out using this technique. For a the cost of some additional instrumentation and time, good dynamic pressure measurements should be obtainable.

VI. Effect of Bends

Background

Prior research on the effect of bends in a fluid transmission line generally supported the assumption that bends have a negligible effect. Swaffield (31) in his study on the influence of bends on fluid transients found that the reflection of a pressure wave from a 90 deg bend with a radius of curvature to line diameter ratio of three or greater is small. Enever (11) in his comments on Swaffield's paper noted that the effect of a bend should be negligible if the wave front of the transient pressure is long compared with the length of the bend, which is true in most practical systems. This agrees with Zur (44) who found no significant effect of sharp bends on the transient response of a hydraulic line. In their experimental study and analysis of a liquid line with a sharp 90 deg elbow, Blade, Lewis and Goodykoontz (6) concluded that the elbow had little effect other than acting as a coupling device between pipe motion and fluid wave motion. The elbow itself caused no appreciable reflection, attenuation or phase shift in the fluid waves. These results, however, were for frequencies well below normal hydraulic system operating frequencies.

Since an aircraft hydraulic system has many bends, experiments were run to determine what effect bends have on the frequency response of a hydraulic system in a range of typical operating frequencies.

Tests

Experiments were run with the test setup in Configuration Four, with the U-shaped bend near the end of the line as shown in Fig. 3.

Data were also taken with the test setup in Configuration One with the U-shaped section at the beginning of the line. However, excessive vibration from the pump in the region of the bends caused the clampon transducer data to be unreliable. The Configuration Four setup, though, had three in-line transducers, which gave reliable data, in the region of the bends. For comparison, data were taken at the same distance from the hydraulic pump under similar test conditions with the setup in Configuration Five, the straight line of length equal to that of Configuration Four. The U-shaped bend consisted of four bends, two 90 deg elbows and two curved pipes with radii of curvature of 2.75 in. and 4.94 in.

Results

Figures 15, 16, 17 and 18 depict the results for flow rates of 0, 2.5, 5.0 and 7.5 gpm respectively. As would be expected considering the results of Swaffield (31), and Blade, Lewis and Goodykoontz (6), the effect of the bends was very small. In most cases, the pressure peaks of the frequency response for the straight line were slightly higher than the peaks for the line with the U-shaped bend. Away from the resonant frequencies, pressures for the straight line and the line with the bends were nearly the same. There is one major difference, however. At the higher flow rates, the system with the bends responded to a much greater extent at the fifth resonant frequency. The resonant peak at 3600 rpm (540 Hz) for a flow rate of 7.5 gpm (Figure 18) and at 3650 rpm (547.5 Hz) for a flow rate of 5.0 gpm (Figure 17) were considerably higher for the line with the bends. Data taken at eight other points along the line using clampon transducers showed the same trend; however, the pressure peaks for

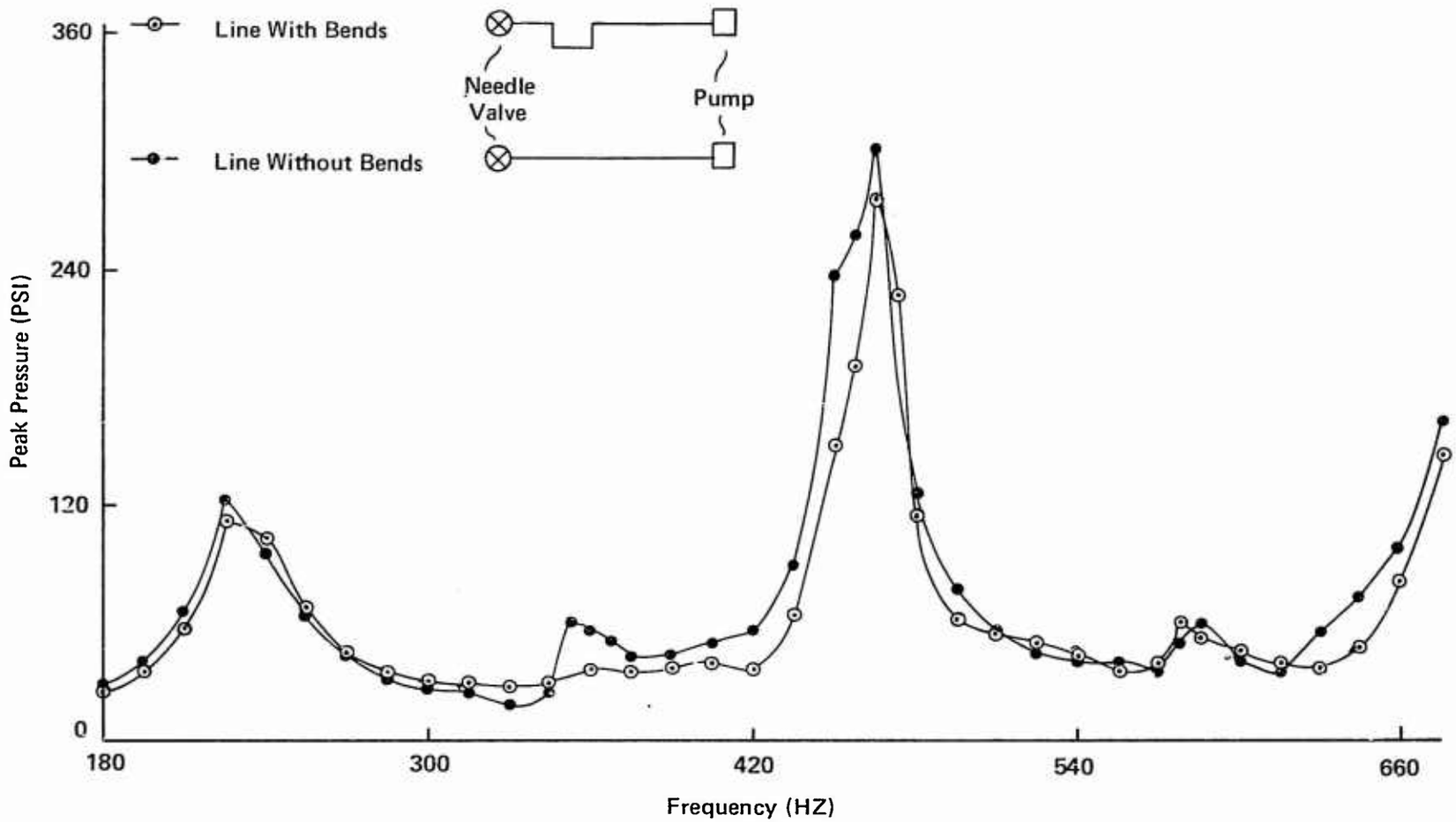

Figure 15. Frequency Response Of Lines With And Without Bends
(In-Line Transducer Data For 0 GPM)

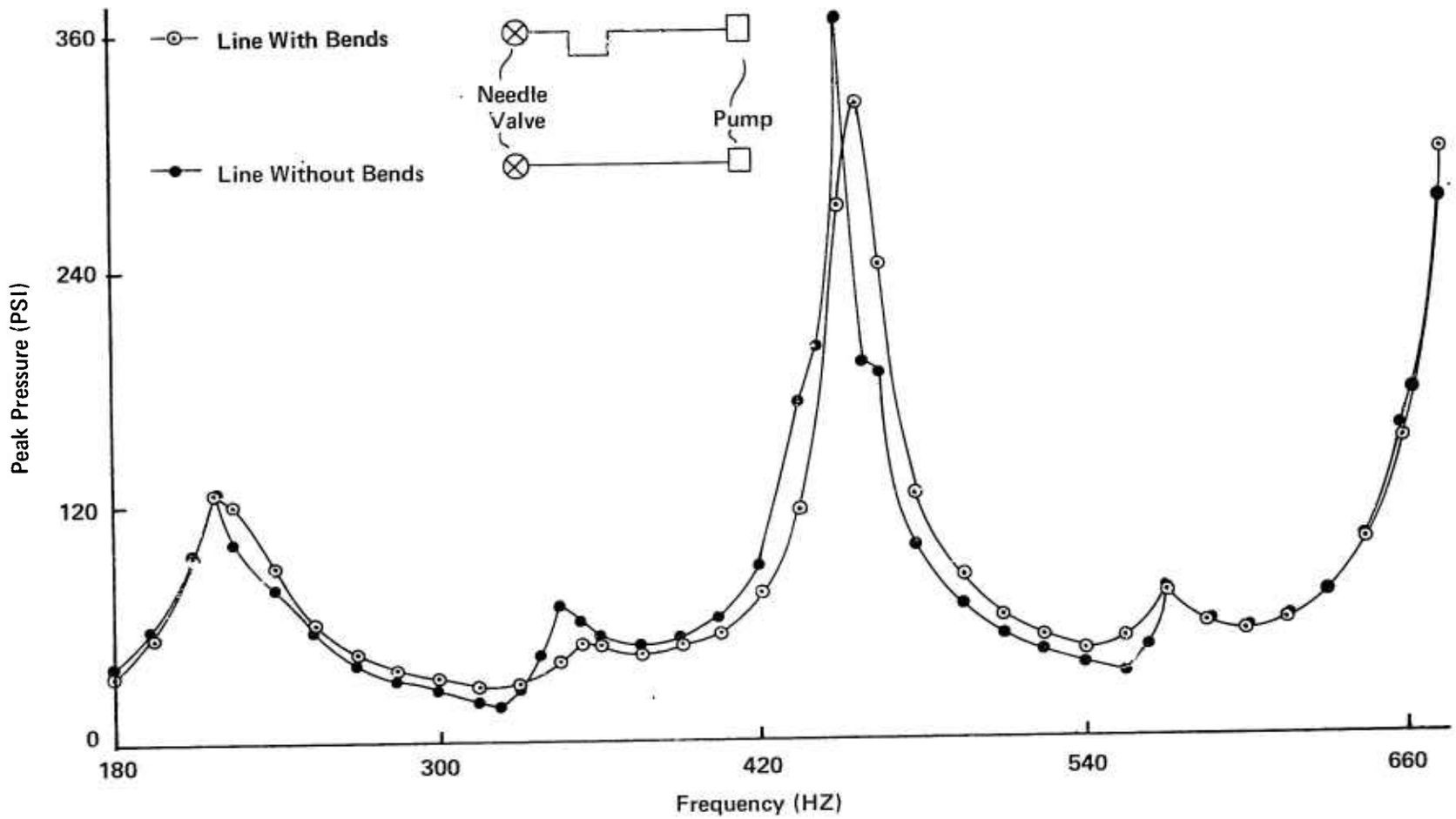

Figure 16. Frequency Response Of Lines With And Without Bends
(In-Line Transducer Data For 2.5 GPM)

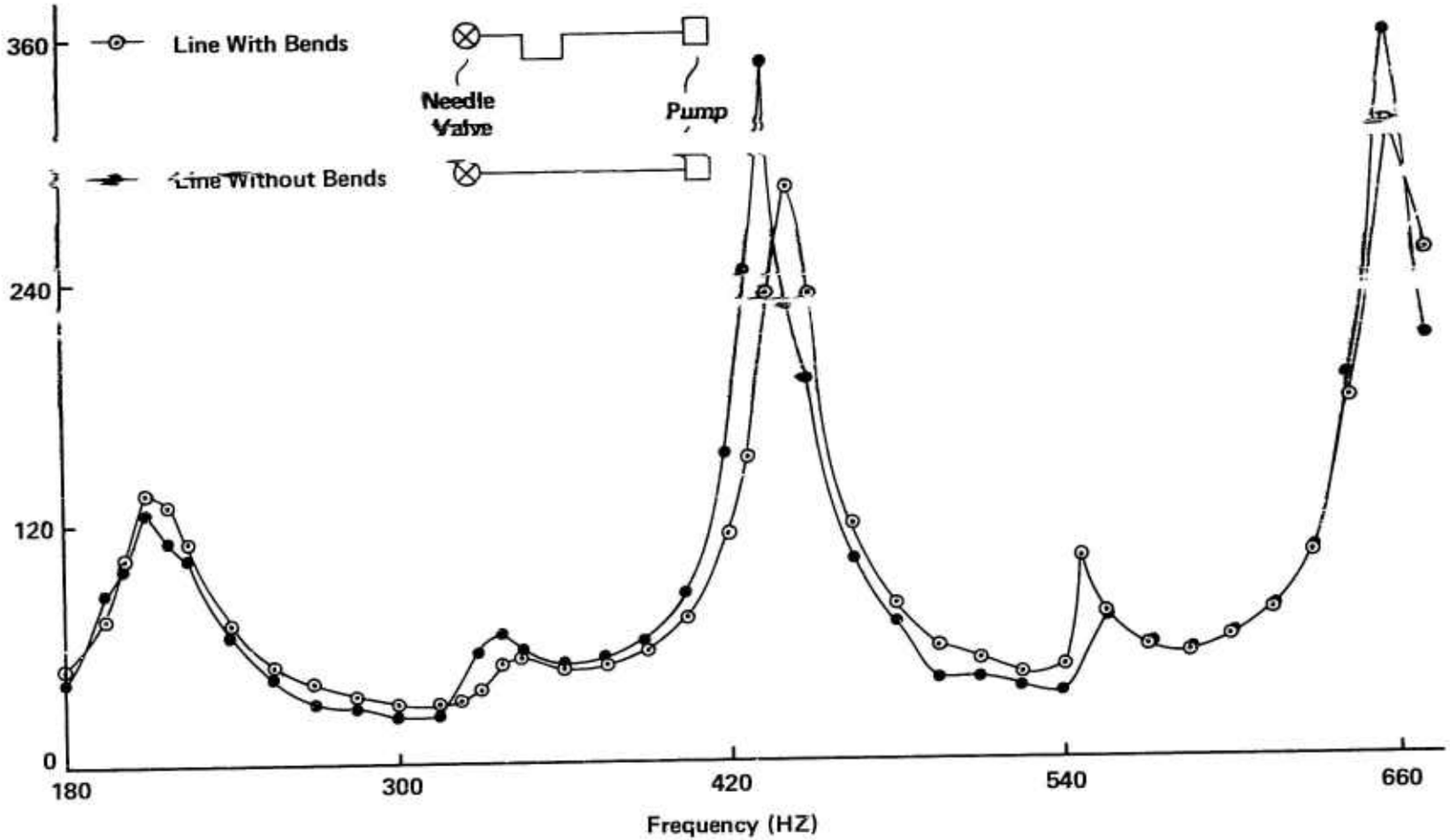

Figure 17. Frequency Response Of Lines With And Without Bends
(In-Line Transducer Data For 5.0 GPM)

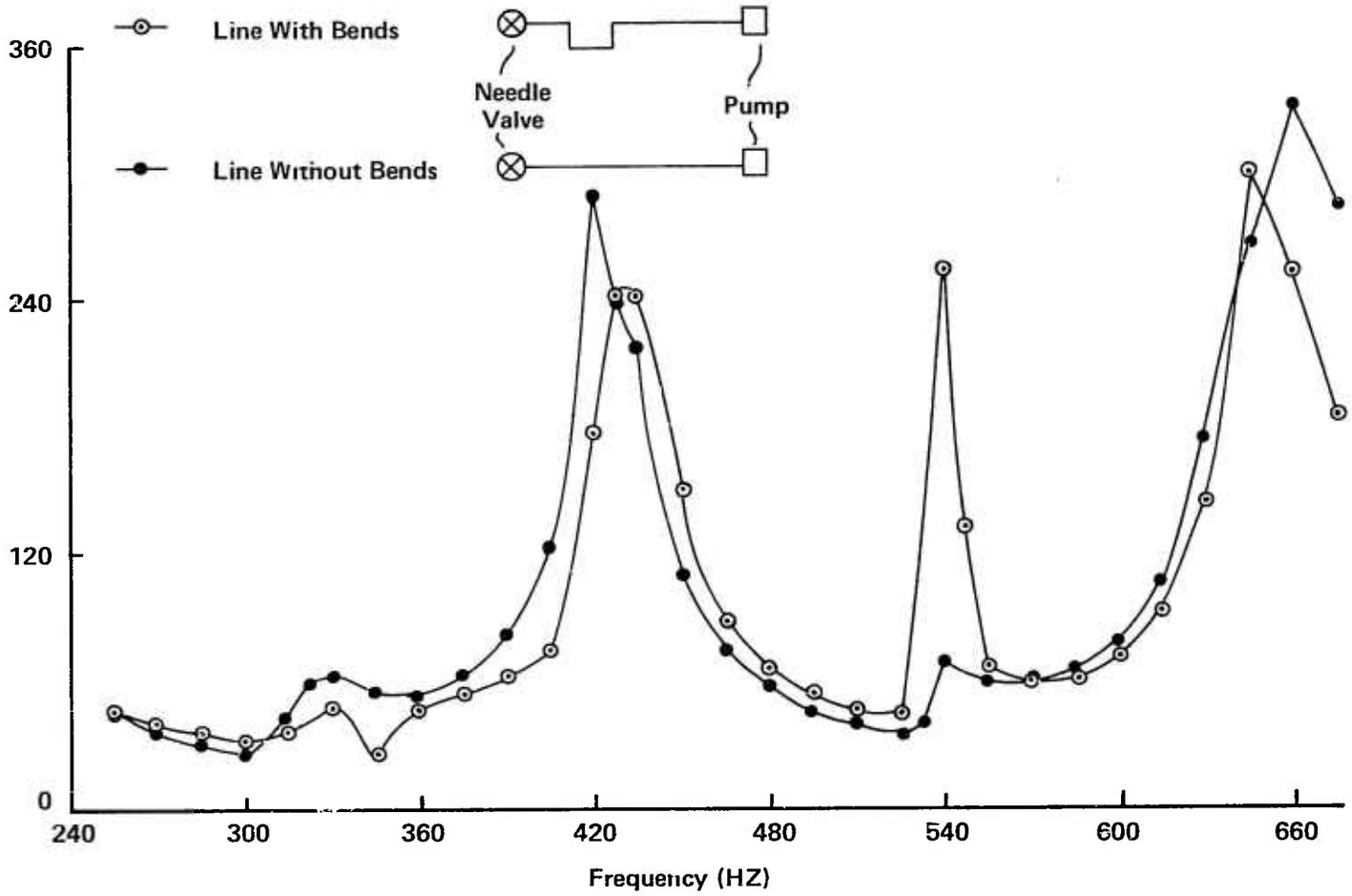

Figure 18. Frequency Response Of Lines With And Without Bends
(In-Line Transducer Data For 7.5 GPM)

both the straight line and the line with the bends were much larger, on the same order as the fourth and sixth resonant frequency peaks. One possible reason for the larger pressure peak at the fifth resonant frequency in the line with the bends at high flow rates is a coupling of the unbalanced pressure forces at the bends with the dynamic pressure. The HSFR program was run to see if it predicted any significant change at these higher flow rates. The HSFR results for both cases showed the same trends as the straight line experimental data. Actually one would not expect HSFR to show much of a difference for the line with the bends since HSFR treats a bend as a small steady-state pressure loss and nothing more. More work needs to be done in this area to fully understand what is happening at the fifth resonant frequency.

The bends did have one other effect as is shown in Figure 19, which compares the vibration in the two cases. For the most part, the line with the bends had higher vibrational displacements. This is due to the additional energy source, the unbalanced pressure forces at the bends from both the steady-state pressure and the dynamic pressure.

Summary

The effect of bends on the frequency response of a hydraulic system was small. An interesting exception to this was the significant increase in the peak pressure at the fifth resonant frequency for the line with the bends at high flow rates. This exception merits further study. Other pressure peaks were slightly lower for the line with the bends and the vibrational displacement was generally larger for the line with the bends.

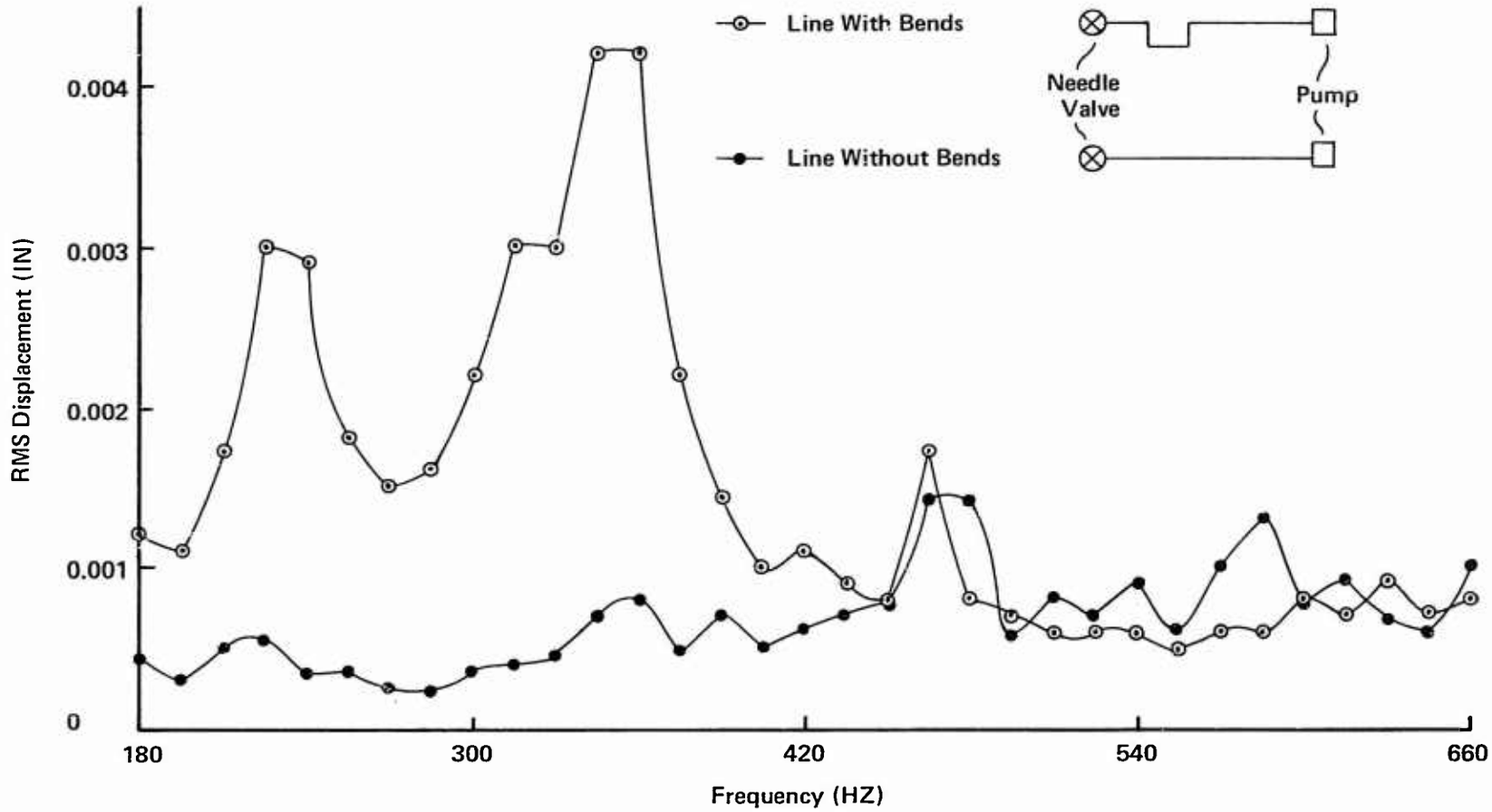

Figure 19. Vibration Displacement For Lines With and Without Bends
(Data Taken 3.5 In. Upstream Of Bend Joint)

VII. Sensitivity Analysis

Introduction

The theoretical analysis of a hydraulic system, whether it is based on the theory using the confluent hypergeometric equation as given in Chapter II, or the theory of D'Souza and Oldenburger (10) which is the basis for the HSFR program, provides an excellent means of obtaining the frequency response of the system. As described in Chapter I, HSFR, the hydraulic system frequency response computer program developed by McDonnell Aircraft Company, uses the same assumptions as the author except that the effect of the coupling between the mean flow and the oscillatory flow is not considered. HSFR calculates the frequency response, in particular the pressure peaks and resonant frequencies. However, the results are only as good as the input data. For practical engineering applications, precise input data are not always possible to obtain. A given input parameter, for example the bulk modulus of the fluid, may be slightly in error. It is important for the engineer to know how small variations in the input parameters will affect the results. Small effects can be neglected, but those parameters causing a large change need to be identified. Once identified, the engineer can make sure these parameters are as accurate as possible. Likewise he will know how his results will vary if his input data are overestimated or underestimated.

Methods of Determining Parameter Sensitivity

A sensitivity analysis was undertaken to determine the effect of small variations about a norm of many typical parameters used in a

hydraulic system analysis. Two methods were used to determine these effects. First HSFR was used to determine the location of pressure peaks in the frequency response. This was done since the frequency response is typically used by the hydraulic engineer in the design process to determine a good operating frequency for the system which is well away from any pressure peaks. Experimental Configuration Five with steady-state conditions of 115°F, 2970 psig and a 5 gpm flow rate was used as the reference and was modeled according to instructions in the HSFR Computer Program User Manual (1). Frequency response data were calculated for points 7.19, 96.25 and 197.25 in. from the pump and the pressure peaks at these points are denoted P_1, P_2 and P_3 respectively. Data were obtained for 5 rpm (0.75 Hz) increments and results are given in terms of the amplitude of the pressure peak and the frequency at which it occurs.

The second method used to ascertain the effect of varying the input parameters was to calculate the change in the attenuation and phase constant of both a left and right traveling wave. Also, the change in the maximum amplitude of the standing pressure wave, denoted as P_{max}, was calculated. For this, the straight line model as described earlier was used. The results showing the variations in the attenuation and the phase constant apply in general while the results showing the change in the maximum amplitude of the standing pressure wave strictly apply only for a blocked line. However, since the line model is used as a basis for reference, the trends determined should be applicable in general. The results were calculated for a pump frequency of 1300 rpm (195 Hz) and a 5 gpm flow rate at 2970 psig and 115°F. The line geometry was the same as used in HSFR.

Effect of Line Length

The line length for Configuration Five is 209.75 in. which is the reference line length. Data were obtained for line lengths of 208.75 and 210.75 in., which corresponds to variations of $\pm$ 0.5%. The results are shown in Table II. The first effect seen is the lowered resonant frequency. A line 0.5% longer than the reference has a resonant frequency 10 rpm (1.5 Hz) lower. The peak pressure changed by about 1% per inch change in line length. The change was both plus and minus indicating that the effect is dependent on position. When the attenuation, αL, and phase constant, βL, are put in dimensional form, i.e., divided by the line length, the resulting dimensional forms are the same for each case. The maximum pressure on the standing wave decreased slightly less than 1% for a one inch increase. The primary effect is the decrease in the resonant frequency of 10 rpm (1.5 Hz) for a one inch increase in line length.

Effect of Radius

The reference radius was 0.2475 in. and data were taken for radii of 0.2375 and 0.2575 in., which is equivalent to a change of 0.01 in. or 4%. As shown in Table III, the resonant frequency increases 10 rpm (1.5 Hz) for an increase in radius of 0.01 in. The peak pressure changed about 4% both plus and minus indicating that this effect is also dependent on position. The attenuation is 4% smaller for an increase in radius of 4% and the phase constant increases, but only a small amount, 0.035%. Likewise P_{max} changed only slightly, a 0.07% decrease which would be too small to be measured by most pressure transducers. The primary effect of a 4% increase in radius is a 4%

Table II. Effect of Line Length

	Line Length		
	208.75 in.	209.75 in.	210.75 in.
P_1	324.9 psi @ 2255 rpm	323.4 psi @ 2245 rpm	321.9 psi @ 2235 rpm
P_2	246.6 psi @ 2255 rpm	250.1 psi @ 2245 rpm	253.3 psi @ 2235 rpm
P_3	122.7 psi @ 2255 rpm	123.1 psi @ 2245 rpm	123.4 psi @ 2235 rpm
$\lvert\alpha_1\rvert L$	0.06174	0.06203	0.06233
$\lvert\alpha_2\rvert L$	0.06243	0.06273	0.06302
$\lvert\beta_1\rvert L$	4.966	4.990	5.013
$\lvert\beta_2\rvert L$	4.986	5.009	5.033
P_{max}	101.08 psi	100.13 psi	99.29 psi

Table III. Effect of Radius

	Radius		
	0.2375 in.	0.2475 in.	0.2575 in.
P_1	332.7 psi @ 2235 rpm	323.4 psi @ 2245 rpm	314.0 psi @ 2255 rpm
P_2	260.7 psi @ 2240 rpm	251.1 psi @ 2245 rpm	240.1 psi @ 2255 rpm
P_3	117.8 psi @ 2235 rpm	123.1 psi @ 2245 rpm	251.3 psi @ 2255 rpm
$\lvert\alpha_1\rvert L$	0.06462	0.06203	0.05966
$\lvert\alpha_2\rvert L$	0.06541	0.06273	0.06027
$\lvert\beta_1\rvert L$	4.986	4.990	4.993
$\lvert\beta_2\rvert L$	5.0077	5.0094	5.0112
P_{max}	100.20 psi	100.13 psi	100.06 psi

decrease in attenuation, accompanied by a 10 rpm (1.5 Hz) increase in resonant frequency.

Effect of Wall Thickness

Data were taken for a wall thickness $\pm$ 0.001 in. from the reference which was 0.065 in. This is a change of $\pm$ 1.5%. The results are shown in Table IV. The peak pressure was not affected significantly as the maximum change was only 0.08%. The resonant frequency was not affected. The attenuation decreased slightly, 0.04%, for an increase in wall thickness of 0.001 in. The phase constant also changed only slightly, decreasing by 0.05%. Likewise there was a small decrease in P_{max}, 0.07%, which again is in the noise level of most pressure transducers. The primary result here is that small variations in wall thickness have no significant effect.

Effect of Temperature

Experiments accomplished before the sensitivity analysis was undertaken demonstrated that small changes in temperature had a significant effect. A temperature change causes viscosity, density, and the bulk modulus to change, resulting in changes to the speed of sound and ω_ν. HSFR data were computed using 115°F, 135°F and 155°F, temperatures that typically occurred in experiments. Results are shown in Table V. Data for three resonant peaks are given to quantify better the large shift in resonant frequency. Figure 20 plots the frequency response showing these three peaks. The computations for α, β, and P_{max} were accomplished for 110°F, 115°F and 120°F. The peak pressures decreased a small amount for the 20°F rise from 115°F to 135°F and increased slightly from 135°F to 155°F. The largest change

Table IV. Effect of Wall Thickness

	Wall Thickness		
	0.064 in.	0.065 in.	0.066 in.
P_1	323.3 psi @ 2245 rpm	323.4 psi @ 2245 rpm	323.3 psi @ 2245 rpm
P_2	249.9 psi @ 2245 rpm	251.1 psi @ 2245 rpm	250.1 psi @ 2245 rpm
P_3	123.2 psi @ 2245 rpm	123.1 psi @ 2245 rpm	123.1 psi @ 2240 rpm
$\lvert\alpha_1\rvert L$	0.062057	0.062034	0.062011
$\lvert\alpha_2\rvert L$	0.062778	0.062729	0.062698
$\lvert\beta_1\rvert L$	4.9917	4.9897	4.9878
$\lvert\beta_2\rvert L$	5.0114	5.0094	5.0075
P_{max}	100.06 psi	100.13 psi	100.21 psi

Table V. Effect of Temperature

	115°F	135°F	155°F
P_1	323.4 psi @ 2245 rpm	322.6 psi @ 2185 rpm	326.5 psi @ 2125 rpm
	360.6 psi @ 3040 rpm	356.0 psi @ 2960 rpm	352.5 psi @ 2875 rpm
	350.2 psi @ 3855 rpm	343.7 psi @ 3750 rpm	337.1 psi @ 3650 rpm
P_2	250.1 psi @ 2245 rpm	249.7 psi @ 2185 rpm	252.9 psi @ 2125 rpm
	273.2 psi @ 3035 rpm	271.7 psi @ 2950 rpm	270.4 psi @ 2870 rpm
	439.8 psi @ 3850 rpm	434.1 psi @ 3750 rpm	428.3 psi @ 3645 rpm
P_3	123.1 psi @ 2245 rpm	122.5 psi @ 2180 rpm	123.8 psi @ 2120 rpm
	54.8 psi @ 3035 rpm	53.9 psi @ 2955 rpm	53.1 psi @ 2870 rpm
	31.0 psi @ 3850 rpm	30.9 psi @ 3750 rpm	30.7 psi @ 3650 rpm

	110°F	115°F	120°F
$\lvert\alpha_1\rvert L$	0.06402	0.06203	0.06179
$\lvert\alpha_2\rvert L$	0.06473	0.06273	0.06085
$\lvert\beta_1\rvert L$	4.9648	4.9897	5.0025
$\lvert\beta_2\rvert L$	4.9843	5.0094	5.0423
P_{max}	101.13 psi	100.13 psi	98.84 psi

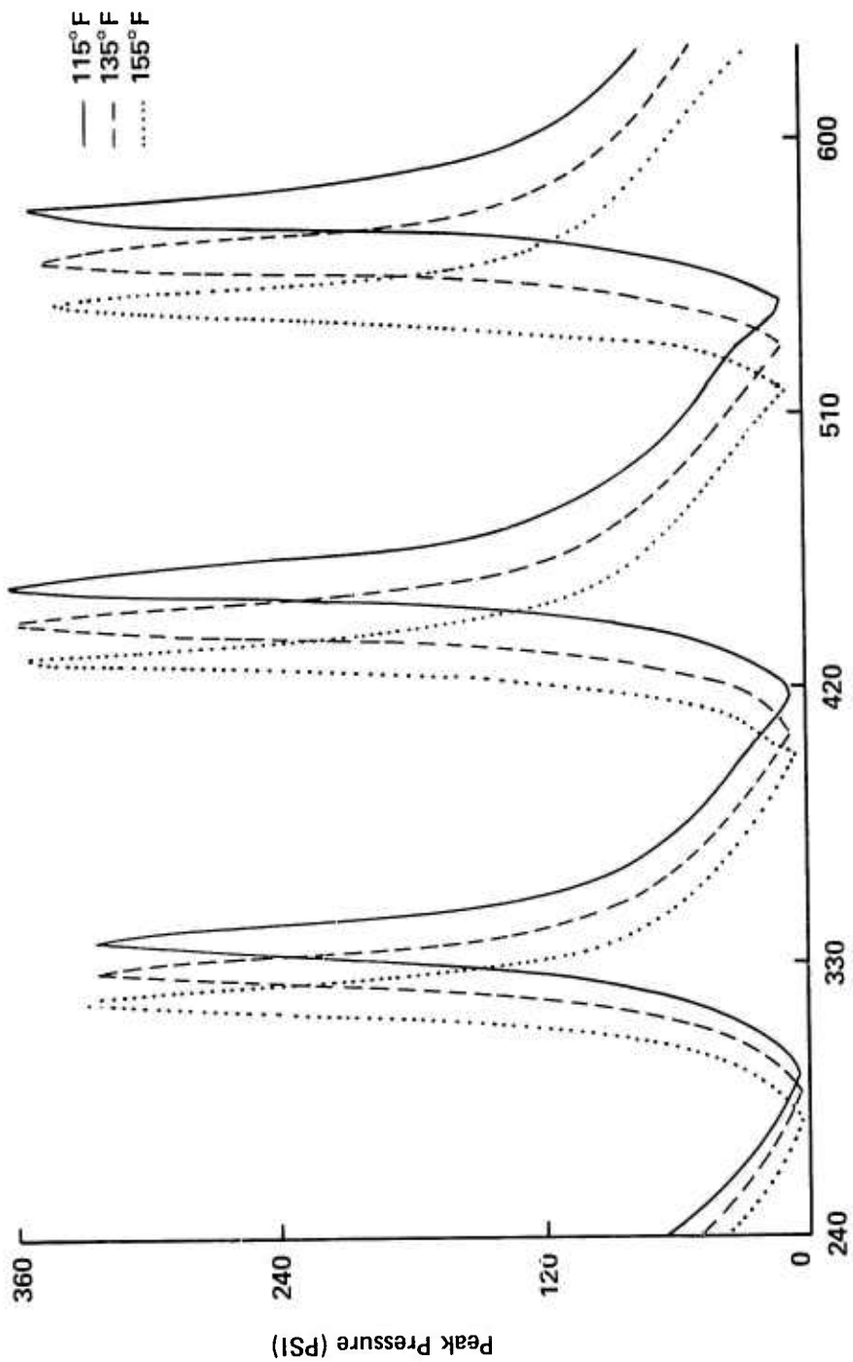

Figure 20. Effect Of Temperature On Frequency Response

was less than 1.5%. The resonant rpm, however, changed significantly as was expected. To understand this effect, the frequency response from 0 to 4000 rpm (600 Hz) must be considered. As calculated by HSFR, the first system resonance occurred at 705 rpm (105.75 Hz) for a system temperature of 115°F, and decreased 20 rpm (3 Hz) for each 20°F rise in temperature. The system responded at near multiples of this first resonant frequency. The data in Table V corresponded to the third, fourth and fifth resonant frequencies. For a 20°F rise in temperature, the third resonant frequency decreased 60 rpm (9 Hz) or 2.7%, the fourth resonant frequency decresed 80 rpm (12 Hz) or 2.7%, and the fifth resonant frequency decreased 100 rpm (15 Hz) or 2.7%. This indicated a leftward shifting of the entire frequency response curve by a significant amount, especially at normal operating frequencies of 3000-4000 rpm (450-600 Hz). This could be critical to the engineer who must design his aircraft hydraulic system to operate away from resonant frequencies for a range of temperatures.

The attenuation, which is also given in Table V, decreased 3.2% for a 5°F temperature rise, primarily due to the smaller viscosity and hence smaller ω_v. The phase constant, however, increased 0.6% due to the decreased speed of sound associated with the 5°F temperature rise. P_{max} decreased slightly, about 1%, for a 5°F temperature increase. Thus, as expected, a temperature increase has two significant effects, decreased resonant frequencies and decreased attenuation.

Effect of Kinematic Viscosity, Density and Bulk Modulus

Considering the large effect of temperature, it was interesting to consider separately the effect of slight variations in fluid

Table VI. Effect of Kinematic Viscosity, Density, and Bulk Modulus

Kinematic Viscosity (in^2/sec)			
	0.0212	0.0228	0.0245
$\|\alpha_1\|L$	0.05976	0.06203	0.06436
$\|\alpha_2\|L$	0.06052	0.06273	0.06509
$\|\beta_1\|L$	4.9875	4.9897	4.9919
$\|\beta_2\|L$	5.0071	5.0094	5.0116
P_{max}	100.22 psi	100.13 psi	100.05 psi

Density ($lbf\text{-}sec^2/in^4$)			
	$0.814x10^{-4}$	$0.817x10^{-4}$	$0.820x10^{-4}$
$\|\alpha_1\|L$	0.06192	0.06203	0.06215
$\|\alpha_2\|L$	0.06261	0.06273	0.06284
$\|\beta_1\|L$	4.9806	4.9897	4.9988
$\|\beta_2\|L$	5.0002	5.0094	5.0186
P_{max}	100.50 psi	100.13 psi	99.77 psi

Bulk Modulus (psi)			
	$0.226x10^6$	$0.233x10^6$	$0.240x10^6$
$\|\alpha_1\|L$	0.06294	0.06203	0.06117
$\|\alpha_2\|L$	0.06365	0.06273	0.06185
$\|\beta_1\|L$	5.0624	4.9897	4.9203
$\|\beta_2\|L$	5.0827	5.0094	4.9394
P_{max}	97.26 psi	100.13 psi	102.93 psi

properties which change with temperature, namely kinematic viscosity, density and bulk modulus. This was done by using reference values at 115°F for two of the three fluid properties and varying the third. Data were not obtained using the HSFR program as only temperature and not the actual fluid properties were read into the program. However, data for α, β, and P_{max} were obtained and are given in Table VI.

The kinematic viscosity values of 0.0212, 0.0228, and 0.0245 in^2/sec are those for MIL-H-5606-B hydraulic fluid at 120°F, 115°F and 110°F respectively. This is equivalent to a variation of $\pm$ 7% from the reference viscosity. The attenuation increased 3.7% for an increase in viscosity equivalent to that due to a 5°F drop in temperature. The phase constant increased only 0.04% for the same viscosity change. Also, P_{max} decreased slightly, 0.8%. Thus the primary effect of increased viscosity is increased attenuation.

The density values of 0.814×10^{-4}, 0.817×10^{-4} and 0.820×10^{-4} $lbf\text{-}sec^2/in^4$ are for MIL-H-5606-B hydraulic fluid at 125°F, 115°F and 105°F respectively. This is equivalent to a variation of 0.37% from the reference density. Both the attenuation and the phase constant increased slightly, 0.2%, for a 0.37% increase in density, while P_{max} decreased 0.4% for a 0.37% increase in density. Thus there is no significant effect due to small density changes.

The bulk modulus values of 0.226×10^6, 0.233×10^6, and 0.24×10^6 psi are those for MIL-H-5606-B hydraulic fluid at 125°F, 115°F and 105°F respectively. This is equivalent to a variation of $\pm$ 3% from the reference bulk modulus. The attenuation and phase constant decreased 1.4% and P_{max} increased 2.4% for an increase in bulk modulus of 3%.

Table VII. Effect of Steady-State Pressure

	Steady-State Pressure (psi)		
	2940	2970	3000
P_1	323.9 psi @ 2245 rpm	323.4 psi @ 2245 rpm	322.4 psi @ 2250 rpm
P_2	250.6 psi @ 2245 rpm	250.1 psi @ 2245 rpm	249.7 psi @ 2250 rpm
P_3	123.3 psi @ 2240 rpm	123.1 psi @ 2245 rpm	123.2 psi @ 2245 rpm

Table VIII. Effect of Young's Modulus

	Young's Modulus (psi)		
	0.29×10^8	0.30×10^8	0.31×10^8
P_1	322.8 psi @ 2245 rpm	323.4 psi @ 2245 rpm	323.6 psi @ 2250 rpm
P_2	249.8 psi @ 2245 rpm	250.1 psi @ 2245 rpm	250.6 psi @ 2250 rpm
P_3	123.3 psi @ 2240 rpm	123.1 psi @ 2245 rpm	123.3 psi @ 2245 rpm
$\lvert\alpha_1\rvert L$	0.06209	0.06203	0.06198
$\lvert\alpha_2\rvert L$	0.06279	0.06273	0.06268
$\lvert\beta_1\rvert L$	4.9940	4.9897	4.9856
$\lvert\beta_2\rvert L$	5.0138	5.0094	5.0053
P_{max}	99.75 psi	100.13 psi	100.30 psi

Effect of Steady-State Pressure

The steady-state line pressure, P_o, for the experiments was 2970 psig. Using this as a reference, data were taken for variations of $\pm$ 1%. No data are given for the attenuation, phase constant or P_{max} because the analysis assumes P_o is constant and uses P_o only for nondimensionalizing dynamic pressure. Thus the analytical results are unaffected by changes in steady-state pressure. The HSFR results, given in Table VII, showed a very small change in peak pressure, 0.3%. The resonant frequency increased slightly, 5 rpm (0.75 Hz) for a 60 psi increase in P_o. Thus small changes in the steady-state pressure have no significant effect. It is important to note that these results are for a hydraulic system, the fluid properties of which are not significantly affected by small changes in the steady-state pressure.

Effect of Young's Modulus

Young's modulus, Y_m, is a measure of the rigidity of the line and affects the speed of sound in the line. The larger Y_m is, the greater the local speed of sound. Y_m has no other effect on the calculations. As seen in Table VIII, a 3.3% increase in Y_m resulted in a small peak pressure change, 0.2%. The resonant rpm did increase 5 rpm (0.75 Hz) for a 6.7% increase in Y_m. Both the attenuation and the phase constant decreased slightly, 0.08% for a 3.3% increase in Y_m. The overall effect of small variations in Young's modulus is insignificant.

Effect of Entrained Air

This effect was looked at prior to any experiments being run to see if special precautions had to be taken to eliminate air bubbles in

Table IX. Effect of Entrained Air on Peak Pressure

	Percent Air by Volume		
	0%	0.01%	0.1%
Peak Pressure	54 psi @ 1275 rpm		4 psi @ 1200 rpm
	83 psi @ 2075 rpm	52 psi @ 1675 rpm	4 psi @ 1500 rpm
	66 psi @ 2925 rpm	41 psi @ 2350 rpm	3 psi @ 2200 rpm
	31 psi @ 3775 rpm	21 psi @ 3050 rpm	4 psi @ 2550 rpm
			3 psi @ 2900 rpm

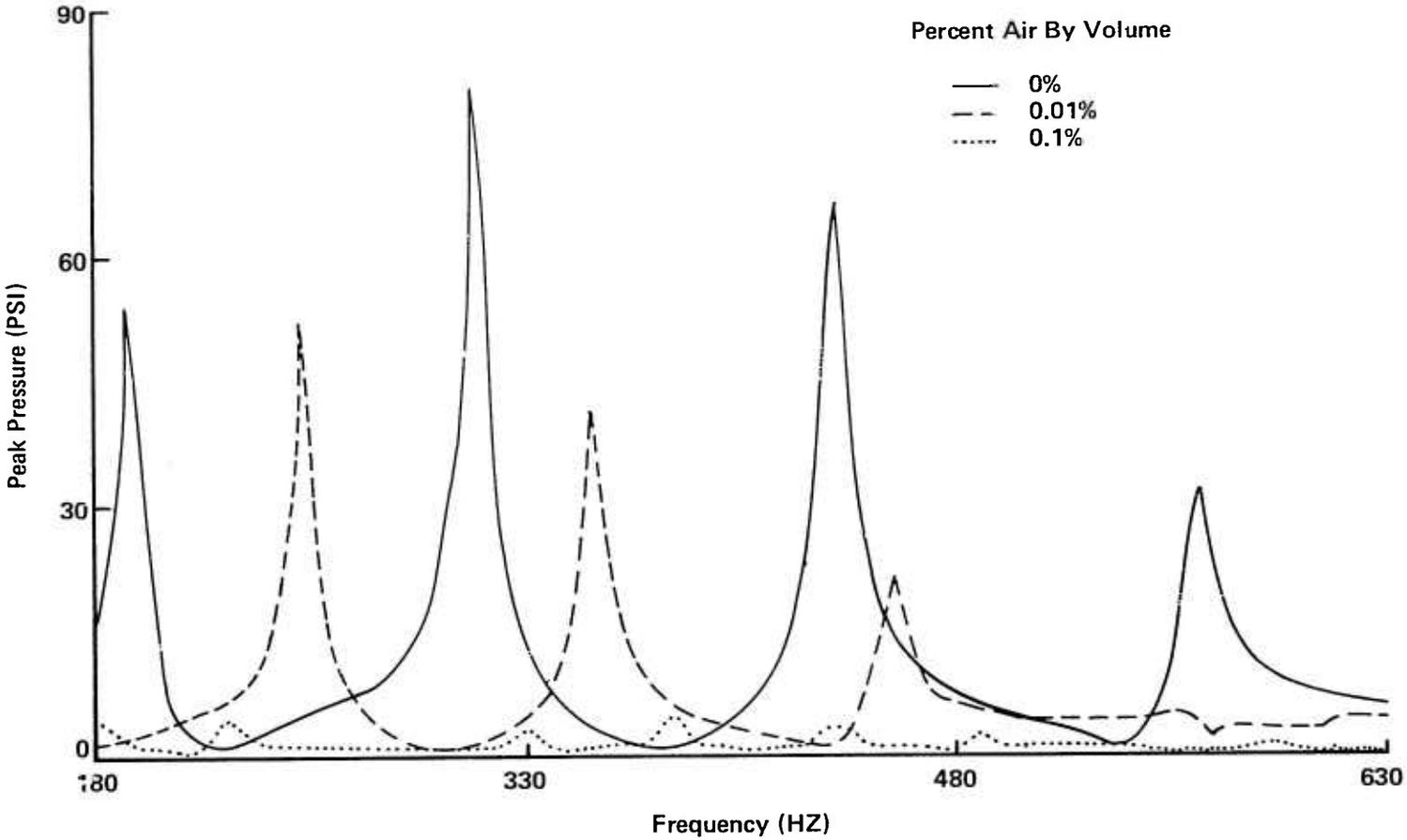

Figure 21. Effect Of Entrained Air On Frequency Response

the line prior to test runs. The HSFR computer program was used with Configuration One modeled for no flow and a steady-state pressure of 3000 psig. The fluid properties, in particular the bulk modulus, were modified to account for the entrained air. Numerical results for a point 42 in. from the pump are given in Table IX and Figure 21 for entrained air quantities of 0%, 0.01% and 0.1% by volume. The frequency response shown in Figure 21 demonstrates how large an effect 0.01% air by volume can have. The peak pressures are lowered 62-68% and the resonant frequencies are 19% lower. When the air volume is 0.1%, the pressure peaks are no longer significant.

These results indicate that even a very small amount of entrained air would cause significant changes to the frequency response of an actual hydraulic system. However, three things must be noted. First, it would be difficult to achieve 0.1% air by volume at 3000 psig. At 14.7 psi, the same air would occupy over two hundred times the volume it does at 3000 psig, assuming isothermal conditions. Thus the line, before the pump is started, would have over 20% air by volume, an unlikely situation for a system that has been bled. Secondly, much of the air that is present in the line will be trapped in the reservoir as the return flow enters the top of the reservoir and the pump intake flow departs the bottom of the reservoir. Thirdly, whatever air does remain in the line will quickly go into solution. Foster and Parker (12) note that at pressures above 500 psi, all entrained air in hydraulic fluid will be in solution and any effect of the air will have disappeared.

For hydraulic systems, the primary effect of entrained air is cavitation and the resulting component damage or failure in regions

where the pressure drops low enough, long enough, to allow air to come out of solution. This can happen near fast acting valves and the port plates of pumps where large pressure fluctuations occur. Detailed information of this effect can be found in an analytical and experimental study by Safwat and Van den Polder (29) of air bubbles coming out of aqueous solution downstream of a fast closing valve.

Effect of a Volume Element

A volume element, meaning a simple cavity attached to a fluid line, is often used to decrease dynamic prssure. Typically volume elements are found near valves in water lines to decrease waterhammer and also are found near hydraulic pumps in aircrft to decrease pump ripple. No-flow experimental data from Configurations 1, 2 and 3, which had volume elements of 19, 15.866 and 0 $in.^3$ respectively, were obtained using clampon transducers. The 19 $in.^3$ volume was a resonator used on F-4 aircraft and the 15.866 $in.^3$ volume was an aircraft filter cavity (filter removed). HSFR data were also obtained for the same three configuratons.

Figure 22 shows the frequency response at a point 191.125 in. from the pump for the three configurations. Similarly, Figure 23 shows the frequency response at a point 128.75 in. from the pump. In this last graph only data for volumes of 15.866 and 19 $in.^3$ are plotted to display better the effect of a small volume change. Likewise HSFR data at a point 40 in. from the pump for volumes of 15.866 and 19 $in.^3$ are plotted in Figure 24. The primary effect of an increase in volume, that of decreased peak pressures, is easily seen in these figures. Figure 22 also shows the leftward shift of the resonant rpm's. Table X gives comparative data for the pressure

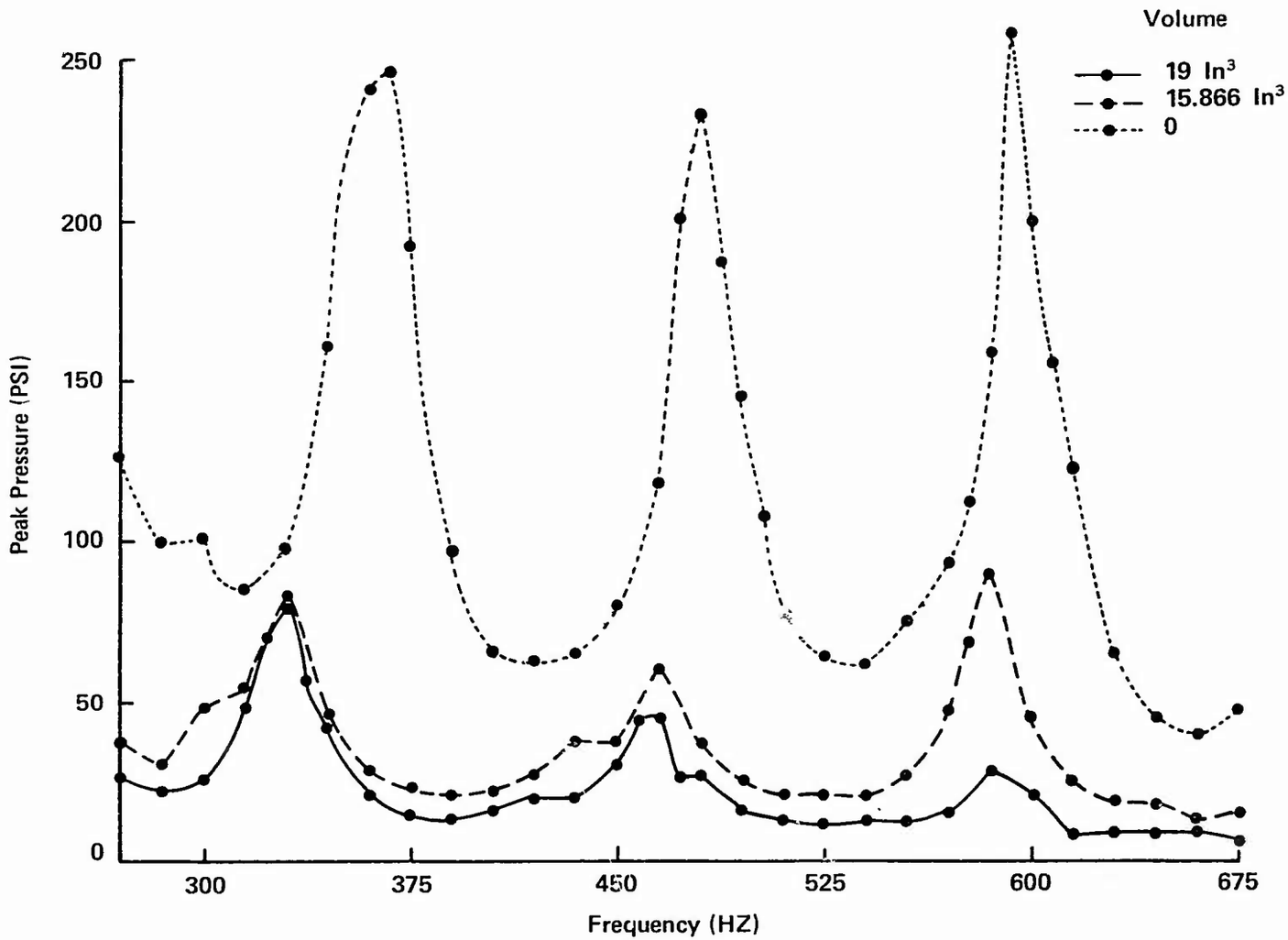

Figure 22. Effect Of Element Volume (Data Taken 191.125 In. From The Pump)

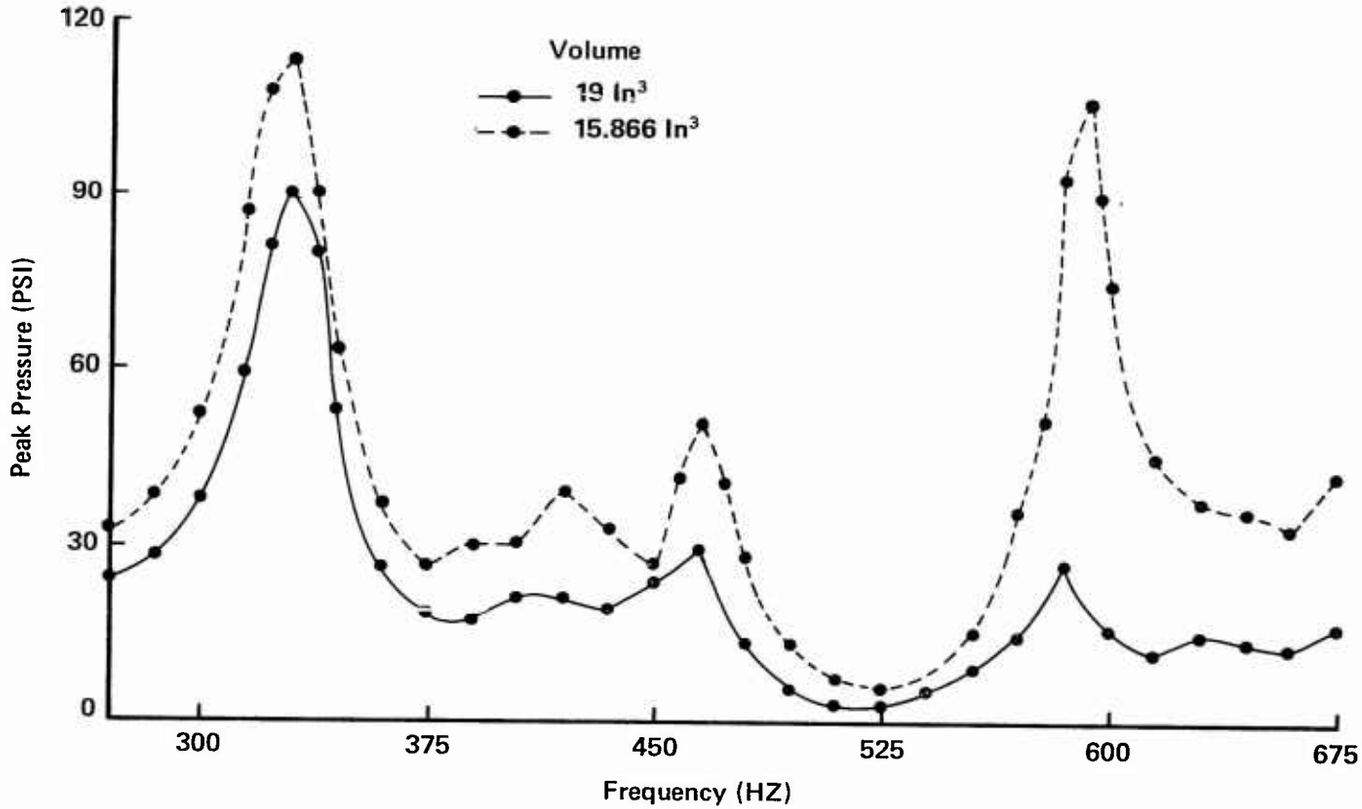

Figure 23. Effect Of Element Volume (Data Taken 128.75 In. From The Pump)

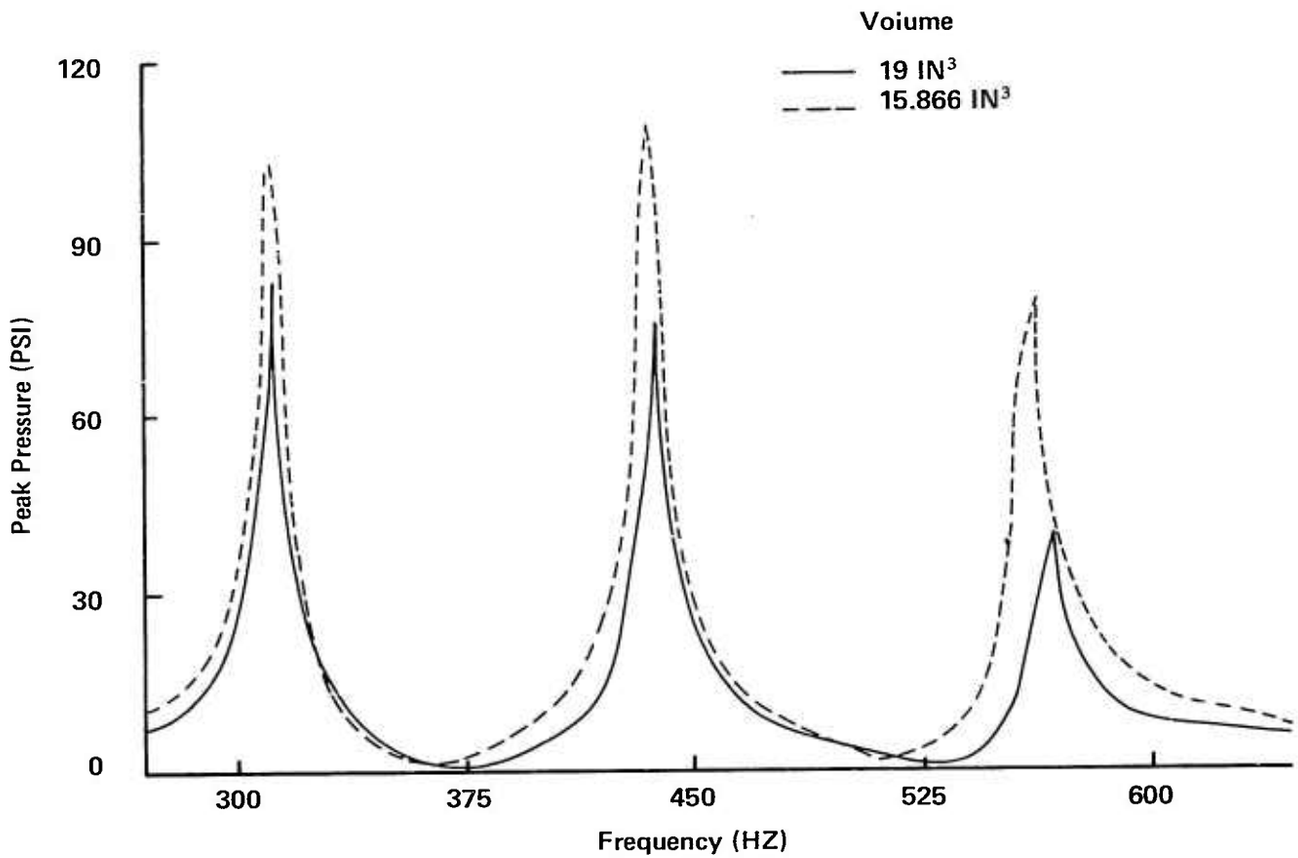

Figure 24. Effect Of Element Volume (HSFR Data For 40 In. From The Pump)

Table X. Effect of Element Volume

Volume ($in.^3$)	Experimental Data 128.75 in. from Pump		HSFR Data 40 in. from Pump	
	Peak Pressure	Resonant rpm	Peak Pressure	Resonant rpm
0	243.7 psi	2400	131.0 psi	2275
15.866	112.3 psi	2200	103.2 psi	2075
19	90.2 psi	2200	82.4 psi	2075
0	85.1 psi	3200	296.6 psi	3075
15.866	51.7 psi	3100	108.5 psi	2900
19	29.4 psi	3100	75.3 psi	2925
0	267.6 psi	3950	358.7 psi	3900
15.866	105.6 psi	3950	79.5 psi	3750
19	27.5 psi	3900	39.8 psi	3775

peaks. The experimental pressure data are probably high due to the effect of vibration on the clampon transducers. The data presented are for a point far from the pump and the bends to minimize the vibration. Despite some vibration error, the trends are valid. Increased line volume causes a large decrease in dynamic pressure, especially at the resonant frequencies. The resonant frequencies themselves are lower; much lower, 200 rpm (30 Hz), at the lower frequencies and only slightly lower at the higher frequencies. Also at the higher rpm's, the decrease in peak pressure is larger than at the lower rpm's. Thus, increased frequency has the effect of accentuating the pressure decrease yet minimizing the resonant rpm shift. Considering that most aircraft hydraulic systems have operating frequencies between 3000 and 4000 rpm (450 and 600 Hz), the small resonant frequency shift can be neglected by the designer, but the large pressure decrease is important. Should other considerations require a system to operate near a resonant frequency, the engineer has a means of eliminating large amplitude dynamic pressure.

Summary

Of the eleven variables considered in this sensitivity analysis, variations in only a few need concern the hydraulic engineer. Generalized results are given in Table XI.

Table XI

Generalized Effect of a Small Increase in Sensitivity Variable

Sensitivity Variable	Peak Pressure	Resonant Frequency	$\|\alpha\|L$	$\|\beta\|L$
L	---	↓↓	NA	NA
R	---	↑↑	↓↓	---
W	---	---	---	---
T	---	↓↓↓	↓↓	↑
ν	NC	NC	↑↑	---
ρ	NC	NC	↑	↑
B_m	NC	NC	↓	↓
P_o	---	---	NC	NC
Y_m	---	---	---	---
Entrained Air	↓↓↓	↓↓↓	NC	NC
Element Volume	↓↓↓	---	NC	NC

Legend:

↑↑	moderate increase	↓↓↓	large decrease
↑	small increase	↓↓	moderate decrease
---	negligible change	↓	small decrease
NC	not calculated	NA	not applicable

VIII. Analytical Results for Hydraulic Lines

Introduction

The analysis based on the confluent hypergeometric function was used to study the effect of mean flow on hydraulic lines. Three results are given: attenuation, the phase constant, and velocity profile data. Eqs (88), (89), (96) and (98) were used to calculate the attenuation and phase constant. Using these results in Eqs (90), (105), (106) and (107), the velocity profile was calculated. Both the attenuation and the phase constant were calculated for flow rates up to 100 gpm for a straight line with the same geometry and fluid properties as Configuration Five from the experiments. The analysis yields the dimensionless propagation constant, $\Gamma = \gamma L$, which is a complex number. The real part of γ is the attenuation, α, and the imaginary part is the phase constant, β. Values of α and β for both left and right traveling waves were calculated. The subscript one is used for the right traveling or forward wave and the subscript two is used for the left traveling or backward wave. The subscript zero denotes the no-flow value. Since γ, as defined by Eq (40), was not set negative, it carries its own algebraic sign. The numerical results for both the real and imaginary parts of γ are negative numbers. This is correct as a positive value for the real part of γ would correspond to signal growth, not attenuation. Considering that both the attenuation and the phase constant are typically quoted as positive numbers in the literature, the negative signs are dropped and all figures and discussions consider α and β as positive.

Quite by accident, solutions were found in which the real and imaginary parts of γ were positive, corresponding to signal growth. The magnitudes of α and β were of the same order as those corresponding to signal attenuation. Since these solutions were not physically realizable, they were discarded. However, the point that there are more than two allowable modes of signal propagation, at least mathematically, was demonstrated.

Most of the results are for flow rates up to 5 gpm. This corresponds to laminar flow conditions with a Reynolds number, based on line diameter, of 1038. These relatively small mean flow velocities, 98 in/sec or M = 0.00178 for 5 gpm, result in small deviations from the classical results using the Bessel function expression for no-flow, Eq (99). The best way to see the effect of flow on α and β is by plotting the deviation from the no-flow case; i.e., $(\alpha_0-\alpha_1)L$ and $(\beta_0-\beta_1)L$. The line length, L, is used as a nondimensionalizing factor.

The classical Bessel function results for the attenuation per wavelength are functions only of ω/ω_ν and for gases the Prandtl number and the ratio of specific heats. The analytical results with flow are much more complicated and are dependent on many more parameters. Numerous calculations for hydraulic systems were made with results compared for data sets having identical values of ω/ω_ν. The parameters varied were the fluid properties and line geometry data. As expected, no-flow results showed no variation, but the results with flow varied slightly. Typically the results matched to three significant figures when an input parameter was varied by a factor of two. For those engineering applications where more accuracy is required,

results given here can be used to identify trends, but a computer solution must be used to determine numerical values.

Attenuation Results

The attenuation for both left and right running waves was calculated for a hydraulic line with a temperature of 70°F. Figure 25 gives the deviation in the attenuation versus flow rate for dimensionless frequencies from 1 to 187. Here ω_ν is 0.96 Hz. Two important trends can be noted from this plot. First, as the flow rate increases, the deviation in the attenuation increases, nearly linearly, for a constant value of ω/ω_ν. This larger deviation corresponds to a smaller forward wave attenuation. Second, the attenuation deviation for a constant flow rate increases with frequency. The calculated results also show that both α_0 and α_1 increase with frequency. Figure 26 depicts the deviation in attenuation plotted against dimensionless frequency, ω/ω_ν. The important thing to note here is that the attenuation deviation, while increasing with frequency for a constant flow rate, does not do so linearly. Rather, as the frequency increases, the attenuation deviation increases by smaller and smaller amounts, implying an asymptotic behavior at high frequencies.

Both of the previous figures presented data for a constant ω_ν. The next two figures show data for a constant frequency, ω, with ω_ν varying. Data for ω_ν = 6.04 rad/sec, the value used in Figures 26, 27 and 28, are compared with data for ω_ν half and twice this value. Figure 27 shows the dimensionless attenuation deviation versus flow rate where ω_ν is varied by changing the radius. Figure 28, on the other hand, depicts dimensionless attenuation deviation versus flow

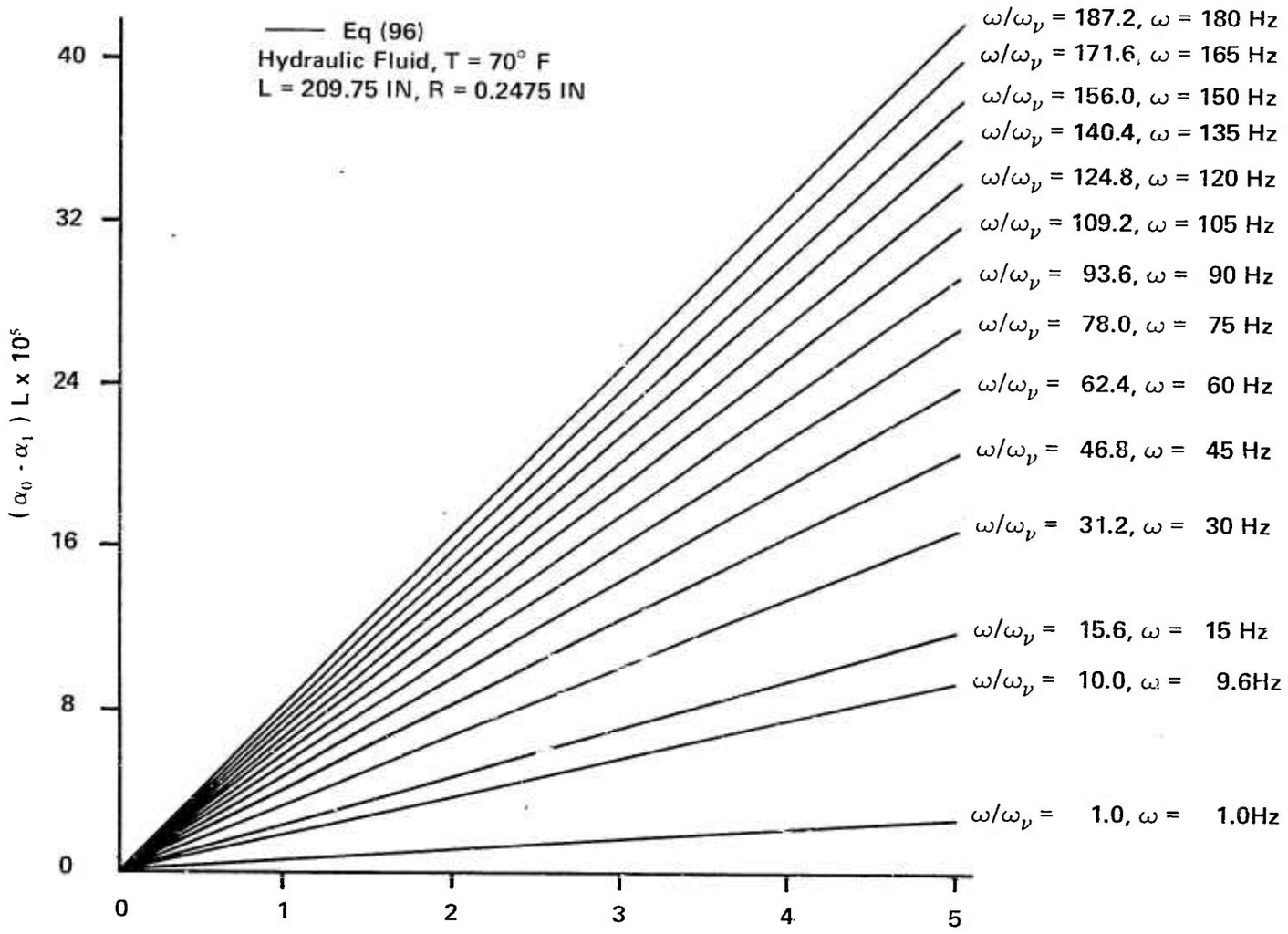

Figure 25. Attenuation Deviation Versus Flow Rate (ω_ν = 1 Hz)

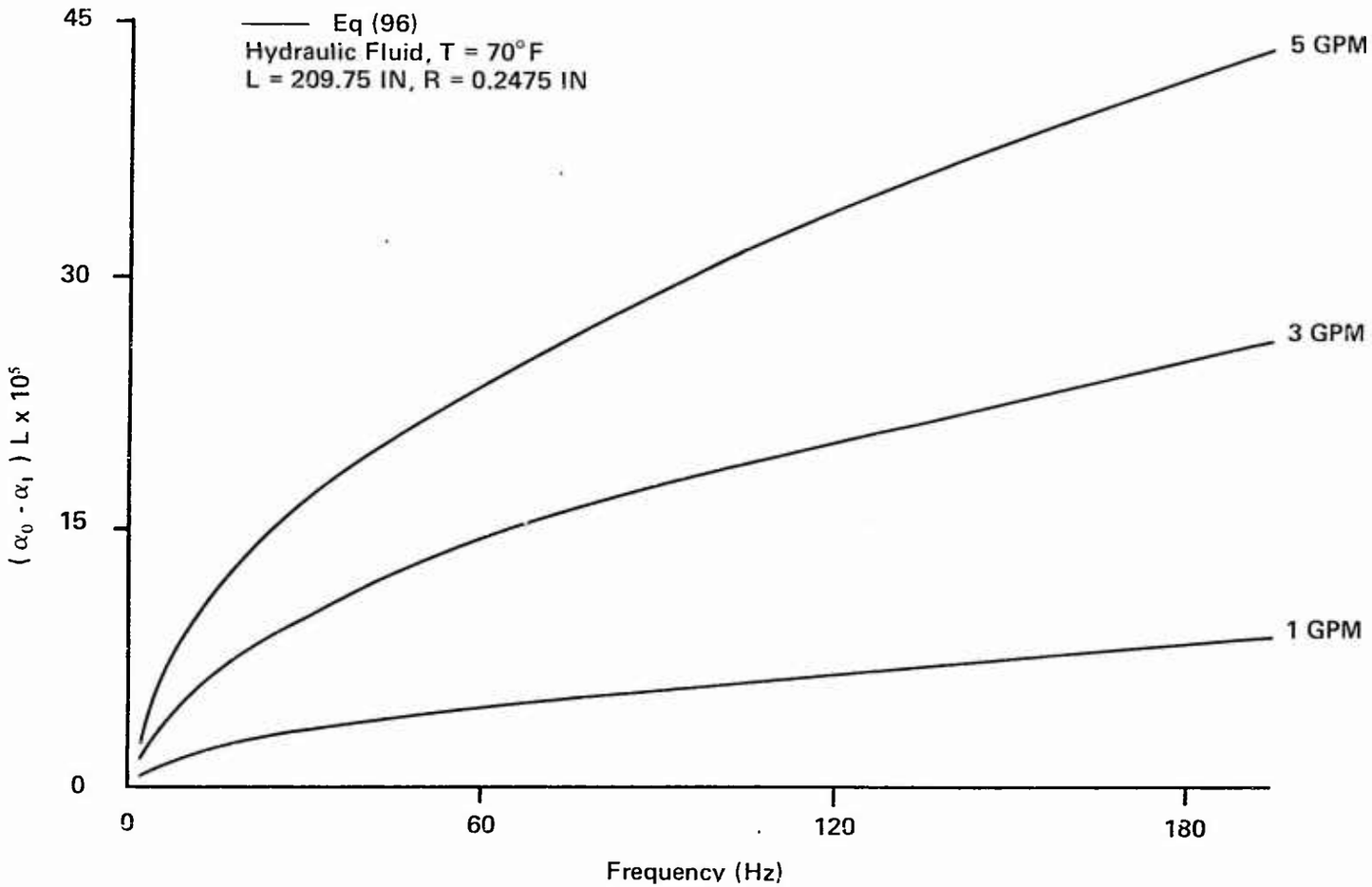

Figure 26. Attenuation Deviation Versus Frequency (ω_ν = 1 Hz)

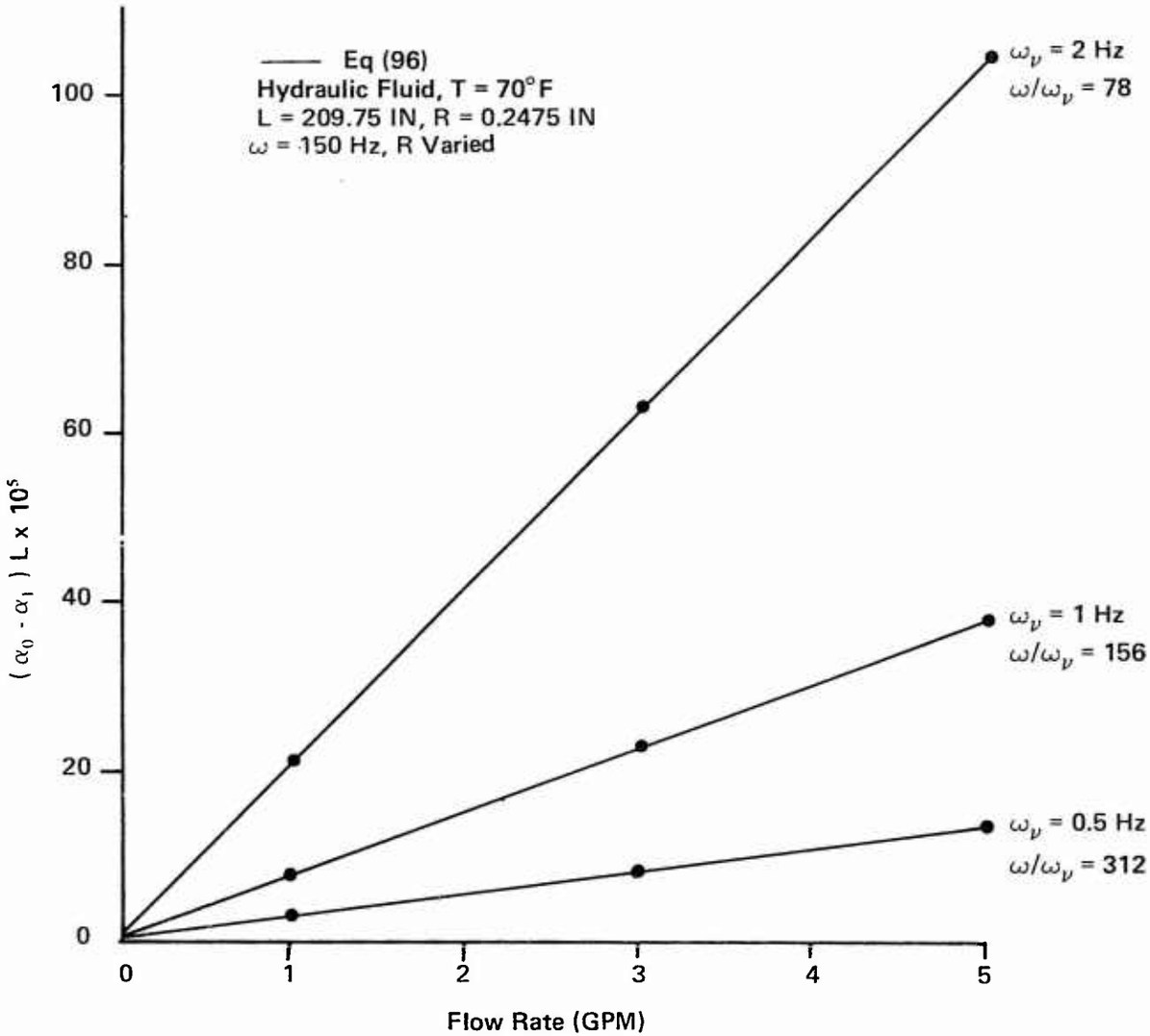

Figure 27. Effect of ω_ν on Attenuation Deviation

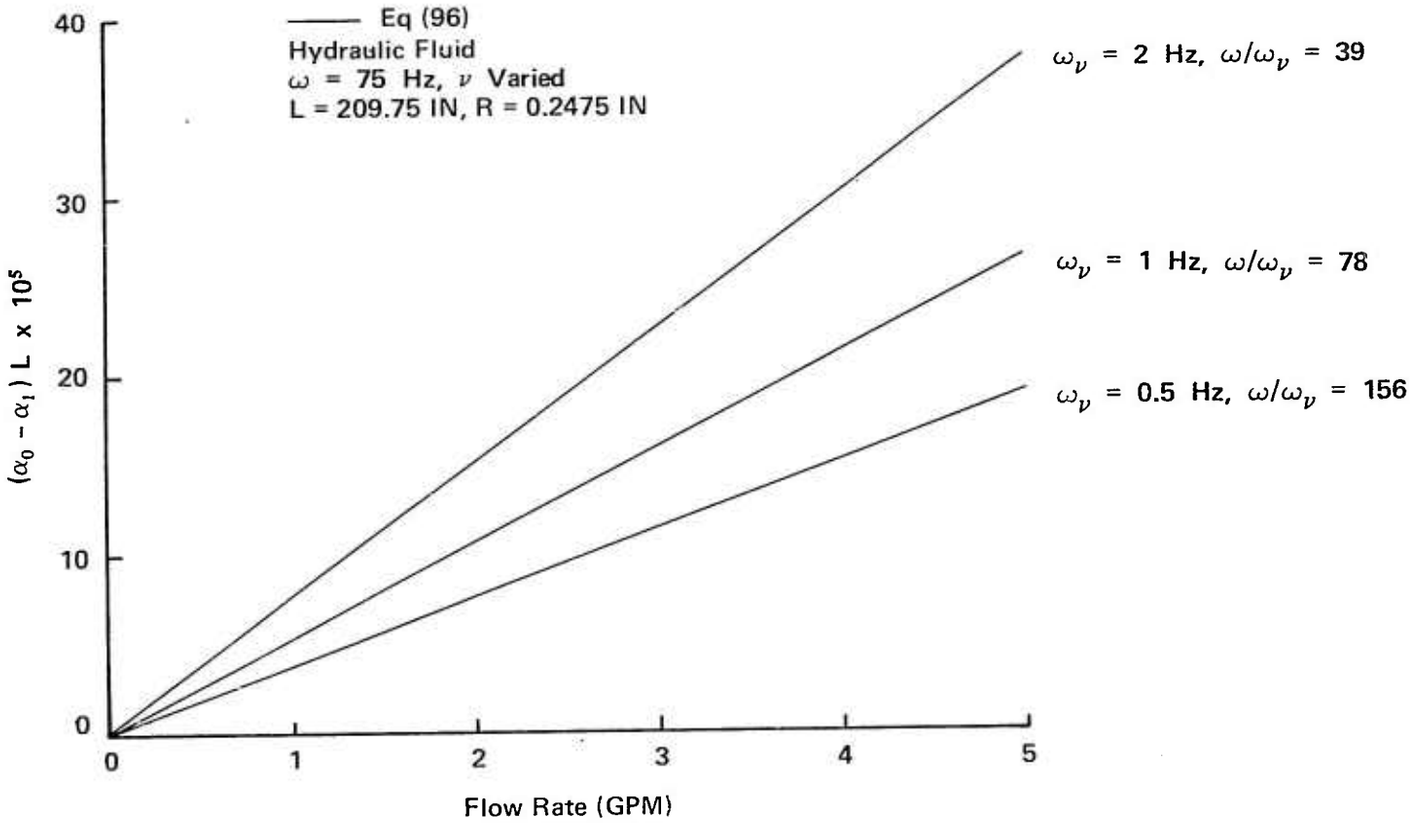

Figure 28. Effect Of ω_ν On Attenuation Deviation

rate where ω_ν is varied by changing the kinematic viscosity. Both graphs show that the attenuation deviation increases with increasing characteristic viscous frequency. Calculated results also show that both α_0 and α_1 increase with increasing ω_ν. Also the deviation increases, nearly linearly, with flow rate. Again this is due to α_1 decreasing with increasing flow rate. This nearly linear relationship was surprising considering the complex mathematical relations used to calculate the results. To check this out further, data were calculated for much higher flow rates, up to 100 gpm, which is equivalent to M = 0.036. Figure 29 shows the results for a frequency of 180 Hz for the same line geometry and fluid properties as used for the data in Figures 27 and 28. Under these conditions the flow would be turbulent for flow rates above 10 gpm, and thus the results given in Figure 29, which are based on laminar flow theory, represent laminar theory extrapolated into the turbulent regime. Figure 30 depicts data for the same line geometry but a frequency of 195 Hz and a kinematic viscosity of 4.72 $in.^2/sec$ which is a hundred times larger than normal. Under these admittedly unrealistic conditions, the flow is laminar at flow rates exceeding 100 gpm. The trend depicted on both curves is the same. The attenuation deviation increases nearly linearly with flow rate. However, a slight dropping off of the curve can be noted at the high flow rates. If a straight line were drawn through the origin and the 5 gpm data point, it would yield a value at 100 gpm for the nondimensional attenuation deviation 3% higher than the turbulent results and 6% higher than the laminar results.

All of the attenuation results just presented are for the forward traveling wave. For all cases α_1 is smaller than α_0 and α_2 is

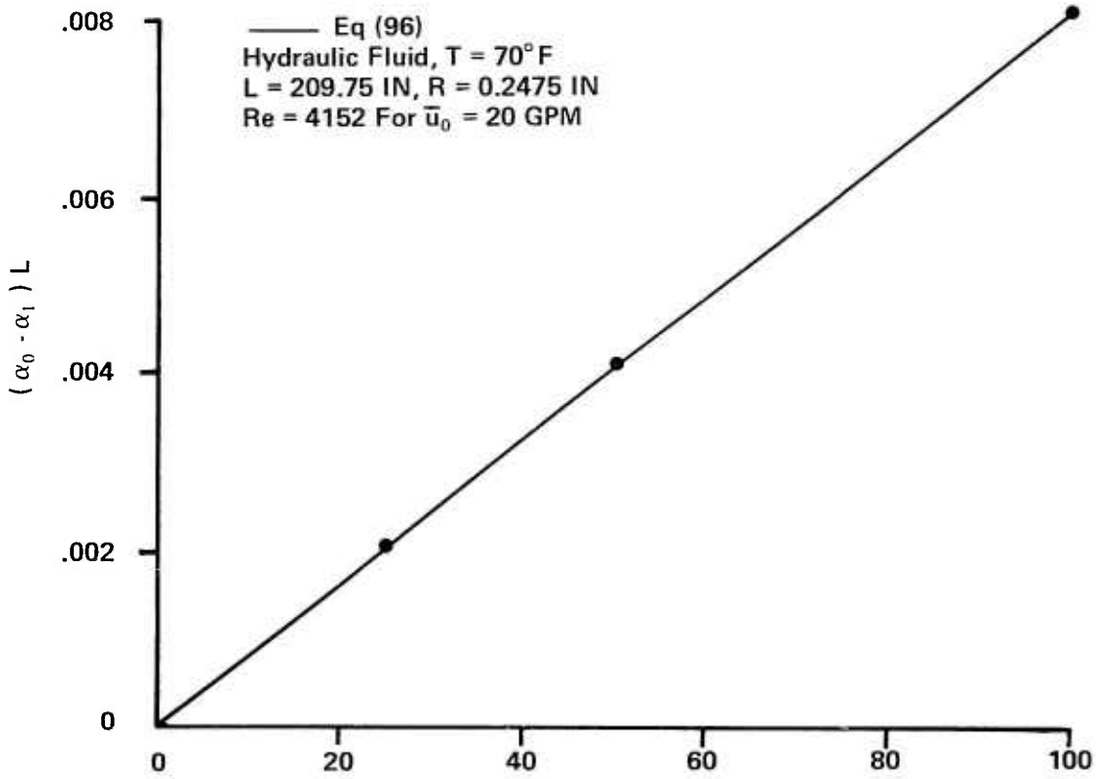

Figure 29. Attenuation Deviation For Large Flow Rates (Turbulent)

ω_ν = 1.0 Hz, ω/ω_ν = 183.5

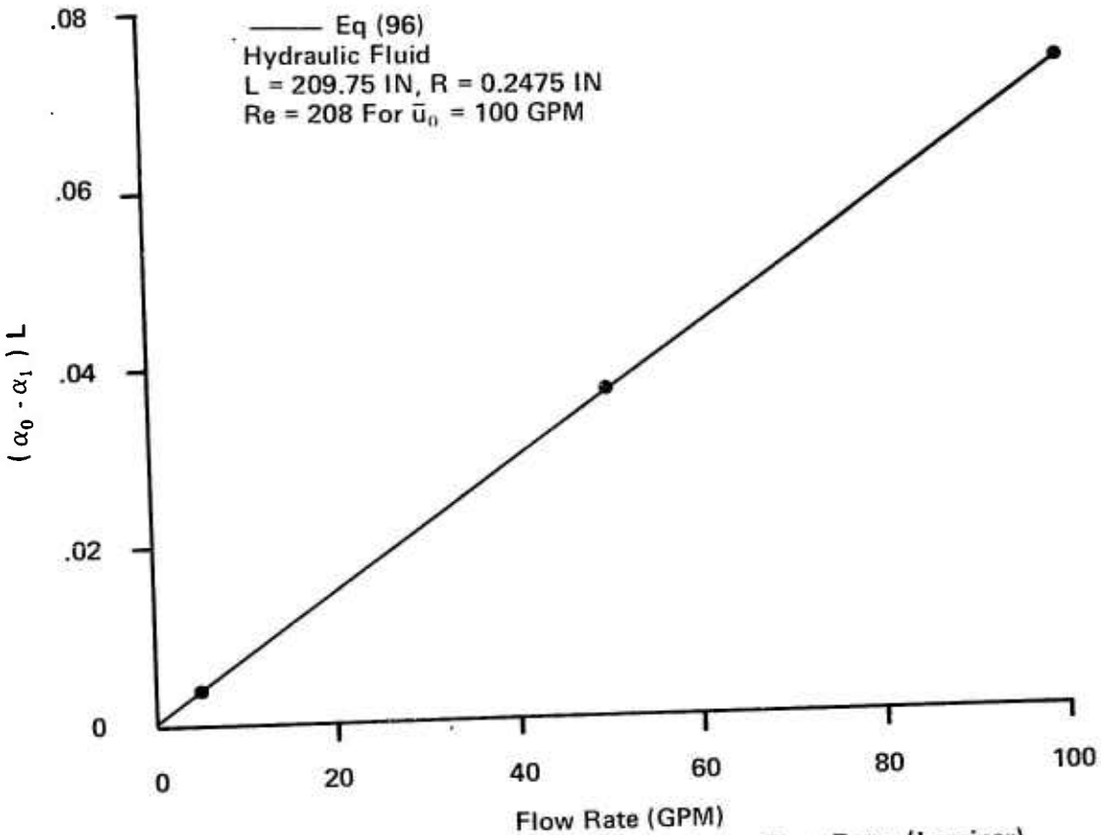

Figure 30. Attenuation Deviation For Large Flow Rates (Laminar)
ω_ν = 96 Hz, ω/ω_ν = 2.0

larger than α_0. At the low mean flows, 5 gpm and less, the backward wave attenuation, α_2, is less than 1% higher than the forward wave attenuation, α_1, and less than 0.5% higher than α_0. The smaller the flow rate, the smaller the difference between α_1 and α_2. The larger backward wave attenuation is due to the inclusion of the parabolic mean flow velocity profile in the analysis.

One main point must be emphasized. While the attenuation data show the effect of mean flow, this effect is very small, at least for the low mean flows considered. Looking back at Figure 25, the largest attenuation deviation, that for 5 gpm at 180 Hz, is 4.2×10^{-4}. For this condition, $\alpha_0 L = 0.0816$ and thus the deviation is only 0.5% of the no-flow attenuation. Even for the worst case, 100 gpm, the deviation is only 6% of the no-flow attenuation. For most engineering purposes the no-flow results are adequate. If further accuracy is required, the no-flow results can be modified using the results of this research. Precise results are possible using the analysis formulated in this research but they are expensive in terms of computer time. For example, the data point for 50 gpm at 180 Hz required 518 seconds of execution time on the CDC Cyber 74 computer.

Phase Constant Results

The phase constant was calculated for the same conditions as the attenuation. In all cases β_1 is smaller than β_0 and β_2 is larger than β_0. Figure 31 plots the dimensionless phase constant deviation versus flow rate for a constant value of ω_ν. Two trends are seen. First the phase constant deviation increases linearly with flow rate for a constant value of ω/ω_ν. This is due to β_1 decreasing with increasing flow rate. Also the phase constant deviation increases with

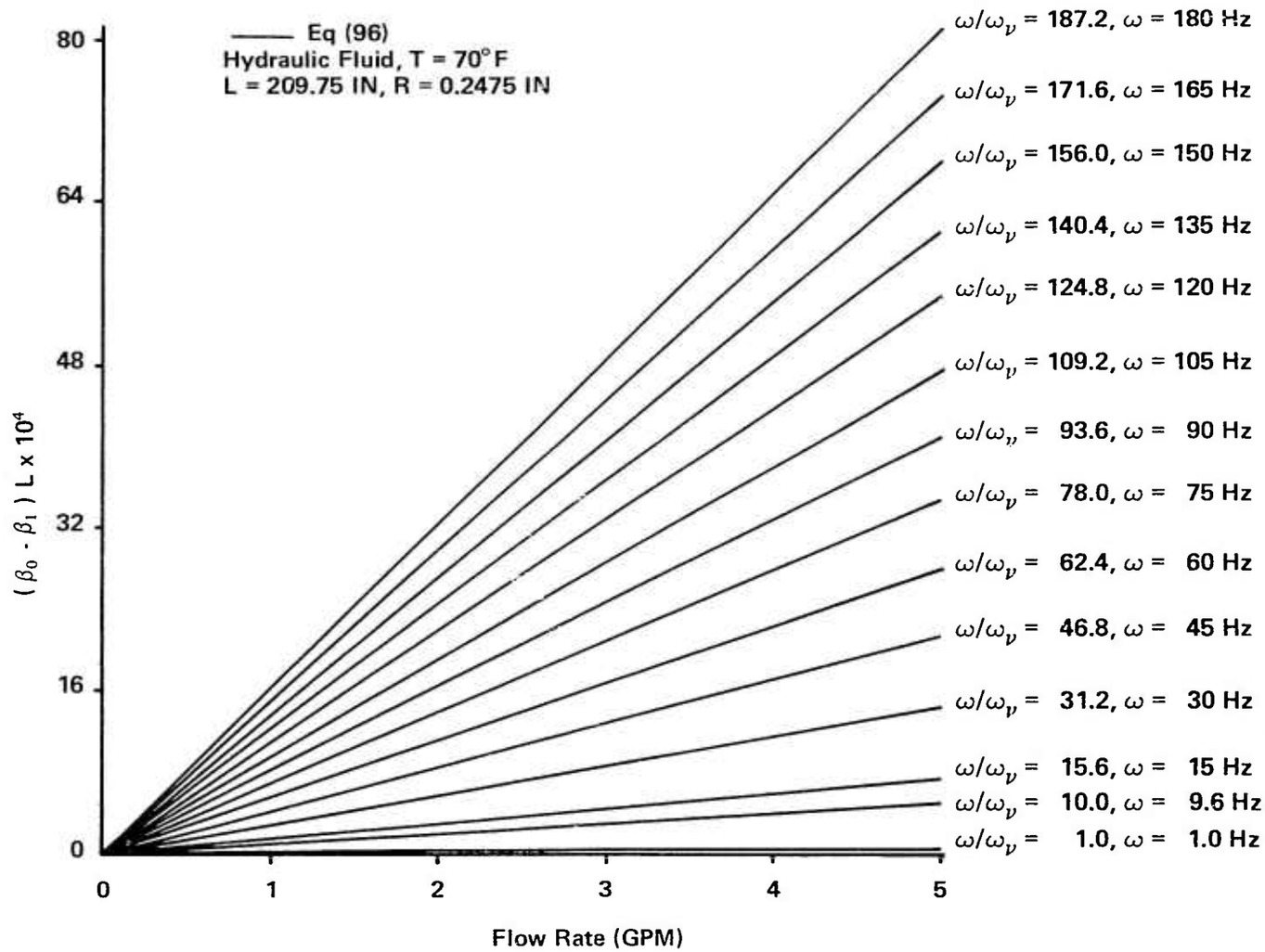

Figure 31. Phase Constant Deviation Versus Flow Rate (ω_ν = 1 Hz)

increasing frequency at a constant flow rate. Not only does $(\beta_0-\beta_1)L$ increase with increasing frequency, but also intermediate computer results show that both β_0 and β_1 increase with increasing frequency too, with β_0 increasing faster than β_1. Figure 32 shows this trend also. Here the deviation is plotted against ω/ω_ν. The phase constant deviation is seen to increase linearly with frequency at a constant flow rate. These last two graphs had a constant value of ω_ν. Figure 33 shows the effect of varying ω_ν with ω held constant. As with the attenuation, the phase constant deviation increases with increasing ω_ν regardless of whether ω_ν is varied by changing the radius or the kinematic viscosity. In the lower plot, the spread between the curves for constant ω_ν is greater than in the upper plot. This is expected since the frequency, 150 Hz, is twice that in the upper plot. The results for large flow rates, given in Figure 34, also show a nearly linear increase in the phase constant deviation for a constant value of ω_ν. If a straight line were drawn between the origin and the 5 gpm data point, it would yield a value at 100 gpm for the nondimensional phase constant 1% higher than the result extrapolated into the turbulent regime and 4% higher than the laminar result.

The phase constant for the background traveling wave is just slightly larger than β_0 and β_1. The larger the mean flow, the larger the difference in the phase constants. The backward wave phase constant is only 0.3% larger than the forward wave constant for 5 gpm at 180 Hz, and 0.18% larger than β_0. Also at this frequency, β_2 is 2% larger than β_1 at 25 gpm and 4% larger at 50 gpm.

The main result of the calculations is that the change in the phase constant at low flow rates is very small. Looking at Figure 31,

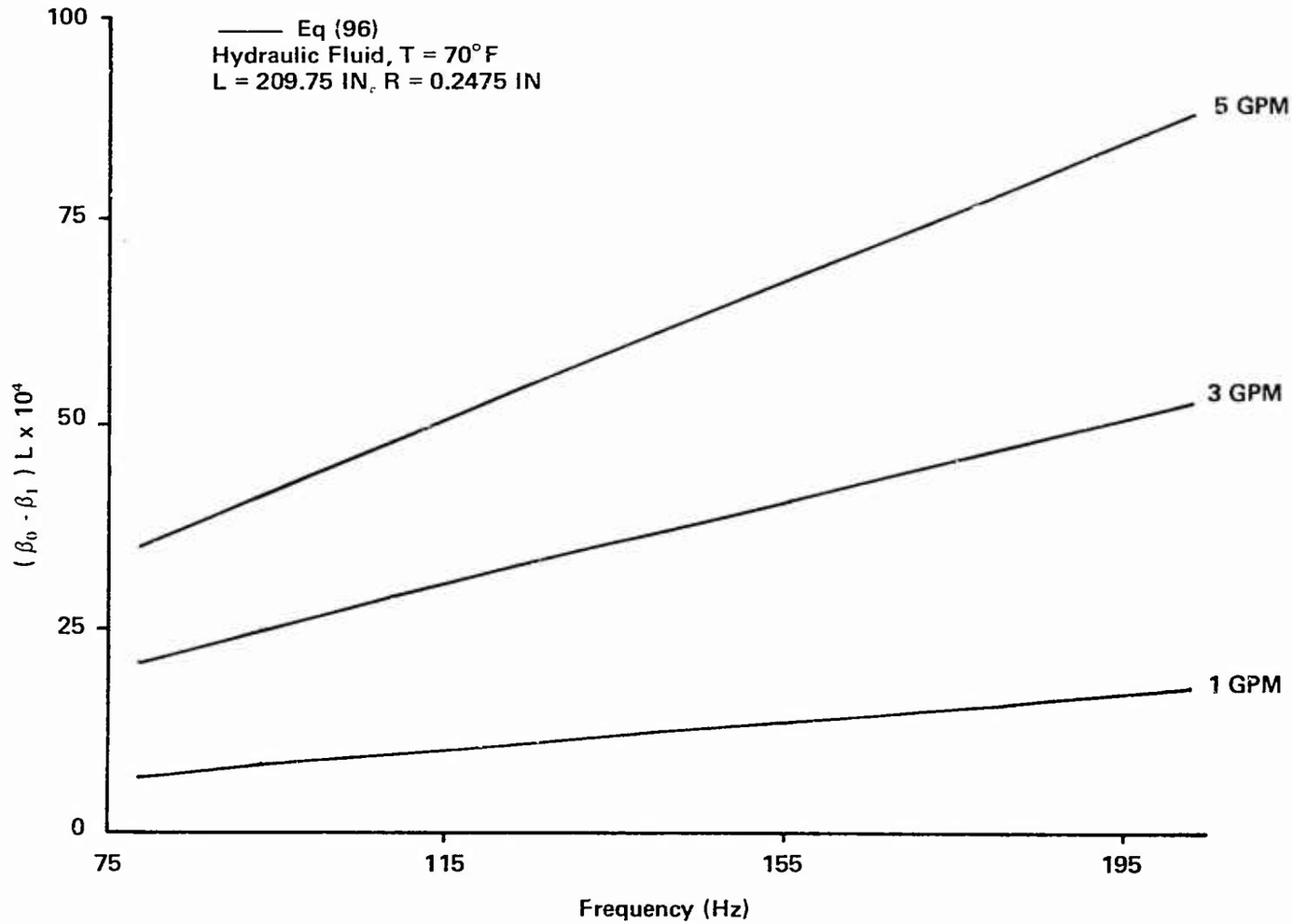

Figure 32. Phase Constant Deviation Versus Frequency (ω_ν = 1 Hz)

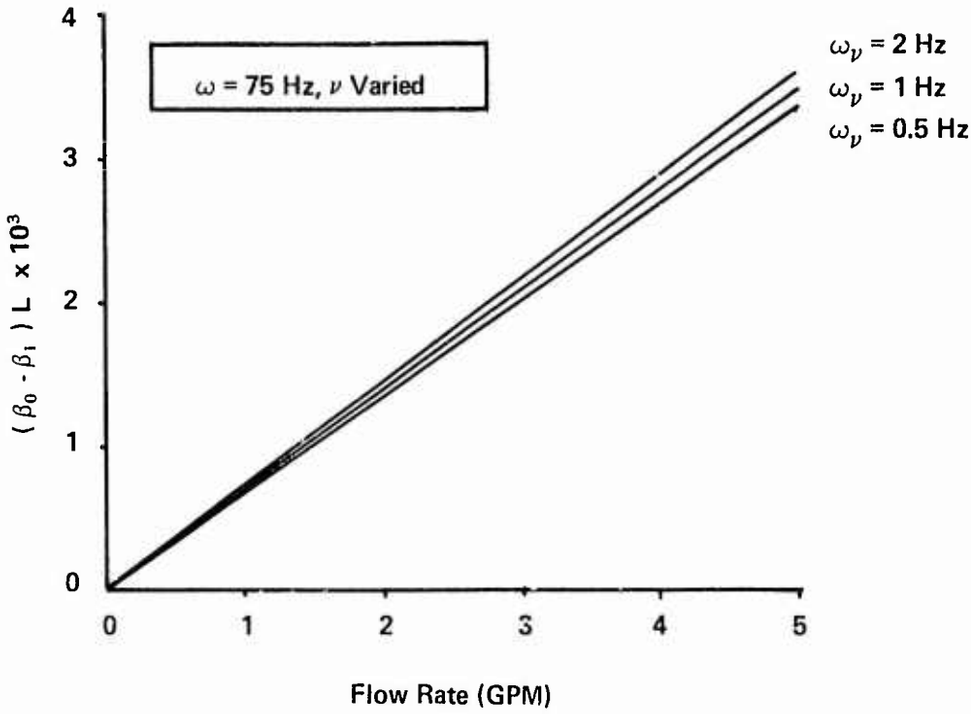

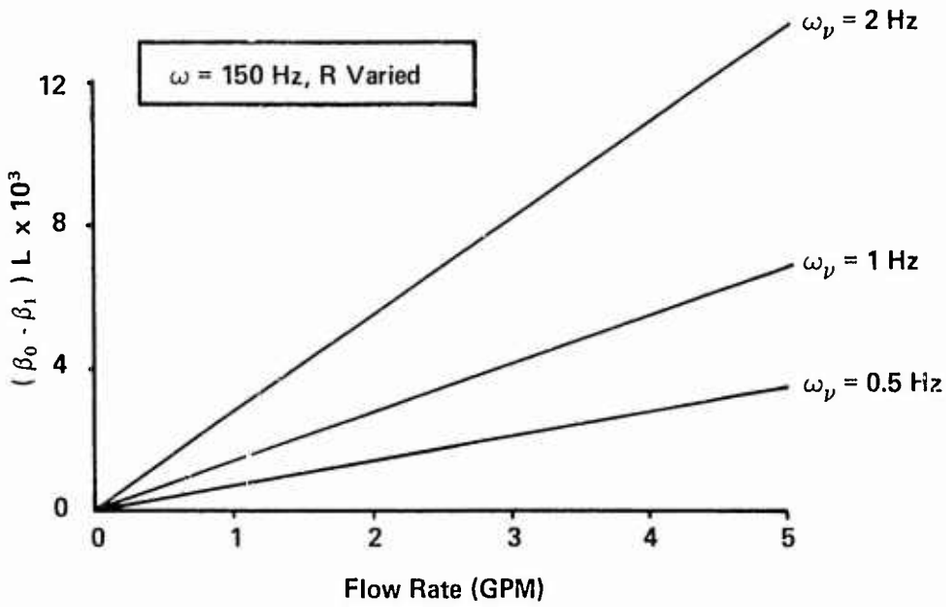

Figure 33. Effect of ω_ν on Phase Constant Deviation
(Hydraulic Fluid, L = 209.75 In)

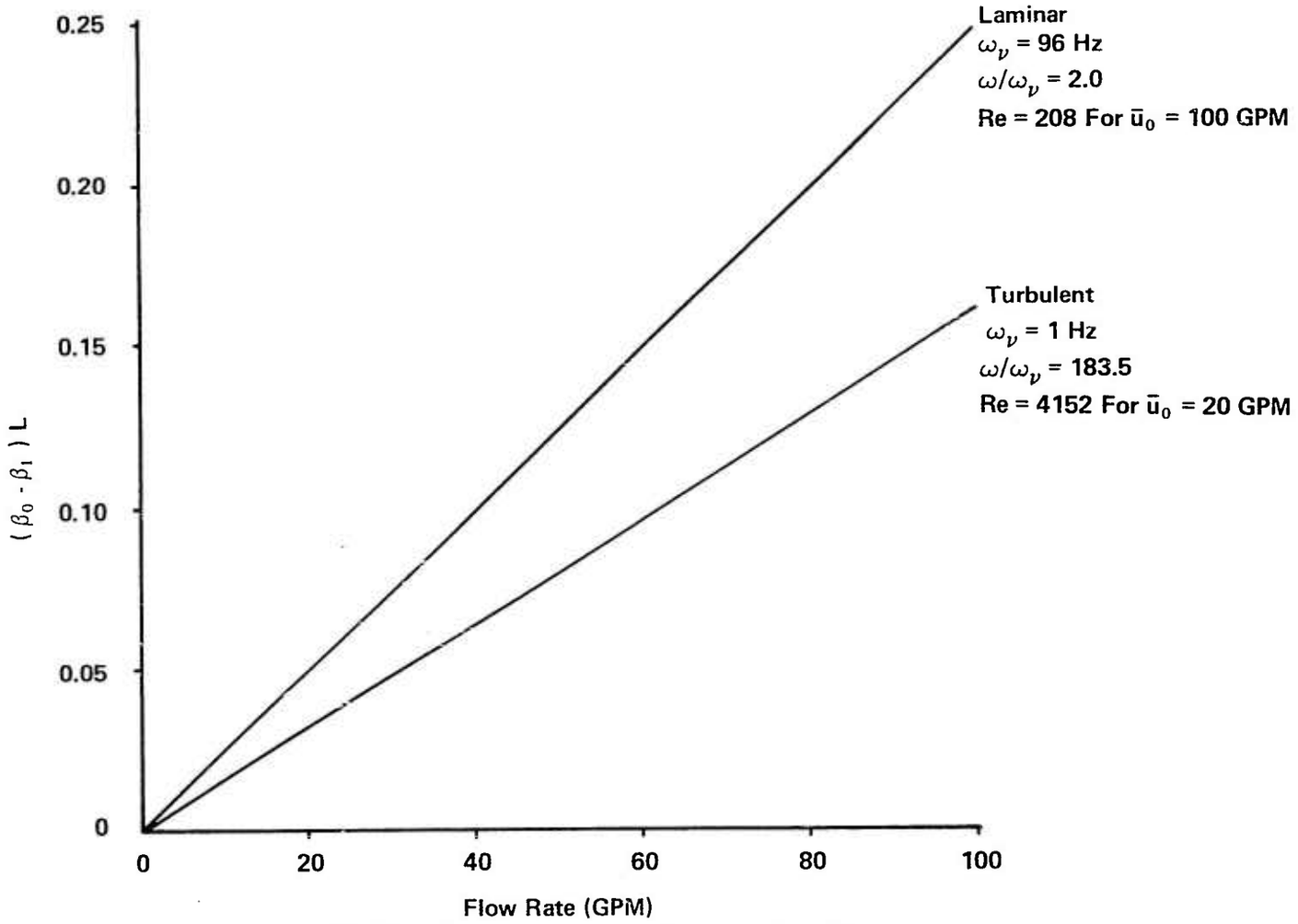

Figure 34. Phase Constant Deviation for Large Flow Rates
(Hydraulic Fluid, L = 209.75 In, R = 0.2475 In)

the largest dimensionless phase constant deviation is 8.1×10^{-3}. For this condition $\beta_0 L = 4.385$ and thus the deviation is only 0.2% of the no-flow phase constant for a mean flow of 5 gpm. Even for the highest flow rate, 100 gpm, the deviation is only 4% of the no-flow phase constant. If the phase constant results are put in an alternate form, namely the speed of propagation, the result for 5 gpm at 195 Hz is only 0.2% higher than for no-flow. At 100 gpm, the forward wave speed of propagation is 4.5% higher. For most engineering purposes, the no-flow results are adequate. If further accuracy is required, the no-flow results can be modified using the results of this research. Again, precise results are possible using the analysis formulated in this work on the computer.

Velocity Profile Results

A third outcome of the analysis is the velocity profile. One of the reasons for the increased accuracy of the analytical results is the inclusion of the mean flow parabolic velocity distribution in the equation of motion. The resulting velocity profile, consisting of the mean flow parabolic velocity profile modified by the oscillating velocity generated by the dynamic pressure, was calculated for the straight line hydraulic system, Configuration Five, at 210 Hz and $105^{\circ}F$ for mean flow rates from 0 to 5 gpm. The results are shown in Figures 35 through 38. The velocity is nondimensionalized using the maximum centerline velocity, $\overline{u}_{C/L}$, for the case of no-flow and $\overline{u}_o$ for the cases with mean flow. The phase angle, ϕ, which corresponds to the maximum value of the perturbation velocity at the centerline, is zero degrees. The effect near the pipe walls is most pronounced. There reverse flow exists for part of a cycle. This is due to the

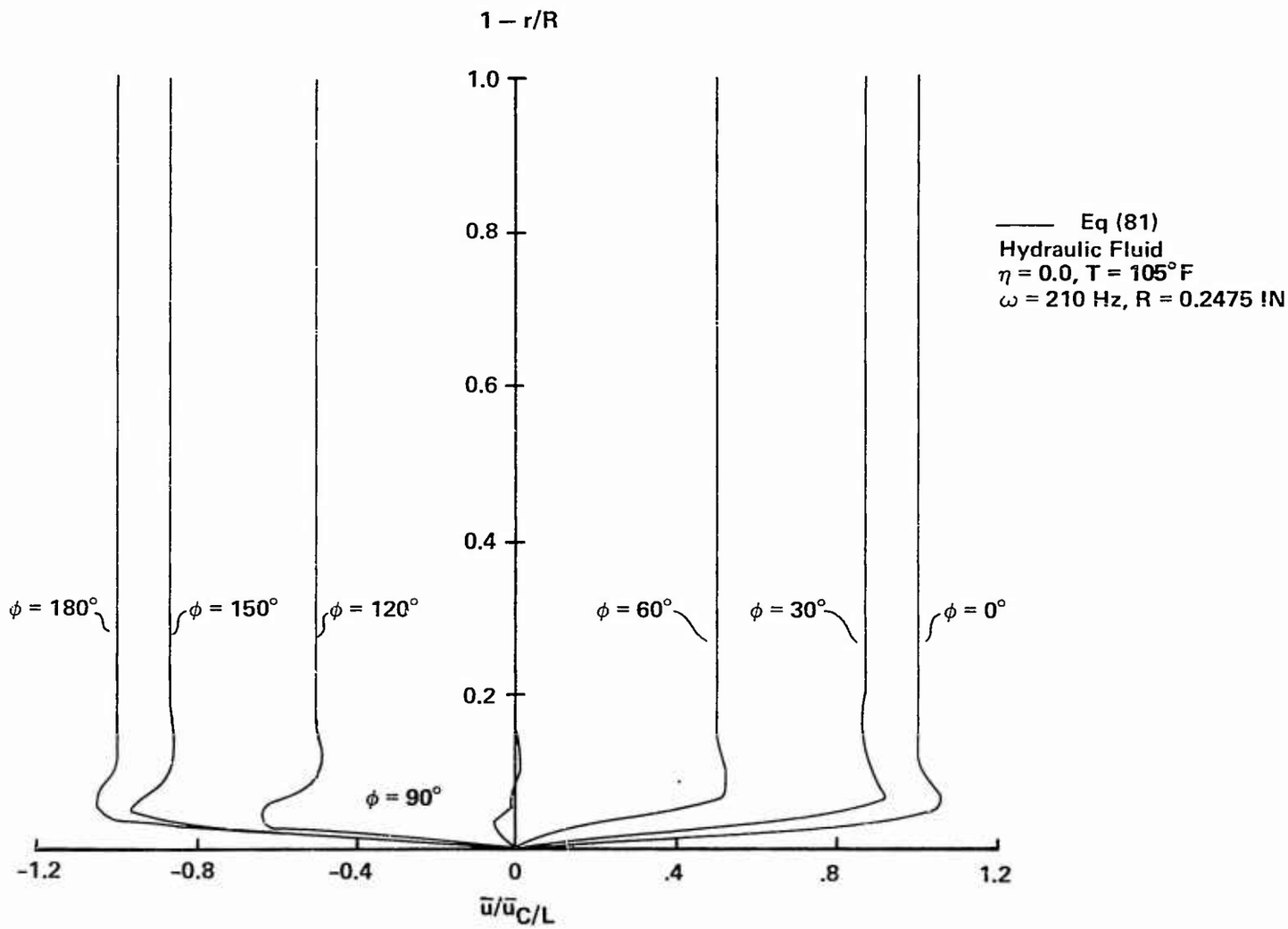

Figure 35. Velocity Profile For A Mean Flow Of 0 GPM

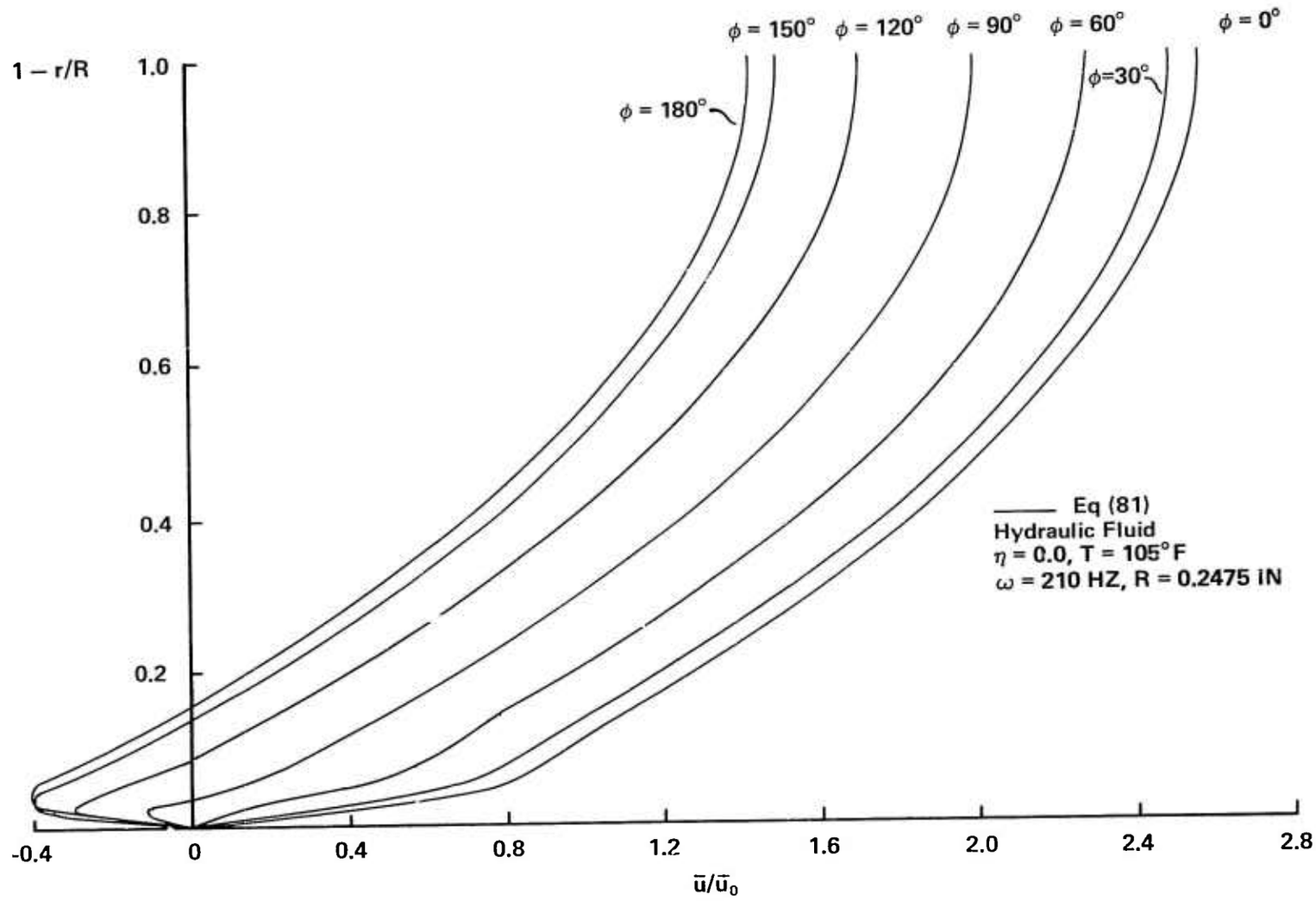

Figure 36. Velocity Profile For A Mean Flow Of 1.5 GPM

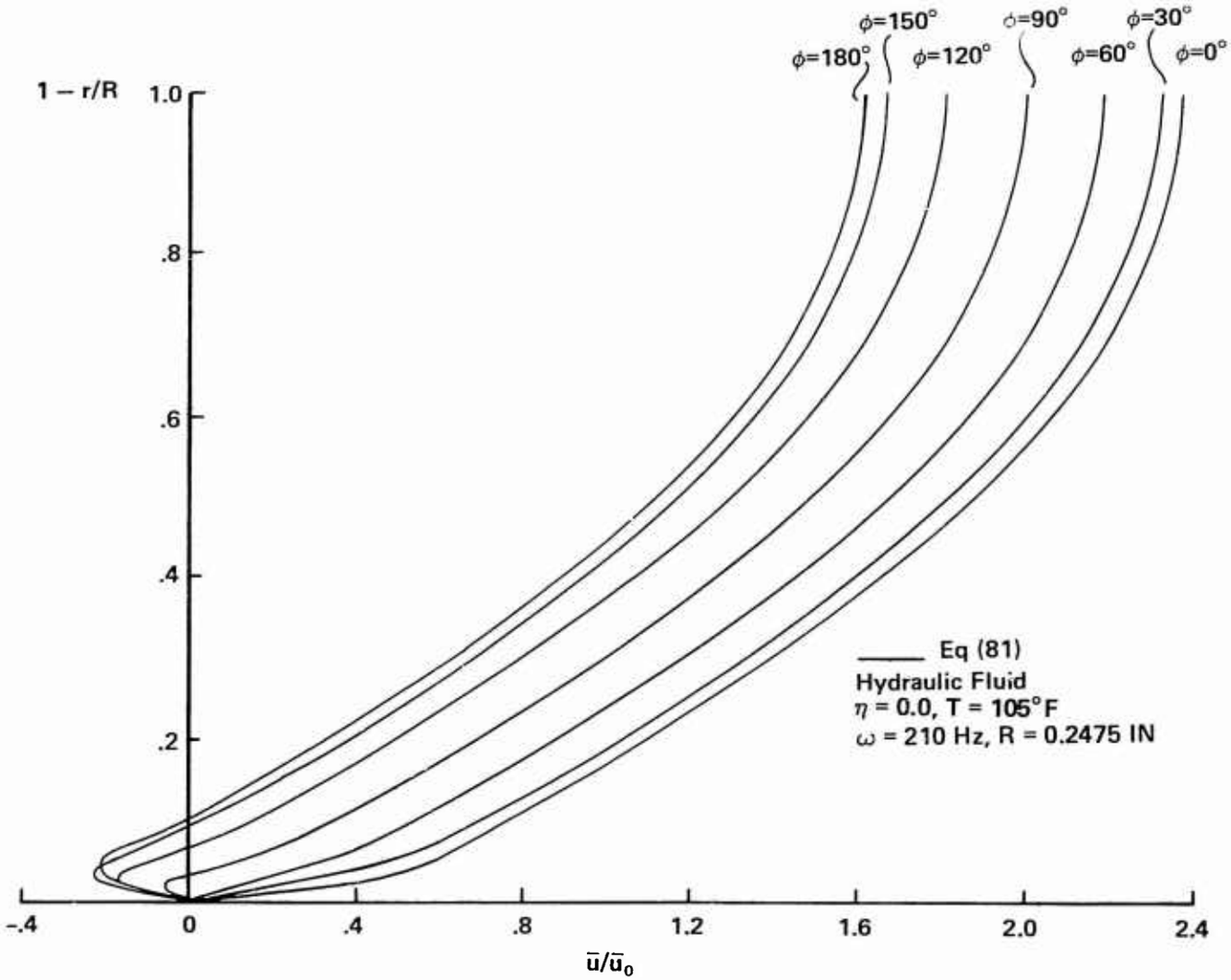

Figure 37. Velocity Profile For A Mean Flow Of 2.5 GPM

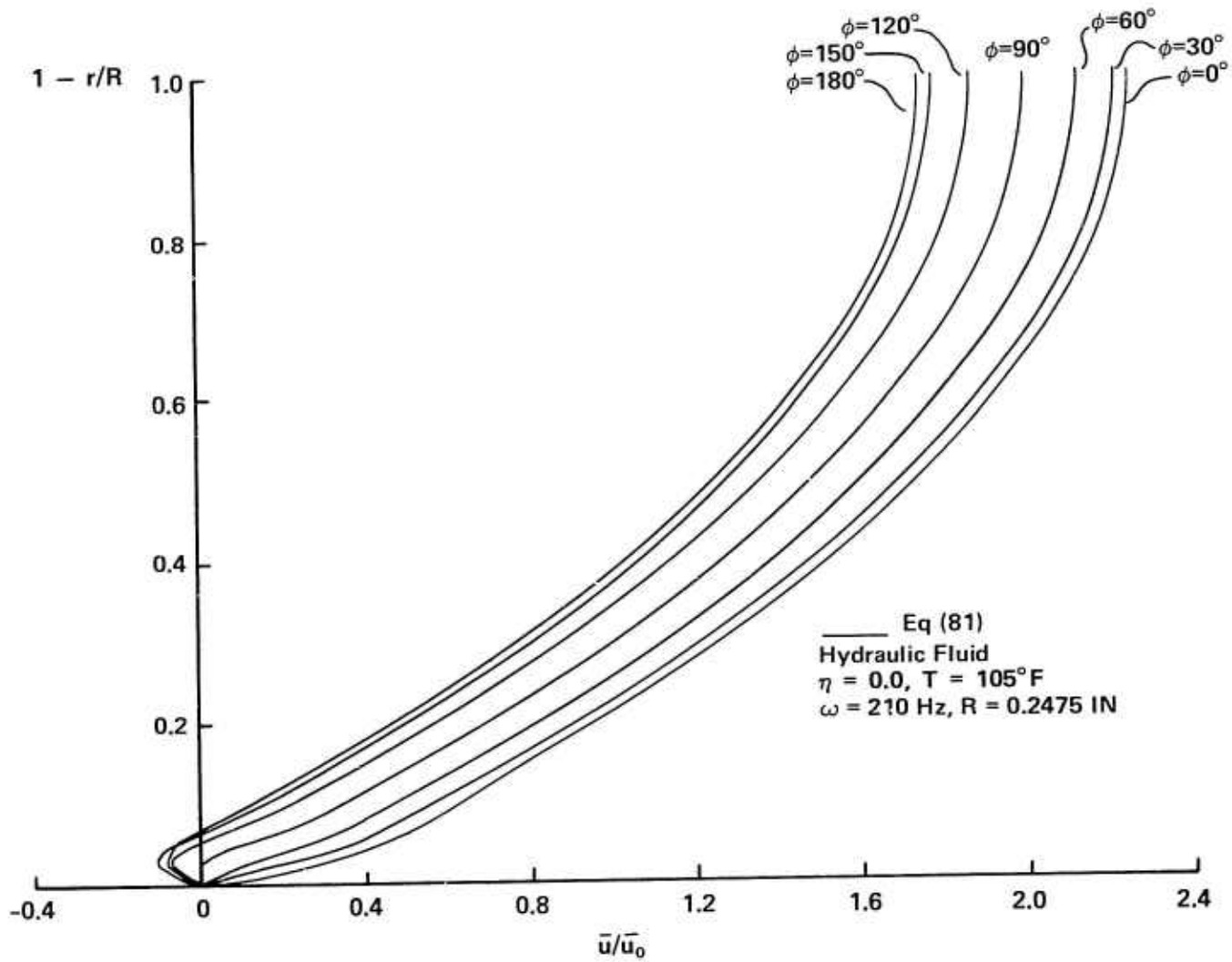

Figure 38. Velocity Profile For A Mean Flow Of 5 GPM

flow near the centerline of the pipe lagging behind the flow near the wall. This effect is the same effect as was observed experimentally by Richardson (27) who termed it the annular effect. Uchida (32) also calculated similar profiles by superposing the parabolic mean flow velocity profile with a periodic velocity profile.

IX. Comparisons with Experiment

Introduction

Experiments described in Chapter III were run to obtain the frequency response and the standing pressure half wave for comparison with analytical results. The straight line hydraulic system, Configuration Five, was used with flow rates up to 5 gpm. At these flow rates the flow was laminar. Experimental data were obtained at nine points along the line. However, the data at only one point, $x/L = 0.4839$, were obtained using an in-line transducer. All other data were obtained using clampon transducers. Thus at the beginning of the line, close to the pump, significant vibration errors were likely. Likewise, at points where the dynamic pressure was large, so was the vibration and the error due to vibration.

The data were read off the spectrum analyzer display. Figure 39 shows two typical displays. The first pressure spike or fundamental, corresponds to the response at the excitation frequency, the pump frequency. The smaller spikes correspond to the response at harmonics of the excitation frequency. Although an in depth study of the pressure harmonics was not undertaken, the data shown in Figure 39 are typical. For the top display, the amplitude of the first harmonic was 9% of the fundamental, the second harmonic 7%, and the third harmonic only 3%. For the bottom display, the first harmonic was 8% of the fundamental and the second harmonic was 4%.

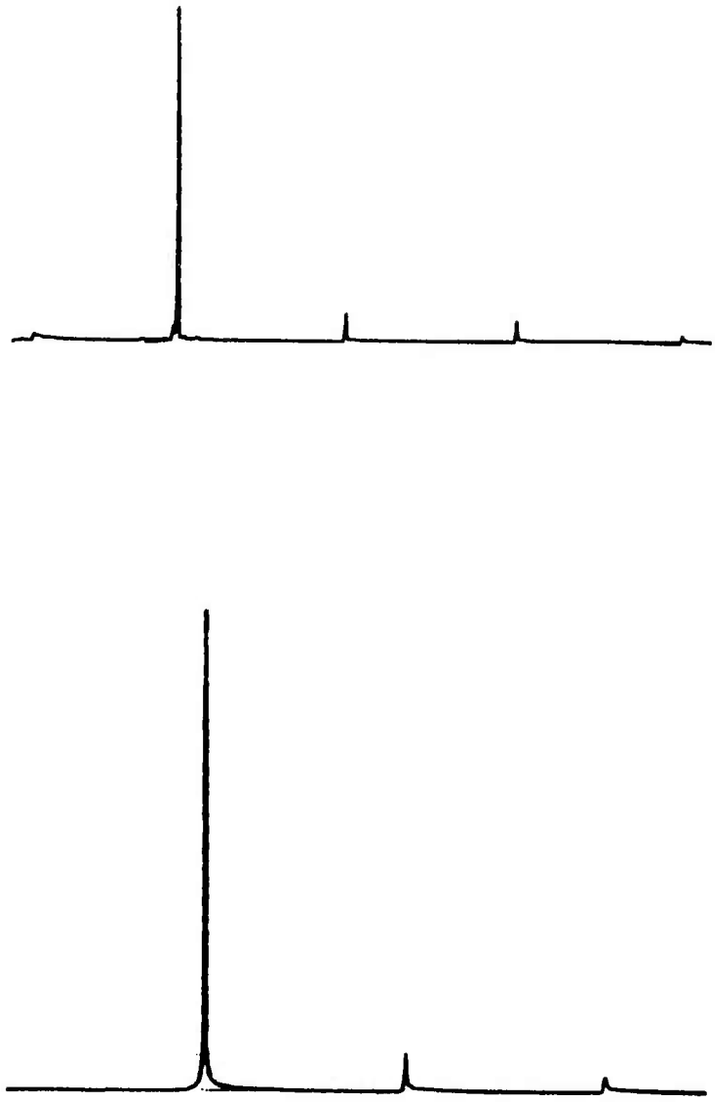

Fig. 39. Spectrum Analyzer Display

Frequency Response

Figures 40 and 41 show the frequency response of the system for flow rates of 0 and 5 gpm respectively. The frequency range is from 180 Hz, the lowest pump frequency obtainable, up to a frequency at which the analysis failed to give accurate results due to convergence problems. The data and analysis agree well except where the vibration error is expected to be large, especially at high dynamic pressures. The largest difference between analytical and experimental values was 13 psi (18%) for the no-flow case and 13 psi (28%) for the case with a mean flow of 5 gpm. The experimental and calculated resonant frequencies agree in each case. The amplitude of the pressure peak does increase slightly with flow rate, 6% from 0 to 5 gpm, while the resonant frequency decreases with increasing flow rate, from 225 Hz at 0 gpm to 210 Hz at 5 gpm. The primary cause for these changes is temperature. The analytical data were calculated using the measured temperature from the experiments, which was different for each flow rate. For the data presented in Figures 40 and 41, the temperature was 40°F higher for the 5 gpm data than it was for the 0 gpm data. Using the rule of thumb given in Chapter VII for the shift in resonant frequency, a temperature increase of 40°F should decrease the resonant frequency 12 Hz. This means the resonant frequency for the line with 0 gpm, but at the same temperature as the 5 gpm line, should be 213 Hz which compares well with the calculated frequency of 210 Hz for 5 gpm. Thus when the effect of temperature is considered, there is no significant shift in resonant frequency due to through-flow. This same result was reported in AFAPL-TR-77-63, "Aircraft Hydraulic Systems Dynamic Analysis" (3) for flow rates up to 10 gpm. The same

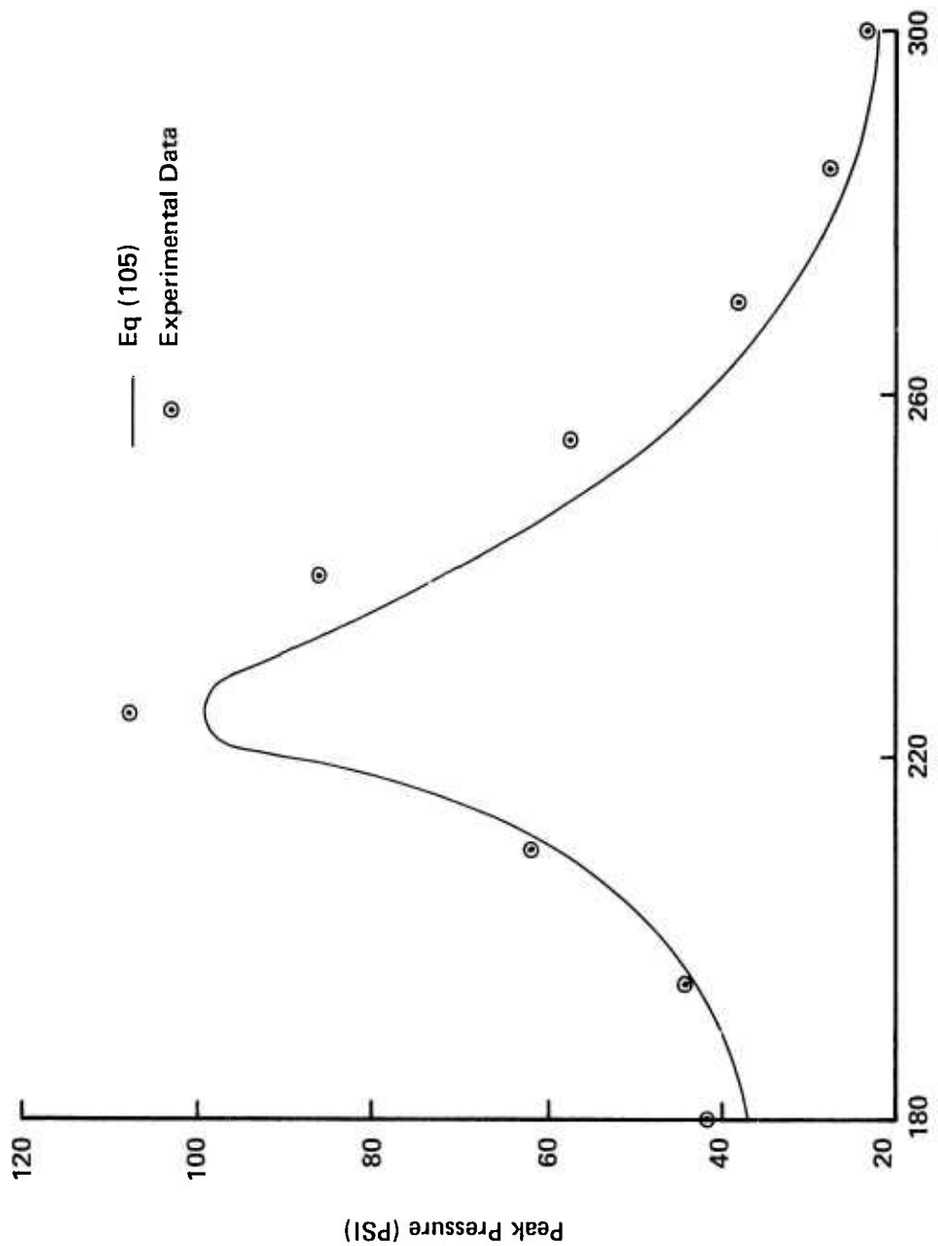

Figure 40. Frequency Response For A Mean Flow Of 0 GPM
(Straight Hydraulic Line, $\eta = 0.876$, T = 75° F, L = 209.75 In, R = 0.2475 In)

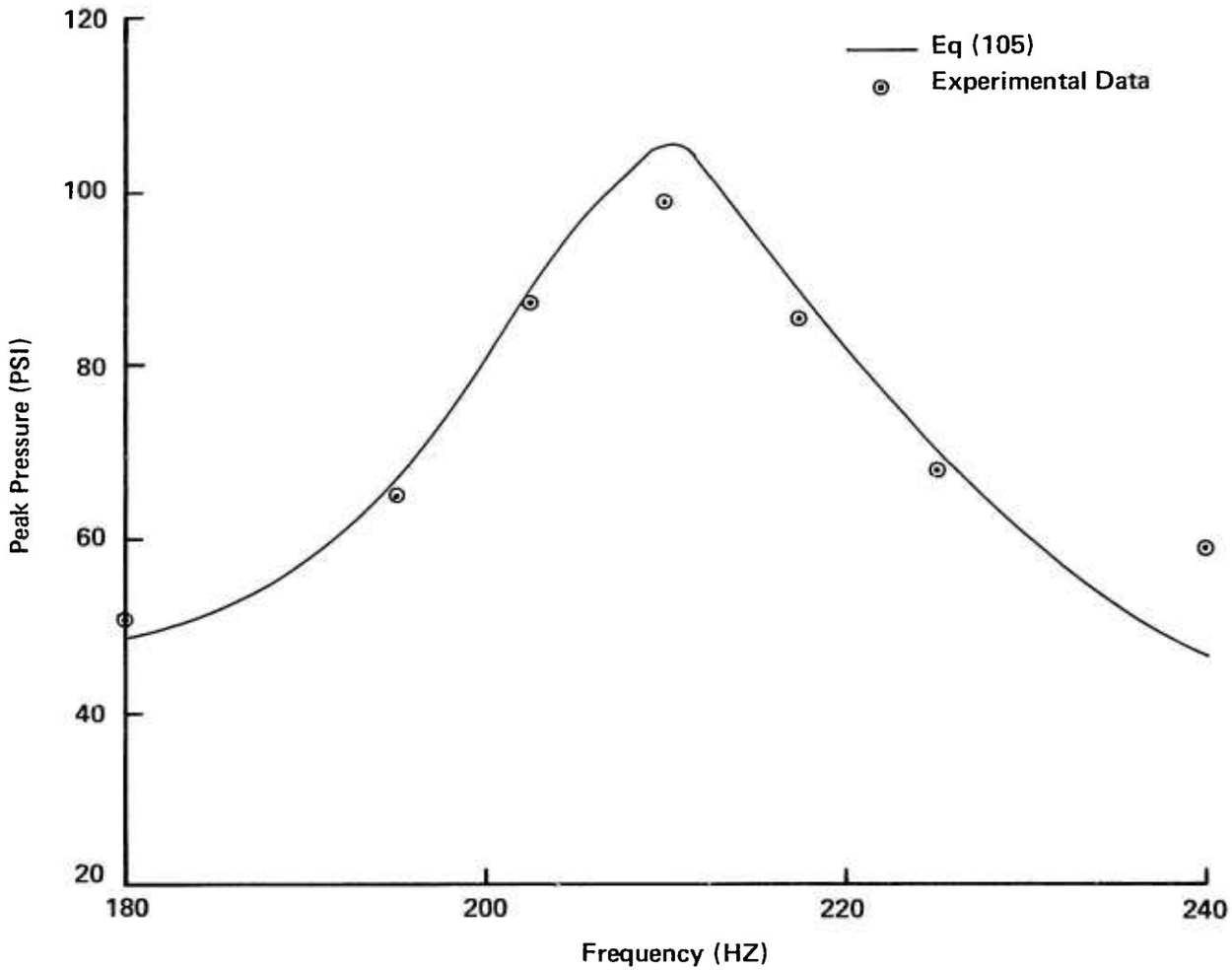

Figure 41. Frequency Response For A Mean Flow Of 5 GPM
(Straight Hydraulic Line, $\eta = 0.876$, T = 115°F, L = 209.75 In, R = 0.2475 In)

technical report states that an increase in pressure amplitude with increasing flow was observed in a long line. This agrees with the trend noted in Figures 40 and 41. The change is so small, however, that it could be solely due to temperature. Other experimental data taken at different resonant frequencies and different flow rates show small pressure amplitude changes, but in both directions, for an increase in flow. The resonant frequencies were unaffected though.

Standing Pressure Half Wave

Figures 42, 43 and 44 show the standing pressure half wave for flow rates of 0, 2.5 and 5.0 gpm respectively. Again, the agreement between experiment and analysis is good except in regions where the vibration is large; namely, near the pump and in regions of high dynamic pressure. In all three figures the pump frequency is the same and the nodes and antinodes occur at the same location, regardless of flow rate. The maximum amplitude does increase with flow rate, but again this is primarily due to the temperature effect which shifts the resonant frequency leftward with increasing temperature. The closer to the nearest resonant frequency a system is, the larger the pressure amplitude should be. It is possible that the pressure amplitude increase was due in part to the increased flow rate, as this effect was noted in AFAPL-TR-77-63 (3) as discussed earlier. In any case the effect is very small. A comparison of the plotted analytical results for 0, 2.5 and 5.0 gpm, after accounting for the temperature differences, shows that the through-flow has very little effect.

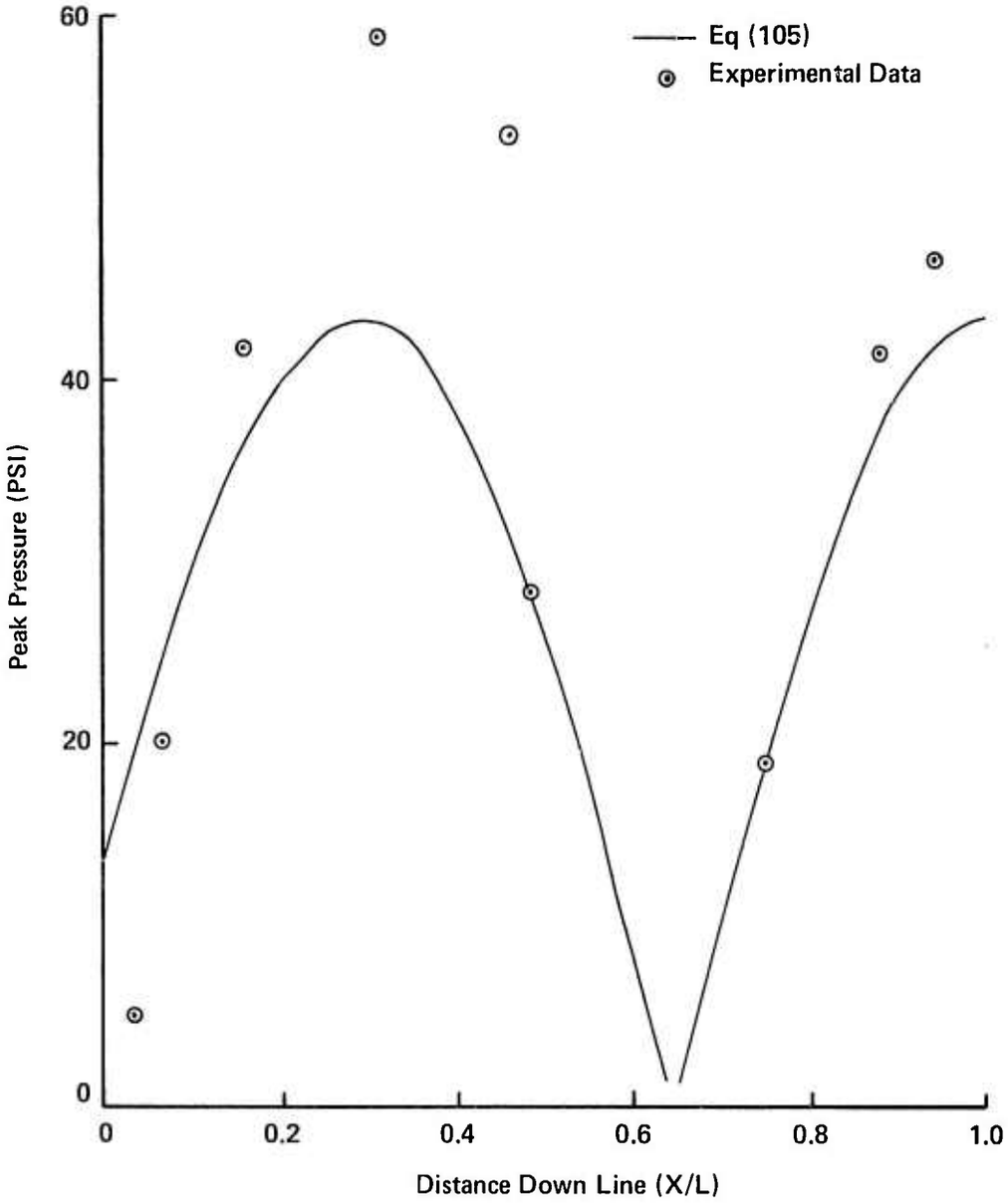

Figure 42. Standing Pressure Half Wave
For A Mean Flow Of 0 GPM
(Straight Hydraulic Line, ω = 180 Hz, T = 75° F, L = 209.75 In, R = 0.2475 In)

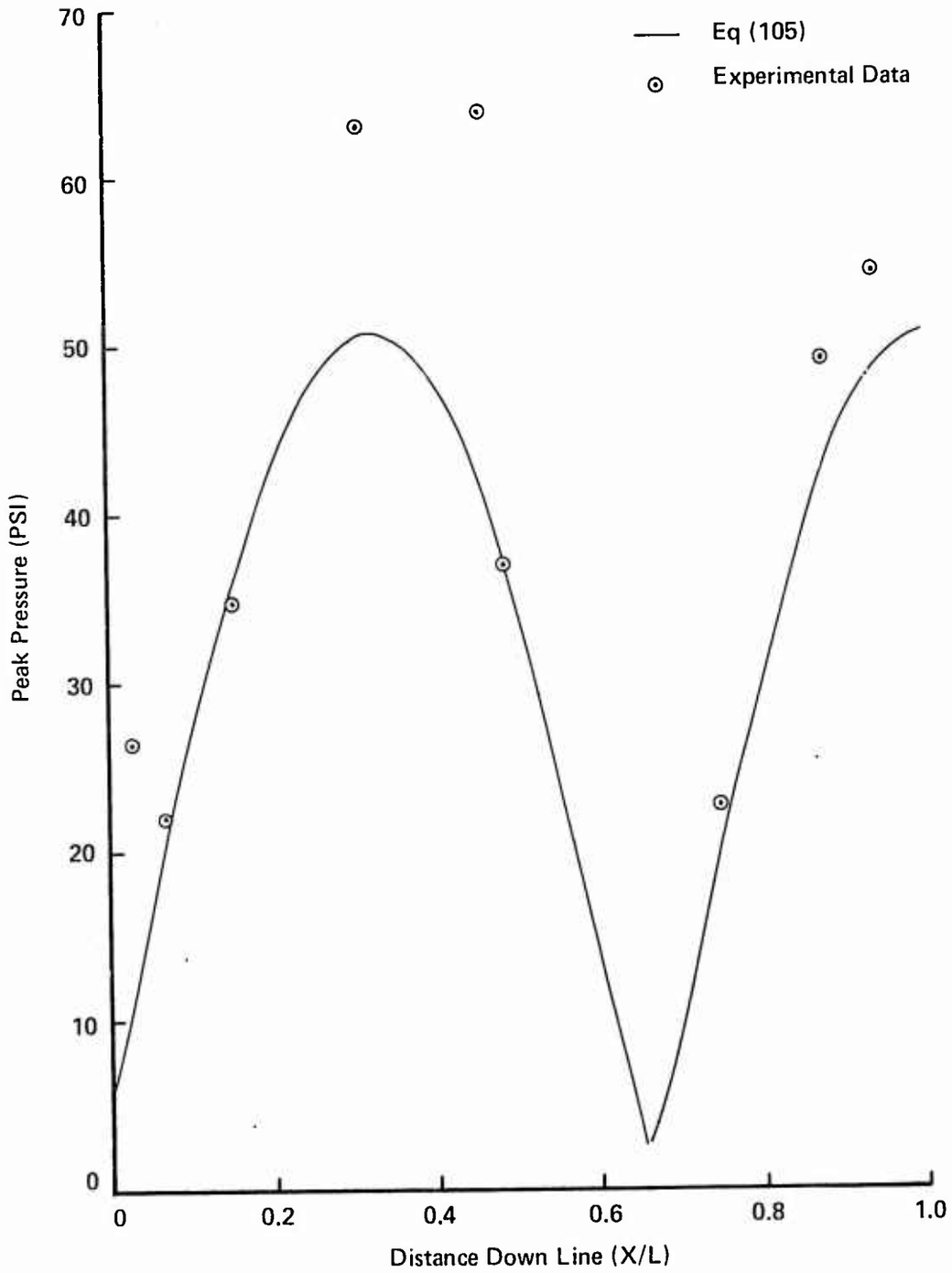

Figure 43. Standing Pressure Half Wave
For A Mean Flow Of 2.5 GPM
(Straight Hydraulic Line, ω= 180 Hz, T = 115° F, L = 209.75 In, R = 0.2475 In)

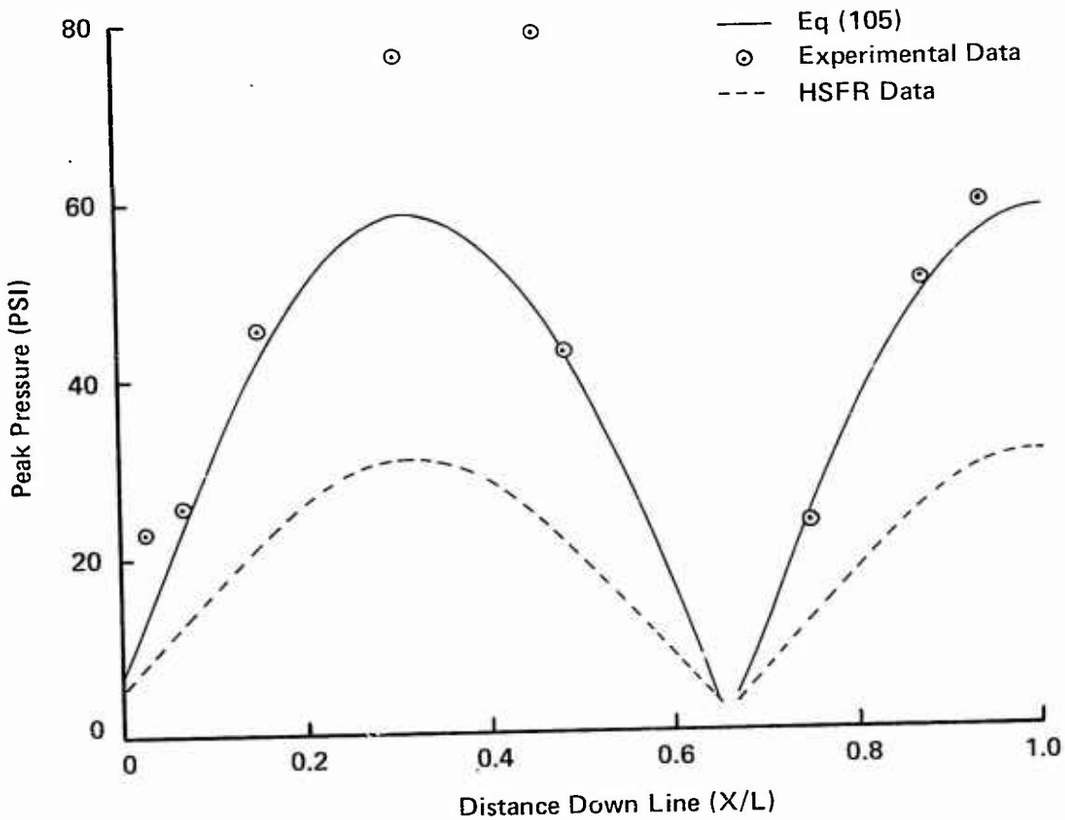

Figure 44. Standing Pressure Half Wave
For A Mean Flow Of 5.0 GPM
(Straight Hydrauiic Line, ω = 180 Hz, T = 115°F, L = 209.75 In, R = 0.2475 In)

Comparisons with Data from the HSFR Program

Figure 44 also shows data from the HSFR computer program. The nodes and antinodes occur at the same line locations as calculated using the analysis reported herein. The amplitude, however, is only about half that given by the analysis and does not agree with the experimental data. The reason for the low amplitudes is that HSFR computed a resonant frequency of 240 Hz compared to the 210 Hz given by the analysis and the experimental data. The primary reason for the error in the HSFR results is the great difficulty involved in accurately modeling the dynamics of a hydraulic pump. The analysis reported here requires a boundary condition and the results are only as accurate as that boundary condition. HSFR does not need a boundary condition, but rather determines one of its own by calculating the pump output pressure and velocity for any given operating conditions.

X. Analytical Results for Air Lines

Introduction

The results of the laminar flow analysis for hydraulic lines showed the effect of through-flow, but the effect was small due to the low mean flow velocities involved. To better understand the effect of through-flow, larger mean flow velocities are required. For this, air lines with Mach numbers up to 0.3 were used. Mach numbers higher than 0.3 would invalidate several of the assumptions used in the derivation of the analytical relations. Even for low Mach numbers, one assumption is violated, that of laminar flow. The Reynolds numbers associated with small diameter air lines at standard temperature and pressure for a Mach number of 0.3 are well into the turbulent regime (Re = 22315 for a 0.125 in. ID line). Lower Reynolds numbers could have been obtained by using values for the radius or viscosity that were physically unrealizable. Since, as noted before, the results do depend on the line geometry and fluid properties, typical values had to be used. Lower Mach numbers would have also resulted in lower Reynolds numbers, but then the flow effects would be small as seen in the hydraulic lines. The high Reynolds number approach was used by Orner (24) and gave good results. At worst, the trends demonstrated with the high Reynolds number data should be valid and should agree with the trends noted for the hydraulic lines with laminar flow.

As before, the analytical results for the air lines are given in terms of the dimensionless attenuation, αL, and phase constant, βL, for both the left and right traveling waves. The phase constant data

are also presented in terms of the speed of propagation, $c = \omega/\beta$. Using these results, the engineer will know how fluid transmission line parameters are affected by flow and can modify easily obtainable no-flow results accordingly. The attenuation and phase constant results are given in three forms. In this way it will be easier for the engineer to extract data most applicable to his problem. Since the no-flow attenuation and phase constant are easily calculated using Eq (99), results for flow are given in terms of first the actual dimensionless values, αL and βL, second the deviation of the values for flow from those with no flow, $(\alpha_0-\alpha_1)L$ and $(\beta_0-\beta_1)L$, and third the ratio of the values with flow to those without, α_1/α_0 and β_1/β_0. The results are plotted against the dimensionless frequency, ω/ω_ν. For those engineering applications where precise results are needed and the trends shown by the results presented here would not suffice to modify no-flow data, a computer solution using the derived analytical expressions is required.

Attenuation Results

Figures 45 through 48 show attenuation results calculated for an 0.125 in. ID air line 23.245 in. long at standard temperature and pressure. The first plot, Figure 45, shows how the forward and backward traveling wave attenuation varies for mean flow velocities from 0 to 0.3 Mach. The attenuation of the forward wave decreases as the mean flow velocity increases while the attenuation of the backward traveling wave increases. This is caused primarily by the decreased time required for a forward wave to travel the length of the line and likewise the increased time required for the backward wave resulting from the fact that the wave is traveling in a moving medium. Also, as

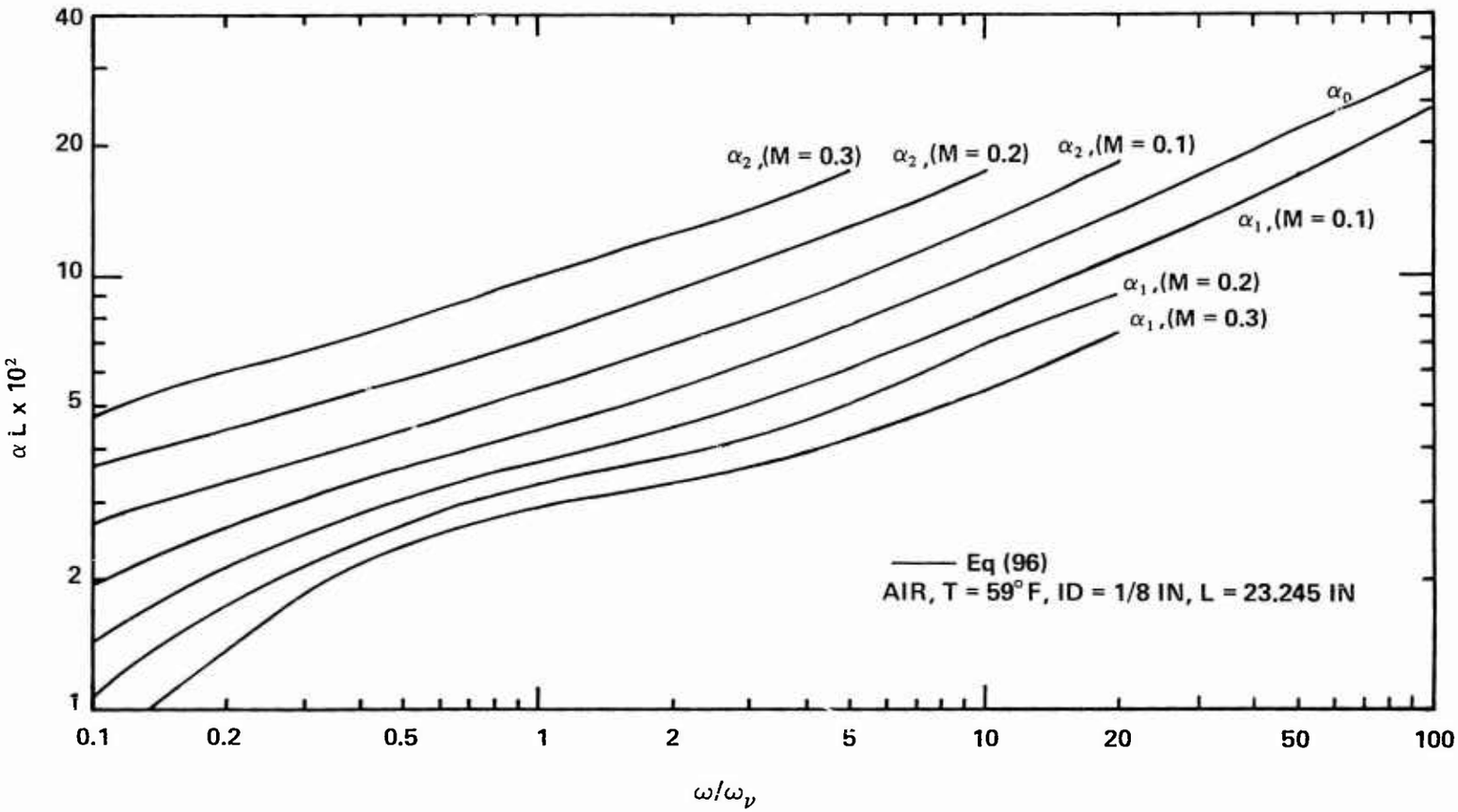

Figure 45. Attenuation Versus ω/ω_ν For Mach Numbers From 0 to 0.3

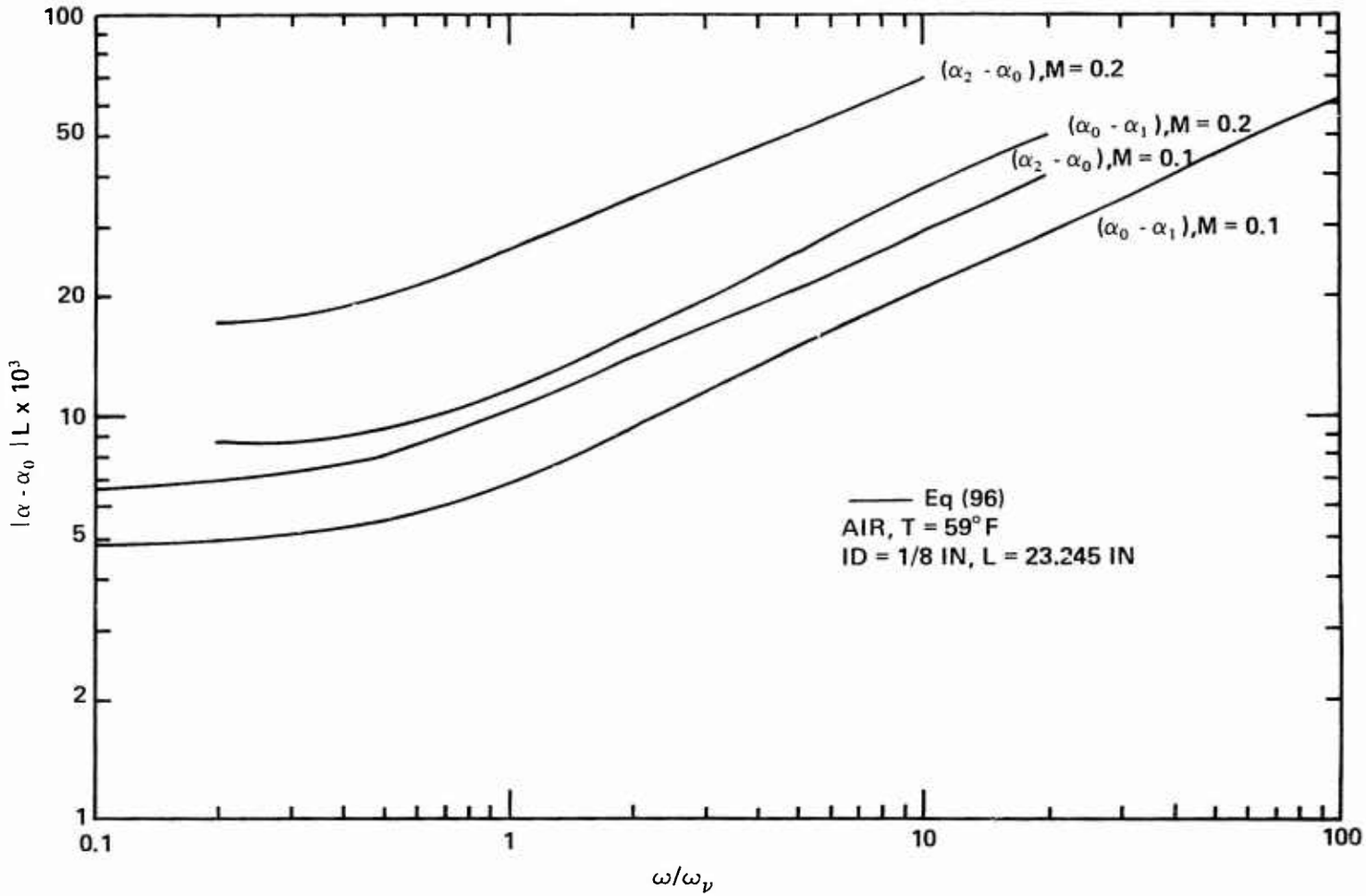

Figure 46. Attenuation Deviation Versus ω/ω_ν for Mach Numbers 0.1 and 0.2

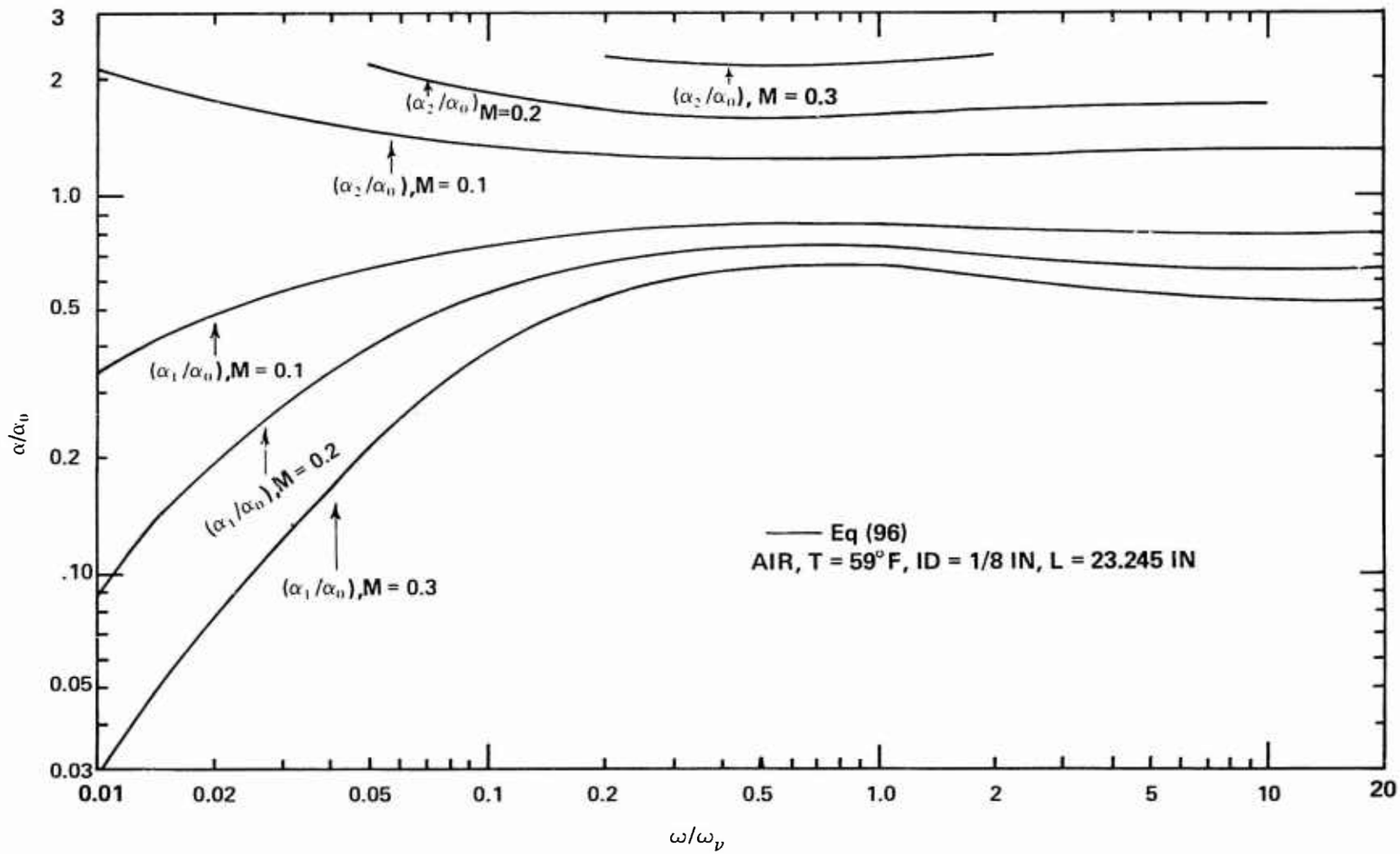

Figure 47. Ratio of the Attenuation with Flow to No-Flow Attenuation Versus ω/ω_v

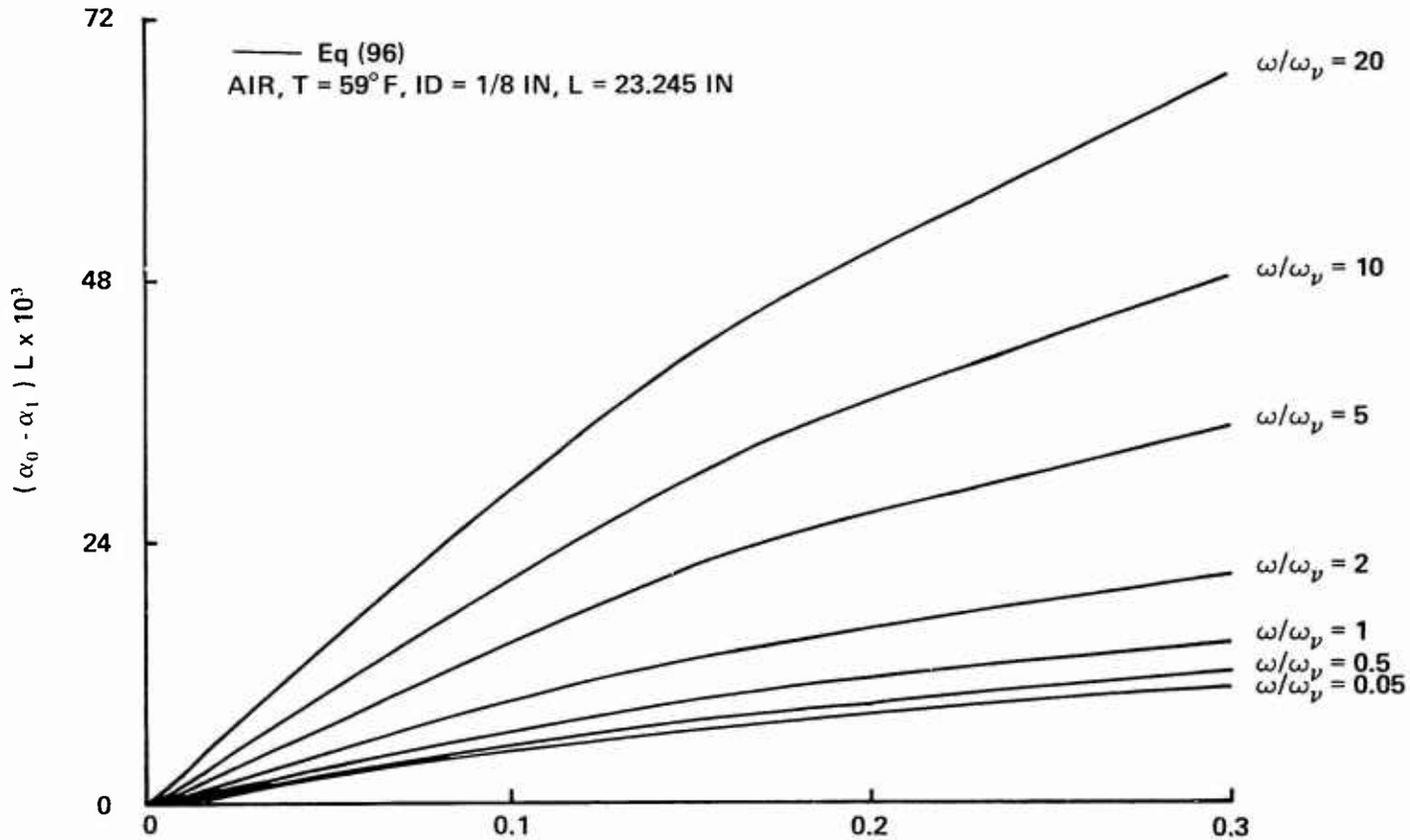

Figure 48. Forward Wave Attenuation Versus Mach Number

the frequency increases, so does the attenuation. This is analogous to electrical transmission lines where high frequency signals attenuate much more rapidly than low frequency signals. Note also that for a mean flow velocity increase, the increase in attenuation for the backward traveling wave is more than the decrease in attenuation for the forward traveling wave due to the mean flow velocity profile. The deviation from the no-flow attenuation is given in the next plot, Figure 46, for both forward and backward traveling waves. The deviation in attenuation for the backward wave is larger than that for the forward wave. If the ratio, $(\alpha_2-\alpha_0)/(\alpha_0-\alpha_1)$ is considered, the largest value, 3.5 for M = 0.3, 2.3 for M = 0.2, and 1.5 for M = 0.1, occurs at $\omega/\omega_\nu = 1$. Also $(\alpha_0-\alpha_1)$ for M = 0.2 is 1.5 to 1.8 times larger than for M = 0.1, depending on the frequency, and $(\alpha_2-\alpha_0)$ is 2.4 to 2.6 times larger for M = 0.2 than for M = 0.1.

Figure 47 shows the ratio of the attenuation of both forward and backward traveling waves for several Mach numbers to the attenuation for no-flow. This plot accentuates the large change in attenuation with flow especially at low frequencies. This is somewhat deceiving, however, since as was seen in Figure 46, the logarithm of the difference in the attenuation with the flow and without flow changes only slightly as frequency increases. This happens since both the flow and no-flow attenuation increase with frequency. Figure 47 also shows that ω/ω_ν must be greater than 20 for the approximation of Katz, Hausner and Eisenberg (17) to be valid. This approximation states that the effect of through-flow on high frequency signals is to reduce attenuation by a factor of (1+M). The approximation would predict $\alpha_1/\alpha_0 = 0.909$ for M = 0.1 while the analytical result for $\omega/\omega_\nu = 20$ is

0.794. Another way of looking at the same data is given in Figure 48. The deviation in the attenuation for the forward traveling wave is plotted against Mach number for several dimensionless frequencies. The same trends as noted before are evident. Data runs were made for negative Mach numbers and, as expected, the calculated values for the forward wave attenuation were identical to those for the backward wave attenuation for positive Mach numbers. Likewise, the forward wave attenuation for positive Mach numbers was the same as the backward wave attenuation for negative Mach numbers.

Phase Constant Results

Calculations for the phase constant were made along with the attenuation calculations and many of the trends are the same. Figure 49 shows the dimensionless phase constant for both forward and backward traveling waves plotted against nondimensional frequency, ω/ω_v, for mean flow Mach numbers from 0 to 0.3. The forward wave phase constant decreases with increasing Mach number while the backward wave phase constant increases. For all Mach numbers, the phase constant increases with frequency. For a given frequency and Mach number, the increase in $\beta_2 L$ from M = 0 is larger than the decrease in $\beta_1 L$. At the higher frequencies, the constant Mach number lines are nearly straight, but appear to curve at lower frequencies. Figure 50, a log-log plot, shows what is happening to the forward wave phase constant at low frequencies. The constant Mach number curves are not straight but curve away from the M = 0 curve. A different perspective is given in Figure 51 which plots the dimensionless phase constant against Mach number for three values of ω/ω_v. The curves bow slightly and show the same trends as noted above.

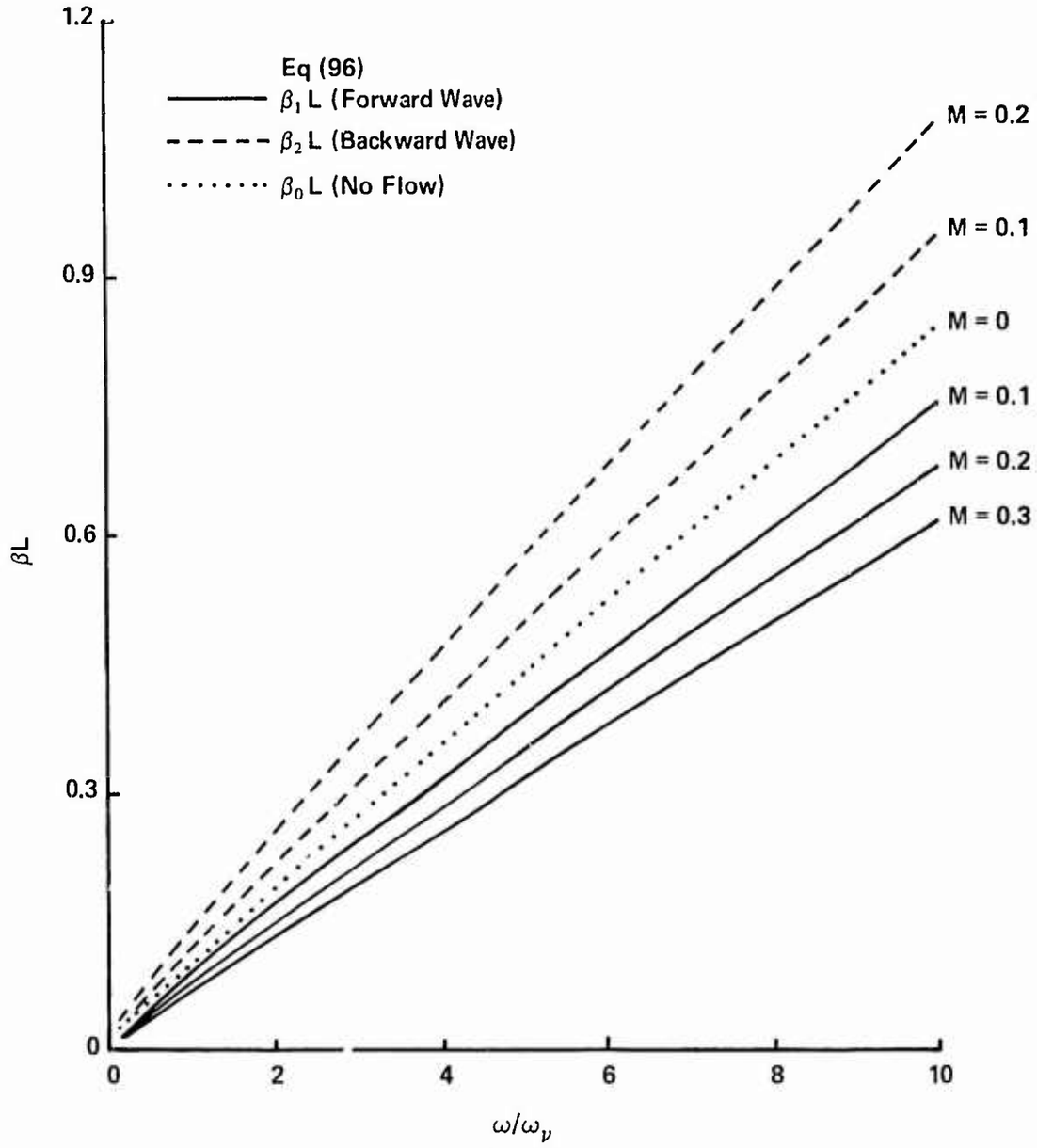

Figure 49. Phase Constant Versus ω/ω_ν For Mach Numbers From 0 to 0.3
(AIR, T = 59°F, ID = 1/8 In, L = 23.245 In)

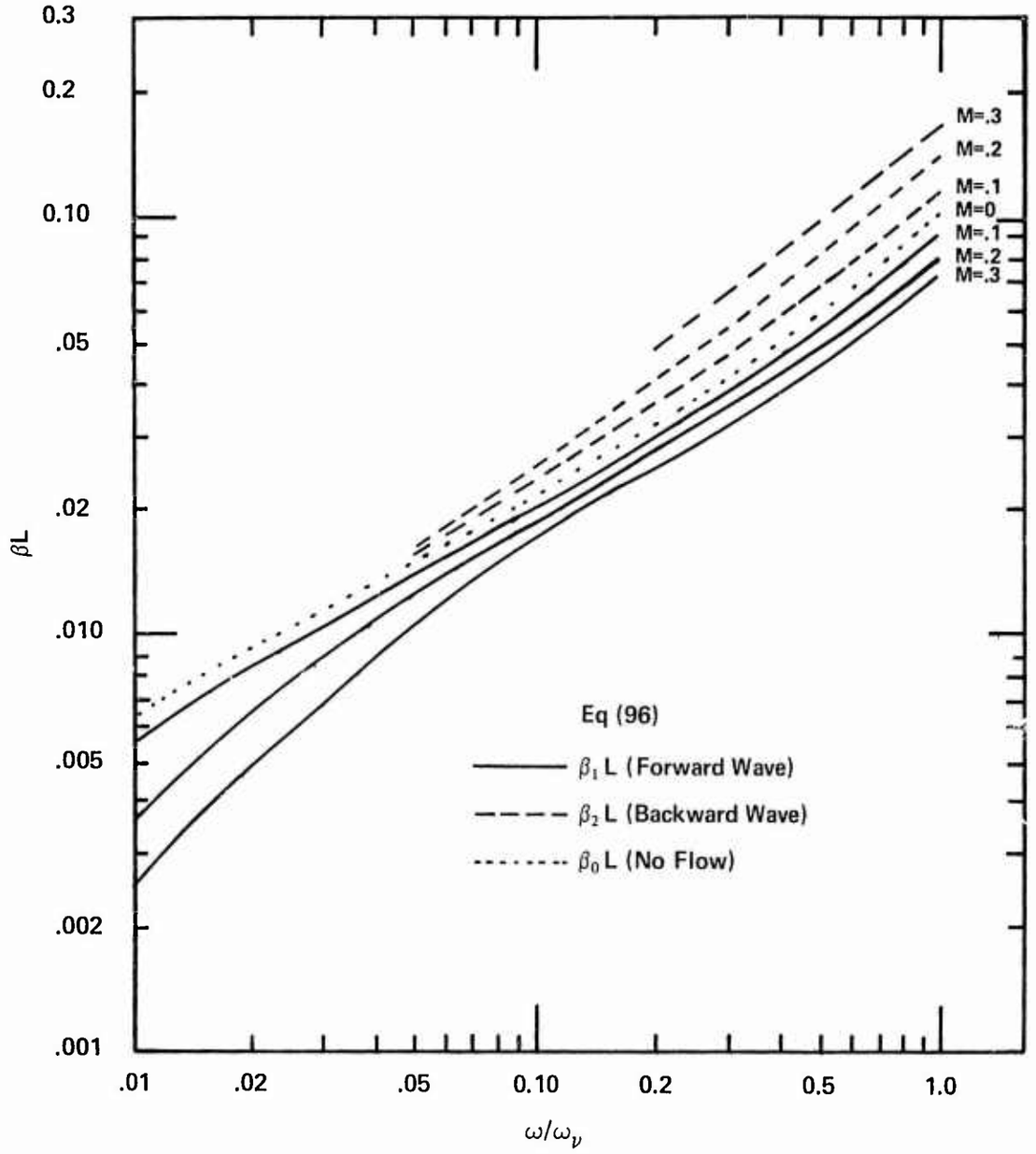

Figure 50. Phase Constant for Small Frequency Ratios
(AIR, T = 59°F, ID = 1/8 In, L = 23.245 In)

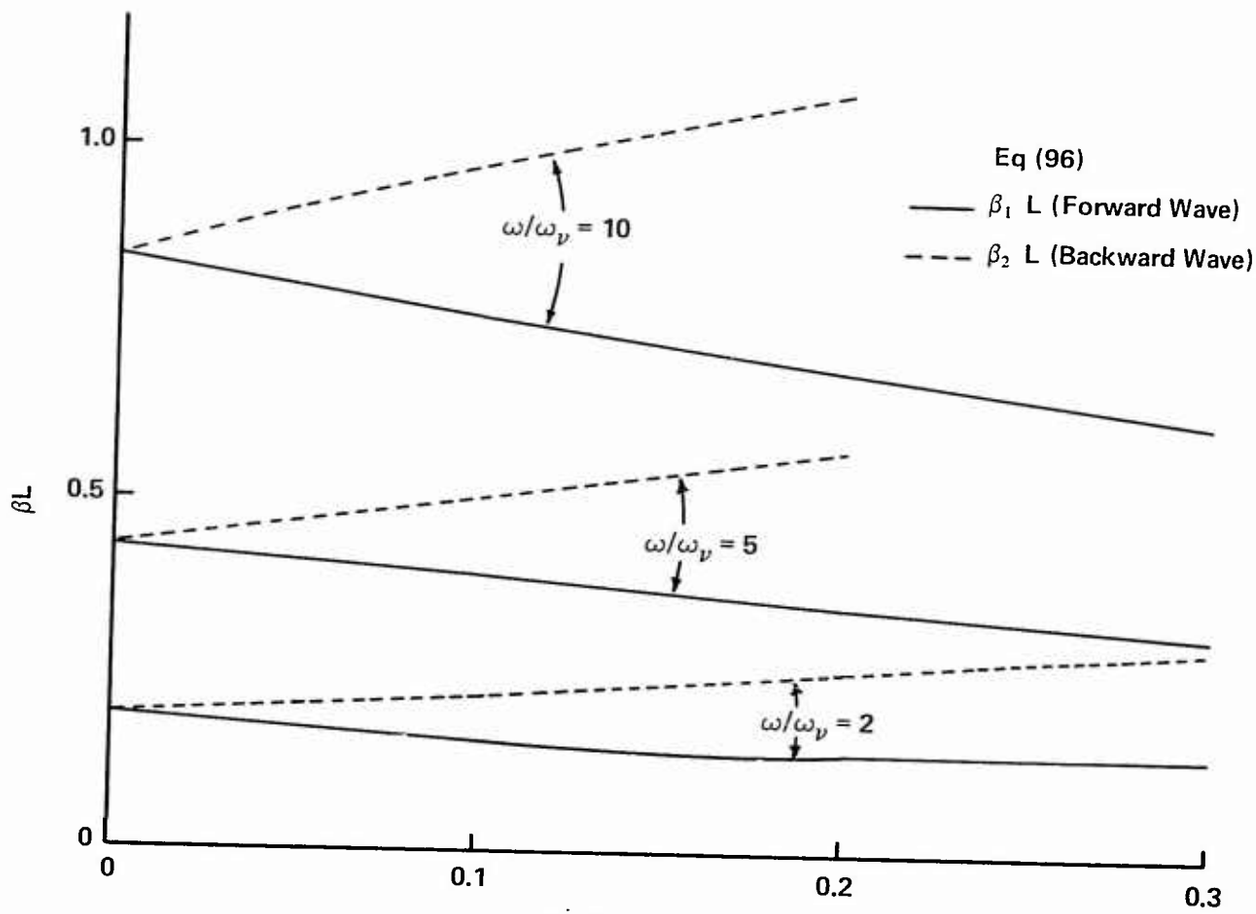

Figure 51. Phase Constant Versus Mach Number
(AIR, T = 59° F, ID = 1/8 In, L = 23.245 In)

The next three graphs, Figures 52, 53 and 54, give the deviation from the no-flow valaue for the phase constant at Mach numbers of 0.1, 0.2 and 0.3. Figure 52 depicts results plotted against frequency. Note that the phase constant deviation is larger for the backward wave than it is for the forward traveling wave. Also, the deviation increases with increasing frequency and Mach number. Similar to the previous plots for the phase constant, the curves are relatively straight at the higher frequencies but appear to curve at the lower frequencies. Figure 53, a log-log plot, shows what actually happens at these lower frequencies. The curves for the forward wave phase constant deviation level off and actually start a gentle rise as the frequency decreases. The actual phase constant decreases as the frequency decreases as is seen in Figure 49, but the deviation does not. Figure 54 plots the forward wave phase constant deviation versus Mach number for several frequencies. The same trends as noted on the prior two graphs are evident. Data for the backward wave phase constant deviation, not plotted, consist of similarly shaped curves located above the curves for $(\beta_0-\beta_1)L$. The next plot, Figure 55, shows the ratio of the forward wave phase constant to the no-flow phase constant. The large change in β_1 relative to β_0 at low frequencies is obvious in this graph which shows better what is happening than the deviation data did. The phase constant is affected by the mean flow more at low frequencies than it is at high frequencies where the curves appear to level off, indicating that both the flow and no-flow phase constants are growing at nearly the same rate.

When the speed of propagation is calculated from the phase constant data, several interesting results appear. Figure 56 shows

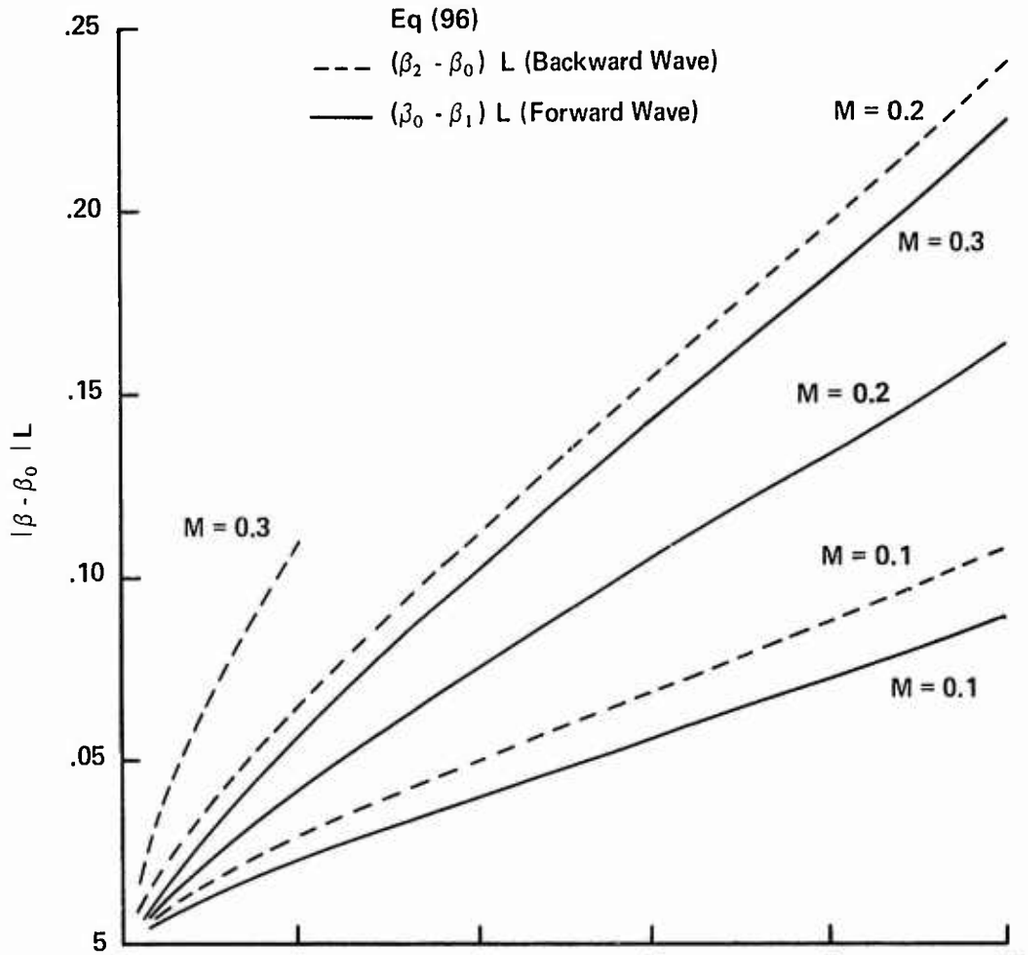

Figure 52. Phase Constant Deviation Versus ω/ω_ν
(AIR, T = 50° F, ID = 1/8 In, L = 23.245 In)

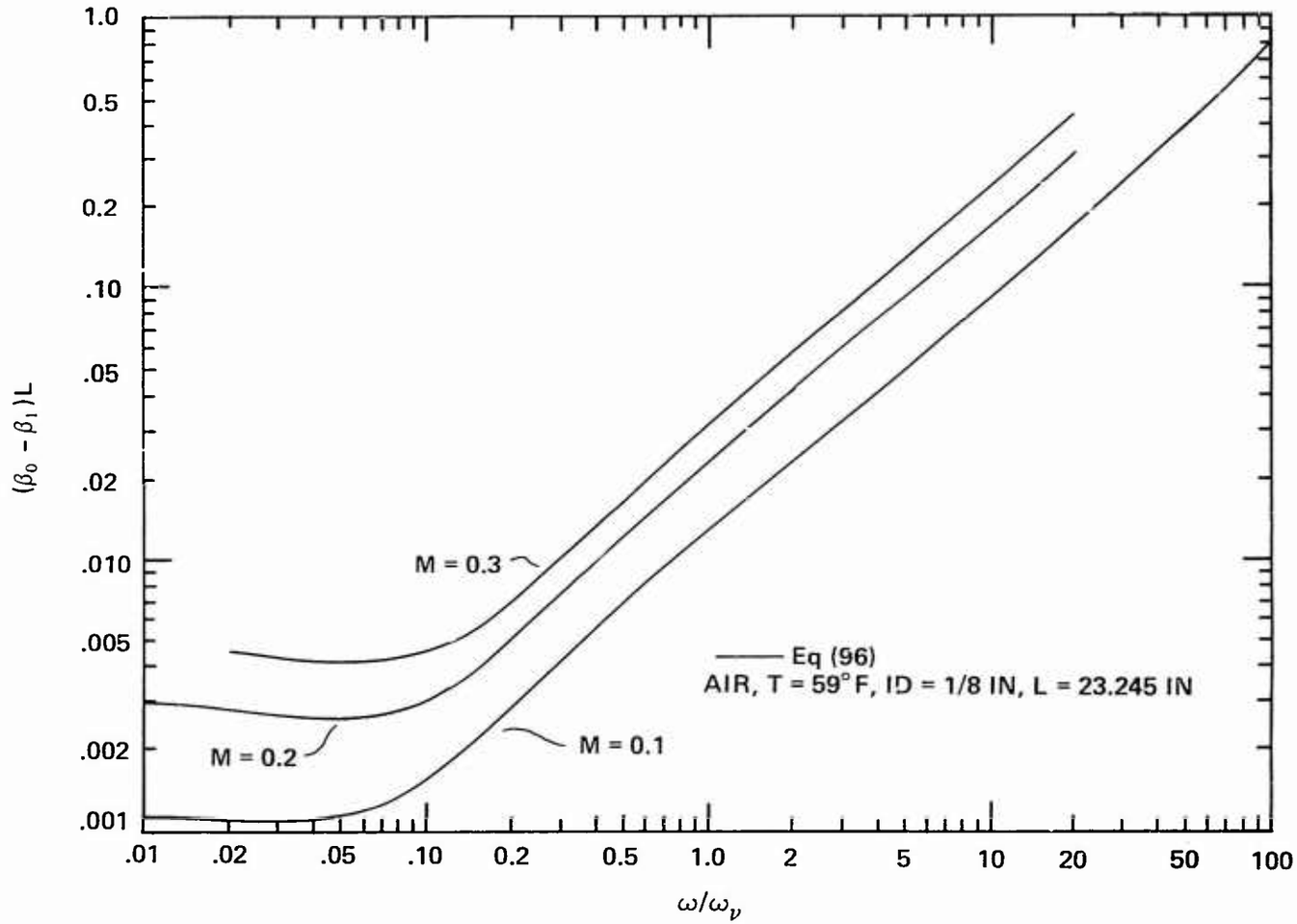

Figure 53. Phase Constant Deviation for Small Frequency Ratios

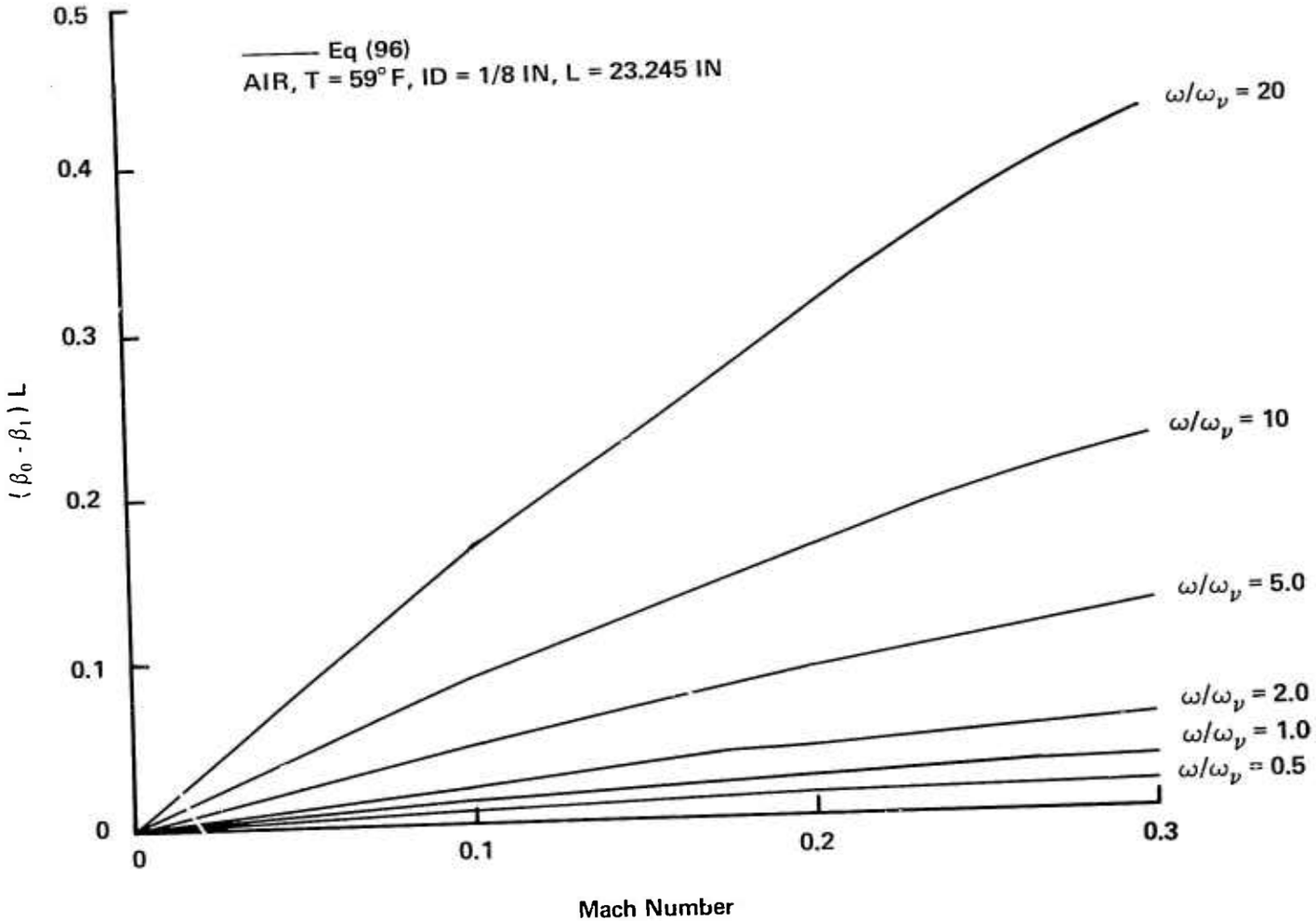

Figure 54. Forward Wave Phase Constant Deviation Versus Mach Number

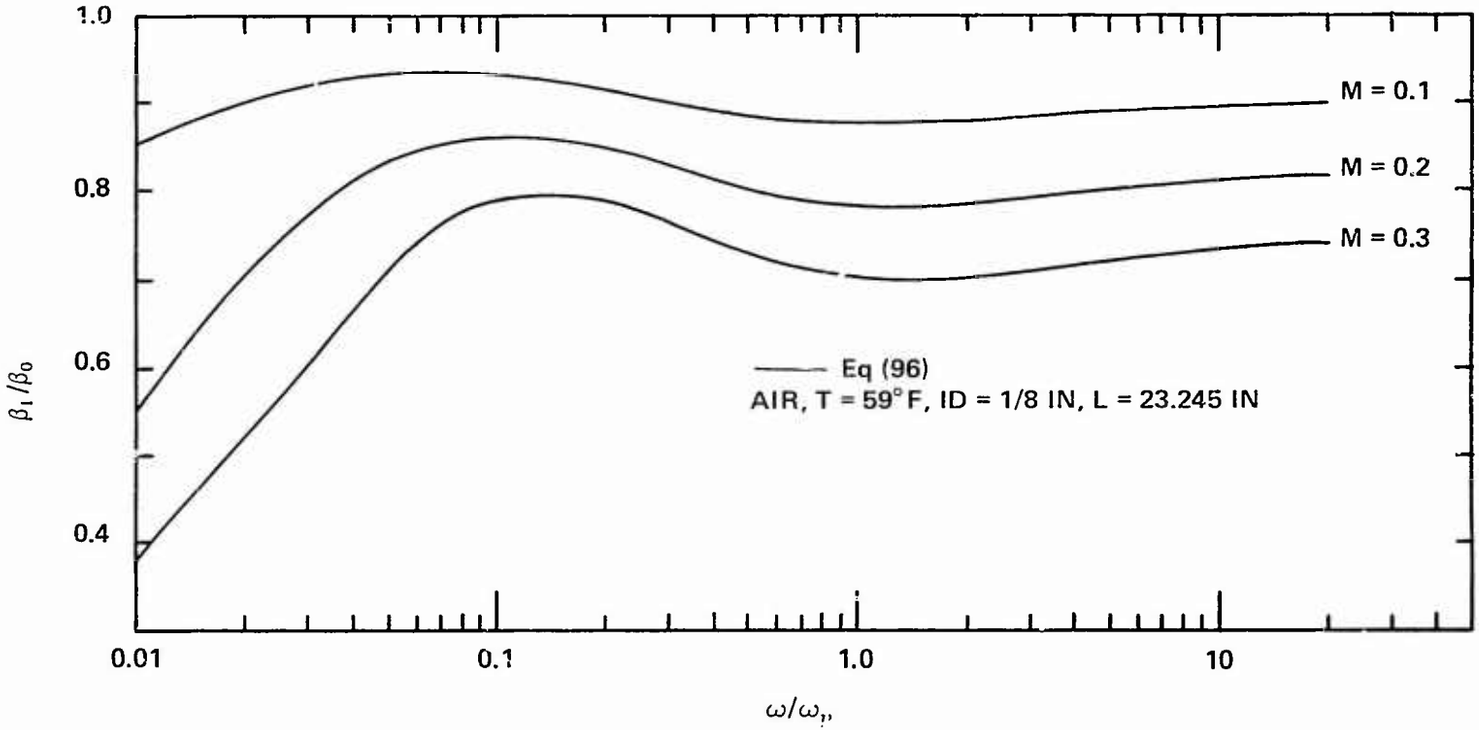

Figure 55. Ratio of the Forward Wave Phase Constant To the No-Flow Phase Constant Versus ω/ω_ν

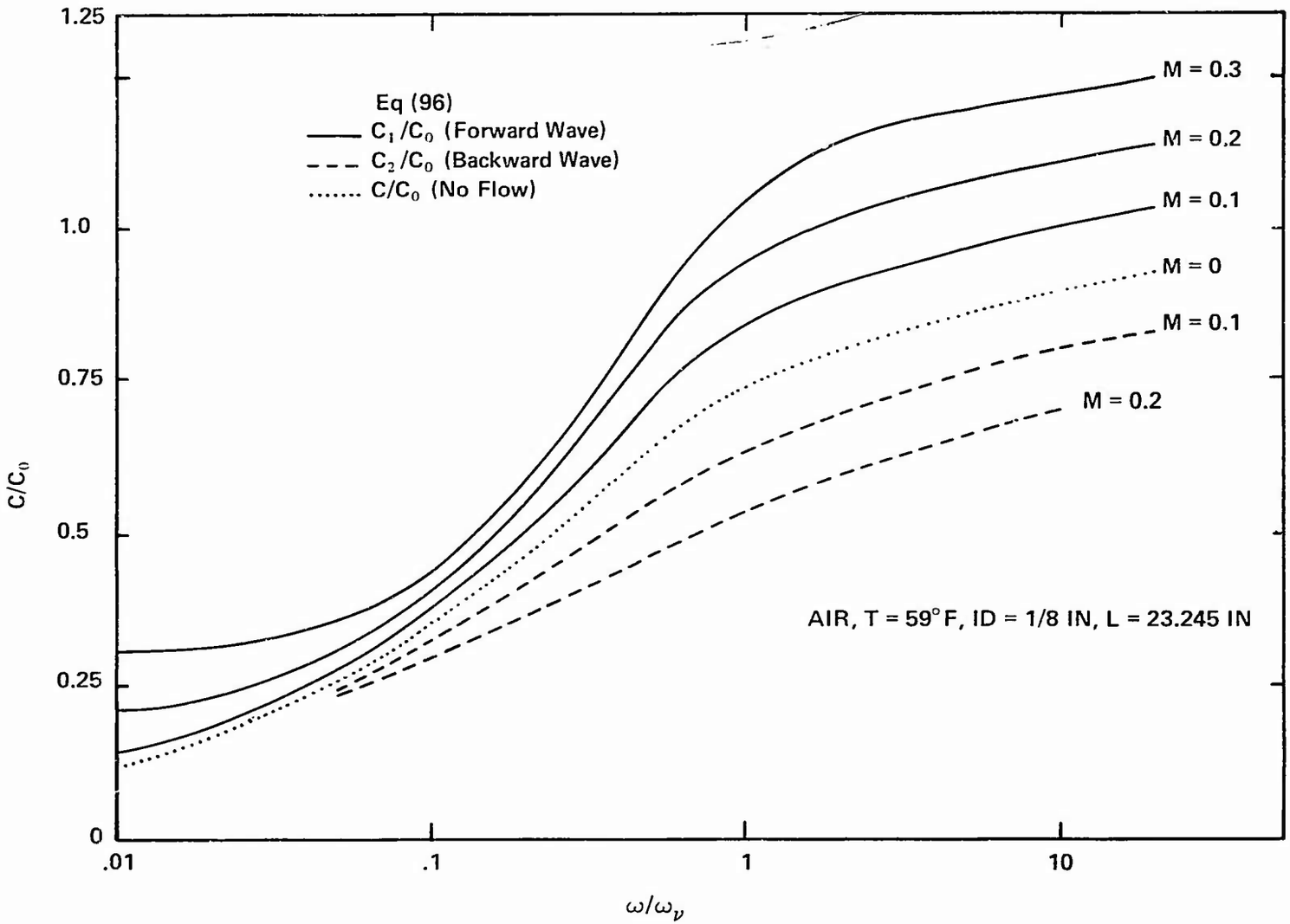

Figure 56. Ratio of the Wave Speed of Propagation to the Isentropic Speed of Sound (C_0 = 13400.9 in/sec)

the ratio of the speed of propagation for both left and right traveling waves to the isentropic speed of sound. As expected, the forward wave with flow propagates faster than the wave with no flow, and the backward wave propagates slower. At high frequencies the curves level off and appear to become asymptotic to (1+M). For frequencies near $\omega/\omega_\nu = 0.1$, the change due to flow is small, but this change increases greatly at lower frequencies. The high frequency behavior has led to a good approximation as given by Katz, Hausner and Eisenberg (17) that $c_1/c_o = 1 + M$. However, in low and mid frequency regimes, the approximation is not valid. Another approximation is

$$\frac{c}{c_o} = \frac{c_{of}}{c_o} \pm M \tag{110}$$

where c_{of} is the speed of propagation calculated for no flow at the frequency of interest. This is a better approximation since it applies in both the mid and high frequency regimes ($\omega/\omega_\nu > 1$). Figures 57 and 58 show how well Eq (110) approximates the actual values of c/c_o for both left and right traveling waves. The agreement is good for frequencies above $\omega/\omega_\nu = 1$. From this point on, the lower the frequency, the worse the approximation.

Isentropic Ideal Gas Results

As an alternative to the rather complex, but frequency dependent process relations, Eqs (18) and (20), derived by Orner (24), the isentropic ideal gas relation, Eq (22), was used for air lines. The weighting function was written as $\Omega = c_v/c_p$ where P_o and ρ_o were absorbed in Ω as was done in Eq (37). This relation was used in lieu of the weighting function given by Eq (20) in calculations for the

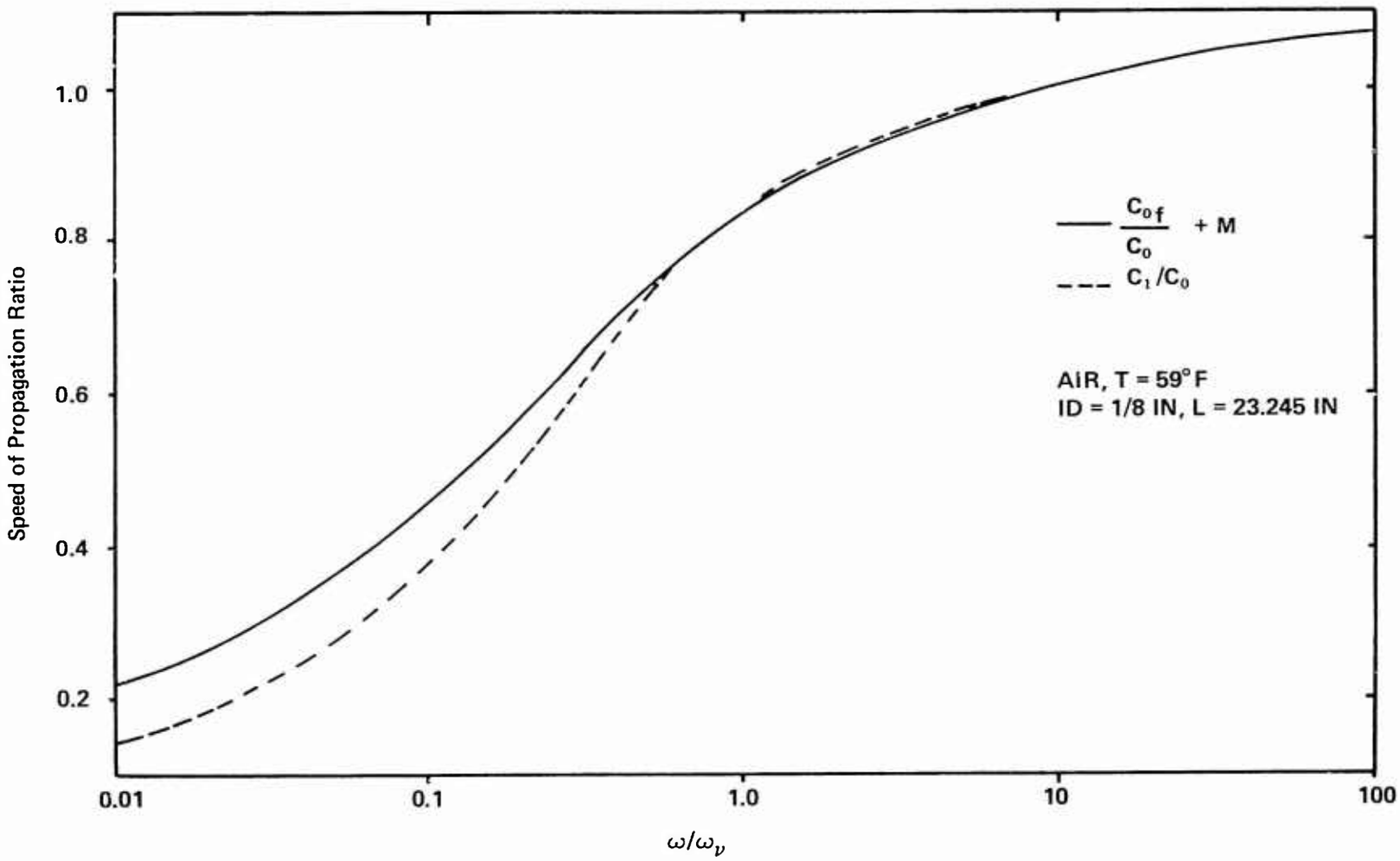

Figure 57. Forward Wave Speed of Progation Ratio for M = 0.1

(C_0 = 13400.9 in/sec)

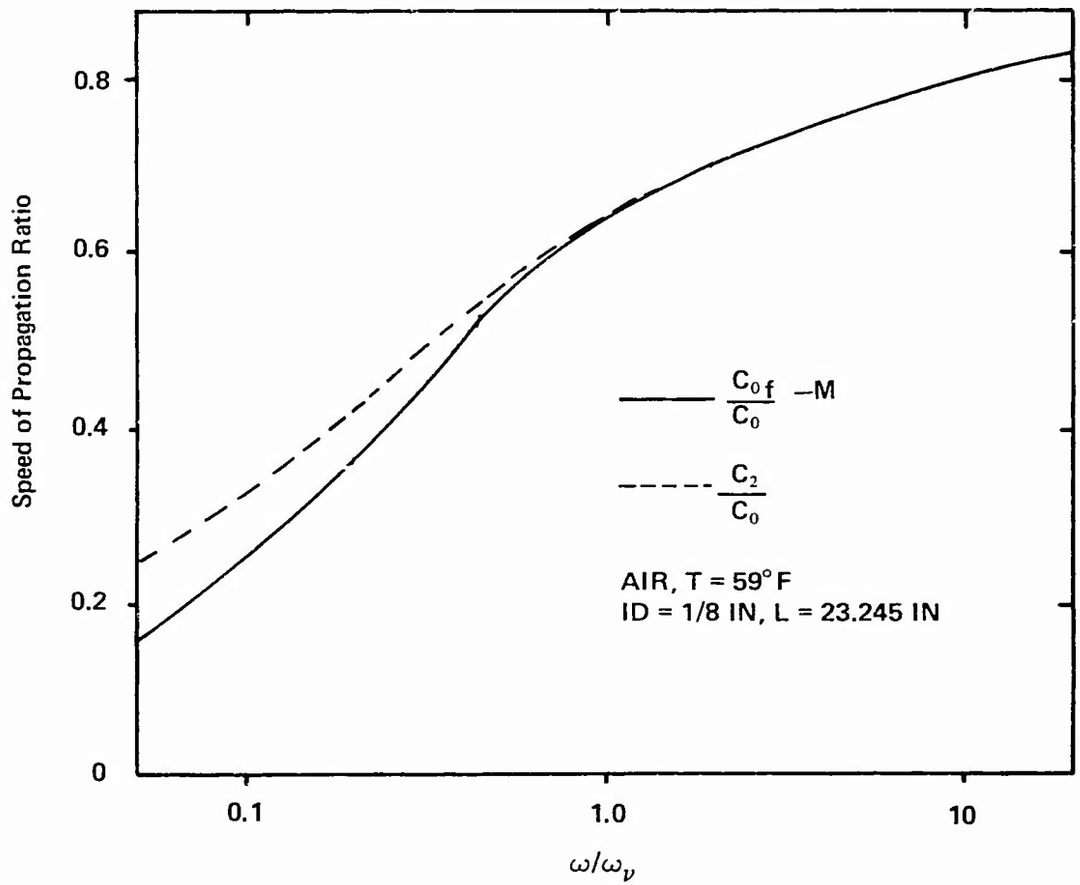

Figure 58. Backward Wave Speed of Propagation Ratio for M = 0.1
(C_0 = 13400.9 in/sec)

propagation constant and the characteristic impedance. The attenuation and the phase constant for both forward and backward traveling waves were smaller when the weighting function based on the isentropic ideal gas law was used. The attenuation was up to 50% smaller and the phase constant up to 18% smaller for M = 0.1. The difference became less as the Mach number increased. Results for $M = 1 \times 10^{-7}$ were much smaller, up to 42% smaller, than classical results for no-flow. The results for the characteristic impedance for no-flow did not agree either. The ideal gas results were up to 18% larger than those calculated using the Bessel function relation. The ideal gas results with flow were also larger than those calculated using Eq (20) and did not agree as well with the data of Katz, Hausner, and Eisenberg. The conclusion is that the isentropic ideal gas relation, Eq (22) is an oversimplification of the pressure-density relation for fluid transmission line problems involving dynamic pressure. A frequency dependent relation, such as Eq (18), is needed for accurate results.

Application of Results

The engineer needs to know when the effect of mean laminar flow must be accounted for. The analytical data given in this chapter show that the effect of mean flow on the attenuation, phase constant and speed of propagation, which was small for hydraulic lines at moderate flow rates, is significant for air lines with higher flow rates. The effect is frequency dependent, being much larger at low frequencies than at high frequencies. In the high frequency regime, $\omega/\omega_\nu > 1$, the effect of mean flow is significant for Mach numbers greater than 0.1. For low frequencies, $\omega/\omega_\nu < 1$, the effect is significant at lower Mach numbers, 0.05 or even lower for very low frequencies. Since the

frequency regime is defined in terms of ω/ω_ν where ω_ν is the viscous characteristic frequency, the effect of radius and kinematic viscosity must be considered also. For a given ω, small radii and large kinematic viscosities make ω/ω_ν small and hence drive ω/ω_ν toward the low frequency regime where the effect of mean flow is more pronounced. The opposite effect occurs for large radii and small kinematic viscosities.

XI. Comparisons with Published Research

Introduction

To assure that this mathematical model of a fluid line with mean flow is indeed representative of an actual fluid transmission line and its associated fluid mechanics, analytical data must be computed and compared with experiment and the results of other researchers. Considering that through-flow is the primary variable included in the analysis which distinguishes this work from prior research, comparisons need to be made for cases with significant through-flow. This necessarily eliminated the use of the available experimental data for hydraulic systems due to the small through-flows. The largest flow rate used was 9.5 gpm (Re = 1973) which equates to a mean flow Mach number of 0.003. However, published results for air lines with significant mean flow are available. Further comparisons were made to ensure that the analysis, when applied to the case of no-flow, generated the same results as given by Nichols (22) and Brown (7). A final comparison is made with the turbulent results of Brown, Margolis and Shah (8) and Moore (20).

Comparisons with the Work of Nichols and Brown

Nichols (22) and Brown (7) studied the response of rigid circular lines to small amplitude laminar disturbances. The lines had no mean flow. Both researchers derived analytical expressions in terms of Bessel functions for attenuation and phase velocity. These two quantities, nondimensionalized in the manner of Nichols and Brown, are plotted in the following figures. Figures 59 and 60 show how the

author's results and those of Brown compare for a liquid. The curves overlap showing that the author's analysis does predict the same attenuation and phase velocity as given by Brown for the case of no-flow. Data for mean flows up to 5 gpm (Re = 1039) showed a deviation from the no-flow curve of less than 1% of the no-flow value.

Results for air lines with Mach numbers up to 0.3 are considered next. Figures 61 and 62 compare the author's results with those of Brown. Again the no-flow curves agree. The curves for M = 0.1, 0.2 and 0.3 show how mean flow affects the attenuation and phase velocity of the forward and backward traveling waves. A comparison with Nichols' results for air is given in Figures 63 and 64. Once again the no-flow curves agree and the curves for M = 0.1, 0.2 and 0.3 demonstrate the effect of mean flow. The curves with mean flow show a large deviation from the no-flow curve at low frequencies. For the forward wave at $\omega/\omega_v = 0.01$ and M = 0.1, the db attenuation per line wavelength is 41% of the no-flow value and c/c_o is 21% higher than the no-flow value. These deviations decrease rapidly with increasing values of ω/ω_v. The deviations are primarily due to the low wave propagation velocities in the line at low frequencies. For these low wave propagation velocities, the mean flow becomes a much larger percentage of the propagation velocity and deviations in β due to mean flow are more pronounced.

Comparisons with Turbulent Flow Results

Moore (20) and Brown, Margolis, and Shah (8) present analytical and experimental results for fluid transmission lines with turbulent mean flows. The effect of the turbulence is given for the attenuation and phase velocity of the forward traveling wave. The magnitude of

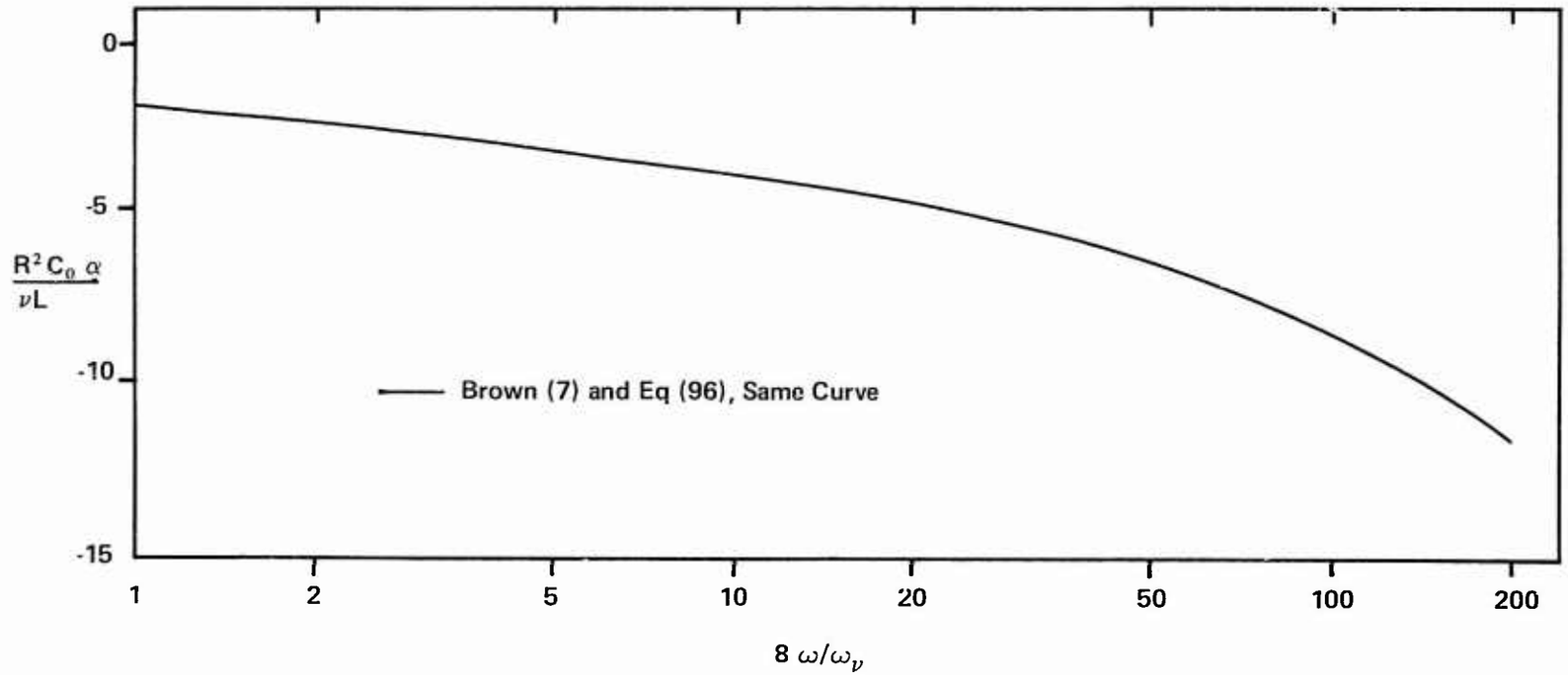

Figure 59. Comparison of Attenuation Results with Those of Brown for Hydraulic Fluid

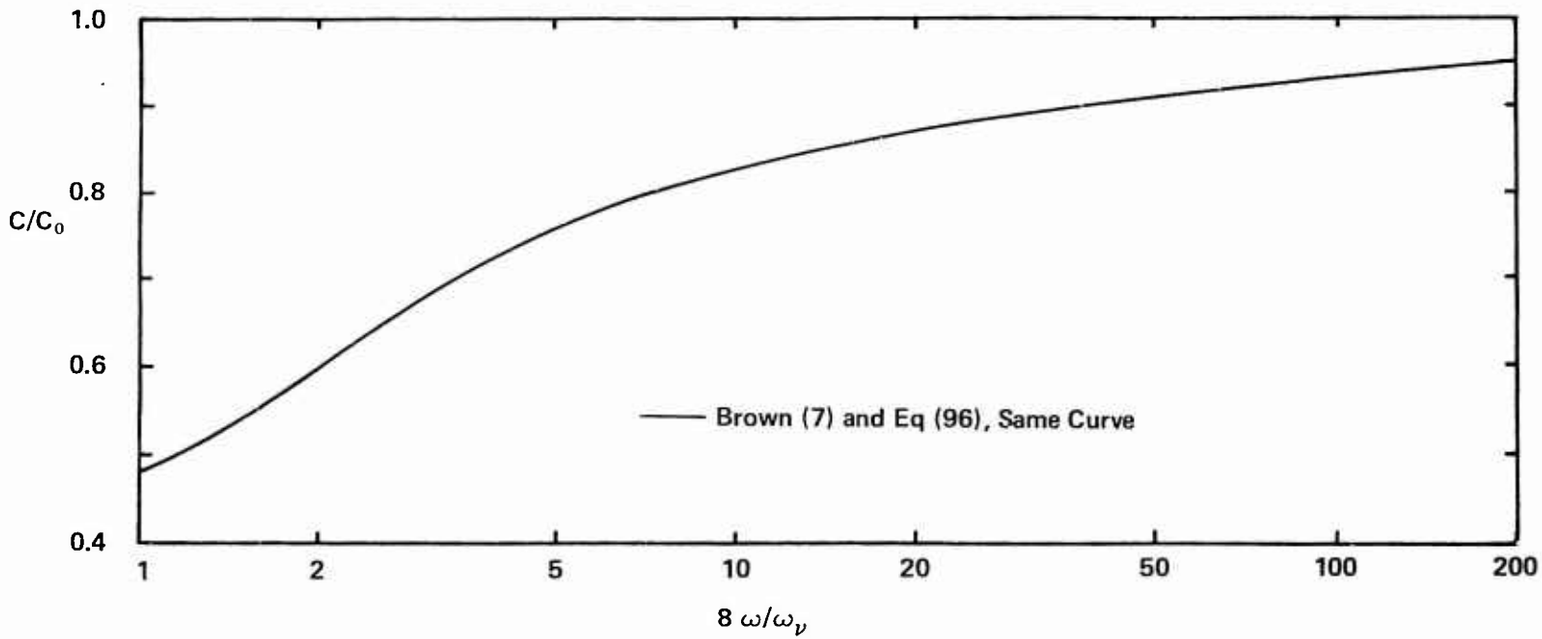

Figure 60. Comparison of Wave Propagation Velocity with Brown's Results for a Liquid (Hydraulic Fluid)

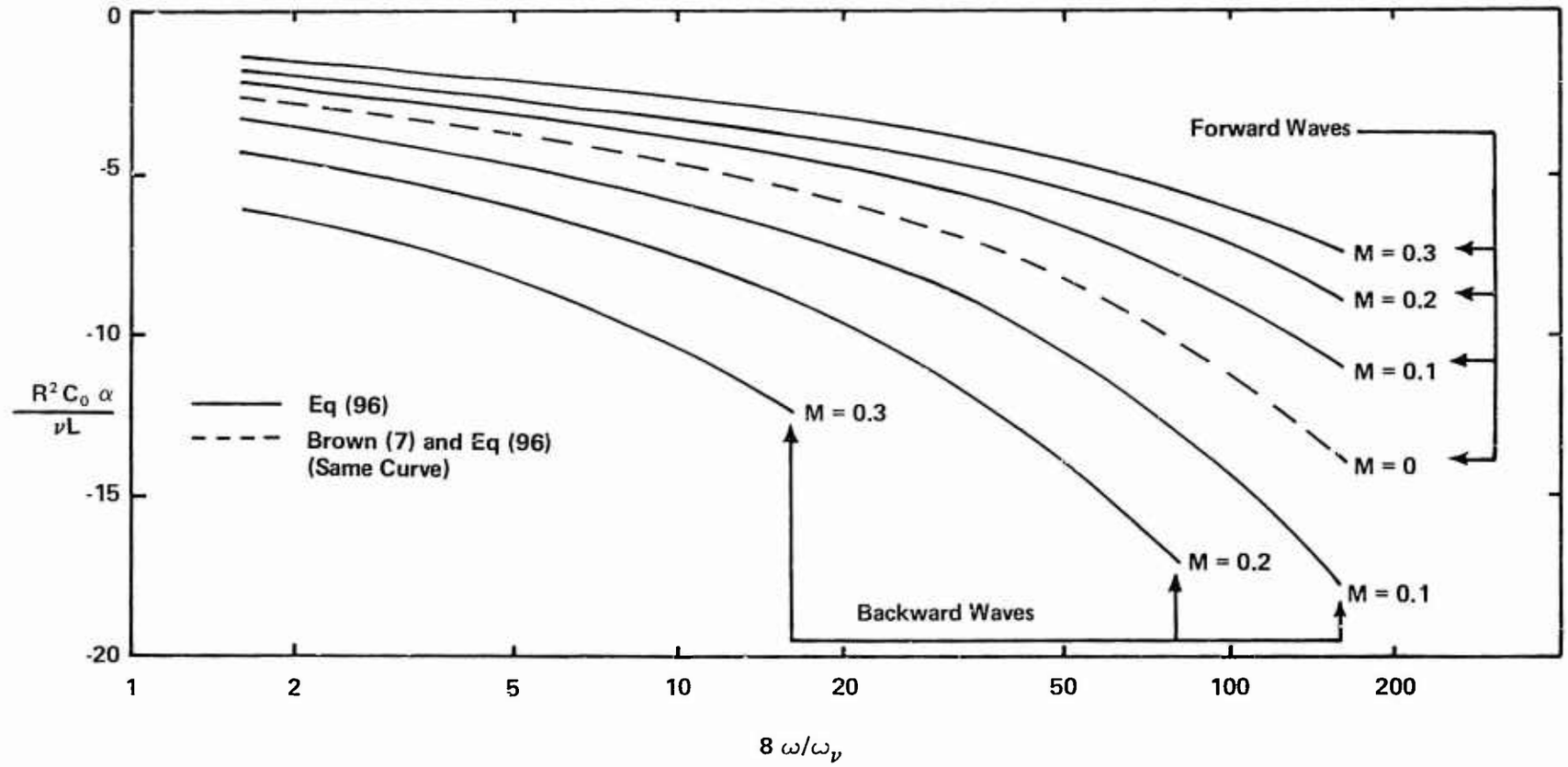

Figure 61. Comparison of Attenuation Results with Those of Brown for Air

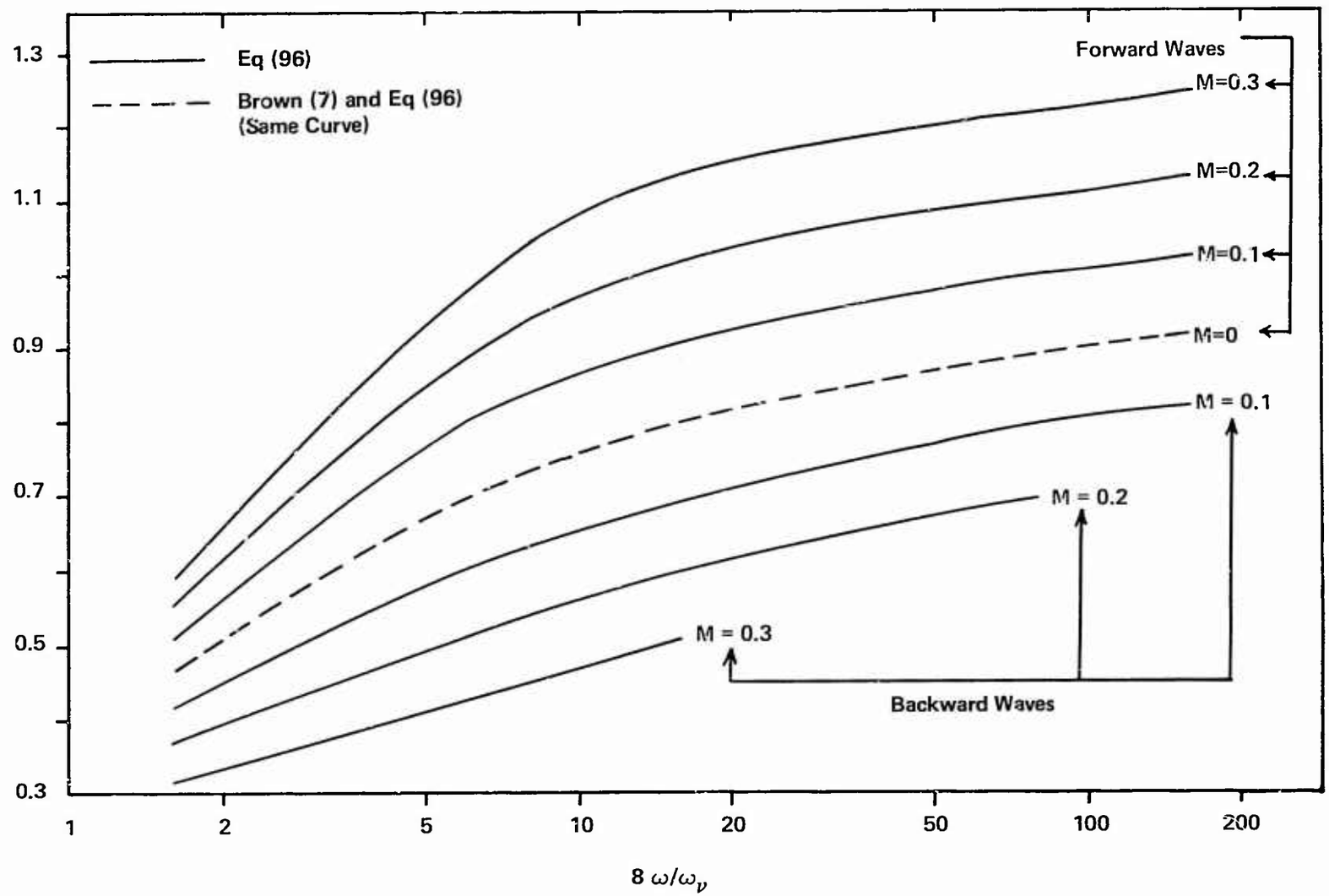

Figure 62. Comparison of Wave Propagation Velocity with Brown's Results for Air

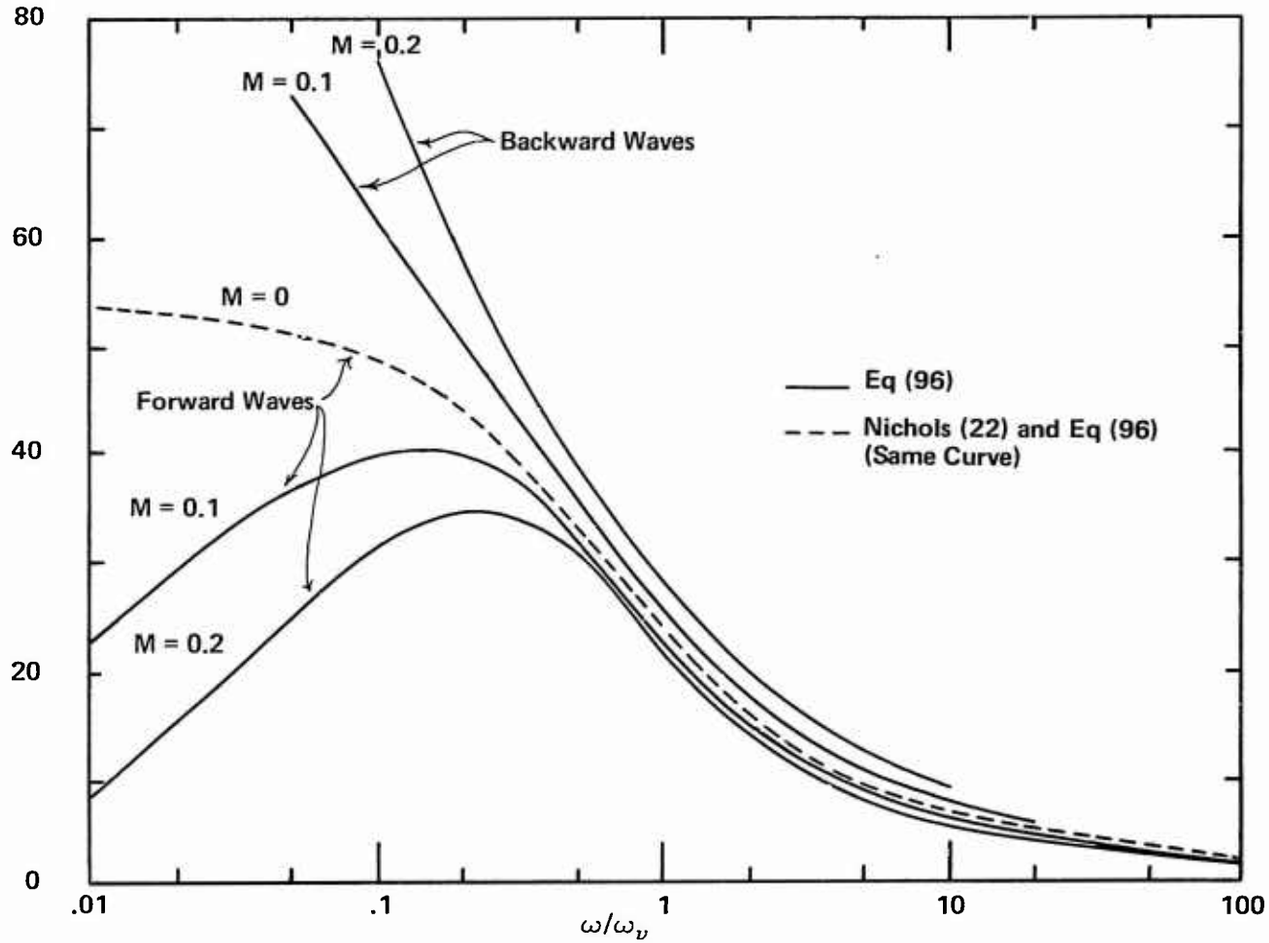

Figure 63. Comparison of Results for the db Attenuation Per Line Wave Length With Those of Nichols for Air

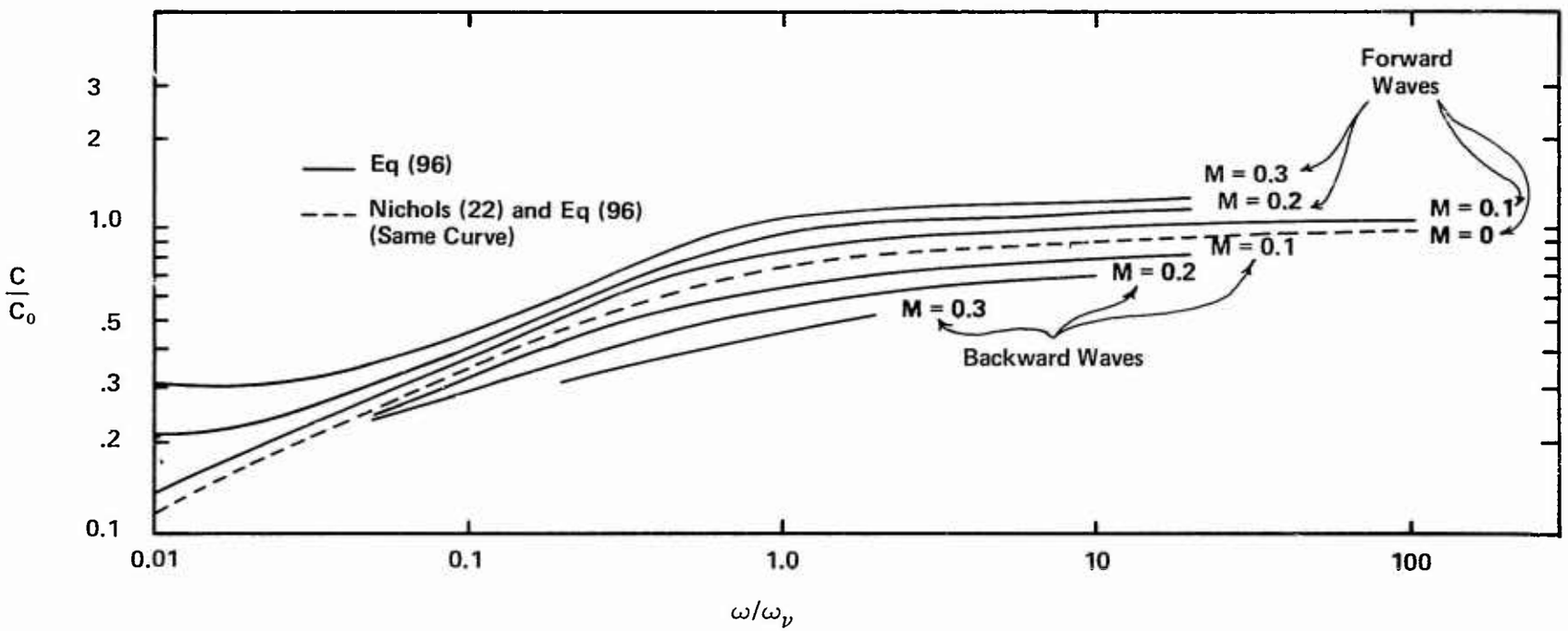

Figure 64. Comparison of the Phase Velocity with Nichols' Results for Air

the attenuation at a given frequency increases from the laminar value with increasing Reynolds number above the critical Reynolds number. The phase velocity also increases with increasing Reynolds number above the critical Reynolds number at a constant but high value of frequency. At lower frequencies, the opposite effect occurs; i.e., the phase velocity decreases with increasing Reynolds number. The curves in Figures 61 and 64 for M = 0.1 (Re = 7438), M = 0.2 (Re = 14877), and M = 0.3 (Re = 22315), as well as the data given back in Chapter X, show a different trend. The attenuation decreases with increasing Mach number and hence Reynolds number. The frequencies plotted in Figure 64 are in the low frequency range as given by Brown, Margolis, and Shah (8) and the turbulent analysis and experimental data showed a decrease in phase velocity with increasing Reynolds number in this range. Just the opposite occurs in Figure 64. Also the apparent resonance in attenuation found experimentally by Margolis and Brown (19) for water at turbulent Reynolds numbers transitioning from low to high frequency is not observed in the laminar data given in Figure 61. Thus the effect of turbulence is not predicted by the author's analysis. This is expected as a laminar mean flow was assumed in the analysis.

For most pneumatic lines (0.125 in. ID and greater), the flow is turbulent for M > 0.05 and thus the laminar results given in X and XI do not apply. For meaningful results with turbulent flows, the turbulent momentum transport must be considered in the analysis.

Comparisons with the Work of Orner and Cooley

A research effort by Orner (24) led to an approximate solution for a fluid transmission line with mean flow. This is a perturbation

solution based on powers of Mach number. Numerical results are given for the admittance parameters of the conventional two-port model for a transmission line; i.e.,

$$u(0) = Y_{11}p(C) + Y_{12}p(1) \tag{111}$$

$$u(1) = Y_{21}p(0) + Y_{22}p(1) \tag{112}$$

where a zero in parenthesis denotes the beginning of the line, one denotes the end of the line, and the Y's are the admittance parameters. Orner's numerical solution retained terms through M^2. In a follow-on paper a year later, Orner and Cooley (25) published the results of experiments designed to determine how well the approximate solution compared with actual line data. The admittance parameters were experimentally determined for Mach numbers of 0 and 0.1 for air at one-fifth atmosphere in a 0.125 in. ID acrylic plastic line. The line temperature was not given in Reference 25, but was assumed to be room temperature, 68^{o}F. Much later it was determined that the actual line temperature was 75^{o}F. For M = 0.1, high laminar flow exists as the Reynolds number is 1454, assuming transition is not triggered early as may happen if vibration is present.

The computer program that calculated the attenuation and phase constant using the confluent hypergeometric equation analysis was modified to calculate the admittance parameters. Due to long run times, only Y_{11}, termed the forward driving point admittance, and Y_{21}, termed the forward transfer admittance, were calculated. These were chosen as they showed the largest changes for an increment in mean flow. Another reason was that the analytical and experimental results of Orner and Cooley were not in agreement, even qualitatively, for Y_{22},

indicating errors in the analysis, the experiment, or both. However, the results for the other admittance parameters agreed qualitatively; i.e., the trends were the same. Vibration is a likely source of any experimental error and may have even triggered transition to turbulent flow. Vytoyannis and Hsu (33) in a careful experiment with curved pipes found transition near a Reynolds number of 900.

Figures 65 and 66 show the computer results along with the experimental results of Orner and Cooley. The magnitude data have been nondimensionalized by Y'_o which is equal to $1/c_o\rho_o$ so as to correspond to the data given by Orner and Cooley. The agreement is good for the magnitudes of the two admittance parameters. The phase angle data agrees qualitatively, however the curves appear to be shifted to the left in comparison with the experimental data. This is possibly due to the temperature for the experiments being slightly higher than room temperature which was used for the computer calculations.

Comparisons with the Work of Katz, Hausner, and Eisenberg

Several years following the work of Orner and Cooley, the results were published of an analytical study on the effect of through-flow by Katz, Hausner, and Eisenberg (17). In their analysis, two models were used. The first, a fixed component model, added convective terms to the conventional transmission line equations. The second, a variable component model, used the continuity, momentum, and energy equations with a uniform velocity profile. The solutions were then placed in transmission line form with the resulting impedance and admittance being functions of the uniform mean flow velocity. In the fixed component model, which also used a uniform velocity profile, the

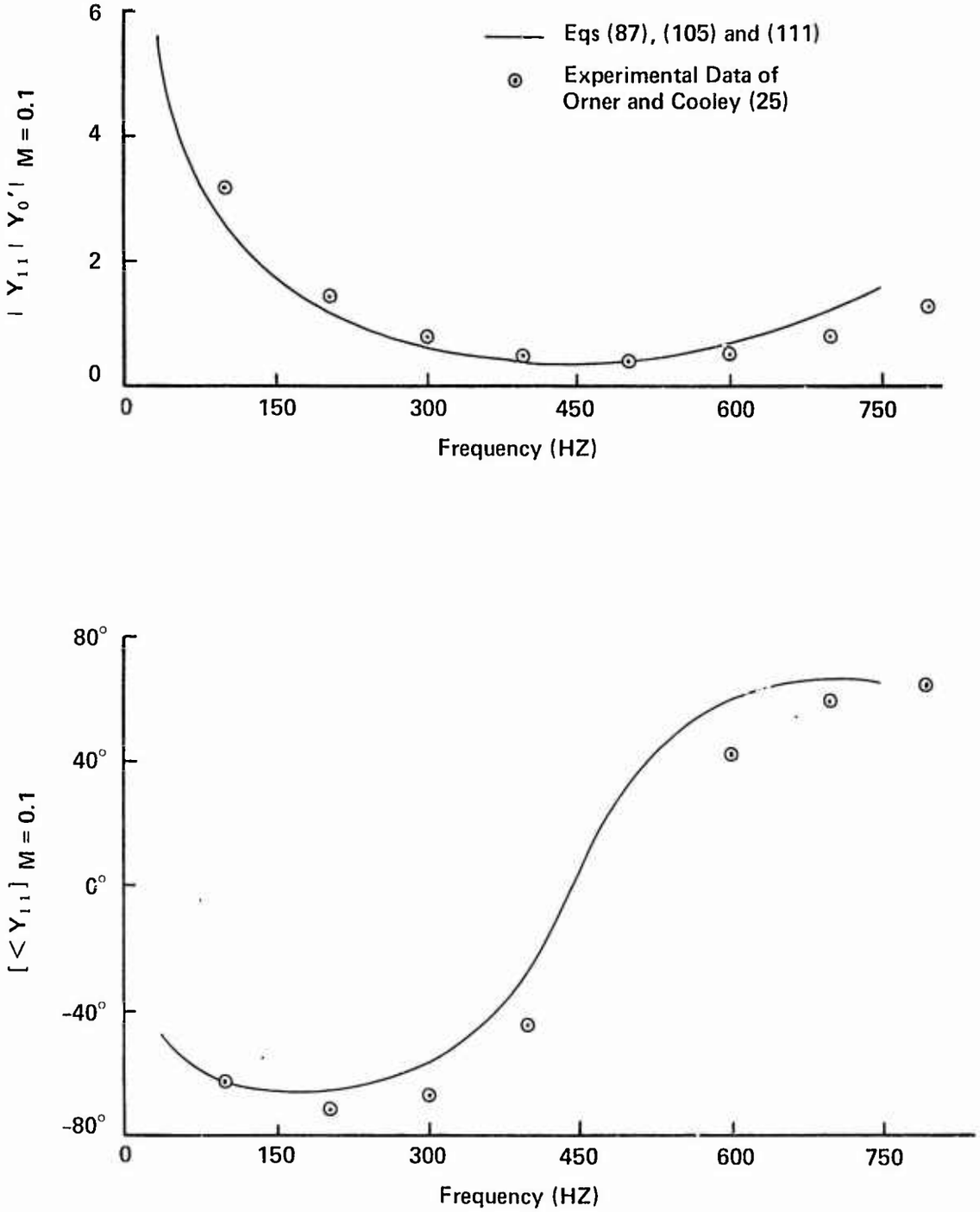

Figure 65. Comparison Of The Analytical And Experimentai Values Of The Forward Driving Point Admittance For M = 0.1

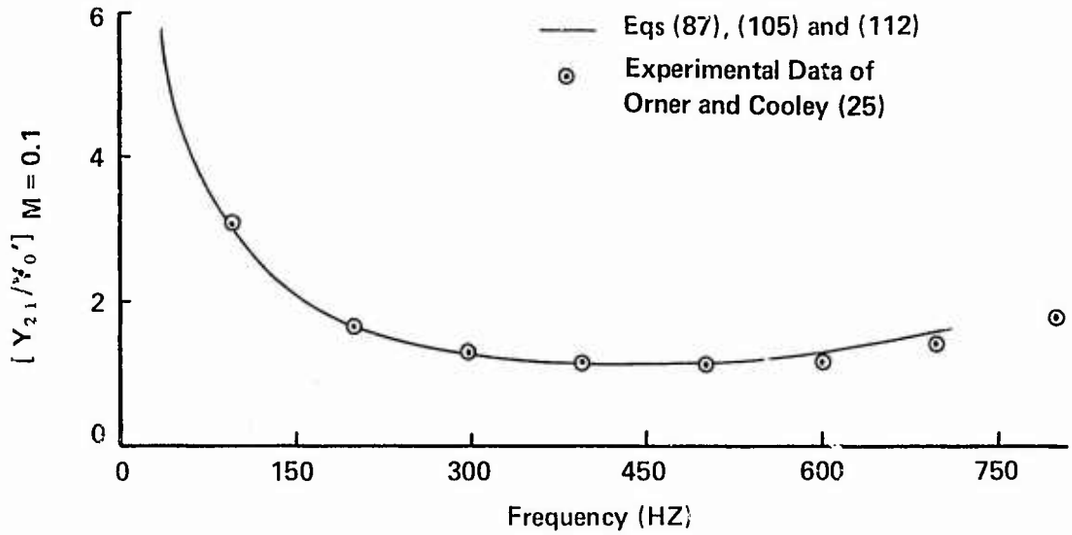

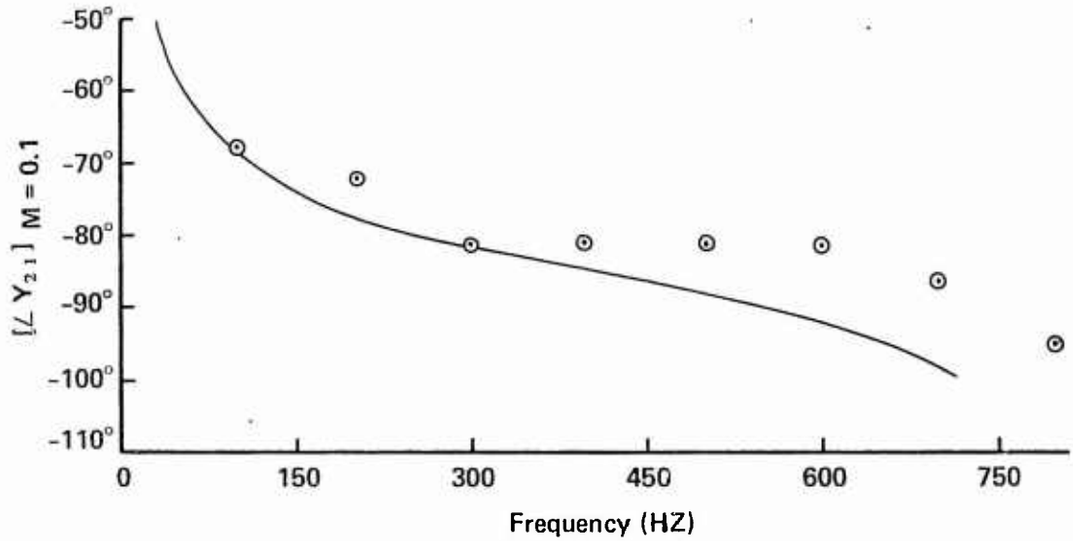

Figure 66. Comparison Of Analytical And Experimental Values Of The Forward Transfer Admittance For M = 0.1

impedance and admittance were not functions of the mean flow velocity. Plots of the real and imaginary parts of the normalized characteristic impedance were given for Mach numbers of 0, $\pm$ 0.2 and $\pm$ 0.3 for the fixed component model and for M = 0.3 for the variable component model. Negative Mach numbers refer to mean flow toward the source of the pressure oscillations. The data were normalized using the adiabatic characteristic impedance, Z_{ca}, which is equal to $\rho_o c_o/(\pi R^2)$.

The characteristic impedance was calculated using the analysis based on the confluent hypergeometric equation by modeling the line as a matched line. This means there is no reflection from the end of the line and thus there exist only forward traveling waves. The pressure and velocity at the end of the line were calculated and used to calculate the characteristic impedance. Results were obtained for conditions of standard temperature and pressure for several Mach numbers. For Mach numbers of 0, 0.1 and 0.2, data were obtained for the entire range of frequencies used by Katz, Hausner, and Eisenberg. For M = 0.3, no data were obtained due to convergence problems. Likewise, convergence problems allowed calculations over only a limited range of frequencies for negative Mach numbers. The results are depicted in Figures 67 and 68.

Figure 69 shows comparisons for the real parts of the dimensionless characteristic impedance for M = 0.2. The M = 0 line is identical for both analyses. This was expected since any analysis with mean flow must reduce to the classical Bessel function formulation for the case of no flow. The two M = 0.2 curves agree qualitatively. Both are consistently below the M = 0 curve, both show large deviations from the M = 0 curve at low frequencies, and both appear to be

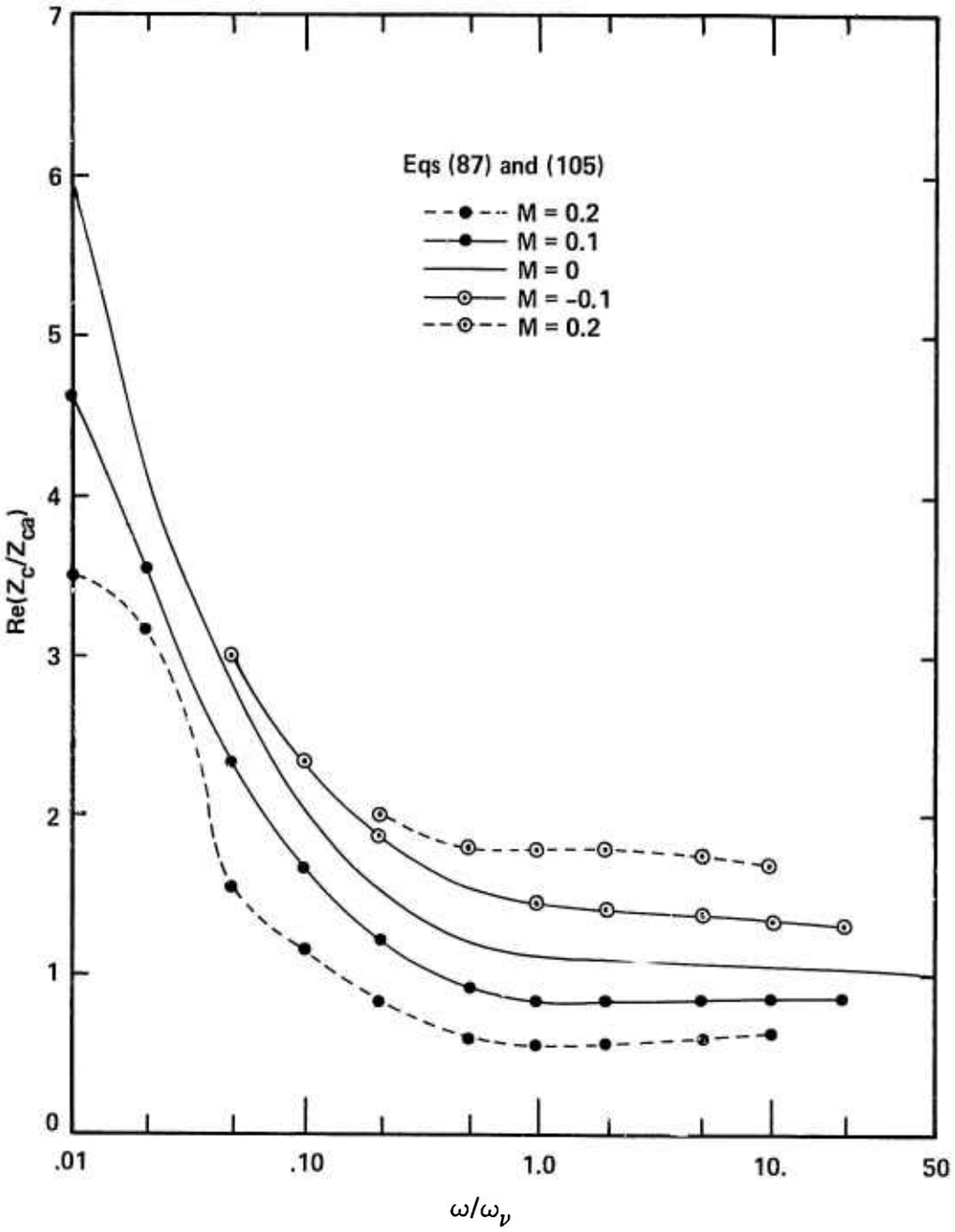

Figure 67. Real Part Of The Normalized Characteristic Impedance Versus ω/ω_ν

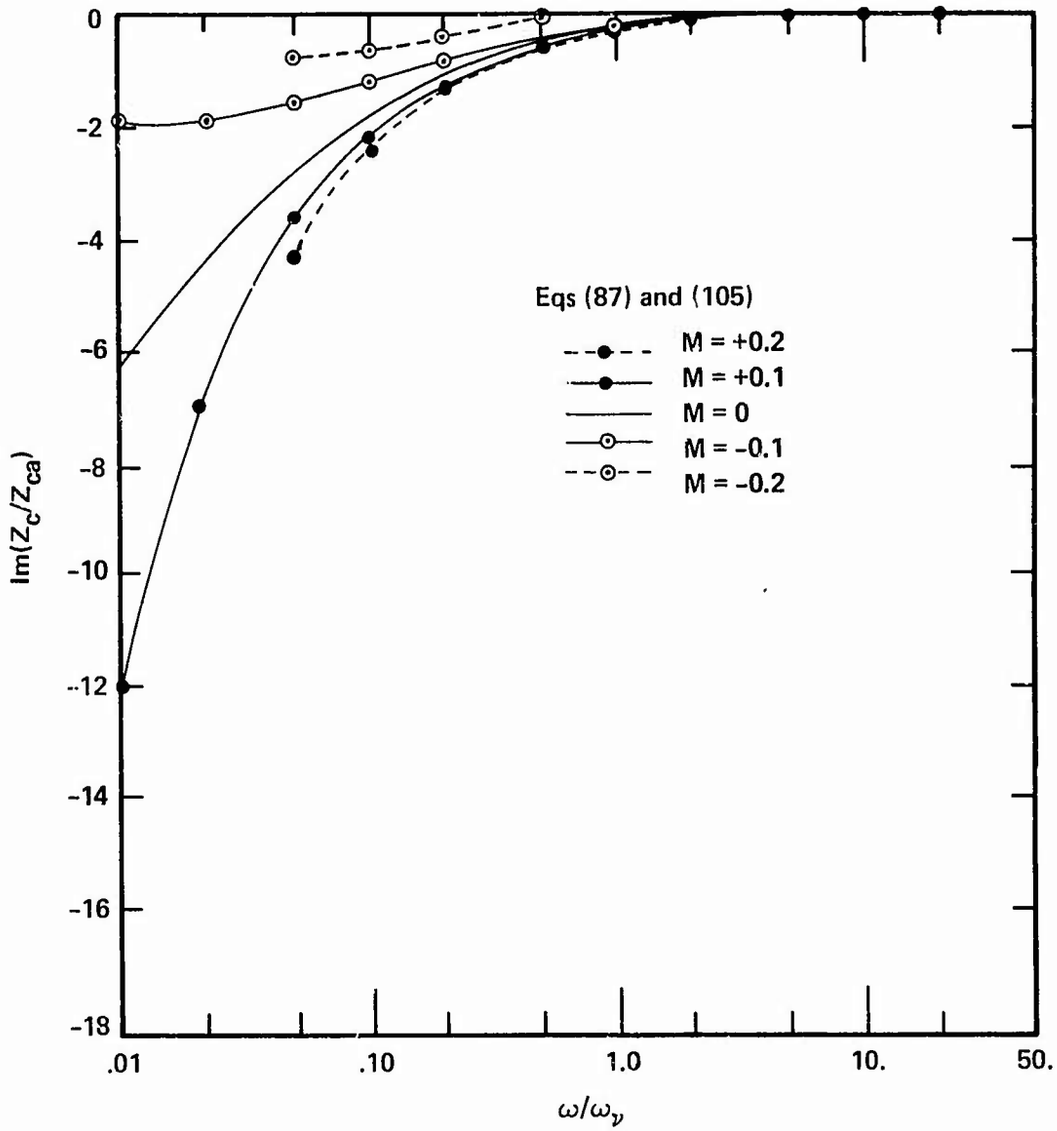

Figure 68. Imaginary Part Of The Normalized Characteristic Impedance Versus ω/ω_ν

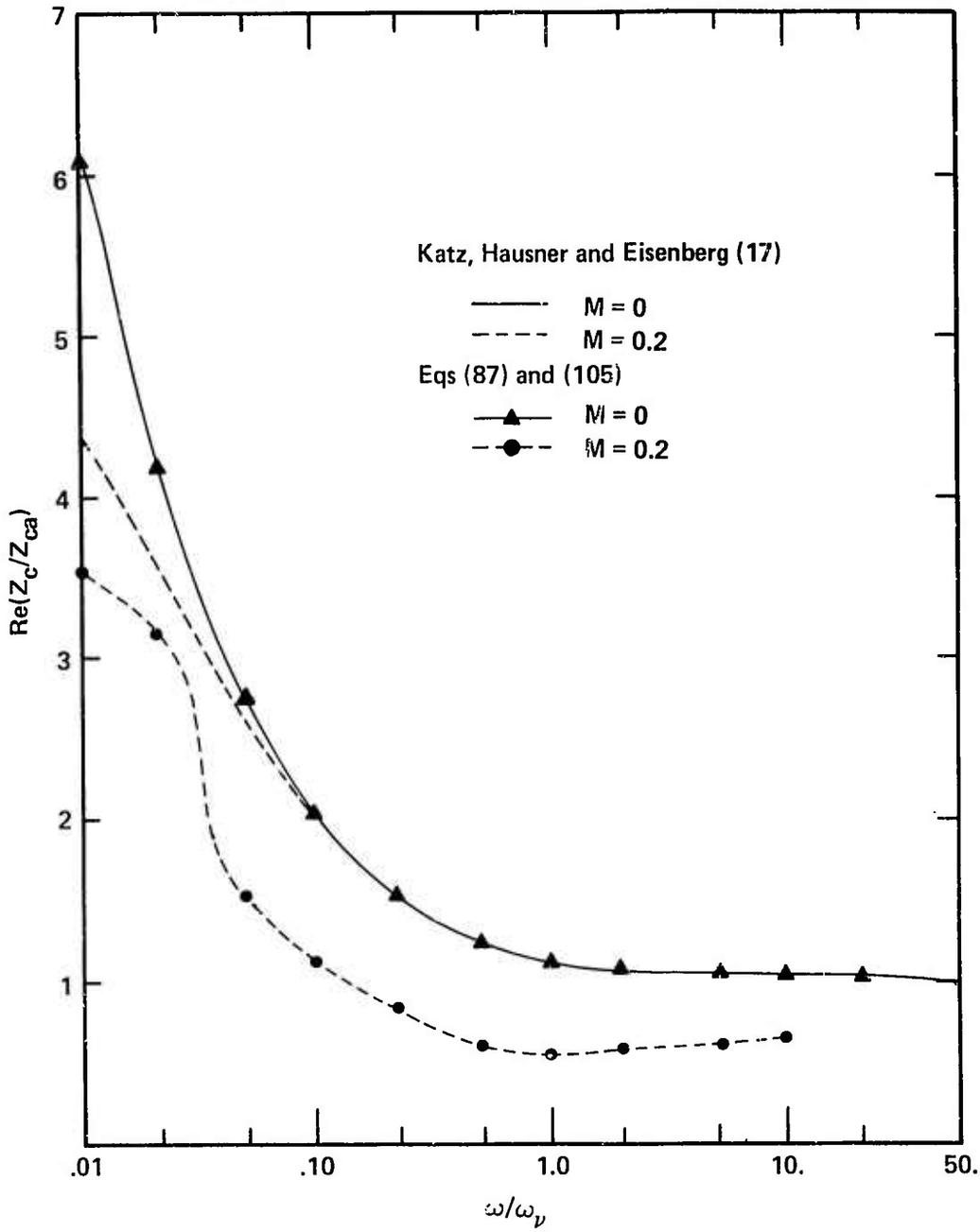

Figure 69. Real Part Of The Normalized Characteristic Impedance For M = 0 And 0.2 Versus ω/ω_ν

approaching one at high frequencies. Two distinctions are apparent. First the analysis based on the confluent hypergeometric equation gives data consistently lower than that of Katz, Hausner and Eisenberg for all frequencies. Due to this, the second distinction occurs; namely, the data do not approach one as fast as the data of Katz, Hausner and Eisenberg. Figure 70 shows the imaginary part of the dimensionless characteristic impedance for Mach numbers of 0 and 0.2. The agreement here is excellent.

Further comparisons are made in Figures 71 and 72 which show data from the confluent hypergeometric equation analysis for $M = \pm 0.1$. Katz, Hausner and Eisenberg did not present data for $M = 0.1$, so their data for $M = \pm 0.2$ is given. The same points noted for the prior comparisons are noted again. The real part of the dimensionless characteristic impedance for $M = 0.1$ is consistently below the $M = 0$ curve and approaches one at high frequency. The data for $M = -0.1$ are consistently above the $M = 0$ curve and likewise approach one at high frequency. These trends are better seen in Figures 67 and 68 which plot only data from the confluent hypergeometric equation analysis. The limited data for $M = -0.2$ fall slightly above the $M = -0.1$ data for the real and imaginary parts of the dimensionless characeristic impedance.

The differences between the two analyses for the real part of the dimensionless characteristic impedance at low frequencies, $\omega/\omega_\nu < 1$, would not be as large if data from Katz, Hausner and Eisenberg for the variable component model had been used. Unfortunately, Katz, Hausner and Eisenberg gave data for the variable component model only for $M = 0.3$. However in this case, for $\omega/\omega_\nu < 0.1$ the

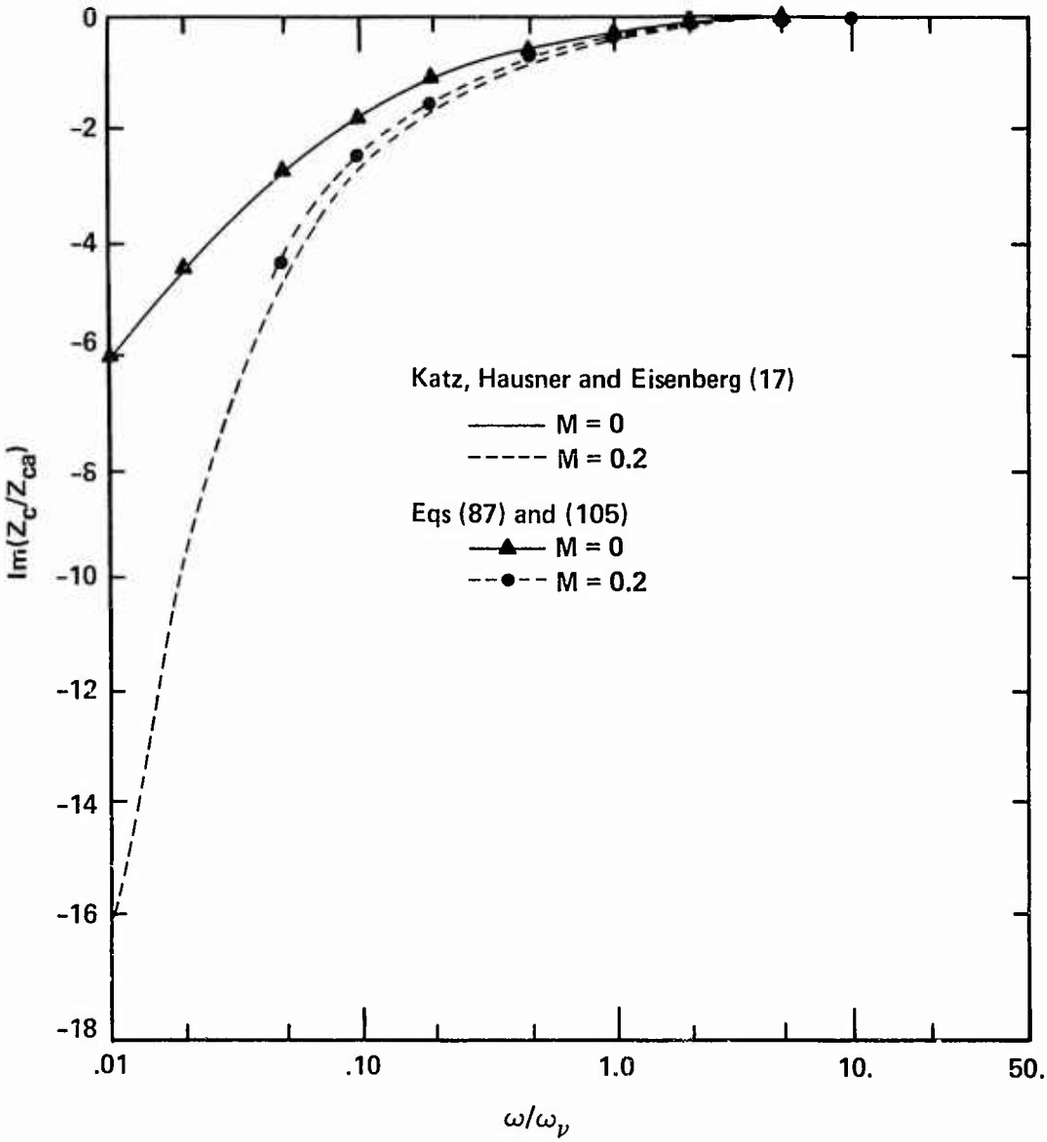

Figure 70. Imaginary Part Of The Normalized Characteristic Impedance For M = 0 and 0.2 Versus ω/ω_ν

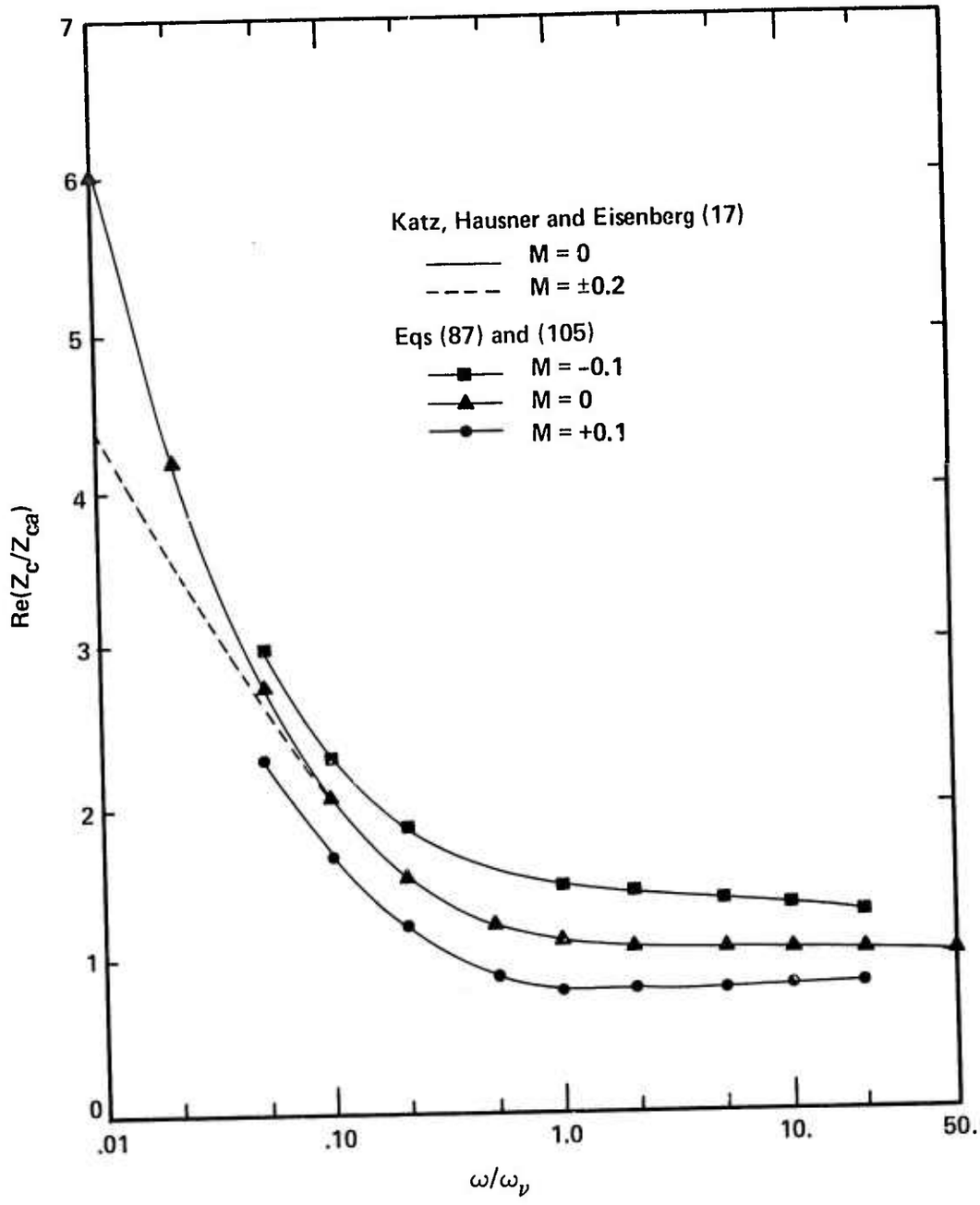

Figure 71. Comparison Of The Real Part Of The Normalized Characteristic Impedance With The Results Of Katz, Hausner, and Eisenberg

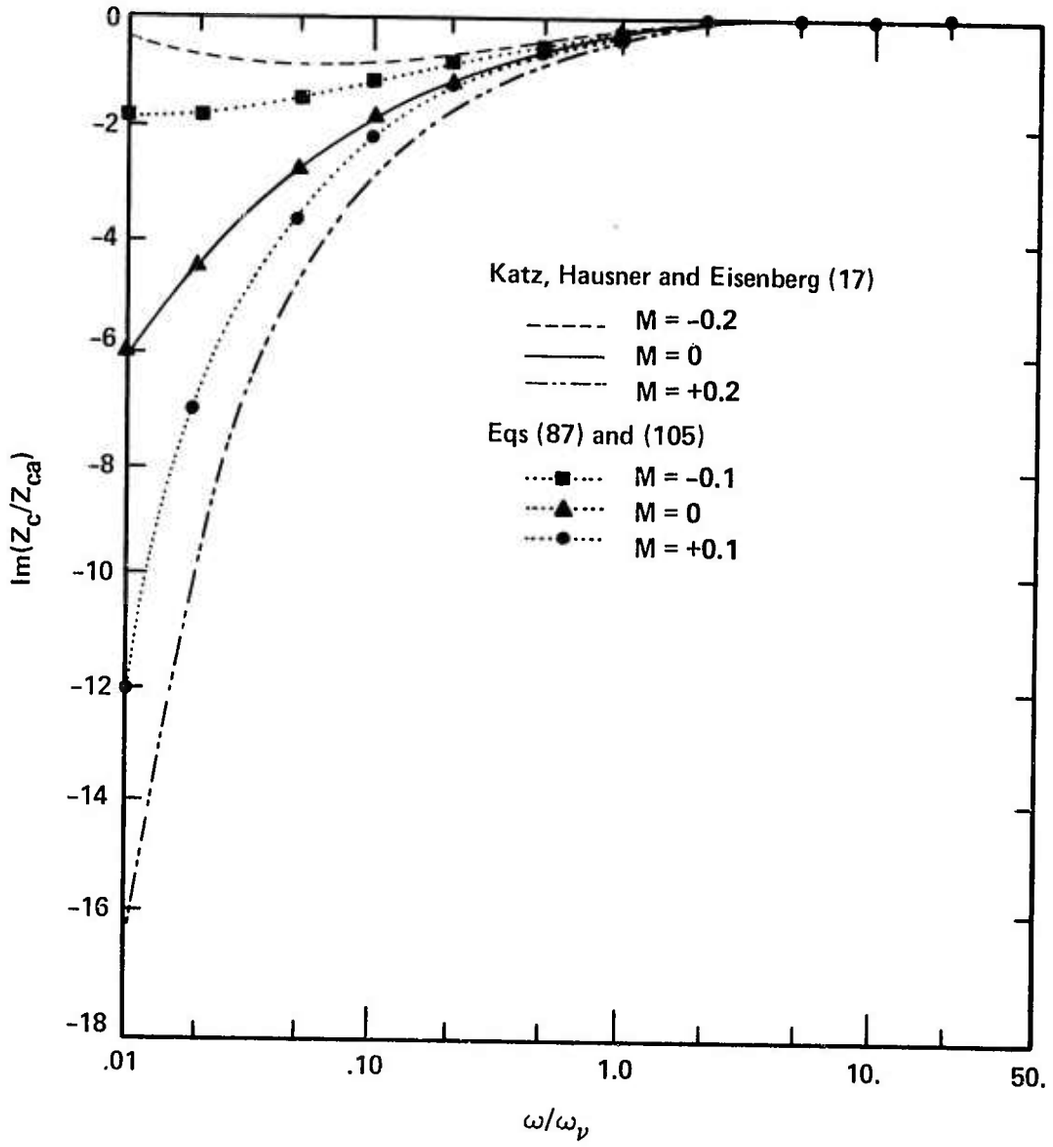

Figure 72. Comparison Of The Imaginary Part Of The Normalized Characteristic Impedance With The Results Of Katz, Hausner, And Eisenberg

real part of the dimensionless characteristic impedance is significantly smaller compared to that for the fixed component model. At higher frequencies, the variable component model gives values only slightly higher than the fixed component model. This closer agreement between the variable component model and the model based on the confluent hypergeometric equation is expected since both analyses are based on the same fundamental equations of fluid mechanics while the fixed component model is based on the transmission line equations.

The differences that do exist between the analysis of Katz, Hausner and Eisenberg are due to two things. First and primarily, Katz, Hausner and Eisenberg assume a uniform velocity profile in their analysis as opposed to the parabolic Hagen-Poiseuille velocity profile used in the analysis based on the confluent hypergeometric equation. This is probably the reason why the real part of the dimensionless characteristic impedance is nearly the same for positive and negative Mach numbers. The second reason for the differences is that both analyses are for laminar flow. The analytical results based on the confluent hypergeometric equation were for a typical pneumatic line at standard temperature and pressure. The Reynolds numbers for all but the M = 0 case were well into the turbulent range. This is probably why convergence problems arose for the higher Mach numbers. The results of Katz, Hausner and Eisenberg do not explicitly involve Reynolds number though it is difficult to think of an actual fluid transmission line with laminar flow at a Mach number of 0.2 or 0.3.

XII. Conclusions and Recommendations for Future Research

Conclusions reached as a result of this research are contained in this chapter. Also, recommendations for future research that would extend this work are given.

Conclusions

1. A new analytical solution for the pressure and velocity in a fluid transmission line with laminar through-flow has been developed. The solution is in the form of an infinite series that converges uniformly. Convergence is fastest for low mean flows and dimensionless frequencies, ω/ω_ν, near one. At very low or high frequencies and at high mean flow rates, the convergence is very slow and numerical evaluation if difficult due to destructive cancellation. For zero mean flow the solution reduces to the classical Bessel function relation. Since the velocity is given as a function of radius, the velocity profile can be calculated.

2. This new analytical solution provides an alternative for the many approximations found in the literature. The transmission line equations have been modified, additional convective terms have been added, and empirical results based on careful experiments are available. Now a solution, not an approximation, based on the fundamental equations of fluid mechanics, not electrical transmission line theory, is available. It considers the radial velocity distribution and the coupling of the mean flow with the oscillating flow. As a result it is complicated and numerical results are expensive in terms of computer time, but the results are accurate. There are several important

applications. For large mean flows, the new solution provides an accurate means of analyzing a system that was not available before. Second, the solution provides a standard against which approximations can be judged. Thirdly, the solution provides an accurate means of determining trends, especially those due to the effect of mean flow, which will help the engineer and designer who do not need the accuracy a complete analytical solution would give.

3. Results calculated using this new analytical solution were compared to the published results of other researchers. The no-flow attenuation, wave propagation velocity, and db attenuation per line wavelength for both air and liquid lines compared very well with that given by the analyses of Brown (7) and Nichols (22). Results were also compared to the turbulent results of Moore (20) and Brown, Margolis and Shah (8) with the expected conclusion that the laminar analysis which included the effect of mean flow, but not turbulent momentum transport, does not predict well for turbulent flows.

Admittance parameters compared well with those given by Orner and Cooley (25). Also the real and imaginary parts of the characteristic impedance compared well with those values given by Katz, Hausner and Eisenberg (17). Increasing positive flow caused the real part of the characteristic impedance to decrease and the imaginary part to become more negative. The one point of disagreement is where Katz, Hausner and Eisenberg show the real part of the characteristic impedance to be nearly the same for both positive and negative Mach numbers, when the new analysis shows a deviation on each side of the $M = 0$ curve. For positive Mach numbers the values fall below the $M = 0$ curve in agreement with the results of Katz, Hausner and

Eisenberg, but for negative Mach numbers the values fall above the M = 0 curve. This is probably due to the inclusion of a parabolic mean flow velocity profile in the new analysis. A uniform velocity profile was used by Katz, Hausner and Eisenberg. In all, the comparisons with published laminar results were very good.

4. Using the new analysis, the attenuation, phase constant and velocity profile were calculated for a straight hydraulic line. Data were obtained for flow rates from 0 to 100 gpm. Dimensionless frequencies ranged from $1 \leq \omega/\omega_{\nu} \leq 203$. The primary conclusion was that the effect of flow was very small at these low mean flow rates. However, the data did show several trends. Both the attenuation and the phase constant increase with frequency. Also the backward wave attenuation and phase constant increase with flow while the forward wave attenuation and phase constant decrease with flow. For a given increase in flow, the increase in the backward wave attenuation and phase constant is greater than the decrease in the forward wave attenuation and phase constant. The attenuation and phase constant deviations increased nearly linearly with flow for a constant ω/ω_{ν}, while the increase with frequency for a constant flow rate was nonlinear. Likewise, both the attenuation and phase constant increase nonlinearly with increasing ω_{ν} for a constant frequency and mean flow.

5. Data for an air line with mean flow Mach numbers up to 0.3 and for dimensionless frequencies, ω/ω_{ν}, from 0.01 to 100 were also calculated. With these large mean flows, the effect of flow is more pronounced. The same trends as found for the hydraulic lines were noted again with the following exception. The nearly linear relationships noted for hydraulic lines over a limited frequency range were

found to be nonlinear when a broader frequency band was considered. At high frequencies, $\omega/\omega_\nu > 1$, the linear results were reasonably valid. However, at low frequencies, $\omega/\omega_\nu < 1$, nonlinearities set in for both the phase constant and the attenuation. The ratio of flow to no-flow values showed this the best. The simple approximation that the forward wave attenuation and phase constant are reduced by a factor of 1 + M is only valid for $\omega/\omega_\nu >> 1$. For lower frequencies the analysis developed in this research must be used. In all, the effect of laminar mean flow needs to be accounted for when $M > 0.1$ for $\omega/\omega_\nu > 1$. For lower frequencies, $\omega/\omega_\nu < 1$, the effect of mean flow is significant at lower Mach numbers, 0.05 or even lower for very low frequencies.

6. Velocity profiles calculated for a hydraulic line compared well with the profiles given by Uchida (32) and Richardson (27).

7. Hydraulic line experiments were conducted to study further the effect of flow and to provide data for comparison with analytical results. The frequency response and standing pressure half wave were determined for flow rates up to 9.5 gpm. However, only data for flow rates up to 5.0 gpm were used as the flow became turbulent at the higher flow rates. The analytical and experimental results compared well. The mean flow had no significant effect on the resonant frequency, nodal point locations or pressure amplitude.

8. The effect of bends in a hydraulic line was studied experimentally. No significant effect was found except for a large increase in the pressure amplitude at the fifth resonant frequency for high flow rates.

9. Pressure measurements were made with a roving clampon transducer which was easily moved and did not disturb the flow. In the absence of vibration, pressure measurements made with the clampon transducer were within 5% of readings taken with a conventional Statham in-line transducer 90% of the time. Vibration does affect the clampon transducer, however. Vibrational displacements in excess of 0.001 in. peak-to-peak were found to cause significant errors. When the vibrational displacement is less than 0.001 in. peak-to-peak, the clampon transducer becomes an excellent tool for the hydraulic engineer.

10. A sensitivity analysis showed how variations in input data can affect results for a hydraulic system. Calculations were made using the analysis developed in this research and also using the HSFR computer program. The most significant input parameters were temperature, line length, radius, kinematic viscosity, element volume, and entrained air content. A summary of these effects is given in Table XI.

Recommendations for Future Research

1. The analysis developed in this research effort applies to laminar flow only. Work needs to be done using turbulent velocity profiles such as the 1/7th power velocity distribution law. Using an appropriate turbulent velocity distribution function instead of the parabolic velocity distribution function for laminar flow, the complexity of the resulting expressions in the analytical development will be greatly increased, but perhaps an infinite series solution that converges uniformly can be found, or at least one that converges in some region of engineering interest. Analytical results thus found

could be compared with turbulent experimental data already gathered in the experiments reported herein.

2. Considering the convergence problems that were encountered when the computerized calculations were attempted for very high and very low frequencies, there needs to be work done in finding another infinite series solution that converges faster in these extremes of frequency. The low frequency regime is most important as good approximations are available for the high frequency regime.

3. As an alternative to the prior recommendation, a new numerical method could be developed to overcome the destructive cancellation which causes the numerical problems. Lacking a new numerical method, one could also use a computer that carries more significant figures. The CDC Cyber 74 computer used for the calculations reported herein carried 29 significant figures.

4. Experiments need to be run to test the idea of putting two clampon transducers 180 deg apart on the same mount and using the combined output, after the transducers have been individually calibrated, to determine dynamic pressure in a line with significant vibration present. If good dynamic pressure measurements can be taken in this manner, the clampon transducer will be an invaluable engineering tool, especially for pressure measurements on operational systems where it is not practical or possible to cut lines and mount conventional in-line transducers.

5. The analysis and the experiments ignored the effect of pressure harmonics. This was done to make the analysis tractable, and the experiments demonstrated that the amplitudes of second and higher harmonics were much smaller than the fundamental and thus could be

neglected. Work needs to be done to determine what effect, if any, they have.

6. The experiments for the hydraulic line with the U-shaped bend showed that the bends had no significant effect except that the pressure amplitude at the fifth resonant frequency increased significantly. Work needs to be done to determine what causes this effect and how it can be predicted.

Bibliography

1. AFAPL-TR-76-43, Vol. III. Frequency Response (HSFR) Computer Program User Manual. Wright-Patterson Air Force Base, Ohio: Air Force Aero Propulsion Laboratory, Air Force Systems Command, February 1977.

2. AFAPL-TR-76-43, Vol. IV. Frequency Response (HSFR) Computer Program Technical Description. Wright-Paterson Air Force Base, Ohio: Air Force Aero Propulsion Laboratory, Air Force Systems Command, February 1977.

3. AFAPL-TR-77-63. Aircraft Hydraulic Systems Dynamic Analysis. Wright-Patterson Air Force Base, Ohio: Air Force Aero Propulsion Laboratory, Air Force Systems Command, October 1977.

4. Amies, G. E. An External Pressure Transducer for Measuring Transient and Oscillatory Pressures in Aircraft Hydraulic Systems. MDC A3134. St. Louis, Missouri: McDonnell Aircraft Company, undated.

5. AMSA Hydrodynamics. The 200 Series Clampon Pressure Transducers Instruction Manual. 2034 Northaire Lane, St. Louis, Missouri, 63138 (undated).

6. Blade, R. J., Lewis, W., and Goodykoontz, J. H. Study of a Sinusoidally Perturbed Flow in a Line Including a 90° Elbow with Flexible Supports. NASA Technical Note D-1216. Washington: National Aeronautics and Space Administration, July 1962.

7. Brown, F. T. "The Transient Response of Fluid Lines." Journal of Basic Engineering, Trans. ASME: 547-553 (December 1962).

8. Brown, F. T., Margolis, D. L., and Shaw, R. P. "Small Amplitude Frequency Behavior of Fluid Lines with Turbulent Flow." Journal of Basic Engineering, Trans. ASME: 678-693 (December 1969).

9. Carnahan, B., Luther, H. A., and Wilkes, J. D. Applied Numerical Methods. New York: John Wiley & Sons, 1969.

10. D'Souza, A. F. and Oldenburger, R. "Dynamic Response of Fluid Lines." Journal of Basic Engineering, Trans. ASME, Series D, Vol. 86, No. 3: 589-598 (September 1964).

11. Enever, K. J. Communications Following "The Influence of Bends on Fluid Transients Propagated in Incompressible Pipe Flow." Proceedings of the Institution of Mechanical Engineers, 1968-1969, Vol. 183, Pt. 1, No. 29: 609-610.

12. Foster, K. and Parker, G. A. "Transmission of Power by Sinusoidal Wave Motion Through Hydraulic Oil in a Uniform Pipe." Proceedings of the Institution of Mechanical Engineers, 1964-1965, Vol. 179, Pt. 1, No. 19: 599.

13. Handbook of Mathematical Functions. Edited by M. Abramowitz and I. Stegun, U. S. Government Printing Office, November 1970.

14. Kantola, R. "Transient Response of Fluid Lines Including Frequency Modulated Inputs." Journal of Basic Engineering, Trans. ASME: 274-282 (June 1971).

15. Kaplan, W. Ordinary Differential Equations. Reading, Mass: Addison-Wesley Publishing Co., Inc., 1958.

16. Katz, Shraga. An Experimental Study of Measuring Oscillatory and Transient Pressure in Hydraulic Systems. Unpublished Thesis. Wright-Patterson Air Force Base, Ohio: Air Force Institute of Technology, December 1978.

17. Katz, S., Hausner, A., and Eisenberg, N. A. "The Effect of Through-flow on Signal Propagation in Fluid Lines." Proceedings of the Fluidic State-of-the-Art Symposium, 30 Sep - 4 Oct 74, Harry Diamond Laboratories, Washington, D. C.: 269-297.

18. Kirshner, J. M. and Katz, S. Design Theory of Fluidic Components. New York: Academic Press, 1975.

19. Margolis, D. L. and Brown, F. T. "Measurement of the Propagation of Long Wavelength Disturbances Through Turbulent Flow in Tubes." Journal of Fluids Engineering, Trans. ASME, Vol. 98, Series I, No. 1: 79-78 (March 1976).

20. Moore, E. F. The Small Signal Response of Fluid Transmission Lines Including Developed Mean Flow Effects. Unpublished Dissertation. Wright-Patterson Air Force Base, Ohio: Air Force Institute of Technology, November 1977.

21. Morse, P. M. and Ingard, K. U. Theoretical Acoustics. New York: McGraw-Hill Book Co., 1968.

22. Nichols, N. B. "The Linear Properties of Pneumatic Transmission Lines." Transactions of the Instrument Society of America, Vol. 1: 5-14 (January 1962).

23. Oldenburger, R. "Theory of Distributed Systems." Journal of Basic Engineering, Trans. ASME, Series D, Vol. 92, No. 1: 1-10 (March 1970).

24. Orner, P. A. "Linear Dynamic Modelling of Flowing Fluid Lines." Journal of Basic Engineering, Trans. ASME, Series D, Vol. 91, No. 4: 740-749 (December 1969).

25. Orner, P. A. and Cooley, W. C. "Experimental Study of Through-Flowing Pneumatic Lines." Journal of Basic Engineering, Trans. ASME, Series D, Vol. 92, No. 4: 849-856 (December 1970).

26. Picard, E. Traite d'Analyse. (Three Volumes, Third Edition) Paris: Gauthier-Villars, 1922, 1925, 1928.

27. Richardson, E. G. and Tyler, E. "The Transverse Velocity Gradient near the Mouths of Pipes in Which an Alternating or Continuous Flow of Air is Established." Proceedings of the Phys. Society of London, Vol. 42: 1-15 (1929).

28. Rosenhead, L. "A Discussion on the First and Second Viscosities of Fluids." Proceedings of the Royal Society of London, Series A, Mathematical and Physical Sciences, Vol. 226: 1-69 (7 December 1954).

29. Safwat, H. H. and Van Den Polder, J. "Experimental and Analytic Data Correlation Study of Water Column Separation." Journal of Fluids Engineering, Trans. ASME: 408-414 (September 1973).

30. Society of Automotive Engineers Aerospace Information Report 1362. Physical Properties of Hydraulic Fluids. New York: Society of Automotive Engineers, Inc., 1974.

31. Swaffield, J. A. "The Influence of Bends on Fluid Transients Propagated in Incompressible Pipe Flow," Proceedings of the Institution of Mechanical Engineers, 1968-1969, Vol. 183, Pt. 1, No. 29: 603-614.

32. Uchida, S. "The Pulsating Viscous Flow Superposed on the Steady Laminar Motion of Incompressible Fluid in a Circular Pipe." ZAMP. Vol. VII: 403-421 (1956).

33. Vytoyannis, C. G. and Hsu, H. "Experimental Study of Effect of Vibration on Friction Factor in Flows Through Curved Pipes." Industrial Engineer's Chemical Process Design Developments, Vol. 9,No. 2: 186-192 (1970).

34. Womersley, J. R. An Elastic Tube Theory of Pulse Transmission and Oscillating Flow in Mammalian Arteries. WADC TR-56-614. Wright-Patterson Air Force Base, Ohio: Wright Air Development Center, 1957.

35. Wright, J. A. An Experimental Study of Hydraulic System Frequency Response Characteristics. Unpublished Thesis. Wright-Patterson Air Force Base, Ohio: Air Force Institute of Technology, March 1977.

Additional References

36. Allievi, L. "Theory of Water Hammer." Symposium on Water Hammer, ASME, 1933.

37. Cohen, L. Heaviside's Electrical Circuit Theory. New York: McGraw-Hill, 1928.

38. Franke, M. E., Karam, J. T., Jr., and Lymburner, F. C. "Experimental Frequency Response of Fluidic Transmission Lines." Paper E1 of the Fourth Cranfield Fluidics Conference. Coventry, England: The British Hydromechanics Research Association, Cranfield, Bedford, England, March 1970.

39. Iberall, A. S. "Attenuation of Oscillatory Pressures in Instrument Lines." Journal of Research, National Bureau of Standards, Vol. 45, July 1950.

40. Joukowsky, N. "Water Hammer." Proceedings of the American Water Works Association, 1904.

41. Rich, G. R. "Water-Hammer Analysis by the Laplace-Mellin Transformation." Trans. ASME, Vol. 67: 361-376 (1945).

42. Rohmann, C. P. and Grogan, E. C. "On the Dynamics of Pneumatic Transmission Lines." Trans. ASME, Vol. 79: 853-874 (1957).

43. Wood, F. M. "The Application of Heaviside's Operational Calculus to the Solution of Problems in Water Hammer." Trans. ASME, Vol. 59: 707-713 (1937).

44. Zur, Arie. Experimental Study of Hydraulic Systems Transient Response Characteristics. Unpublished Thesis. Wright-Patterson Air Force Base, Ohio: Air Force Institute of Technology, December 1978.

Appendix A

Demonstration that Orner's Solution is Incorrect

Orner solved Eqs (41) and (42) obtaining Eq (48) which does satisfy the radial boundary conditions as given in Eq (39). Comparing Eq (40) with Eq (48) and using Eq (42) for an expression for exp ($\gamma\eta$), one finds

$$E(\varepsilon) = \frac{\exp(D_2\varepsilon^2)}{B+4D_2}\left[1 - \frac{M\left(1/2 - \frac{B}{8D_2};\ 1;\ 2D_2\varepsilon^2\right)}{M\left(1/2 - \frac{B}{8D_2};\ 1;\ 2D_2\right)}\right] \tag{113}$$

where

$$B + 4D_2 = K_1 \tag{114}$$

Now let

$$E(\varepsilon) = \exp(-D_2\varepsilon^2)W(\varepsilon) = \exp(-z/2)W(z) \tag{115}$$

where

$$z = 2D_2\varepsilon^2 \tag{116}$$

Substituting Eq (115) into Eq (41) yields

$$zW''(z) + (1-z)W'(z) - \left(1/2 - \frac{B}{8D_2}\right)W(z) = \frac{K_1\exp(z/2)}{8D_2} \tag{117}$$

where ' denotes a derivative with respect to z.

Note that the homogeneous form of Eq (117) is the confluent hypergeometric equation. Now let

$$W(z) = V(z)\left[1 - \frac{M\left(1/2 - \frac{B}{8D_2};\ 1;\ z\right)}{M\left(1/2 - \frac{B}{8D_2};\ 1;\ 2D_2\right)}\right] \tag{118}$$

Substituting Eq (118) into Eq (117) yields the following differential equation for V(z):

$$zV''\left[1 - \frac{M\left(1/2 - \frac{B}{8D_2};\ 1;\ z\right)}{M\left(1/2 - \frac{B}{8D_2};\ 1;\ 2D_2\right)}\right] - 2zV' \frac{M'\left(1/2 - \frac{B}{8D_2};\ 1;\ z\right)}{M\left(1/2 - \frac{B}{8D_2};\ 1;\ 2D_2\right)}$$

$$+ (1-z)V'\left(1 - \frac{M\left(1/2 - \frac{B}{8D_2};\ 1;\ z\right)}{M\left(1/2 - \frac{B}{8D_2};\ 1;\ 2D_2\right)}\right) - V\left(1/2 - \frac{B}{8D_2}\right)$$

$$= \frac{K_1 \exp(z/2)}{8D_2} \tag{119}$$

Now if Orner's solution is correct,

$$V(z) = \frac{K_1 \exp(z)}{B + 4D_2} \tag{120}$$

and substitution of Eq (120) into Eq (119) should yield an identity. Substitution yields

$$\left(1/2 + \frac{B}{8D_2}\right)[\exp(-z/2)-1] = -\frac{2zM'\left(1/2 - \frac{B}{8D_2};\ 1;\ z\right)}{M\left(1/2 - \frac{B}{8D_2};\ 1;\ 2D_2\right)}$$

$$- \frac{M\left(1/2 - \frac{B}{8D_2};\ 1;\ z\right)}{M\left(1/2 - \frac{B}{8D_2};\ 1;\ 2D_2\right)} \tag{121}$$

Since it is not obvious whether this is an identity or not, two methods can be used to determine if Eq (121) is an identity or a contradiction. First, evaluate Eq (121) at z = 0 noting that

$$M\left(1/2 - \frac{B}{8D_2};\quad 1;\quad 0\right) = 1 \tag{122}$$

which is easily noted by looking at the infinite series

$$M\left(1/2 - \frac{B}{8D_2};\quad 1;\quad z\right) = \sum_{K=0}^{\infty} \frac{\left(1/2 - \frac{B}{8D_2}\right)_K z^K}{(K!)^2} \tag{123}$$

Also note that

$$M'\left(1/2 - \frac{B}{8D_2};\quad 1;\quad z\right) = \sum_{K=1}^{\infty} \frac{\left(1/2 - \frac{B}{8D_2}\right)_K K z^{K-1}}{(K!)^2} \tag{124}$$

Thus

$$M'\left(1/2 - \frac{B}{8D_2};\quad 1;\quad 0\right) = 1/2 - \frac{B}{8D_2} \tag{125}$$

Using Eqs (122) and (125) and substituting into Eq (121) yields

$$\frac{1}{M\left(1/2 - \frac{B}{8D_2};\quad 1;\quad 2D_2\right)} = 0 \tag{126}$$

This could be true only if

$$M\left(1/2 - \frac{B}{8D_2};\quad 1;\quad 2D_2\right)$$

were unbounded for all values of B and D_2, which it is not. This term was calculated for several values of B, which is a function of frequency, with the result being a finite complex number in each case.

A second way of showing the same contradictions is by writing Eq (121) in terms of the infinite series representations and then equating coefficients of like powers of z. An identity should result if Eq (121), and hence Orner's solution, is correct. The result for z^1 is

$$\left(1/2 - \frac{B}{8D_2}\right) \Big/ \left(1/2 + \frac{B}{8D_2}\right) = \frac{M\left(1/2 - \frac{B}{8D_2};\ 1;\ 2D_2\right)}{4} \qquad (127)$$

Neither Eq (126) nor Eq (127) is an identity. These contradictions which were generated from Orner's solution demonstrate that his solution is not correct.

Appendix B

Proof of Uniform Convergence

For Eq (117) let

$$a = 1/2 - \frac{B}{8D_2} \tag{128}$$

and

$$W(z) = \sum_{m=0}^{\infty} c_m z^m \tag{129}$$

Thus

$$z\sum_{m=2}^{\infty} m(m-1)c_m z^{m-2} + (1-z)\sum_{m=1}^{\infty} mc_m z^{m-1} - a\sum_{m=0}^{\infty} c_m z^m = \frac{K_1}{8D_2}\sum_{m=0}^{\infty}\frac{z^m}{2^m m!} \tag{130}$$

After some manipulation of the summation indices

$$\sum_{K=1}^{\infty} K(K+1)c_{K+1}z^K + \sum_{K=0}^{\infty}(K+1)c_{K+1}z^K - \sum_{K=1}^{\infty} Kc_K z^K = \frac{K_1}{8D_2}\sum_{K=0}^{\infty}\frac{z^K}{2^K K!} \tag{131}$$

Equating coefficients of z^K yields

$$c_{K+1} = \frac{K+a}{(K+1)^2}c_K + \frac{K_1}{8D_2 2^K K!(K+1)^2} \tag{132}$$

which is a two term recursion formula. Noting that c_K is complex in the general case

$$|c_{K+1}| \leq \frac{|K+a|}{(K+1)^2}|c_K| + \left|\frac{K_1}{8D_2}\right|\frac{1}{2^K K!(K+1)^2} \tag{133}$$

Now suppose for some K

$$|c_K| \leq \frac{D}{\sqrt{K!}} \tag{134}$$

where D is a positive real number. Then

$$|c_{K+1}| \leq \frac{|K+a|D}{(K+1)^2\sqrt{K!}} + \left|\frac{K_1}{8D_2}\right| \frac{1}{2^K K!(K+1)^2} \tag{135}$$

or

$$|c_{K+1}| \leq \frac{|K+a|D}{(K+1)^{3/2}\sqrt{(K+1)!}} + \left|\frac{K_1}{8D_2}\right| \frac{1}{2^K(K+1)^{3/2}\sqrt{(K+1)!}\sqrt{K!}} \tag{136}$$

Now if

$$\frac{|K+a|D}{(K+1)^{3/2}} + \left|\frac{K_1}{8D_2}\right| \frac{1}{2^K(K+1)^{3/2}\sqrt{K!}} \leq D \tag{137}$$

then

$$|c_{K+1}| \leq \frac{D}{\sqrt{(K+1)!}} \tag{138}$$

By induction

$$|c_{K+J}| \leq \frac{D}{\sqrt{(K+J)!}}, \quad J = 2, 3, 4, \ldots \tag{139}$$

To show that Eq (137) and hence Eq (138) is valid, rewrite Eq (137) as

$$A \geq \left|\frac{K_1}{8D_2}\right| \frac{1}{2^K(K+1)^{3/2}\sqrt{K!}\left[1 - \frac{|K+a|}{(K+1)^{3/2}}\right]} \tag{140}$$

Note that

$$\left|\frac{K_1}{8D_2}\right|$$

is a constant;

$$2^K (K+1)^{3/2} \sqrt{K!}$$

is monotone increasing; and

$$1 - \frac{|K+a|}{(K+1)^{3/2}}$$

is monotone increasing. Therefore

$$\left|\frac{K_1}{8D_2}\right| \frac{1}{2^K (K+1)^{3/2} \sqrt{K!} \left[1 - \frac{|K+a|}{(K+1)^{3/2}}\right]}$$

is monotone decreasing. Thus a value of D that satisfies Eq (134) for one value of K, say K_o, satisfies Eq (134) for all $K \geq K_o$.

Since $|c_K|$ is some finite constant, a value of D can always be found such that two conditions are satisfied:

$$1) \quad |c_K| \leq \frac{D}{\sqrt{K!}}, \quad K \geq K_o \tag{141}$$

$$2) \quad D \geq \left|\frac{K_1}{8D_2}\right| \frac{1}{2^K (K+1)^{3/2} \sqrt{K!} \left[1 - \frac{|K+a|}{(K+1)^{3/2}}\right]}, \quad K \geq K_o \tag{142}$$

This assures that

$$|c_{K+1}| \leq \frac{D}{\sqrt{(K+1)!}}, \quad K \geq K_o \tag{143}$$

Then by the comparison test with the known uniformly convergent series

$$\sum_{K=0}^{\infty} \frac{\eta z^K}{K!}$$

the series

$$\sum_{K=0}^{\infty} c_K z^K$$

is also a uniformly convergent series. Note, however, that nothing is said about the relative magnitude of the terms, i.e., $|c_{K+1}|$ may be larger or smaller than $|c_K|$. The only guarantee is that

$$\lim_{K\to\infty} |c_K| = 0 \tag{144}$$

As a result numerical problems may occur depending on the size of z, K_1, D_2 and a. Many terms in the series may be needed for accurate numerical evaluation if K_o is a large number. Note also that term-by-term differentiation and integration is possible due to the uniform convergence property.

Appendix C

Demonstration that the Solution Satisfies the Differential Equation

The solution to Eq (117) is

$$W(z) = \frac{K_1}{8D_2} \sum_{K=1}^{\infty} \left\{ \sum_{m=1}^{K} \frac{(a+m)_{K-m}}{(m)^2_{K-(m-1)}(m-1)!2^{m-1}} \right\} \left\{ z^K - (2D_2)^K \frac{M(a,1,z)}{M(a,1,2D_2)} \right\} \quad (145)$$

Differentiating Eq (145) term-by-term, which is valid due to the uniform convergence property, and substituting the results into Eq (117) yields

$$\sum_{K=1}^{\infty} \left\{ \sum_{m=1}^{K} \frac{(a+m)_{K-m}}{(m)^2_{K-(m-1)}(m-1)!a^{m-1}} \right\} \left\{ K^2 z^{K-1} - (K+a) z^K \right\} = \sum_{K=0}^{\infty} \frac{z^K}{2^K K!} \quad (146)$$

where the confluent hypergeometric equation,

$$zM''(a,1,z) + (1-z)M'(a,1,z) - aM(a,1,z) = 0 \quad (147)$$

is subtracted out since the confluent hypergeometric function, $M(a,1,z)$, satisfies it identically. Also the infinite series representation for $\exp(z/2)$ is included in Eq (146).

The terms with an "a" in them cancel out as can be seen by calculating the coefficient of z^{K-1} for any $K \geq 1$ from Eq (146). The remaining terms, which do not have an "a" in them, on the left hand side of Eq (146) should equal the coefficient of z^{K-1} in the series for the exponential. They do; in fact the resulting equation after the "a" terms have been cancelled out is

$$\sum_{K=1}^{\infty} \frac{z^{K-1}}{(K-1)!2^{K-1}} = \sum_{K=1}^{\infty} \frac{z^{K-1}}{(K-1)!2^{K-1}} \tag{148}$$

Thus it has been demonstrated that the solution, Eq (145), to Eq (117) can be substituted into Eq (117) with an identity resulting. The solution then does satisfy the differential equation.

Appendix D

Reduction of the Solution for Zero Through-Flow to the Bessel Function Velocity Profile

Starting with Eq (81) and reversing several of the transforms yields

$$u_1 = \frac{R^2}{4\rho_o \nu} \frac{dp_1}{dx} \exp(-j\sqrt{A}\varepsilon^2/2) \sum_{K=1}^{\infty} \left\{ \sum_{m=1}^{K} \left[\frac{\left(1/2 + \frac{\sqrt{A}}{4j} + \frac{\omega R^2}{4\nu\sqrt{A}} + m\right)_{K-m}}{(m)^2_{K-(m-1)}\,(m-1)!\,2^{m-1}} \right] \right.$$

$$\left. \otimes \left[(j\sqrt{A})^{K-1} \left(\varepsilon^{2K} - \frac{M(a,1,j\sqrt{A}\varepsilon^2)}{M(a,1,j\sqrt{A})} \right) \right] \right\} \tag{149}$$

Looking at the confluent hypergeometric functions,

$$\lim_{\overline{u}_o \to 0} M(a,1,j\sqrt{A}\varepsilon^2) = \lim_{A \to 0} M\left(1/2 + \frac{\sqrt{A}}{4j} + \frac{\omega R^2}{4\nu\sqrt{A}},\ 1,\ j\sqrt{A}\varepsilon^2\right) \tag{150}$$

From the Handbook of Mathematical Functions (13)

$$\lim_{\hat{a} \to \infty} M(\hat{a},b,-\hat{z}/\hat{a})/\Gamma(b) = \hat{z}^{1/2-b/2} J_{b-1}(2\sqrt{\hat{z}}) \tag{151}$$

Let

$$j\sqrt{A}\varepsilon^2 \left[\frac{\frac{1}{2} + \frac{\sqrt{A}}{4j} + \frac{\omega R^2}{4\nu\sqrt{A}}}{\frac{1}{2} + \frac{\sqrt{A}}{4j} + \frac{\omega R^2}{4\nu\sqrt{A}}} \right] = -\hat{z}/\hat{a} \tag{152}$$

where

$$\hat{a} = \frac{1}{2} + \frac{\sqrt{A}}{4j} + \frac{\omega R^2}{4\nu\sqrt{A}} \tag{153}$$

$$-\hat{z} = \varepsilon^2 \left[\frac{j\sqrt{A}}{2} + \frac{A}{4} + \frac{j\omega R^2}{4} \right] \tag{154}$$

$$b = 1 \tag{155}$$

$$\Gamma(1) = 1 \tag{156}$$

Then

$$\lim_{A\to 0} M\left(\frac{1}{2} + \frac{\sqrt{A}}{4j} + \frac{\omega R^2}{4\nu\sqrt{A}}\ ,\ 1,\ j\sqrt{A}\varepsilon^2\right) = \lim_{\hat{a}\to\infty} M(\hat{a},1,-\hat{z}/\hat{a}) = J_o(2\sqrt{\hat{z}}) \tag{157}$$

Also

$$\lim_{A\to 0} \hat{z} = -\varepsilon^2 \left[\frac{j\omega R^2}{4\nu} \right] \tag{158}$$

The result after reversing some transforms is

$$\lim_{A\to 0} M\left(\frac{1}{2} + \frac{\sqrt{A}}{4j} + \frac{\omega R^2}{4\nu\sqrt{A}}\ ,\ 1,\ j\sqrt{A}\varepsilon^2\right) = J_o(rj^{3/2}\sqrt{\omega/\nu}) \tag{159}$$

Similarly,

$$\lim_{A\to 0} M\left(\frac{1}{2} + \frac{\sqrt{A}}{4j} + \frac{\omega R^2}{4\nu\sqrt{A}}\ ,\ 1,\ j\sqrt{A}\right) = J_o(Rj^{3/2}\sqrt{\omega/\nu}) \tag{160}$$

Also

$$\lim_{A\to 0} \exp(-j\sqrt{A}\varepsilon^2/2) = 1 \tag{161}$$

The next term is

$$\sum_{m=1}^{K} \left[\frac{(a+m)_{K-m}}{(m)^2{}_{K-(m-1)}\,(m-1)!\,2^{m-1}} \right] (j\sqrt{A})^{K-1}$$

In the limit as $A \to 0$, the only terms that remain are clearly

$$\sum_{m=1}^{K} \left\{ \frac{\left(\frac{\omega R^2}{4\nu\sqrt{A}}\right)_{K-m}}{(m)^2_{K-(m-1)}(m-1)!2^{m-1}} \right\} (j\sqrt{A})^{K-1}$$

as all the other terms have a positive power of $\sqrt{A}$ in the numerator. Remembering that $(a)_K = a(a+1)(a+2)\ldots(a+K-1)$, one notes that

$$\left(\frac{\omega R^2}{4\nu\sqrt{A}}\right)_K$$

will have a factor, $(1/\sqrt{A})^K$ and thus

$$\sum_{m=1}^{K} \left(\frac{\omega R^2}{4\nu\sqrt{A}}\right)_{K-m}$$

has one and only one term with the factor, $(1/\sqrt{A})^{K-1}$ and all other terms have a factor, $(1/\sqrt{A})^n$, where $n < K-1$. Thus only one term of the sum survives as $A \to 0$, the $m = 1$ term. Thus

$$\lim_{A\to 0} \sum_{m=1}^{K} \left\{ \frac{\left(\frac{\omega R^2}{4\nu\sqrt{A}}\right)_{K-m}}{(m)^2_{K-(m-1)}(m-1)!2^{m-1}} \right\} (j\sqrt{A})^{K-1} = \left(\frac{j\omega R^2}{4\nu}\right)^{K-1} \left(\frac{1}{K!}\right)^2 \qquad (162)$$

Piecing everything together and noting that

$$\sum_{K=1}^{\infty} \frac{(-1)^K \left(j\sqrt{j\omega R^2\varepsilon^2/\nu}\right)^{2K}}{2^{2K}(K!)^2} = J_o\left(j\sqrt{j\omega R^2\varepsilon^2/\nu}\right) - 1 \qquad (163)$$

which utilized the series representation

$$J_o(z) \sum_{m=0}^{\infty} \frac{(-1)^m z^{2m}}{2^{2m}(m!)^2} \qquad (164)$$

where the -1 in Eq (163) comes from the omitted first term (K=0) in Eq (164), one finds the final result

$$\lim_{\bar{u}_o \to 0} j\omega u_1 = -\frac{1}{\rho_o}\frac{dp_1}{dx}\left[1 - \frac{J_o(rj^{3/2}\sqrt{\omega/\nu})}{J_o(Rj^{3/2}\sqrt{\omega/\nu})}\right] \tag{165}$$

This is exactly the well-known form of the Bessel function velocity profile for zero through-flow as cited by many authors including Nichols (22).

Vita

Major John H. Pletcher, Jr. was born [redacted] In 1967 he graduated from the United States Air Force Academy and went on to Illinois Institute of Technology where he earned a MS degree in Mechanical and Aerospace Engineering. After a year in pilot training, Major Pletcher was assigned to the 39th Rescue and Recovery Squadron (ARRS), Cam Ranh Bay, Republic of South Vietnam, flying rescue HC-130 aircraft. During his tour Major Pletcher participated in numerous rescue operations for downed pilots in hostile areas, including the Son Tay POW Camp raid. His next assignment was with the 76th ARRS, Hickam AFB, Hawaii, where he provided rescue coverage for the Skylab mission. While in Hawaii, Major Pletcher moved to the 41st Aerospace Rescue and Recovery Wing, where he served as Current Operations Officer, planning and managing rescue operations such as the Mayaquez rescue and the Phenom Phen evacuation. In September 1975 Major Pletcher started his studies at the Air Force Institute of Technology.

His permanent address [redacted]

UNCLASSIFIED

SECURITY CLASSIFICATION OF THIS PAGE *(When Data Entered)*

REPORT DOCUMENTATION PAGE		READ INSTRUCTIONS BEFORE COMPLETING FORM
1. REPORT NUMBER AFIT/DS/AA/79S-1 ✓	2. GOVT ACCESSION NO.	3. RECIPIENT'S CATALOG NUMBER
4. TITLE *(and Subtitle)* AN ANALYTICAL AND EXPERIMENTAL STUDY OF AIRCRAFT HYDRAULIC LINES INCLUDING THE EFFECT OF MEAN FLOW		5. TYPE OF REPORT & PERIOD COVERED PhD Dissertation 6. PERFORMING ORG. REPORT NUMBER
7. AUTHOR*(s)* John H. Pletcher, Jr. Major, USAF		8. CONTRACT OR GRANT NUMBER*(s)*
9. PERFORMING ORGANIZATION NAME AND ADDRESS Air Force Institute of Technology (AFIT-EN) Wright-Patterson AFB, Ohio 45433		10. PROGRAM ELEMENT, PROJECT, TASK AREA & WORK UNIT NUMBERS Work Unit Number 31453013
11. CONTROLLING OFFICE NAME AND ADDRESS Air Force Aero Propulsion Laboratory AFAPL/POP-3, Wright-Patterson AFB, Ohio 45433		12. REPORT DATE 13. NUMBER OF PAGES 236
14. MONITORING AGENCY NAME & ADDRESS*(if different from Controlling Office)*		15. SECURITY CLASS. *(of this report)* Unclassified 15a. DECLASSIFICATION/DOWNGRADING SCHEDULE

16. DISTRIBUTION STATEMENT *(of this Report)*

Approved for public release; distribution unlimited.

17. DISTRIBUTION STATEMENT *(of the abstract entered in Block 20, if different from Report)*

JOSEPH R. HIPPS, Maj, USAF
Director of Public Affairs

18. SUPPLEMENTARY NOTES

19. KEY WORDS *(Continue on reverse side if necessary and identify by block number)*

Frequency Response
Fluid Transmission Lines
Through-Flow Effects
Hydraulic Lines
Clampon Pressure Transducer
Effect of Bends in Lines
Vibration Measurements
Nonhomogeneous Confluent Hypergeometric Equation

20. ABSTRACT *(Continue on reverse side if necessary and identify by block number)*

A mathematical model of a fluid transmission line was developed which included the effect of mean flow coupling with oscillatory flow. The analysis centered on solving the nonhomogeneous confluent hypergeometric equation with complex parameters using an infinite series and evaluating the solution using Ward's method.

Experiments were run using an aircraft hydraulic system. The frequency response, vibration displacement, and standing pressure half wave were → next page

DD FORM 1 JAN 73 1473 EDITION OF 1 NOV 65 IS OBSOLETE

UNCLASSIFIED

SECURITY CLASSIFICATION OF THIS PAGE *(When Data Entered)*

20. Abstract (continued)

measured in a straight line and a line with bends for flow rates up to 9.5 gpm. A clampon transducer, which did not disturb the flow and could be easily moved, was used for the pressure measurements. In the absence of vibration the clampon transducer measurements were within 5% of readings taken with a conventional Statham in-line transducer.

A sensitivity analysis showed the effect of small changes in geometry, temperature, steady-state pressure, fluid properties, entrained air content, and element volume. Using the new mathematical model, the attenuation and phase constant were calculated for hydraulic and air lines. Results compared well with experiment and published data. The new analysis and line model provide a means for the fluid systems engineer to accurately account for mean flow effects.